TECHNO-ECONOMIC EVALUATION OF A LIQUID REDOX PROCESS EMPLOYING AMINO ACID SALTS FOR SOUR NATURAL GAS TREATMENT

vorgelegt von
M.Sc.
Hatice Gülşah Sönmez
geb. in Nizip

von der Fakultät III – Prozesswissenschaften
der Technischen Universität Berlin
zur Erlangung des akademischen Grades

Doktorin der Ingenieurwissenschaften
- Dr.-Ing. -

genehmigte Dissertation

Promotionsausschuss:

Vorsitzende: Prof. Dr. Tetyana Morozyuk
Gutachter: Prof. Dr.-Ing. George Tsatsaronis
Gutachter: Prof. Dr.-Ing. Klaus Görner

Tag der wissenschaftlichen Aussprache: 09.03.2017

Berlin 2017

For my family

DANKSAGUNG

Diese Arbeit entstand im Zeitraum von April 2014 bis Dezember 2016 während meiner Tätigkeit in der Abteilung Technology and Innovation, Power and Gas Division, der Siemens AG im Industriepark Höchst, Frankfurt am Main. Hiermit möchte ich meinen Dank all denjenigen entgegenbringen, die zu dem guten Gelingen beigetragen haben.

Mein Dank gilt zuerst meinem Doktorvater, Herrn Prof. Dr.-Ing. George Tsatsaronis, für die bereichernde Betreuung dieser Arbeit vonseiten der Technischen Universität Berlin. Er hatte stets ein offenes Ohr, lieferte mir wertvolle Ratschläge und ermöglichte mir den nötigen Freiraum bei der Anfertigung der Arbeit.

Außerdem gehört mein Dank Herrn Prof. Dr.-Ing. Klaus Görner von der Universität Duisburg-Essen für die Übernahme des Zweitgutachtens und für seine umfassende Durchsicht der Arbeit.

Frau Prof. Dr. Tetyana Morozyuk danke ich für die Übernahme des Vorsitzes im Promotionsausschuss.

Weiterhin geht ein besonders herzliches Dankeschön an alle Kolleginnen und Kollegen der Siemens AG im Industriepark Höchst, stellvertretend insbesondere:

- Herrn Dr.-Ing. Rüdiger Schneider für die Ermöglichung der Doktorandentätigkeit in der Abteilung Technology and Innovation der Siemens AG sowie für die Bereitstellung der labortechnischen Einrichtungen,

- Herrn Dr.-Ing. Kevin Brechtel für die ersten wegbereitenden Ideen und Impulse, die mir den Zugang zu der Thematik sowie den Mut zur Anfertigung dieser Dissertation eröffneten,

- Herrn Dr. Ralph Joh für die fachliche Betreuung und die Durchsicht der Arbeit seitens der Siemens AG, für das mir entgegengebrachte Vertrauen sowie für die zahlreichen konstruktiven Gespräche,

- Frau Dipl.-Ing. Katrin Raake und den Herren Dipl.-Ing. Torsten Schliepdiek, Dr.-Ing. Henning Schramm, Dr. Markus Kinzl und Dipl.-Ing. Stefan Hauke für die bedingungslose Unterstützung in allen Bereichen des Tagesgeschäfts und vor allem für die Freude an der Arbeit und auch außerhalb,

- Herrn Wolfgang Nickelfeld für die tatkräftige Unterstützung bei Aufbau und Betrieb verschiedener Versuchsanlagen,

- Herrn Dr. Ansgar Kursawe für die konstruktiven Hinweise bei der Entwicklung spezieller Analytik-Methoden im Rahmen dieser Arbeit.

Herzlich danken möchte ich auch den Studierenden, die mit ihren Praktika, Bachelor- sowie Masterarbeiten sehr engagiert und konstruktiv mitgewirkt haben:

- Rainer Hessler, Alexander Behringer, Benita Sommer, Ivo Kühnrich und Lorenz Abduly.

Mein außerordentlicher Dank gilt Herrn Dr.-Ing. Albert Reichl. Die mehrfache Durchsicht der Arbeit, die kritischen Betrachtungen und differenzierten Anmerkungen, vor allem aber sein stetiger Beistand, haben mir Kraft und Mut zur Vollendung der Dissertation gegeben.

Tief verbunden bin ich all meinen Freunden in Deutschland und in der Türkei für das liebevolle Verständnis und die Aufmunterungen in dieser herausfordernden Zeit.

Mein ganz persönlicher Dank gilt aber meiner Familie, die es mir ermöglicht hat, immer meinen Weg zu gehen, auch wenn er mich weit weg von der Heimat führte. Die Widmung gebührt daher euch:

„Canım ailem, doktora tezimi size armağan ediyorum, desteğiniz için çok teşekkür ederim !“.

ABSTRACT

Abundant sour natural gas fields have been left untapped so far due to barriers limiting their economic and environmental viability for power generation. Considering the long-term projections of global energy demand, supply and prices, sour gases could be utilized to supply the regional energy demand of gas producing countries, if there were inexpensive, reliable and environmentally friendly ways for their treatment. Siemens AG has developed an **integrated technology** which enables the in-situ removal of mainly the H_2S from sour gases and the direct conversion of the sulfuric components in the liquid phase into elemental sulfur by the **liquid redox technique** (treatment plant) as well as the generation of electricity from the treated gas in a gas turbine (power plant) – for both onshore and offshore applications. The proprietary liquid redox solvent system consists of an amino acid salt (AAS) as absorbent and a chelated iron as oxidation catalyst in aqueous solution to overcome the limitations of the state of the art technologies, e.g. the infeasibility of them in case of high CO_2 contents. The economics of the new technology are directly related to the solution properties. This gave the motivation for research on and development of new solvent systems in the scope of this work by theoretical and experimental approaches - meaning selection, screening, formulation and techno-economic evaluation. Three test rigs were constructed and operated to explore the suitability of the formulations when employing them for the liquid redox process, which consists mainly of absorption, catalyst regeneration (with air) and sulfur separation. Firstly, possible constituents were identified by reviewing potentials and niche of the common gas sweetening solutions, leading to the pre-selection of 7 AASs as absorbents and 8 chelating agents. In subsequent **screening tests**, the stability of these was examined in sparged cell reactors in continuous mode under severe conditions. It was seen that the thermodynamics of the chelating phenomenon and the molecular structure of the AASs played decisive roles regarding their durabilities (primary AASs degraded much more rapidly compared to secondary, tertiary or sterically hindered ones). As a result, 2 secondary AASs, 1 tertiary AAS (dimethylglycinate) and 2 chelators (e.g. EDTA) were labelled as attractive in terms of thermodynamic, thermal and/or oxidative stability. In the **technical evaluations,** different solvent systems were formulated from those constituents (variation of components and composition). Since the application of AAS based chelated-iron solutions in the Siemens liquid redox technology is first of its kind, data on the regeneration kinetics of the chelated iron and on the desulfurization performance of the developed formulations are so far absent in open literature. Thus firstly, the regeneration behavior of 3 solutions identified as characteristic and therefore selected was investigated in a stirred cell reactor in batch mode. The iron and the dissolved oxygen concentration as well as temperature and pH were found to be the key interacting parameters regarding the catalyst regeneration. A remarkable change in the rate determining reaction step was observed at higher iron concentrations. The type of the AAS affected the stereochemical equilibria of the complex and in turn its regeneration kinetics. Considering these findings, 13 new solutions with different types and/or concentrations of AASs, chelators and iron were formulated. 7 gas compositions were involved for the determination of the overall performance behavior, and thus in total 91 test runs were conducted during 2000 hours in a continuously operated lab test rig containing bubble columns and representing the absorption and regeneration step of the treatment plant. The stable, efficient and economic operation regime of each formulation was indicated by the decisive cost driving factors: the required solution pump around ratio and the regeneration air demand per dosed H_2S. The technical evaluation was completed with the theoretical and experimental examination of possible **degradation pathways** and the determination of the optimal conditions for suppressing these. The formulation called “Sol.13” - with one of the secondary AASs and a high chelated-iron concentration - showed the most superior performance even at ultra-high sour gas concentrations. Consequently, “Sol.13” was chosen for the **economic analysis** to obtain commercial figures of the integrated technology for a semi-industrial demo phase. Evaluation was done by determining the levelized cost of electricity (LCoE, ct/kWh) with the total revenue requirement method. The LCoE was broken down to the plant parts and the single cost components. The operational expenses of the treatment plant were found to be the dominating component driven by chemical costs resulting from mechanical losses during the separation of sulfur product. The commercial aspects of the utilization of “Sol.13” for the integrated technology were assessed by comparing with performance parameters of alternative solvent systems and with the LCoE obtained from the combustion of sweet natural gas. Based on several sensitivity analyses (e.g. residual moisture after sulfur separation), proposals for optimization were given. Taking all into account, the “Sol.13” was found to be effective (low capital invest and footprint) and promising (significant reduction potentials in operational expenses) and thus appropriate to be tested and optimized further in the piloting respectively demo phase of the technology.

ZUSAMMENFASSUNG

Angesichts ökonomischer und ökologischer Hindernisse werden die meisten Sauergasvorkommen bislang nicht zur Stromerzeugung genutzt. Gestützt auf Langzeitprognosen zum weltweiten Energiemarkt wäre ein Einsatz von Sauergas zur Energieversorgung erdgasfördernder Staaten denkbar, falls kostengünstige, verlässliche und umweltschonende Aufbereitungsverfahren verfügbar wären. Die Siemens AG hat eine **integrierte Technologie** entwickelt, bei welcher maßgeblich das H_2S aus dem Sauergas abgetrennt werden (Treatment Plant basierend auf dem **Liquid Redox Verfahren** mit direkter Umwandlung des absorbierten H_2S in der flüssigen Phase zu elementarem Schwefel) und auch das gereinigte Gas in einer Gasturbine verstromt wird (Power Plant). Als Solvent-System wird eine wässrige Formulierung aus einem Aminosäuresalz (AAS) als Absorbent und einem Eisen-Chelat als Oxidationskatalysator verwendet, da diese eine deutliche höhere pH-Pufferkapazität gegenüber herkömmlichen Waschlösungen aufweisen. Die Motivation zur Entwicklung neuer Solvent-Systeme für Liquid Redox resultierte aus der Erkenntnis, dass die Wirtschaftlichkeit des Verfahrens entscheidend von den Eigenschaften der Komponenten in der Waschlösung abhängt. Im Rahmen dieser Arbeit wurden hierzu theoretische und experimentelle Ansätze gewählt – Vorauswahl, Screening, Formulierung, technische Bewertung und Wirtschaftlichkeitsanalyse. Um die Eignung neuer Formulierungen für den Liquid Redox Prozess (bestehend im Wesentlichen aus Absorption, Regeneration des Katalysators mit Luft und Schwefelabtrennung) zu testen, wurden 3 Laboranlagen aufgebaut und betrieben. Zunächst wurden durch Vergleich mit den Vor- und Nachteilen konventioneller Entschwefelungsverfahren 7 AAS als Absorbentien und 8 Chelate vorausgewählt. In nachfolgenden **Screening-Tests** wurde deren Stabilität in kontinuierlich durchströmten Glasapparaturen unter harschen Einsatzbedingungen getestet. Es zeigte sich, dass die Thermodynamik der Komplexbildung und die Molekülstruktur der AAS entscheidend waren für die Stabilität. Die primären AAS zersetzten sich viel schneller als sekundäre, tertiäre oder sterisch gehinderte. Dementsprechend wurden 2 sekundäre AAS, 1 tertiäres ASS (Dimethylglycinat) und 2 Chelatoren (darunter EDTA) als vielversprechend erkannt hinsichtlich thermodynamischer, thermischer und oxidativer Stabilität. Für die **technischen Bewertungen** wurden verschiedene Formulierungen aus diesen Komponenten angesetzt. Da chelatierte AAS-Lösungen zum ersten Mal im Rahmen der von Siemens entwickelten Liquid-Redox-Technologie zum Einsatz kommen, sind in der Literatur bislang keine Daten zur Kinetik der Regeneration des chelatierten Eisens und zum Entschwefelungsverhalten der Formulierungen verfügbar. Es wurden daher zuerst die Regenerationskinetiken von 3 typischen Formulierungen in diskontinuierlich betriebenen Rührzellenreaktoren untersucht. Als wichtigste Parameter hinsichtlich der Regeneration des Katalysators wurden die Konzentration des Eisens und des gelösten Sauerstoffs sowie Temperatur und pH-Wert identifiziert. Der AAS-Typ beeinflusste das stereochemische Gleichgewicht des Komplexes und dementsprechend auch die Reaktionskinetik. Vor dem Hintergrund dieser Erkenntnisse wurden 13 neue Formulierungen mit verschiedenen Typen bzw. Konzentrationen von AAS, Chelator und Eisen angesetzt. Mit 7 unterschiedlichen Gaszusammensetzungen ergaben sich insgesamt 91 Versuchsreihen über 2000 Std. Es wurde eine kontinuierlich betriebene Laborapparatur mit Blasensäulenkolonnen benutzt, welche den Absorptions- und den Regenerationsschritt der Treatment Plant repräsentierten. Bei jeder Messreihe zeigte sich der stabile und wirtschaftliche Betriebspunkt durch zwei entscheidende, kostenrelevante Faktoren: erforderlicher Solvent-Umpump und spezifischer Bedarf an Luft zur Regeneration (per zudosiertem H_2S). Die technischen Bewertungen wurden vervollständigt durch die theoretische und experimentelle Untersuchung der **Zersetzungsmechanismen** und die Bestimmung optimaler Bedingungen zu deren Unterdrückung. Die Formulierung mit der Bezeichnung „Sol.13“ – mit einem sekundären AAS und einer hohen Konzentration an komplexiertem Eisen – zeigte beste Eigenschaften, sogar bei sehr hohen Anteilen von sauren Komponenten im Gas. Dementsprechend erfolgte die Auswahl von „Sol.13“ für die **Wirtschaftlichkeitsanalysen** der Technologie im semi-industriellen Maßstab. Dazu wurden die sog. „Levelized Cost of Electricity (LCoE, ct/kWh) nach der „Total Revenue Requirement Methode” ermittelt. Es zeigte sich, dass die Betriebskosten und hier im Wesentlichen die Solvent-Verluste bei der Schwefelabtrennung entscheidend waren. Der Einsatz von „Sol.13“ bei der integrierten Technologie wurde unter kommerziellen Gesichtspunkten mit alternativen Formulierungen sowie mit den LCoE für die Verbrennung von konventionellem Erdgas verglichen. Aus Sensitivitätsanalysen (z.B. Restfeuchte des Filterkuchens bei der Schwefelabtrennung) ließen sich Empfehlungen für Optimierungen ableiten. Schlussendlich erwies sich „Sol.13“ als am besten hinsichtlich Investkosten und Flächenbedarf und als vielversprechend hinsichtlich einer möglichen Reduzierung der Betriebskosten. „Sol. 13“ ist daher ein geeigneter Kandidat für weitere Tests während einer Pilot- bzw. Demonstrationsphase der Technologie.

TABLE OF CONTENTS

1 INTRODUCTION

For decades to come, natural gas will be the energy source of choice to meet the increasing global energy demand (EIA, 2016a). Following profound forecasts, the main part of the world´s energy demand, almost 80 %, will be covered by fossil fuels throughout 2040, whereby the market share of natural gas will be 28 % by 2035. Such a market interest for natural gas is due to the utilization of it in power generation where it is less costly per unit of energy and releases the fewest pollutant emissions in comparison to the other fossil fuels. Worldwide proven natural gas reserves are roughly 200 trillion normal cubic meters. It is stated that tapped reserves, containing standard quality gases or so-called sweet gases, will last for the next few decades. However, they would not be able to cover the worldwide energy demand beyond that period of time, considering an annual increase by 1.8 % in the global natural gas consumption. The oil and gas field operators who mainly have preferred to produce gas from reservoirs delivering best-quality products will have to develop fields with higher acidic gas content in the future. At the moment, almost 40 % of the gas fields lying undeveloped contain high amount of sour contaminants. Without purification, these so-called sour gases are currently not tradable in the world market, since proven and potential resources are estimated to contain significant fractions of non-hydrocarbon gases, mainly hydrogen sulfide (H_2S) and/or carbon dioxide (CO_2). Especially high H_2S contents (from trace amounts to greater than 30 vol%) severely limit the economic and environmental viability of sour gas resources. Among others, corrosiveness and toxicity of sour gases pose obstacles for further processing them in gas turbines. Because of these handicaps sour gases have been often regarded as commercially unusable in power generation. The improvement of cost effective H_2S removal processes would enable the on-site utilization of sour natural gases in gas turbines. By processing these gases in combustion units, the local utilities would be provided with an opportunity to significantly cut down cost of electricity, since the domestic price of sour natural gas would be cheaper than the price of sweet natural gas (Canty, 2012). The sour gas deposits are located mainly in the Middle East, Central USA and the Russian Federation. Others can be found in Western Europe, South East Asia and North Africa.

There are already commercially available H_2S removal processes; however they are not applicable economically for all sour gas reserves. The most common approach of them is the absorption of acidic gases in an amine employing absorber unit and stepwise conversion of the stripped H_2S to elemental sulfur of good quality by the help of a Claus unit along with its supplementaries (Kohl, A. L. et al., 1997). Since the technology of the amine unit, Claus unit and accompanying tail gas treatment (TGT) unit is reportedly capital and equipment intensive, alternative processes are more economical to recover the sulfur, in case of small capacities of H_2S-bearing gases. The liquid redox technique, which allows removal of H_2S from gases and subsequent direct conversion of it into elemental sulfur in the liquid phase, is in that case the process of choice due to lower capital requirement as well as simple and compact design. Common liquid redox processes have been established only for low H_2S removal capacities and are sensible towards various CO_2 fractions of sour gases. However, the Middle Eastern sour gas reserves holding the largest volumes are contaminated with CO_2. Therefore, Siemens AG has developed a proprietary liquid-redox technology applying amino acid salts (AAS) containing a chelated metal for the simultaneous removal of H_2S and CO_2 from sour natural gases. This technology is especially designed to be an integrated sour gas treatment plant for application with combined and/or open cycle power plants to enable direct conversion of the treated gas into electricity by simultaneously covering the regional energy demand. Characteristics of the solvent system employed in the liquid redox method are crucial for achieving robust operation, small footprint and cost-effectiveness and are therefore the main focus of this work.

Parts of Chapter 1 are published as:
Sönmez, H. G. et al. (2015). Investigations on characterization of catalytically activated liquid systems for sour gas treatment. Paper presented at GPA Europe Technical Conference – Gas Treatment and Liquefaction Processes for Natural Gas, Hamburg, Germany, April 22-24, 2015.

1.1 Constituents, classification and reserves of natural gas and sour gas

Raw natural gas comprises of liquefied and/or gaseous components occurring in deposits and varies substantially in composition from source to source. The simplest hydrocarbon, the methane (CH_4), is always the major component of the natural gas, typically 70-90 vol%, but also significant amounts of ethane (C_2H_6), some propane (C_3H_8) and butane (C_4H_{10}) or other higher hydrocarbons are contained (see **Table 1-1** (Speight, 2013)). There can also be a wide range of different non-hydrocarbon components in it. The non-flammable, non-hydrocarbon constituents such as water, carbon dioxide, nitrogen as well as oxygen and rare gases are often present in minority and are regarded as undesirable impurities. In addition, natural gas may possess other contaminants with an even higher potential for disturbance such as hydrogen sulfide, mercaptanes also called thiols (RSH - molecules composed of a sulfur-hydrogen-bond attached to an organic group) and carbonyl sulfide (COS).

Table 1-1 Typical ranges for the composition of natural gas (Speight, 2013)

Component	Formula	Volume [%] of dry gas
Methane	CH_4	70 – 90
Ethane	C_2H_6	0 – 20
Propane	C_3H_8	
Butane	C_4H_{10}	
Pentane and higher hydrocarbons	C_5H_{12} etc.	0 – 10
Carbon dioxide	CO_2	0 – 8
Hydrogen sulfide	H_2S	0 – 5
Nitrogen	N_2	0 – 5
Oxygen	O_2	0 - 0.2
Rare gases	He, Ar, Ne, Xe	Trace
Mercaptanes, carbonyl sulfide, carbonyl disulfide	RSH, COS, CS_2	Trace

Note: Ranges are roughly representative for all worldwide presently known natural gas sources

The classification of the natural gas, depending on the composition of the constituents mentioned above, varies in a wide range from well to well where the gas is tapped from as it is presented in **Table 1-2** (Devold, 2010).

Table 1-2 Classification of natural gas depending on its origin (Devold, 2010)

Origin of the gas		Classification of the gas	
Conventional reservoirs	Oil, gas or condensate wells Oil wells Gas or condensate wells	Raw gas Associated gas Non-associated gas	
Unconventional reservoirs	Low permeable sandstone rocks Coal deposits Shale deposits Methane hydrate deposits	Tight gas Coalbed methane Shale gas Methane gas hydrate	Wet gases

Raw natural gas comes from three types of conventional reservoirs: oil wells, gas wells and condensate wells. These wells are highly porous and permeable; therefore, enable easy extraction of the gases by standard vertical drilling. Associated gas either comes along with crude oil or is the methane recovered from oil wells, whereas non-associated gas, namely dry natural gas, originates from gas and/or condensate wells and may contain almost pure CH_4. Unlike these conventional gases, wet natural gases (continuous gases) are drilled horizontally from very low permeable unconventional resources and contain usually a higher percentage of ethane, propane and/or butane.

These are mainly tight gas, shale gas, coalbed methane and methane hydrates. Worldwide proven total natural gas reserves (conventional and unconventional) have been estimated to be approx. 200 trillion normal cubic meters (Nm^3). According to (EIA, 2016a) about 40 % of gases from both conventional and unconventional reservoirs are sour, meaning they contain > 100 ppmv H_2S. They are geographically uneven distributed around the world. The most sour gas reserves are located in the Middle East, where 60% of the total reserves contain sour gas, while 34% of the reserves in the Russian Federation are sour. A simple definition of the sour gas is given by (Wu, Y. et al., 2012) and classified in **Table 1-3**.

Table 1-3 Classification of the sourness of sour gas (Wu, Y. et al., 2012)

Sourness classification	Quantity of the sour component
Sweet raw gas	Less than 100 ppmv H_2S
Low sour gas	Less than 1%, but greater than 100 ppmv H_2S
Moderate sour gas	1 to 10 vol% H_2S
High sour gas	10 to 25 vol% H_2S
Ultra-high sour gas	Greater than 25 vol% H_2S

Note: The quantity of the CO_2 in sour gas may vary from trace amounts up to 50 vol% and does not influence the sourness classification. Since other components containing sulfur (e.g. RSH, COS, CS_2) are usually present in natural gas only in traces, they are also not considered for the classification.

Despite the abundance of such reserves, the undesired components, in particular H_2S and CO_2, make it necessary to process these gases before utilization. This will be described in the following section.

1.2 Parameters for the specification of natural gas

Once produced, natural gas will need some treatment in order to assure secure distribution to and handling by the end user and to meet performance as well as emission requirements of combustion units. Natural gas cleaning processes executed near the well are mainly classified as removal of acidic gases, removal of water and separation of heavier hydrocarbons to maximum allowable limits depending on the requirements of the specific utilization (Younger, 2004). In order to avoid varying gas compositions throughout the network and to maximize the flexibility of natural gas without compromising operability of gas appliances, the European Association for Streamlining of Energy Exchange (EASEE) has determined pipeline and downstream specifications of natural gas as shown in **Table 1-4**.

Table 1-4 EASEE specifications of natural gas (Abbott, D. J. et al., 2009)

Parameter	Unit	Min.	Max.
Wobbe Index	MJ/Nm^3	47	52
Gross heating value	MJ/Nm^3	36.5	47.2
Relative density (respective gas vs. dry air at same T and P)	m^3/m^3	0.555	0.70
Total inert gases (CO_2,N_2,He,Ar,Xe)	mol %	-	7.0
Oxygen	mol %	-	0.01
Carbon dioxide	mol %	-	2.5
Water content	mg/Nm^3	-	50
Water dew point	°C at 70 bara	-	-8
Hydrocarbon dew point	°C at 70 bara	-	-2
Total sulfur	mg/Nm^3	-	30
Hydrogen sulfide + Carbonyl sulfide (H_2S +COS as S)	mg/Nm^3	-	5
Mercaptans (RSH as S)	mg/Nm^3	-	6
Organo halides (C-X) (X as F, Cl, Br, I)	mg/Nm^3	-	1.5

Note: Normal conditions: 273.15 K and 1.01325 bar

Although the Wobbe Index (denominating the combustion characteristics) and the heating value of a gas are regarded as critical parameters with respect to safety in the combustion unit, there are also other important features which need to be considered as part of the overall gas quality specification as they can have adverse impacts on gas transportation (usually through pipelines) and on the utilization in large scale combustion plants or in other gas burning applications (CER, 2008):

- The hydrocarbon dew point and water dew point are the temperatures at which these components begin to condense out of the gas stream. The presence of liquid water and hydrocarbons leads to formation of solid hydrates which e.g. causes plugging of valves and fittings in the pipeline.

- Oxygen (O_2) in the presence of water can promote metal corrosion within pipelines and associated systems. If excess water in the gas condenses, it can absorb CO_2 and sulfur compounds creating a corrosive liquid in the pipeline, as well.

- Sulfur compounds do not only lead to corrosion in the presence of liquid water, but are also fatal in case of exposure to the environment in a concentration higher than allowable limits (e.g. 5 mg/Nm^3 or approx. 4 ppmv of H_2S and COS in natural gas) (Younger, 2004). In addition, sulfur poses obstacles during the combustion such as emissions of sulfur oxides (SOx) as well as condensation and/or deposition of corrosive sulfates on associated equipment which will be explained in detail in the following section.

To sum up, exact specifications for the treated natural gas and necessary processing operations vary depending on the purpose of the end use and the type of raw natural gas. The following section gives an overview on desired characteristics of natural gas as fuel for utilization in power generation in industrial size gas turbines.

1.3 Impacts of natural gas characteristics on gas turbine performance and operation

In gas turbines, varying natural gas characteristics and/or composition, beyond acceptable limits, may have adverse impacts on turbine performance and operation such as (CER, 2008):

- increased emissions (particularly nitrogen oxides (NOX) and carbon monoxide (CO))
- decreased operability including part load operation
- reduced reliability
- decreased component life.

Two factors which mainly affect the performance and operation of a gas turbine are the pressure ratio (gas turbine in/out) and the firing temperature (Boyce, 2012). Elevated pressure ratios yield a higher thermal efficiency of the turbine when accompanied with an increase in the firing temperature. However, raising the pressure ratio beyond a certain value can actually result in lowering the overall cycle efficiency. Besides that, very high pressure ratios tend to reduce the operating range of the turbine compressor which in turn can lead to a compressor surge (a flameout) or even to more serious damage/failure of the related turbine components.

The two main fuel characteristics influencing the combustion behavior of a gas are the heating value and the Wobbe Index (WI) (Boyce, 2012). The higher heating value (HHV) is a parameter for the heat content of the gas and expressed as the amount of heat produced by the complete combustion of a specified volume at defined temperature and pressure, usually by re-cooling and condensing the vapor (as a product of combustion) at T = 15°C and P = 1.01325 bar. The lower heating value (LHV), also known as the net heating value, is calculated by subtracting the heat of vaporization of water from the measured HHV and assumes that all products of combustion including water remain in the gaseous phase. Gas turbines do not operate with condensing exhaust systems and it is common that gas turbine industry practice to utilize the LHV when calculating the overall cycle thermal efficiency. In addition, the heating value depends on the composition of the gas.

Despite the fact that the inert components (e.g. the CO_2 and the N_2 among others) are not poisonous, they contribute to a lower heating value and obstruct the compression of the gas to the desired pressure. Accurate determination of the composition and the LHV of the fuel gas allow for optimal adjustment of the air-to-fuel ratio, thus enabling the combustion turbine to operate at its most cost-effective and efficient point with respect to pressure ratio and firing temperature while reducing NOx emissions. As expressed in Eq.1-1, the WI is calculated by dividing the LHV by the square root of the relative density[1] of the gas.

$$\mathrm{WI} = \mathrm{LHV} \Big/ \sqrt{\rho_g / \rho_a} \qquad \text{(Eq.1-1)}$$

The WI is an indication of the energy flow into the system at given gas pressure and pressure drop, thus, a critical factor for combustion dynamics and safety (Boyce, 2012). Turbine damage can result from varying flame dynamics caused by changes in the WI. If two fuel gases with different compositions have the same WI, the pressure drop will be identical for both gases. Typically, fluctuations of up to ±5 % are allowed in a combustor before problems will be encountered. In all gas combustors, the gas flow is regulated by a hole or orifice of given size, while the pressure is controlled at a certain value. The higher the WI of a gas, the greater the LHV per quantity of it which flows through an orifice of given size in a given time frame. Therefore, a WI too high can result in over-heating of appliances or so-called sooting as well as CO formation due to incomplete combustion whereas a WI too low can result in extinguishing of flames.

After gaining an understanding of chief parameters of fuel natural gas impacting combustion performance, thus now, the influences of its composition on the turbine operation will be highlighted: As mentioned before, untreated sour natural gas has been left as commercially unused in direct power generation, since the combustion of these fuels can be extremely detrimental to gas turbine life due to corrosion, erosion, and fouling of the blades. Operational problems in gas turbines caused by H_2S and other sulfur species can be termed as (Soares, 2015):

- corrosion (hot gas path and downstream units)
- elemental sulfur deposition
- selective catalytic reduction (SCR) deactivation with subsequent increase in NOx emissions
- SOx emissions.

Hot path corrosion has a major impact on gas turbine performance and the service life of crucial components which are shown in **Figure 1-1** illustrating the cost-intensive parts of one of the Siemens gas turbines, the SGT-8000H (Bierdel, T. et al., 2013).

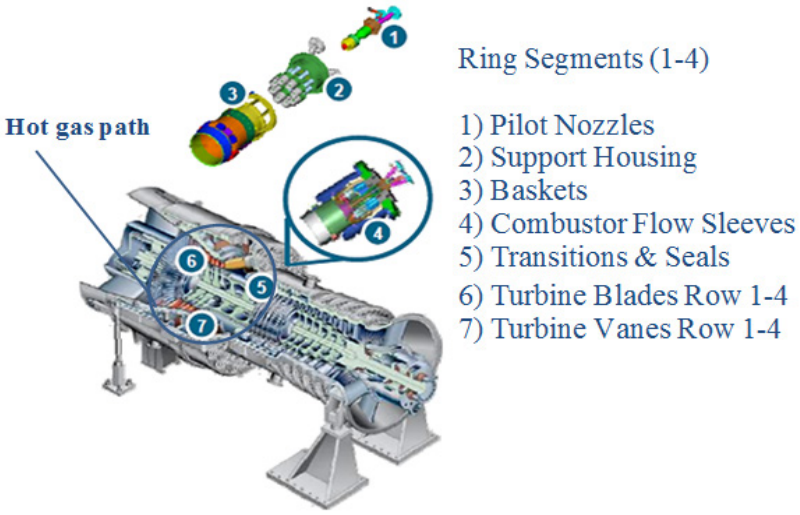

Figure 1-1 Hot gas path components of SGT-8000H (Bierdel, T. et al., 2013)

[1] The relative density is the density of the respective gas divided by the density of dry air – at the same pressure and temperature.

Besides these, other problems can be exacerbated by sulfur content, such as corrosion of components downstream of the gas turbine e.g. the Heat Recovery Steam Generator (HRSG) in combined cycle plants. Furthermore, **solid elemental sulfur deposition** can occur in gas fuel systems, downstream of pressure reducing stations or gas control valves (Soares, 2015). High gas temperatures (e.g. 55°C for a H_2S content of 5 ppmv) are required at the inlet to the gas control valves to avoid deposition, depending on the sulfur concentration. In reciprocating engines, deposition can result in engine knock, negative changes in engine performance, and decreased parts life. Furthermore, **the SCR deactivation** is described as formation of quite corrosive sulfur deposits in units which utilize ammonia injection downstream of the gas turbine for NOx control. These deposits containing ammonium sulfate [$(NH_4)_2SO_4$] and ammonium bisulfate [$(NH_4)HSO_4$] are formed on low-temperature downstream equipment and may cause decrease in HRSG performance as well as increase in back pressure to the gas turbine. In addition, high levels of sulfur compounds in the gas increase the amount of **SOx-emissions** when gas is burned. It is important to notice that comparably moderate levels of total sulfur, which are however still in excess of pipeline supply limits (approx. 25 ppmv to 100 ppmv), may have little effect on corrosion rates of hot turbine parts except in the presence of alkali metals. These include sodium (Na), potassium (K), calcium (Ca), lead (Pb), vanadium (V) and manganese (Ma). Reportedly, limiting values of V, Ca, K, Pb and Na are lesser than 0.5, 10.0, 0.5, 1.0, and 0.5 ppmwt, respectively (CER, 2008). Small amounts of V, naturally found in liquid fuels, are subject to low-temperature-melting (677 °C), and thus, vanadium pentoxide (V_2O_5) ash is created. At typical gas turbine operation temperatures, these ash deposits are in molten form and accelerate oxidation of turbine blades and vanes (Parts 6 and 7 in **Figure 1-1**). The presence of other alkali metal contaminants in the fuel, e.g. the Na and K salts, leads to formation of sodium or potassium sulfates (Na_2SO_4 or K_2SO_4) by reaction with sulfur (S) in the fuel (the sulfidation attack), resulting in pitting of the hot path components (Soares, 2015). The problems occurring due to the presence of alkali metals are typically dealt with by:

- appropriate control of fuel temperature (however temperature reduction leads to reduced performance)
- removal of water-soluble salts i.e. Na and K by on-site fuel washing
- injection of high-temperature corrosion additives for the treatment of non-soluble ones i.e. the vanadium.

Besides these measures, to meet emission regulations and to avoid problems occurring during the combustion of natural gas containing considerable contents of sulfur, a wide variety of H_2S removal (so-called “sweetening”) technologies has been developed. The following section provides an overview on the developed and/or commercially utilized gas sweetening processes.

1.4 Common sour gas sweetening processes

Before outlying the classification and application cases of available gas sweetening processes, it must be noted that, similar to the classification of sour gas according to **Table 1-3**, which was solely linked to the H_2S (sulfur) content, the term “gas sweetening” is related only to the removal of H_2S and theoretically also other sulfuric components, which are however usually not contained in natural gas in considerable amounts. The simultaneous removal of CO_2, which also contributes to the acidity, is in many cases desired, however not denoted as “gas sweetening”.

1.4.1 Classification

To be economical, the removal of acidic gas components (e.g. the H_2S and CO_2) from moderate to ultra-high sour gases requires the optimum choice of the process. For every technology, the size and the cost of the sour gas treatment (i.e. transformation of the H_2S into sulfur, shipping of the produced sulfur, acidic gas compression and reinjection facilities) increase with the quantity of acidic gas components to be separated, but not linearly. Therefore, various cost-efficient technologies are necessary to remove different fractions and amounts of acidic gases. As illustrated in **Table 1-5**, there are already commercially available chemical and/or physical separation processes to remove H_2S and/or CO_2 from sour gases in order to meet the pipeline and downstream specifications listed in **Table 1-4**.

Table 1-5 Classification of common gas sweetening technologies –compiled from ((Younger, 2004) and (Perry, R. C. et al., 1973))

Removal principle	Operating mode	Technology and operating fluids	Commercial name (process and/or solvent)	Application ranges
Chemical absorption	Regenerative, continuous	Amines	MEA, DEA, MDEA, DIPA, DGA, formulated solvents	-Gas flowrate >10 MNm^3/d -H_2S_{in} up to 80 vol%; H_2S_{out} < 4 ppmv -CO_{2in} up to 70 vol%; CO_{2out} < 0.1 vol%
		Potassium carbonate	Benfield, Catacarb, Giammarco-Vetrocoke	-Gas flowrate < 7 MNm^3/d -H_2S_{in} up to 10 vol%; H_2S_{out} < 4 ppmv -CO_{2in} up to 40 vol%; CO_{2out} < 50 ppmv
		Alkaline salts of amino acids	Alkacid-DIK, Alkacid-M	Removal of 85 ppmv and 320 ppmv H_2S with and w/o CO_2 in feed gas,respectively
				(T_{Abs}≈ 30-60 °C, P_{Abs}≈ 5-120 bara)
	Non-regenerative, continuous	Sodium hydroxide	-	-Gas flowrate < 3 MNm^3/d -H_2S_{in} < 0.1 vol%; H_2S_{out} < 5 ppmv -CO_{2in} < 0.1 vol%; CO_{2out} < 300 ppmv (T_{sys}≈ ambient, P_{sys} ≈ practically no limit)
Physical absorption	Regenerative, continuous	Physical solvents	Selexol, Rectisol, Purisol, Fluor Solvent, IFPexol	-Gas flowrate ~ 3 to 12 MNm^3/d -H_2S_{in} > 3.5 bara; H_2S_{out} < 4 ppmv -CO_{2in} > 3.5 bara ;CO_{2out} < 1 vol% (T_{sys}≈ -18 °C to ambient, P_{abs} ≈ 69 bara)
Physical-chemical absorption	Regenerative, continuous	Physical-chemical (hybrid) solvents	Amisol, Sulfinol, Ucarsol LE 701, 702 & 703, Flexsorb PS	-Gas flowrate ~ 1 to 12 MNm^3/d -H_2S_{in} >7.6 bara; H_2S_{out} < 4 ppmv -PCO_{2in}>7.6 bara; CO_{2out} < 1 vol% (T_{sys}≈ ambient to 60 °C, Pa_{bs} ≈ 69 bara; P_{reg}≤3bara)
Physical adsorption	Regenerative, continuous	Molecular sieves	5A (Zeochem), LNG-3, (UOP)	-Gas flowrate ~ 0.4 to 3 MNm^3/d -H_2S_{in} up to 2 vol%; H_2S_{out} < 4 ppmv -CO_{2in} up to 2 vol%; CO_{2out} < 50 ppmv (Ta_{ds}≈30 to 60 °C; T_{reg}≈350 °C, P_{ads} ≈ 14 to 69 bara)
Chemical adsorption	Cyclic	Dry bed by metal compounds	Sulfa-Treat®, Iron Sponge, Zinc oxide	-Gas flowrate <10 Nm^3/h -H_2S_{in} 10 to 1,000 ppmv; H_2S_{out}<0.2-0.5 ppmv -Almost no CO_2 removal (T_{ads}≈30 to 60 °C; T_{reg}≈260°C, P≈practically no limit)
Permeation	Continuous	Membranes	Separex, Cynara, Z-top, Medal	-Gas flowrate >10 Nm^3/h -H_2S_{in} up to 90 vol%; H_2S_{out} < 1 ppmv -CO_{2in} up to 70 vol%; CO_{2out} < 2 vol% (T_{sys} < 60 °C, P_{sys}≈27 to 100 bara)
Chemical conversion	Continuous	Direct conversion by metal compounds, Liquid redox	Stretford, Takahax, Thylox, Ferrox, Perox, Sulfint, SulFerox®, LO-CAT®	-Gas flowrate ~65 Nm^3/s to 12 MNm^3/d -H_2S_{in} up to 25 vol%; H_2S_{out} < 1 ppmv -Almost no CO_2 removal (T_{sys}≈20-60°C, P_{abs}≈1-100 bar(g), P_{reg}≈0.5-4 bar(g)

A detailed description of each technology can be found in (Kohl, A. L. et al., 1997), (Younger, 2004) and (Perry, R. C. et al., 1973). Each process utilizes a specific removal mechanism. Some have their own benefits or niche, but there are still cases where different technologies compete for the same application. For choosing a processing method, mainly the following factors are to be considered related to economics and environmental issues:

- the type, concentration and relation (e.g. CO_2 to H_2S ratio) of contaminants in the gas
- the desired removal degree of them
- the selectivity of the required acidic gas removal
- temperature, pressure, volume, flowrate and composition of the gas.

To this end, some particular characteristics of respective technologies listed in **Table 1-5** can be summarized as following:

In **chemical absorption processes**, the acidic gases react reversibly with the liquid absorbent after absorption into it (T ≈ 30-60 °C, P ≈ 5 to 120 bara). The regeneration of the absorbent is subsequently done by steam stripping (T ≈120-140 °C, P ≈ 1 to 2 bara). They are particularly applicable when partial pressures of acidic gas components are low and/or when the desired removal degree of the contaminants is high. Examples for this type of processes are as follows:

- The most common approach is the absorption of acidic gases in an alkanolamine based solution in an absorber unit and subsequent conversion of the stripped H_2S to elemental sulfur with the help of a Claus unit (Goar, B. G. et al., 1986).
- Absorption of acidic gases with potassium carbonate solutions shows similar operation with that of alkanolamines except the requirement of higher temperatures in the absorber (T ≈ 110-120 °C, P ≈ 60-120 bara). This method is typically used for feed gases with relatively significant fractions of CO_2 (i.e. CO_2 to H_2S ratio greater than 3) and containing other contaminants such as carbonyl sulfide (COS) and carbon disulfide (CS_2) (Kohl, A. L. et al., 1997). Reportedly, performance improvement of the potassium carbonate solutions for CO_2-capture can be achieved by addition of amines (e.g. MEA) into the solutions (Görner, K. et al., 2013).
- Non-regenerative chemical scavengers like sodium hydroxide are only suitable for the removal of small amounts of acidic gases (T ≈ ambient temperature, P ≈ 2 to 70 bara) (Kohl, A. L. et al., 1997).

Contrary to the chemical absorption processes, in **physical absorption processes** the acid gases do not react with the absorbent but are solved in it (T ≈ -18 °C to ambient, P ≈ 10 to 70 bara) (Younger, 2004). This phenomenon allows the regeneration of the absorbent by the change of thermo-physical conditions of it e.g. the pressure (depending on the desired removal degree). They are usually applied in cases where the partial pressure of the acidic components is high, bulk removal of these is required or a selective removal of H_2S is needed. Compared to the thermally regenerated chemical solvents, the regeneration of physical solvents requires less energy.

Absorption with hybrid solvents, (T≈ambient to 60 °C, P≈15 to 70 bara), keeps many similarities with chemical absorption into alkanolamines. However, hybrid systems have some advantages over chemical absorption technique associated to physical absorbent constituent of the system (i.e. lower heat requirement for regeneration).

Physical adsorption is reportedly appropriate for low inlet acidic gas contents. However, it is capable to achieve very low outlet concentrations (see **Table 1-5**). This method is generally applied in gas liquefaction trains (for LNG production), when H_2S and mercaptanes or other sulfur compounds are also to be removed. Use of **chemical adsorption** technique (e.g. dry box), which will be discussed in detail later, is not usual to remove exclusively CO_2.

Membranes serve as a barrier to separate acidic gas components. At the surface of the membrane (mostly polymer based), the components to be removed are dissolved and permeate to the other side of it (T < 60 °C, P ≈ 27 to 100 bara).

The permeation kinetics is determined by the characteristics of the membrane. Although **permeation technique** shows high turn down capacity in terms of acidic gas concentration and gas flow rate, it seems to lose its competitiveness, if higher removal degree of CO_2 than 2 vol% is desired (see **Table 1-5**). The regeneration of loaded membranes is achieved by the change of operating parameters i.e. either the P or the T.

In **chemical conversion technique**, the acidic gases react with a catalytic agent in the liquid absorbent through irreversible chemical reactions. This allows direct conversion of the absorbed H_2S to elemental sulfur in the liquid phase. This method competes with amine employing treatment processes regarding the smaller footprint of the technology -when applied for lower acidic gas capacities- and overcomes the chemical adsorption method by featuring high flexibility in the terms of acidic gas concentrations (see **Table 1-5**), however, heretofore, it has been applied for the removal of H_2S alone.

Chemical absorption with alkanolamines, chemical adsorption by metal compounds and chemical conversion by redox couples have been the most frequently used methods for the removal of the H_2S from sour gas streams. Thus, these technologies will be presented in detail in the scope of the following subsections, respectively.

1.4.2 Absorption and conversion of hydrogen sulfide to elemental sulfur by the Claus process

One of the most common processes for the treatment of industrial sour gases is the absorption of the H_2S with alkanolamines, which have at least one hydroxyl group and one amino group. The hydroxyl group reduces the vapor pressure while the amino group provides the proper alkalinity in aqueous solutions to enforce the absorption of acidic gases (Goar, B. G. et al., 1986). The whole sour gas treatment plant consists of an amine unit, a Claus unit and a TGT unit is shown in **Figure 1-2** as deduced from (Dalrymple, D. A. et al., 2005).

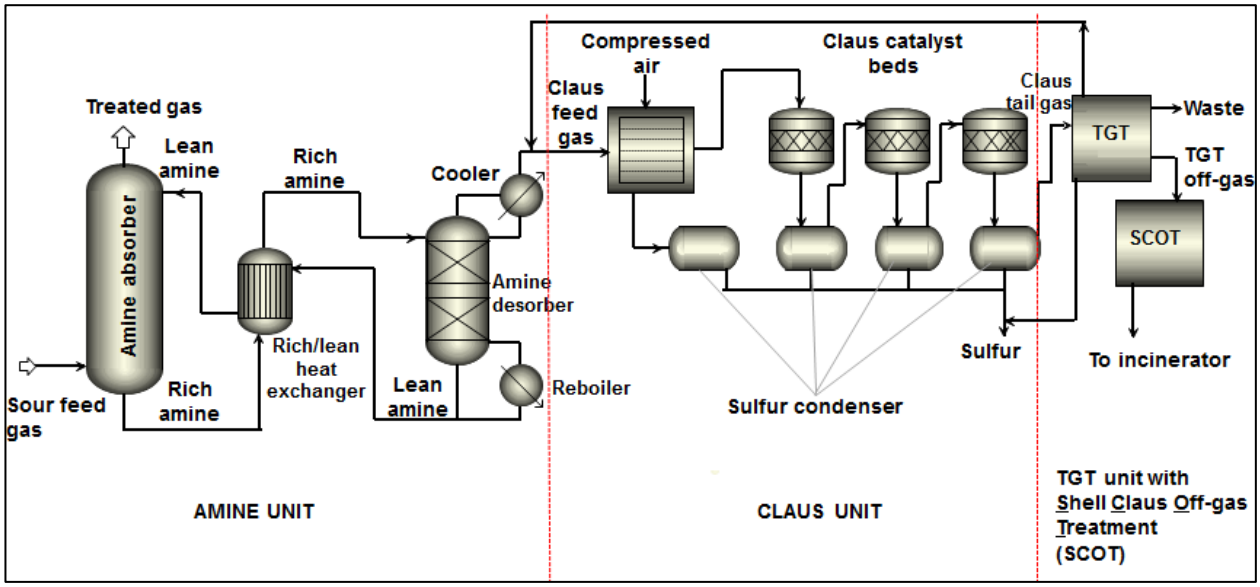

Figure 1-2 Process scheme of a conventional amine/Claus/TGT unit -deduced from (Dalrymple, D. A. et al., 2005)

Accordingly, feed sour gas containing H_2S and CO_2 is contacted with lean amine solution in a countercurrent absorption tower of the amine unit (T ≈ 30-60 °C, P ≈ 5 to 120 bara). On top of the absorber, the treated sweet gas (the desired product) is gained.

The rich amine, containing H_2S and some of the CO_2, is sent to the regenerator after being heated in the lean/rich exchanger by the hot lean amine from the bottom of the regenerator. Stripped acidic gas is then cooled on top of the reboiler (T ≈ 140 °C, P ≈ 1 to 2 bara) to condense a major portion of the water vapor. This condensate is fed back to the system as a reflux which enables a) realization of a multi-staged washing concept, b) balancing the concentration of the amine solution and c) minimizing the loss of amine vapors with the acidic gas stream (Goar, B. G. et al., 1986). The stripped H_2S is then converted into substances such as sulfur or sulfuric acid in a sulfur recovery plant i.e. the Claus Unit and the TGT Unit. When only trace amounts of H_2S are present, it might also be directly flared.

As shown in **Figure 1-2**, a common Claus unit comprises of a thermal stage and two or three catalytic stages. The H_2S-bearing feed gas and compressed combustion air flow to a burner within a reaction furnace. Approximately one third of the H_2S in the feed gas is thermally converted there to sulfur dioxide (SO_2) at high temperatures (>900 °C) and pressures of 1.5 bara without aid of a catalyst according to reaction Eq.1-2 (Younger, 2004). This reaction is exothermic and not limited by the equilibrium between hot sulfur gases (H_2S) and produced SO_2 vapor.

$$H_2S_{(g)} + 3/2\ O_{2(g)} \rightarrow SO_{2(g)} + H_2O_{(g)} \qquad \text{(Eq.1-2)}$$

The unburned H_2S in the acidic gas (the remaining 2/3 of H_2S) then reacts with the thermally produced SO_2 to form elemental sulfur vapor in the thermal stage by reaction Eq.1-3. This reaction is enabled by cooling to approx. 285-315 °C with simultaneous production of steam and is referred as Claus reaction (Bryan Research & Engineering, Inc., 1997). It can convert approximately 50% to 70% of the remaining sulfur gases (H_2S) to sulfur vapor (S_2). The reaction Eq.1-3 is endothermic and limited by the equilibrium between produced sulfur vapor species and reactant sulfur gases, since the reaction between them is a function of temperature. In the sulfur condenser of the thermal stage, elemental liquid sulfur is formed by cooling with water and simultaneously generating steam at temperatures around 160 °C and pressures around 4 bara. The condensed sulfur is drained from the condenser by a hydraulic seal and routed to a sulfur collection pit.

$$2H_2S_{(g)} + SO_{2\ (g)} \leftrightarrows 3/2\ S_{2(g)} + 2H_2O_{(g)} \qquad \text{(Eq.1-3)}$$

The thermal stage is followed by catalytic stages. The unconverted H_2S in the process gas, which comes from the first sulfur condenser of the thermal stage, is transferred to elemental sulfur vapor in the catalytic stages of the Claus Unit. Each catalytic section consists of a series of three steps: reheating, conversion of sulfur gases to sulfur vapor and subsequent condensation of them to liquid sulfur. Upstream of each catalytic bed reactor, the hot gases are heated up to approx. 230 - 280 °C. Downstream of each bed reactor the gases are cooled to approx. 160 – 175 °C by producing low-pressure steam in a separate sulfur condenser. The resulting liquid sulfur is removed in a separator section within each condenser and flows by gravity to a sulfur storage tank. The Claus plant tail gas is routed to a TGT unit for further processing (Borsboom, H. et al., 2001). The so-called Shell Claus off-gas treating unit (SCOT) is mainly utilized for the further treatment of TGT-off-gas. The SCOT unit consists of three stages: (1) catalytic reduction stage, (2) feed conditioning stage and (3) solvent regeneration stage. In the catalytic reduction section, the TGT-off-gas is heated and catalytically reacted with hydrogen so that all remaining sulfur constituents in the off-gas are reduced to H_2S. In the feed conditioning stage, the hot gas leaving the catalytic reduction section is cooled by quenching. In the solvent regeneration stage, the H_2S in the cooled gas is absorbed selectively into an organic solvent. Subsequently, the rich solvent is regenerated to strip out the H_2S, which is then injected back into the sour feed gas of the Amine Unit. The downstream stream of the SCOT unit (which mainly consists of the CO_2 absorbed from the sour feed gas in the Amine Unit) routed directly to a thermal oxidizer to incinerate all of remaining sulfur compounds in the tail gas to SO_2 before dispersing the effluent to the atmosphere. The process has to be controlled in an appropriate way to obey the emission limits with respect to SOx.

Since its inception, the Claus process has been the standard for the industrial sour gas treatment and the sulfur recovery industry, but limitations related to feed gas composition, complexity, footprint and energy demand for regeneration restrict its effectiveness (Bryan Research & Engineering, Inc., 1997).

It is stated that, depending on the H_2S concentration in the feed gas, 94 to 95 % conversion efficiencies can be achieved with one thermal stage combined with two catalytic conversion stages and 96 to 97 % with three catalytic conversion stages, so that a supplementary TGT which yields a 99.7% or higher overall sulfur recovery is required (Kohl, A. L. et al., 1997). Acidic gas streams containing less than about 40-45 mol % H_2S are considered as lean H_2S streams and usually require the application of different, more complex flow schemes than that shown in **Figure 1-2** because a stable flame cannot be sustained in the Claus reaction furnace while burning only 1/3 of the H_2S in the feed. The more non-H_2S components are present in the stream, more severe operating problems and lesser sulfur recovery efficiency will be encountered. Since the capital expenditures (CAPEX) of a plant do not linearly decrease with the plant size, complex processes are disadvantageous for small capacities. Therefore, an amine based Claus unit with supplementary of TGT and SCOT units is too cost intensive for the sweetening of sour gases with small to moderate absolute amounts of acidic components i.e. below 25 long tons equivalent sulfur per day (LTPD) (Kohl, A. L. et al., 1997). Thus, above this amount and in the case of low to moderate sour gases it should be more economical to recover the sulfur by some other process.

The H_2S removal by metal compounds e.g. the liquid redox technology, which allows the in-situ removal of H_2S from gases along with the direct conversion of it into elemental sulfur by the chelated metal catalyst in the liquid phase, may be the process of choice in cases where Claus units are not suited, due to lower CAPEX, higher turn down ratios as well as high conversion efficiencies (i.e. 99 %) (Kohl, A. L. et al., 1997). For a variety of sour gases which have been disposed of so far, high performance, simplicity and reduced footprint of this separation method would enable economical direct utilization of the treated gas in integrated open or combined cycle power generation plants constructed on the drilling rig. The following section provides an overview on the basic chemistry of separation processes involving metal compounds and their evolution during the 20th century.

1.4.3 Hydrogen sulfide removal from gaseous streams by metal compounds

1.4.3.1 Dry box processes with iron oxide

The most common dry chemisorption technology is iron sponge process (Kohl, A. L. et al., 1997). The method which employs hydrated iron oxide (sponge) (Fe_2O_3) that is impregnated on wooden chips in a dry bed is one of the oldest ways to separate undesired sulfur compounds from gas streams. As shown in **Figure 1-3**, the feed gas bearing the H_2S flows through series of fixed beds (dry boxes) while the acidic gas components are adsorbed on these beds.

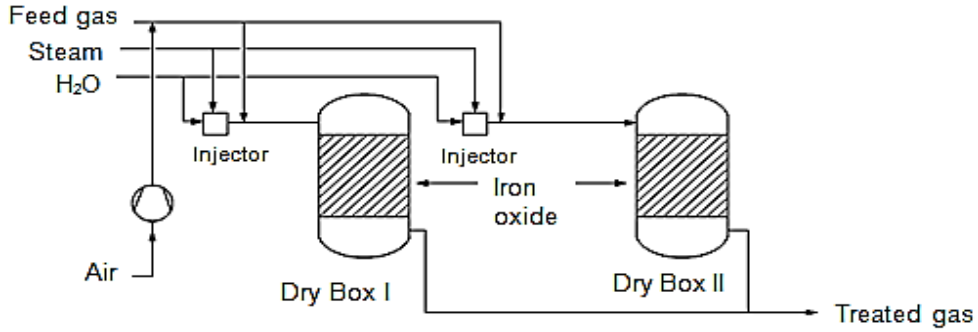

Figure 1-3 Process flow scheme of dry box H_2S removal technology (Kohl, A. L. et al., 1997)

The Fe_2O_3 in the beds reacts exothermically with H_2S to iron sulfide (Fe_2S_3) at low to moderate pressures up to 83 bara and temperatures around 35 °C (see Eq.1-4).These kinds of processes are usually operated batch-wise i.e. when the loading capacity of one dry box is reached, it has to be regenerated (or finally replaced).The formed Fe_2S_3 can partly be regenerated to sulfur (S) and Fe_2O_3 by oxidation with air at room temperature and pressures of 1.01325 bar, referring Eq.1-5.

Chemical leaching or washing beds with high pressure water are considered as feasible treatment methods to subsequently remove the formed elemental sulfur from beds (Wang, H. D. et al., 2008).

$$Fe_2O_{3(s)} + 3H_2S_{(g)} \rightarrow Fe_2S_{3(s)} + 3H_2O_{(aq)} \quad \text{(Eq.1-4)}$$

$$Fe_2S_{3(s)} + 3/2\ O_{2(g)} \rightarrow 3S_{(s)} + Fe_2O_{3(s)} \quad \text{(Eq.1-5)}$$

Dry box iron oxide technique (e.g. Sulfa-Treat® etc.) is widely used for removing H_2S from small volumes of low sour natural gas (usually less than 10 Nm^3/h containing 10 to 1,000 ppmv H_2S (Anerousis, J. P. et al., 1984)). However, utilization of this technology for treating larger volumes or concentrations of sour gases is reportedly not economic, since its design requires slow gas velocities due to disadvantageous sorption kinetics. Therefore, large gas flow rates even with low H_2S concentrations will necessitate large vessels and thus result in large footprint. Moreover, requirement of bed regeneration and/or of substitution after a certain number of regeneration steps lead to operational difficulties and standstill. Additional bottlenecks are high labor costs and production of low quality sulfur. At last, the continuous injection of sufficient water or steam is very important in order to prevent the ignition of the wooden chips by the exothermic reaction.

The abovementioned drawbacks of the iron oxide employing dry box processes and the limitations of the Claus technology as well as disadvantageous features of other common technologies listed in **Table 1-5** have enforced the development of liquid redox processes for removal of H_2S which convert the H_2S direct into pure elemental sulfur in a liquid phase. As a rule of thumb, dry box technique is applied in systems with less than 200 kg/day of sulfur recovery, while Amine-Claus unit with TGT technology is employed at ranges greater than 25 LTPD of sulfur (but only feasible for H_2S-concentrations higher than 40 mol%) (Merichem Company, 2015). The liquid redox technology is recommended for any sour gas capacity in between and low, moderate as well as high sour gases (see **Table 1-3**). The following section gives an overview on the principals of the liquid redox technique.

1.4.3.2 Liquid redox technique

1.4.3.2.1 Basic chemistry and overview

The basic chemistry of the liquid phase reduction-oxidation (i.e. the liquid redox) is derived from a cyclic reduction and oxidation of a redox couple (Nagl, G., 2001). This comprises two basic simultaneous reactions: where the gaseous H_2S is first physically absorbed in an appropriate aqueous absorbent solution containing an oxidizing agent (Ox/Red) (see Eq.1-6), which, in a second step, is capable of rapidly oxidizing aqueous H_2S to solid elemental sulfur (see Eq.1-7). Then, the chelated oxidizing agent is regenerated back to its active form by the reaction Eq.1-8, typically using oxygen from air.

$$H_2S_{(g)} \rightarrow H_2S_{(aq)} \quad \text{(Eq.1-6)}$$

$$2Ox_{(aq)} + H_2S_{(aq)} \rightarrow S_{(s)} + 2Red^-_{(aq)} + 2H^+_{(aq)} \quad \text{(Eq.1-7)}$$

$$2Red^-_{(aq)} + 1/2\ O_{2(aq)} + 2H^+_{(aq)} \rightarrow 2Ox_{(aq)} + H_2O_{(aq)} \quad \text{(Eq.1-8)}$$

In the equations above, the terms Ox and Red^- denote the redox couple - the oxidized (active) and the reduced (inactive) form of the oxidizing component, respectively.bThe sulfur product is thereafter removed by an appropriate filtration method. Heretofore, as redox couples, arsenic (As^V/As^{III}), vanadium (V^V/V^{IV}), cobalt (Co^{III}/Co^{II}) and iron (Fe^{III}/Fe^{II}) have been applied in such processes. During the 20th century, over 25 different technologies have been developed; however,

most of these have not been promoted due to very little commercial prospects of safety reasons (especially arsenic). Although all of the liquid redox processes utilize the same basic principle as mentioned above, they can be distinguished and classified by the chemical nature of the absorbent solution, comprising the absorbent itself and the redox couple (see **Table 1-6**).

Table 1-6 Categorization of liquid-redox processes depending on the absorbent solution (Kohl A. L., 1997)

Absorbent solution	Redox couple	Process name
Polythionate solutions	$(S_xO_6^{2-})/(S_{x-1}O_3^{2-})$	Feld process, Koppers C.A.S.
Iron-cyanide solutions	Fe^{III}/ Fe^{II}	Fischer, Staatsmijnen-Otto, Autopurification
Sodium carbonate and iron oxide solutions	Fe^{III}/ Fe^{II}	Ferrox, Burkheiser, Manchester, Gluud
Thioarsenates and arsenites solution	As^{V}/ As^{III}	Thylox, Giammarco-Vetrocoke
Sodium carbonate or vanadate of anthraquinone disulfonic acid (ADA) or aqueous ammonia solutions with hydroquinone	V^{V}/ V^{IV}	Quinone: Perox, Takahax Quinone + metal salt: Stretford, Hiperion, Vanadate: Sulfolin, Unisulf
Chelated iron solutions	Fe^{III}/ Fe^{II}	C.I.P., Cataban, LO-CAT®, Sulfint, SulFerox®

The processes based on polythionate ($S_xO_6^{2-}$), iron oxide (Fe_2O_3) and iron-cyanide ($[Fe(CN)_6]^{3-}$) solutions are primarily of historical interest. Although, all of them showed sulfur removal efficiencies in a range of 85 to 100 %, only iron oxide processes have been used commercially, since chemical nature of polythionate and cyanide solutions led to non-soluble salt formation (Lundtorp, 2001). The thioarsenate processes were mainly used to purify coke-oven gas. Another group of liquid redox processes involve technologies where quinone and/or a mixture of them with vanadium salts are employed. This category can be divided into three subgroups regarding the composition of the washing solution:

1. Perox and the Takahax process which employ only quinones as catalytic agent.
2. Stretford and the Hiperion process i.e. both using a combination of quinone compounds and metal salts. The Stretford process reached remarkable success and was utilized commercially (Holmes, 1974).
3. The third subgroup can be characterized by the use of vanadium salts in a mixture with other organic additives than quinones. Examples for this type of processes are the Unisulf and the Sulfolin which are similar to the Stretford process except for the use of an organic nitrogen vanadium promoter instead of a quinone compound to reduce side-reactions caused by hydrogen peroxide generation.

To sum up, the liquid redox technologies employing vanadium (V^{V}/V^{IV}) and arsenic (As^{V}/As^{III}) redox couples showed a high potential for the removal of H_2S from gas streams but their toxicity and thus health, safety and environmental issues (HSE) lead to their abandonment. Avoiding this problem, consequently processes with iron (Fe^{III}/Fe^{II}) as catalytic agent have been developed and promoted.

1.4.3.2.2 State of the art - Chelated iron solutions for liquid redox technique

The evolution of the use of iron as a regenerable oxidant for the conversion of H_2S to S is traced from inception as solid phase dry box processes employing Fe_2O_3, through aqueous, alkaline Fe_2O_3 suspensions to aqueous, homogeneous redox catalysts using salts of poly aminopolycarboxylated (APC) chelated iron.

In principle, the basic chemistry of the iron based liquid redox technique is similar to the previously mentioned processes (Heguy, 2003). The solvent system (also called as “liquid phase”, “liquid system” and “solution”) in these technologies is assembled of the following primary components:

- **Absorbent** in aqueous solution, responsible mainly for providing the required alkalinity to enable the transition of the H_2S from the gas to the liquid phase
- **Catalytic agent** (also called “oxidizing agent” or “redox couple”), responsible for the conversion of the H_2S to elemental sulfur
- **Chelating agent** (also called “ligand” or “chelator”), responsible for keeping the catalytic agent in solution and preventing it from precipitation.

Besides that, the solvent system can also contain additives (i.e. secondary components; see section 2.2). It must be noted that, in the scope of this study, chelating agent and catalytic agent form a complex will be called as “chelate” or - in case of iron as catalytic agent as “chelated-iron”.

As absorbents, mainly aqueous alkali components, for example potassium hydroxide (KOH), are used. Iron has become the standard oxidizing agent due to its non-hazardous features and high reactivity towards H_2S. Since the solubility of iron in aqueous solutions is very low, various chelating agents (ligands) have been used to form water-soluble complexes of it. Examples of chelating agents mostly applied are alkali or ammonium salts of (among others) hydroxyl ethyl ethylene diamine tri acetic acid (HEDTA), ethylene diamine tetra acetic acid (EDTA), nitrilo tri acetic acid (NTA). Their main purpose is to prevent the precipitation of the respective metal reagent (Welch, K. et al., 2002). Commercially important processes of this type like the Sulfint, LO-CAT® and SulFerox® will be presented in further sections of this work in detail.

The chemistry of the different iron chelate based liquid redox processes is comparable to each other. In the first step, the H_2S is absorbed from the gas into the mildly alkaline liquid phase, in which the ferric ions (Fe^{3+}) complexed with a ligand i.e. chelating agent (Lig) have been dissolved (Nagl, G., 2001). Subsequently, the elemental sulfur (S^0) is formed by the reduction of the ferric (Fe^{III}) to ferrous (Fe^{II}) ions[2].

$$H_2S_{(aq)} + 2(Fe)^{3+} \bullet Lig_{(aq)} \rightarrow S^0_{(s)} + 2(Fe)^{2+} \bullet Lig_{(aq)} + 2H^+{}_{(aq)} \qquad \text{(Eq.1-9)}$$

Regeneration is performed utilizing oxygen from air[2]:

$$2(Fe)^{2+} \bullet Lig_{(aq)} + 1/2O_{2(aq)} + 2H^+{}_{(aq)} \rightarrow 2(Fe)^{3+} \bullet Lig_{(aq)} + H_2O \qquad \text{(Eq.1-10)}$$

All of the processes employed so far have their own niche, benefits or drawbacks, and several disadvantages can be improved. The conventional absorbent solutions of liquid redox processes have a simple formulation - water based alkaline solution containing a chelated metal catalyst. This makes them only feasible for low H_2S loads as well as low CO_2 concentrations due to the sensitivity of the process towards changes of the acidic gas concentration of the sour feed gas and in turn the solution-pH (Kohl, A. L. et al., 1997). The applied solutions reportedly have a very low capacity for dissolved sulfides resulting in large liquid circulation rates, equipment size and hence high power consumption. It was also realized that all these organic chelating compounds are only suitable above a pH minimum (Wubs, 1994). Furthermore, their thermodynamic stabilizing effect on metal catalyst decreases above a certain pH maximum because the bond between the chelator and the metal (Fe^{III}) is weakened, which leads to undesired precipitation of ferric hydroxide ($Fe(OH)_3$).

[2] The charge of the ligand is omitted for reasons of clarity.

Selection of the appropriate absorbent and the chelating agent is a critical issue for every application since their performance depends on several factors such as the solubility of the chelator in the solvent, the degradation rate of the chelating agent as well as the cost of the chelating agent and the solvent. On the whole, alternative liquid systems, which are feasible for highly variable gas loads as well as H_2S and CO_2 contents and for more robust operability, would be beneficial and have a high commercial interest, as presented in the following section.

1.5 Liquid redox technique applying amino acid salts (AAS) - Siemens sour gas treatment process

As it was given in **Table 1-5**, both liquid absorbents and solid adsorbents are used for the removal of acidic gases (mainly H_2S and CO_2) from sour gas streams. Nevertheless, technologies employing liquid absorbents have been mostly preferred mainly due to their loading capacity, flexibility regarding the presence of other contaminants than H_2S and/or CO_2 in the gas, high purity of the treated gas and ease of regeneration. Alkanolamines are commonly utilized as liquid absorbents in the amine unit of Claus technology, but they feature high oxygen degradation potential, and thus, cannot be used in liquid redox processes because of the presence of oxygen in the regeneration step. Furthermore, they feature a negligible vapor pressure. Due to their molecular structure, the amino acid salts (AAS) show better resistance to oxidation and thermal degradation compared to alkanolamines, so that undesired absorbent loss and emissions of volatile degradation products can be avoided. In addition, their reactivity with CO_2 is rather high and thus comparable to aqueous alkanolamines of related classes (Hook, 1997). Alkaline salts of amino acids (commercial names Alkacid-DIK and Alkacid-M) have been already proposed for absorbing either H_2S or CO_2, or for absorbing both simultaneously (Kohl, A. L. et al., 1997) (refer to **Table 1-5**). In both Alkacid-technologies, acidic gases are removed in absorption-stripping cycles, whereas supplementary units are required for e.g. the conversion of H_2S into sulfur or handling of the stripped CO_2. Furthermore, there is a commercially available Siemens-CO_2 capture process, PostCap^{TM}, which employs an AAS as scrubbing solution (Reichl, A. et al., 2014). The process is beneficial due to the near-zero vapor pressure of the AAS, non-toxic ionic components and low energy demand for solvent regeneration. Reported favorable features of Alkacid technologies as well as the positive experiences, gained with the Siemens PostCap^{TM} process, put alkaline salts of amino acids into a class of absorbents of potential commercial interest for sour gas treatment. Therefore, adding a chelated catalytic metal agent to an aqueous AAS absorbent solution (see **Figure 1-4**) makes such systems suitable for the direct chemical conversion of H_2S to elemental sulfur in liquid phase by liquid redox method and poses an attractive alternative to conventional liquid redox absorbent systems as well as to alkanolamines.

Figure 1-4 Schematic structure of the solvent system applied in Siemens liquid redox technology

After reviewing potentials and limitations of common gas sweetening processes and outlying the properties of the solvent system of the Siemens sour gas treatment process, the targets set for the scope of this study will be highlighted in the following section.

1.6 Objectives of the study

Siemens AG has developed a proprietary liquid redox technology which is mainly intended to be designed as a sour gas treatment plant integrated into combined and/or open cycle power plants. The driving force to develop such a new process is to provide a way to ensure high H_2S removal capacity per unit circulation, low absorbent and chelating agent degradation rate as well as a simple and compact process design. This technology uses an aqueous AAS solution as absorbent containing a chelated metal as oxidizing agent (see **Figure 1-4**). The presence of the AAS supplies the required alkalinity to the washing medium which improves absorption rates of H_2S and also of CO_2, if the latter is also contained in the gas. Initial laboratory studies showed that the utilization of AAS in liquid redox technology is very feasible. First cost evaluations based on operation parameters of a test rig revealed that significant fractions of the total expenditures (TOTEX) of the technology are the costs related to properties of the employed solvent system (Sönmez, 2014). This indicates that the development of alternative, appropriate solvent systems is a central part of improving and optimizing the applied H_2S removal method based on liquid redox technique. The targets of this PhD-thesis are focused, therefore, on features of solvent systems and their effects on process design, performance, operability and economics. The identification of cost driving factors related to properties of applied solvent systems enables design flexibility and reduction in total expenditures (TOTEX) by improvements in these properties. In addition, degradability could prevent otherwise promising systems from being utilized at energetically beneficial conditions. Therefore, thorough investigations on the behavior of potential candidates for various AAS based solvent systems have to be executed with special focus on (among others) absorption and regeneration efficiency as well as on stability in order to characterize the suitability of them at industrial scale under corresponding operation conditions. Test runs are to be performed by piloting the technique in a research prototype test rig in lab scale.

Chapter 2 gives a review on the features of the state of the art liquid redox processes with the properties of heretofore commercially employed solvent systems. In addition to design considerations of representative processes, application fields of each technology, key process variables those influence the process performance and cost driving factors will be discussed in detail with special focus on their relation to solvent properties.

Chapter 3 describes a holistic approach in solvent system development i.e. chelating agent and absorbent selection to successfully address past and current operating issues with the aim to enforce improvements of the solvent system properties. Besides these, absorbent and chelator screening tests on oxidative and thermal stability will be presented to identify promising constituents, and thus, formulations of several solvent systems for the subsequent benchmarking experiments.

In **Chapter 4**, different liquid systems will be formulated based on experimental findings in the previous chapter. By benchmarking these, impacts of solution properties mainly on the performance, the key design operation parameters and the quality of the obtained solid product (among others) will be highlighted. Identification of these impacts will help to optimize solvent system formulation and describe required modifications on system design with respect to the applied absorbents and/or chelators. Thus, a profound understanding about chelated-iron containing AAS as new liquid redox solutions will be gained.

Chapter 5 focuses on the stability of solvent systems, since the solvent degradation can lead to high chemical make-up costs up to the degree of non-economical operation of the process. In order to emphasize this, a brief literature review on possible reaction pathways leading to degradation as well as earlier studies on the ligand decomposition will be presented. Subsequently, the experimental investigations will be described and discussed. Altogether, with these studies it is intended to gain a better understanding of the catalyst degradation in the applied solutions and to reduce it by the use of appropriate additives and by adjusting the operating conditions.

Chapter 6 gives an overview on the economic studies of the evaluated process with the selected formulations based on experimental findings from a lab scale test rig. The main purpose of this chapter is to evaluate the economic feasibility of the selected formulations when they are applied in a demo plant in semi-industrial scale by analyzing their impact on the resulting levelized cost of electricity (LCoE, ct/kWh). Identifiying the main drivers of the LCoE and analyzing the sensitivity of the LCoE to these will enable to examine the further technical and economic optimization potentials of the technology during the piloting (pre-industrial) phase. Therefore, the proposals done as results of this chapter will help to take an optimal transition step between lab scale to pilot scale.

In **Chapter 7**, a summary of the obtained results is presented together with conclusions and recommendations for future applications.

The results will lead to a better understanding of the liquid redox technology with AAS as absorbents and will give answers to the so far unknown techno-economic and environmental impacts. Important goals are the reduction of the solvent pump around ratio, the required air for regeneration and the chemical make-up in order to make the process more economical and more attractive -also for relatively high fractions of acidic components in the gas- due to smaller equipment sizes and lower operating costs. With liquid redox as an economical treatment method, the utilization of untapped sour gas reserves will contribute to supply the regional energy demand in the vicinity of the gas wells. Reduced plant footprint will even enable the direct conversion of the treated sour gas into electricity especially on the offshore drilling platforms.

2 STATE OF THE ART LIQUID REDOX PROCESSES WITH CHELATED IRON

As it was mentioned in section 1.4.3.2.2, iron-chelate systems have been preferred over the other liquid redox technologies and actively marketed primarily because of the non-hazardous character of their scrubbing solutions. In most of these, the liquid phase is mildly alkaline (pH 7 to 8.5) while the iron is held in solution by ligands and serves as oxidizing agent (Kohl, A. L. et al., 1997). Although the basic chemistry of all iron-chelate systems is comparable (see section 1.4.3.2), several technological differences exist resulting from the applied solvent system. The following sections will give an overview on the design, operational principles, features or bottlenecks of conventional chelated-iron liquid redox processes and will thus provide a basis for the comparison of them. Reviewing and understanding the process configurations and specific characteristics of these technologies will also help to make optimization proposals of the evaluated process in the later chapters of this study (refering the chapter 4, chapter 5 and chapter 6).

2.1 Configurations of unit operations

Iron-chelate employing liquid redox systems comprise three basic unit operations:

- absorption & subsequent oxidation of the H_2S
- regeneration of the operating solution
- separation of produced sulfur.

A large variety of design options has been reported for these units depending on the purpose of the application. **Figure 2-1** gives an overview of the preferably used equipment and the process flow. In the very most cases "H_2S Absorption & Oxidation" is first followed by "Catalyst Regeneration", before "Sulfur Separation" takes place. However, there are also processes (e.g. Sulfint HP, see **Table 2-6**) where sulfur is withdrawn upstream of the regeneration.

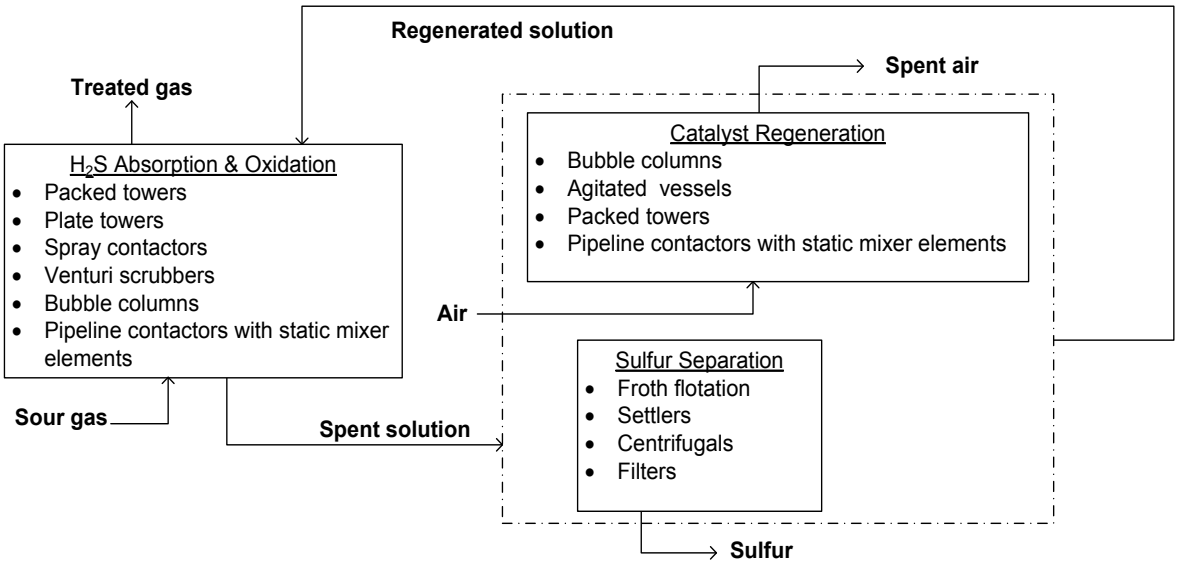

Figure 2-1 Simplified process flow scheme of conventional chelated-iron liquid redox units with options for equipment (Hardison & McManus, 1987)

Units for "H_2S Absorption & Oxidation" and "Catalyst Regeneration" can be summarized as gas-liquid contactors. The following subsection gives a combined overview on the application of gas-liquid-contactors in absorption processes in general and in liquid redox technique in particular.

2.1.1 Gas-liquid contactors for liquid redox processes

The gas-liquid contactors used industrially can be generally divided into two categories depending on the phase which is dispersed (Fair, J. R. et al., 1997). In the first group, gas (G) is the

continuous phase in which the liquid (L) is dispersed. In the other group which can also be called sparged columns, the gas (G) is dispersed into the liquid (L) phase. Both types can be operated in counter, co or cross-current and also as up or downstream modules. Since systems containing solids are particularly prone to fouling (e.g. sulfur fouling in liquid redox technique), gas dispersion into liquid has been the method of choice. In liquid redox absorbers, the dissolved H_2S is converted in-situ to elemental sulfur by oxidation with the active form of chelated iron (Fe^{3+}•Lig) whereas the reduced catalyst (Fe^{2+}•Lig) is oxidized back to its active form by air in a regenerator. These two successive reactions are referred to Eq.1-9[2] and Eq.1-10[2], respectively. Both reactors have been configured to be operated under a wide variety of conditions which are presented in **Table 2-1** (Wubs, 1994).

Table 2-1 Range of operation conditions of liquid-redox contactors (Wubs, 1994)

Operation parameter	Absorber	Regenerator
Temperature,°C	20-60	20-60
Pressure, bar (gauge)	1-100	0.5-4
H_2S content of the feed gas, vol%	0.01-25	-
CO_2 content of the feed gas, vol%	0-99	-
Fe^{3+}/H_2S, mol/mol	2-8	-
O_2/Fe^{2+}, mol/mol	-	0.3-10
Ligand/metal ratio, mol/mol	1-2	
Residence time, sec	2-120	2-2,400

The design of liquid redox reactors depends mainly on the volumetric gas flow rate, the available pressure drop (ΔP), the required H_2S removal efficiency as well as on the physical and chemical properties of the applied solvent system (Smith R. , 2005). An appropriate configuration will provide enough mass transfer surface area to enable transition between phases and will feature liquid sections (static pressure drop) which can be overcome with a minimum expenditure of energy. An optimum between capital investment and operational expenditure must be the goal. The following section gives examples of industrially used liquid redox absorbers, their features or bottlenecks.

2.1.1.1 Absorbers

The absorption and subsequent oxidation of the H_2S in a liquid containing chelated-iron is reportedly irreversible due to instantaneous reaction in the liquid phase (Kohl, A. L. et al., 1997). The driving force for the absorption of H_2S into the liquid is the higher partial pressure of it in the feed gas. Theoretically, the concentration of H_2S in the treated gas can be effectively reduced to almost zero, if sufficient catalyst, mass transfer area and residence time are provided by applying an appropriate gas-liquid contactor. The design of choice is normally the approach that leads to the most convenient and economical method of obtaining the required number of transfer units (NTU_{req}) to reduce an available inlet concentration of H_2S ($c[H_2S]_{in}$) to the desired outlet concentration of it ($c[H_2S]_{out}$) at the top of absorber (Vancini & R., 1985). As expressed in Eq.2-1, the NTU_{req} is the natural logarithm of the ratio between inlet and outlet gas concentrations.

$$\mathrm{NTU_{req}} = \ln\left(\frac{\mathrm{c[H_2S]_{in}}}{\mathrm{c[H_2S]_{out}}}\right) \qquad \text{(Eq.2-1)}$$

Generalized figures for the NTUs attainable with the four types of contactors are illustrated in **Table 2-2** along with other typical design data obtained from ((Smith R. , 2005), (Kohl, A. L. et al., 1997), (Vancini & R., 1985), (Strigle, 1994)).

Table 2-2 Typical design data of liquid redox absorbers ((Smith, 2005), (Kohl, A. L. et al., 1997), (Vancini, C. A., and Lari R., 1985), (Strigle, 1994))

Absorber type	**Packed columns**	**Plate columns**	**Spray columns**	**Venturi scrubbers**
∆P (mbar)	2-25	3-50	4-10	30-200
L/G (vol/vol)	0.05-5	0.01-10	1-20	0.5-5
Phase state	L distributed over G by internals	L distributed over G by internals	L dispersed in G	L dispersed in G
Interface generation	Co, counter or cross-current	Counter-current	Counter-current	Co-current
υ(m/s)	2-2.5	1-2	3-3.5	10
F-factor ($Pa^{0,5}$)	1-3	0.8-2	2-4	n.a.
Attainable NTUs	>10	>10	1-5	1-4
Configurations	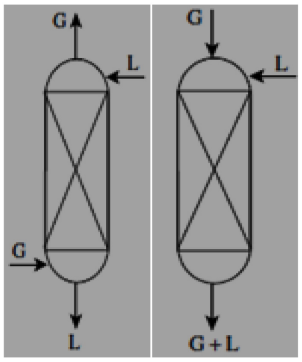	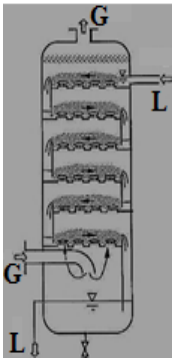	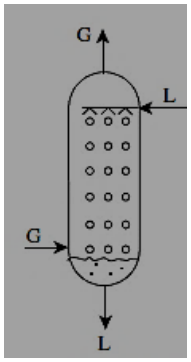	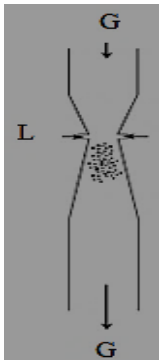

Various types of contactors used in liquid redox technique were listed in the box for absorption unit in **Figure 2-1** (Hardison & McManus, 1987) each has their own characteristic (refer to **Table 2-2**), advantages and drawbacks depending on the application case which will be highlighted as follows:

In applications in which high removal efficiency of H_2S or an NTU greater than 3 is required (especially for low sour gases refer to **Table 1-3**), **packed towers** are preferred as they feature primarily high mass transfer efficiencies (Strigle, 1994). In addition, they are well-suited when the $c[H_2S]_{in}$ is relatively low, since packings are prone to fouling, in cases where the circulating solution has high sulfur loadings. In general, co-current flow mode (shown at the right hand side in **Table 2-2**) will give a poorer performance than the counter-current arrangement (at left). However, co-current flow is claimed to be preferable if the flow of gas is much greater than the flow of liquid due to the relatively high mass transfer coefficients in the gas phase (Ludwig, 1997). Reportedly, at most part of these columns, the mass transfer velocity for the H_2S is limited in gas phase whereas the mass transfer velocity for the CO_2 is limited in the liquid phase. Thus, the co-current type features reportedly a higher selectivity for H_2S (Satterfield, 1975). Another design parameter, commonly employed to characterize the gas loading, is the gas loading factor, F, which is the product of the superficial gas velocity (υ) and the square root of the gas density (ρ_g), referring Eq.2-2 (Ludwig, 1997).

$$F = \upsilon\sqrt{\rho_g} \qquad \text{(Eq.2-2)}$$

The range for the tolerable F-factor depends on the type and size of the applied packing and is a critical design parameter with respect to operation safety and efficiency. If the F-factor is increased, a point is eventually reached where the maldistribution of the liquid occurs and the liquid hold-up begins to increase significantly. This is called as loading point. Raising the gas flow rate further will lead to a condition where the liquid begins to fill the whole tower causing an intense elevation of the pressure drop up to the so-called flooding with significant decrease of the

mass transfer efficiency. As indicated in **Table 2-2**, recommended gas loading factors for a packed column are between 1 to 3 $Pa^{0,5}$ in order to ensure safe operation.

Plate towers can be utilized when high removal efficiency even at moderate H_2S concentrations is required (see **Table 1-3**). Reportedly the NTU per tray is equivalent to approx. 0.6 (Kohl, A. L. et al., 1997). They offer the advantage that the height of a mass transfer unit is independent of the absorbent flow rate (Fair, J. R. et al., 1997). This permits efficient operation even at very low liquid-to-gas (L/G) ratios (refer **Table 2-2**) and bulk removal of the H_2S. Drawbacks of plate columns are their relatively high ΔP, their complex construction and sensitivity to fouling. In addition, they are unsuitable for the treatment of fluctuating gas flows as their absorption capacity declines drastically with small gas flow rates.

Spray contactors can be installed ahead or instead of packed columns as they feature low pressure drop and fouling tendency (Smith R. , 2005). However, they are limited to applications with low requirements towards mass transfer. They are operated in counter-current flow mode. In this type of equipment, the absence of internals, which would provide contact area, generates small specific mass transfer areas, which in turn leads to increased contactor size (i.e. height and diameter). Although this is a drawback with respect to CAPEX and footprint, it results in longer lifetime of falling drops along with lower coalescence of them and hence, a longer residence time is provided. However, ensuring even gas distribution by an appropriate geometry is an essential design feature because of the low ΔP in the column. In addition, entrainment of fine droplets caused by liquid spraying is reported to be a specific problem for spray contactors which may necessitate use of a demister which should be leached with fresh water to prevent deposits.

Likewise spray contactors, **venturi scrubbers** are insensitive to blocking up. However, contrary to spray contactors, the interfacial area is provided co-currently. (Rothery, 1986). They are used in cases where the required NTU is between 1.5 and 2.5 (Kohl, A. L. et al., 1997) and bulk removal of H_2S from high and/or ultra-high sour gases (refer **Table 1-3**) is desired. For example in a jet type venturi scrubber, the mass transfer between gas and liquid occurs across the boundary layer on the surface of the droplets produced by the spray nozzle. As shown in **Table 2-2**, the liquid is introduced through a single nozzle at a pressure sufficiently high to convey the gas through the throat section of the venturi without significant ΔP, which leads to high absorption efficiencies (Smith R. , 2005). However, they feature low turndown ratios unless the nozzle is changed. Depending on the required final gas purity, several scrubbers in series may be needed to provide sufficient gas liquid mass transfer.

Bubble columns or pipeline contactors are usually the absorber configurations of choice for liquid-redox applications, since they feature high turndown ratios for treatment of low to ultra-high sour gases (Fair, J. R. et al., 1997). They can be applied both as liquid redox absorbers or regenerators due their broad operating range and low investment cost. However, installment of an appropriate gas distributor is essential to an efficient operation of these contactors. This will be discussed in the following part of the work.

2.1.1.2 Regenerators

In general, the processes in the regenerator (absorption of O_2 in the aqueous scrubbing solutions and subsequent regeneration of the reduced complex (Fe^{2+}•Lig)) are more difficult than those in the absorber (absorption of H_2S and conversion of it to elemental sulfur). Therefore, they require longer residence times (Wubs, 1994). Wubs stated that the regeneration reaction rate for any given ligand increases with the Fe^{2+} concentration and the oxygen partial pressure in the solution. However, the latter reportedly promotes the oxidative decomposition of chelators, thus necessitating chemical make-up which results in higher OPEX. Consequently, the configuration of a regeneration unit must be such that the mass transfer rate of oxygen is enhanced but the oxidative decomposition of chelating agent is minimized. As shown in **Figure 2-1**, the variety in regenerator design is therefore less numerous compared to the H_2S absorbers.

Usually sparged towers such as bubble columns, agitated vessels and pipeline contactors with in-line static mixing elements and to a minor extent packed towers were used (Hardison & McManus, 1987). General characteristics of these units are given in **Table 2-3** (Fair, J. R. et al., 1997).

Table 2-3 Design data of typical liquid redox regenerators (Fair, J. R. et al., 1997) and (Smith R. , 2005)

Regenerator type	**Bubble columns**	**Agitated vessels**	**Pipeline contactors with static mixers**
∆P (mbar)	70-700		20-50 *per element
NTU	1-10		0.05-10
Phase state	G dispersed in L		G dispersed in L
Interface generation	Co or counter-current		Co-current
υ (m/s)	0.03-0.3		0.8-5
μ (cP)	1-62	5.10^3-20.10^3	0.4-19.50
Configurations	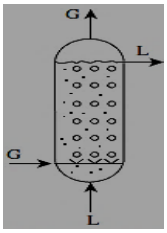	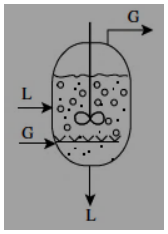	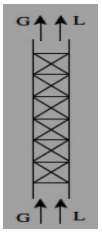

Note: Bubble columns and pipeline contactors are also frequently used as liquid-redox absorbers

Pipeline contactors can be used both for absorber and regenerator units. They are applied for the dispersion of gases in liquids usually in co-current flow, performed either in vertical vessels upwards or downwards or in horizontal vessels (Smith R. , 2005). However, with flow in an empty pipe, adequate radial mixing can in most cases only be achieved by an impractical length of pipe. Inserting a static mixer significantly accelerates the mixing and subsequent reaction. This technique is desirable wherever a continuous, inexpensive and fast operation is required. Since there are no moving parts in the static mixer, it is basically maintenance-free and can be installed as easy as any piece of pipe. Design factors for selection of the type of static mixer include allowable ∆P, heating/cooling requirements, residence time or flow rates, length of piping, and liquid viscosity. (Grozs-Röll, 1982). Pipeline contactors with an inline static mixing element can be used with liquids of a wide range of viscosities (e.g. 0.4 to 19.50 cP) even at high pressures due to their mechanical benefits i.e. requirement of a thinner wall than a large-diameter column.

In contrary to pipeline contactors, **bubble columns** necessitate the construction of more pipelines in parallel to achieve the same performance that would be achieved by a large-diameter column. In addition, they tend to have lower performance and higher ∆P characteristics than packed towers. However, the simple arrangement features two advantages compared to a packed bed. Firstly, the liquid hold-up per reactor volume is higher, which provides longer residence time for a slow reaction at a given liquid flowrate. Secondly, bubble columns are very resistant to sulfur plugging. The key variables that affect the design of gas dispersed liquid-redox regenerators i.e. the dynamics of bubbles and flow as well as their behavior during their residence time in the contactor are (Kohl, A. L. et al., 1997):
(1) geometrical aspects of the gas sparger (influencing the required respectively the possible air flow)
(2) chemical and physical properties of the applied solvent (influencing the required liquid volume).
These parameters have to be determined by experimental methods. The required air flow is reportedly directly proportional to the amount of sulfur being produced and inversely proportional to the useful height of liquid in the column, and it also depends on the effectiveness of air-liquid contact.

The operation principal and the design characteristics of bubble columns and **agitated vessels** are similar except for the presence of a mechanical stirring device in agitated vessels as presented in **Table 2-3** (Fair, J. R. et al., 1997). The choice between a bubble column and an agitated vessel depends primarily on the physical and ionic character of the liquid (viscosity, density, surface tension and corrosiveness) as well as on the rate of the chemical reaction (Smith R. , 2005). A disadvantage of bubble columns compared to agitated vessels is that they will be ineffective if the viscosity in the liquid is beyond a certain limit (e.g. for dynamic viscosities μ>>100 cP) because mixing in such systems is comparably slow due to low diffusivity. If the liquid is significantly viscous, agitated vessels are preferred since the agitator both enforces the gas to be dispersed as small bubbles and the liquid to be circulated. Thus, a good contact between the gas and the liquid is maintained. The shape of these units may be flat, dished, or conical, or specially contoured, depending on factors such as ease of emptying or the need to suspend solids. Reportedly, if the overall reaction rate is five times greater than the mass transfer rate in a simple bubble column, a mechanical agitator will be beneficial. However, due to the fact that H_2S is a very corrosive gas, the stirrer and the shaft in an agitated vessel have to be made from high-grade material which results increase of CAPEX. Higher OPEX for agitated vessels are due to the consumption of electrical power and more effort for maintenance. (Fair, J. R. et al., 1997). Another disadvantage of rotating equipment is the higher risk of process interruptions. Therefore, it is advantageous to improve the mass transfer in a simple bubble column by a modification of the set-up and thus overcome the necessity of a mechanical stirring. An effective dispersion of the gas into the liquid phase leads to a high mass transfer, and smaller size of the bubbles enlarges the interface. The mass transfer rate increases proportionally to the interfacial area of the two phases. Thus, the device for dispersion of the gas is of particular interest. There are two basic types of **gas dispersion devices** (see **Figure 2-2**): circular perforated spargers (in two versions: perforated pipe or porous septum) and eductor mixers.

Perforated pipe Porous septum Eductor mixer

Figure 2-2 Different types of gas dispersion devices (Fair, J. R. et al., 1997)

Besides achieving of efficient gas dispersion, also maintaining the homogene flow regimes is important to sustain stable operation. Reportedly, bubble columns and agitated vessels can be operated stable with superficial gas velocities, u, of 0.03 to 0.3 m/s (see **Table 2-3**). Within this range, different flow regimes in the column occur, as shown in **Figure 2-4**.

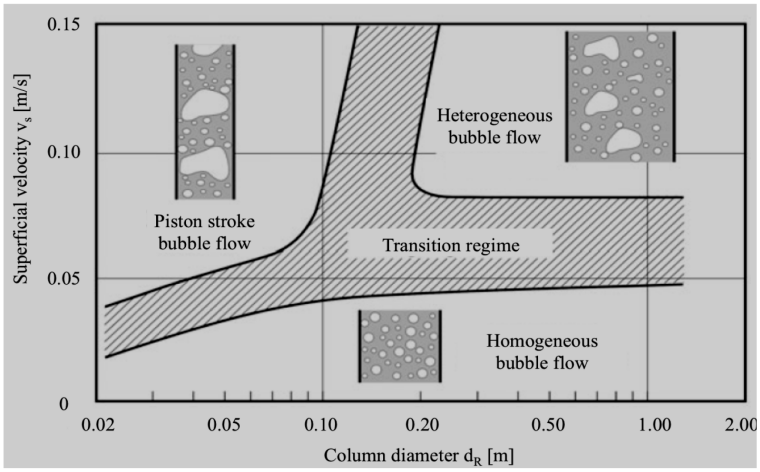

Figure 2-3 Flow patterns in bubble columns in correlation with the superficial gas velocity (without application of an eductor mixer) (Fair, J. R. et al., 1997)

In a homogeneous regime (refer to **Figure 2-4** for υ < 0.045 to 0.060 m/s), porous septa will often give considerably higher overall mass-transfer coefficients than perforated plates or pipes because of the formation of tiny bubbles that do not coalesce. In a turbulent regime (refer to **Figure 2-4** for υ > 0.045 to 0.060 m/s), inexpensive perforated pipe spargers can be used (Fair, J. R. et al., 1997). At higher gas velocities (corresponding to the heterogeneous regime), eductor mixers are recommended, where the gas is dispersed through the nozzles. Since they provide a very high mass-transfer coefficient between the oxygen and the liquid, they have been preferably applied in liquid redox processes. Another advantage of this kind of surface aerator is that it promotes bubbles upward through the regenerator to accomplish the sulfur flotation which will be discussed in the following section, together with other sulfur separation methods (Vancini & R., 1985).

2.1.2 Sulfur separation units for liquid redox processes

The desired sulfur quality, the complexity of the set-up and the sulfur removal efficiency are crucial criteria for the design of the sulfur removal process. Besides that, catalyst losses vary with the sulfur removal method. That is why the selection of the proper method also enables to reduce OPEX resulted from compensation of chemicals due to mechanical catalyst loss. **Figure 2-4** gives an overview on the applied sulfur separation techniques and equipment in the history of liquid redox processes (Smith R. , 2005) and (Quinlan, 1991). Whereas froth flotators and settlers can either be separate pieces of equipment, or this process can be realized simultaneously with regeneration in one contactor, centrifuges and filters are always separate downstream units. Usually sulfur removal is realized in several consecutive steps, especially for stringent quality requirements. If high sulfur purity must be reached, the methods displayed in **Figure 2-4** have to be followed by e.g. a melting step.

Froth flotation is a gravity separation process that exploits differences in the surface properties of particles. The air not only encompasses the sulfur generation by oxygen, but also acts as a flotation agent for the sulfur, which then collects at the surface of the solution as froth. There are two types of froth flotators (Foxall, 1986): In a **conventional flotation cell (Figure 2-4a)**, gas bubbles are injected directly into a liquid by some form of sparging system (presented above) and become attached to solid particles or immiscible liquid droplets, causing these particles or droplets to rise to the surface. Sulfur removal by conventional froth flotation requires good control of the solution level and vigorous mixing in the balance tank. In **air skimming flotation** units **(Figure 2-4b),** bubbles are generated by dissolution of air in a circulated liquid under pressure and then liberation of it into the regenerator by reducing the pressure; if the catalyst in the spent solution coming from the absorber is oxidized by a co-current, upwards stream of air. The froth is withdrawn from the top of the regenerator. For both types of flotators, the froth is further concentrated in a consecutive step. The equipment most commonly used for this purpose is a settler, but in large plants centrifuges or filters are also applied (Quinlan, 1991).

In most iron chelate-based redox processes, **settling** has been the preferred first-stage sulfur removal method where particles are separated from a fluid by gravitational forces acting on them (Kohl, A. L. et al., 1997). The **settler** diameter is a function of the solution flow rate, which is determined by the sulfur production rate (refer to **Figure 2-4c**). The settler depth is a function of the retention time needed to yield the desired sulfur slurry concentration. When high concentrations of particles are present during settling, the surrounding particles interfere with the ones in the middle and the settling becomes hindered. A sedimentation device is called a **thickener**, if the main purpose of it is to produce concentrated slurry. However, if the main function of the sedimentation is to remove solids from a liquid, the device is known as a **clarifier**. Both types are often similar in design as it is shown in **Figure 2-4d**.

Figure 2-4 Configurations of different sulfur separation units-compiled from (Smith R. , 2005) and (Quinlan, 1991)

<table>
<tr><th>Mechanism</th><th>Froth flotation</th><th>Settling</th><th>Centrifuge</th><th>Filtration</th></tr>
<tr><td></td><td>Flotation</td><td>Gravitational force</td><td>Centrifugal force</td><td>Pressure/Permeation</td></tr>
<tr><td rowspan="2">Configuration</td><td>a. Conventional flotation
 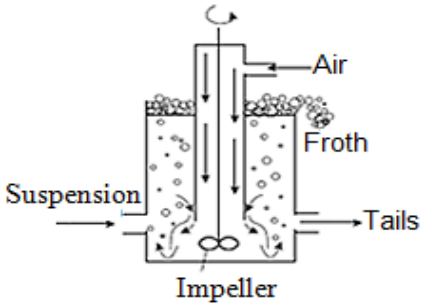
</td><td>c. Settler
 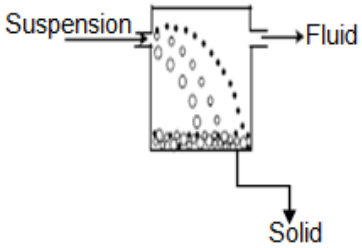
</td><td>e. Hydrocylone
 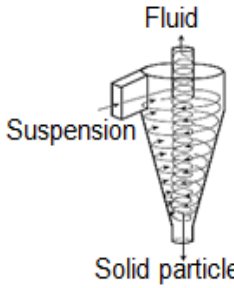
</td><td>g. Bag or pressure filter
 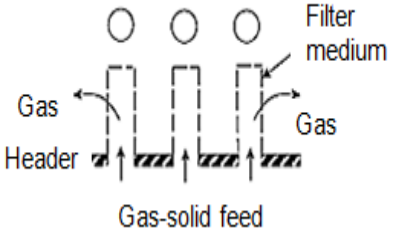
</td></tr>
<tr><td>b. Air skimmed flotation
 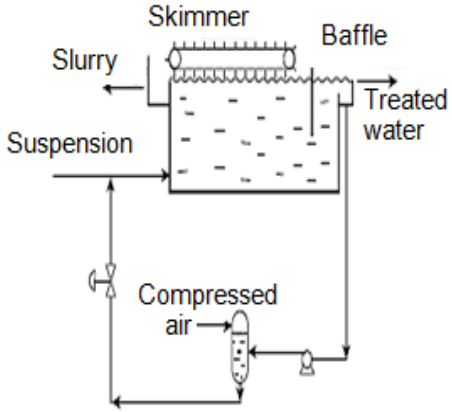
</td><td>d. Thickener/Clarifier
 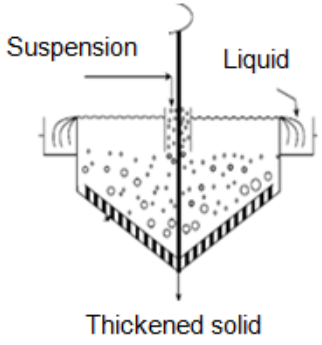
</td><td>f. Centrifuge
 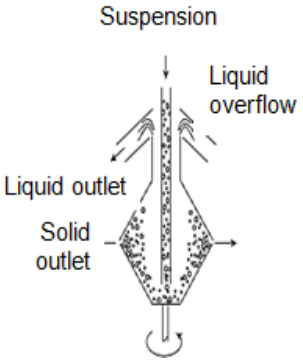
</td><td>h. Belt filter
 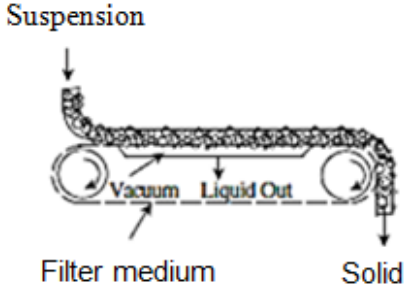

i. Rotary drum filter
 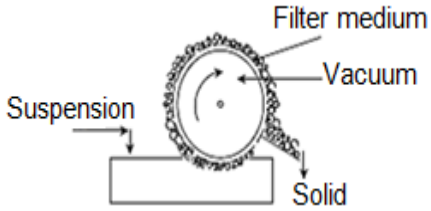
</td></tr>
</table>

Sometimes gravity separation may be too slow, if the densities of the particles and the fluid are too close together or if small particle sizes lead to low settling velocities. Particles that do not settle readily in gravity settlers can often be separated from fluids by centrifugal forces (Smith R. , 2005). **Centrifugal separators** take the idea of an inertial separator a step further and make use of the principle that an object whirled about an axis at a constant radial distance from the point is acted on by a force. For example, in **hydrocyclones** (see **Figure 2-4e**) the mixture enters through a tangential inlet in a cylindrical part near the top, and the rotating motion created in this way develops centrifugal force that throws the dense particles radially towards the wall. The fluid flows downward in a spiral adjacent to the wall, which becomes conical. When the fluid reaches the bottom, it spirals upward in a smaller spiral through an inner pipe. The downward and upward spirals are in the same sense of rotation. The particles of dense material are creeping downwards the wall and leave the bottom of the cone. In **centrifuges**, a cylindrical bowl is rotated to produce the centrifugal force (illustrated in **Figure 2-4f**). The feed is thrown radially to the walls of the container. Whereas the liquid rises and leaves the bowl on top through an overflow, the particles settle outward horizontally. Centrifuges usually run much more stable compared to hydrocyclones (which are prone to disturbances in operation), but due to their high maintenance costs, they have been replaced by **filters** in most applications.

In **filtration**, suspended solid particles in a gas, vapor or liquid are removed by directing the mixture through a porous medium that retains the particles and lets the fluid pass. For liquid-redox plants processing more than 1 LTPD of sulfur, it is reportedly cost effective to concentrate the sulfur solids in a filter press (Kohl, A. L. et al., 1997). **Bag or pressure filters (Figure 2-4g)**, in which the cloth is arranged as a thimble or candle, are used when thickening of the slurry is to be performed without a separate thickener vessel (Smith R. , 2005). As the particles build up on the inside of the thimble, the unit is periodically taken off-line, and the flow is reversed to recover the filtered particles. **Figure 2-4h** shows a **belt filter** where a horizontal filtering surface is employed. This arrangement permits gravity filtering before vacuum is applied additionally. It is claimed that this type of filter is ideal for cake washing and cake dewatering. However, belt filters require substantial floor space. **Figure 2-4i** shows a **rotating drum** in which the drum moves through the slurry (Grande, 1987). In both latter types, the flow of liquid is induced by the creation of a vacuum. The vacuum provides the driving force to draw the solution through the filter cake.

Froth flotators and settlers usually have to be followed by centrifuges or filters to gain slurry or filter cake, which can then be forwarded to further purification stages in order to produce commercial sulfur product for several purposes:

- sulfuric acid production
- building material (e.g. as sulfur-polymer-cement)
- explosives
- fertilizer.

The sulfur in the filter cake of liquid-redox processes contains entrained water and residual catalyst. Thus, sulfur content ranges between 60 wt% and 90 wt% (Hydrocarbon Processing®, 2004). This product can be upgraded to 99.9 wt% pure sulfur by **melting**. It is stated that in systems where the sulfur is fed into a melter, there would be almost no filter cake solution losses, but high temperatures (>60°C) would lead to enhanced thermal degradation of the applied ligand. Therefore, the purification of liquid-redox sulfur to molten-grade sulfur usually is not profitable. But there are potential uses for this “impure” sulfur. With the sulfur being formed in the liquid phase at low temperatures, the particles are rather amorphous compared to solidified molten sulfur (melting point is 115 °C) and have a smaller particle size (typically from 8 to 45 microns) (Quinlan, 1991). The iron and chelators remaining in the sulfur act as soil nutrients, pH adjusters and as fungicides. All these characteristics of liquid-redox sulfur support good utilization of it in agricultural applications. Nevertheless, the physical and chemical properties of the end product and thus the potential usage mainly depend on the chemical nature of the original absorbent solution. The next section covers the constituents of conventional chelated-iron liquid systems and their impacts on the whole process.

2.2 Formulations of state of the art chelated-iron solvent systems

In all of chelated-iron liquid redox processes, the liquid system consists of the absorbent (providing the alkalinity) in aqueous solution, the catalytic agent (iron for all systems discussed here) and a ligand allocated to iron (see section 1.4.3.2.2), as primary components. Depending on the purpose of application, other constituents in the solution may be needed additionally:

- to strengthen the physical stability of the iron-ligand-complex
- to modify reaction pathways, to accomplish sulfur flotation or sinking
- to control biological activity
- to aid H_2S/CO_2 selectivity
- or to enforce CO_2 absorption capability.

Conventional liquid redox solution systems based on iron-chelate share certain similarities in their liquid formulation, which are listed in **Figure 2-5**[3] and will be discussed in the scope of this section (deduced from (Wubs, 1994) and (Kohl, A. L. et al., 1997)).

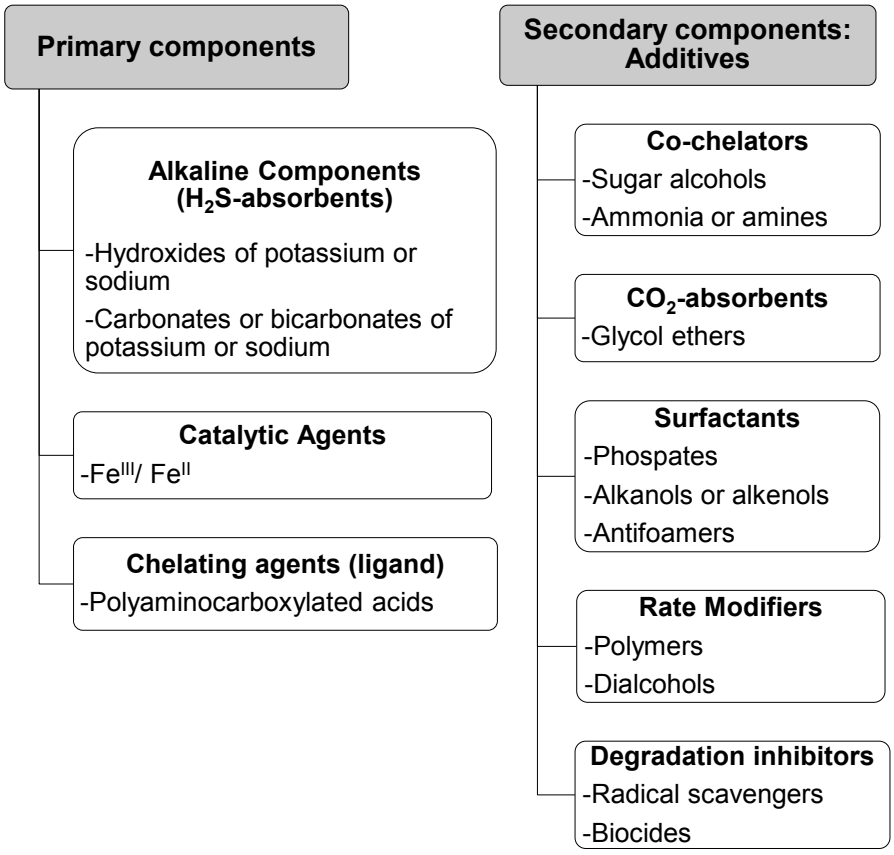

Figure 2-5 Constituents[3] of conventional iron-chelate solution systems deduced from (Wubs, 1994) and (Kohl, A. L. et al., 1997)

2.2.1 Primary components

Alkaline components: To ensure that the process operates within the desired pH range so that neither the lower nor the upper pH limit specifications are exceeded (for solution of the applied chelating agent, absorption of H_2S and/or CO_2 and prevention of side reactions), the scrubbing medium shall be mildly alkaline and buffered (Hardison & McManus, 1987). Salts of potassium (K) or sodium (Na) have been mostly chosen as alkali component so that purge streams drawn from the system with the sulfur product is highly water soluble. In gas streams bearing only H_2S, potassium or sodium hydroxide (KOH or NaOH) are added to the water (Kohl, A. L. et al., 1997) - KOH is preferred for higher buffering capacities, but it is more expensive than NaOH.

[3] All constituents are in aqueous solutions.

If the gas to be treated contains also CO_2, but H_2S should be separated selectively, carbonates (K_2CO_3 or Na_2CO_3) as well as bicarbonates ($KHCO_3$ or $NaHCO_3$) of these alkali metals are applied. Carbonates cause selectivity in absorbing H_2S relative to CO_2 besides maintaining the pH, thus they exert more than one specific characteristic. This can also be the case for other components.

Chelating agents: In the reaction process for converting the sulfur ions in elemental sulfur the Fe ions (both (Fe^{III}) and (Fe^{II})) serve as the donor and acceptor of electric charges, see Eq.1-9 and Eq.1-10. The ligand, however, does not take part in these reactions, but keeps the Fe-ions dissolved in water to reach a defined concentration varying from 600 ppmwt to 4 wt%, thus exceeding saturation of non-chelated Fe in water (Hardison & McManus, 1987). As it was already mentioned in section 1.4.3.2 as well as 1.4.3.2.2 and listed in **Table 1-6**, various chelating agents have been used in former liquid redox processes (Kohl, A. L. et al., 1997). These can be categorized as organic compounds (e.g. cyanides, thionates etc.), quinones (e.g. anthraquinone, benzoquinone etc.) and sulfonates (water soluble polymers e.g. salt of ADA etc.). For iron-chelated iron processes, however, solely either alkali or ammonium salts of poly aminopolycarboxylates (APC) (EDTA, HEDTA, NTA etc.) are used as chelating agent and the iron as metal catalyst. Because of this unique combination the chelated iron solutions have been claimed to persist longer and to be environmentally friendlier than those of others (Martell, A. E. et al., 1996). Such chelators feature high solubility and subsequent thermodynamic stability towards hydrolysis due to the presence of multiple carboxylate anion groups in their molecular structure. They are either neutral or anions, containing at least one atom (e.g. nitrogen (N), oxygen (O), sulfur (S) or phosphor (P)) which is able to serve as an electron donor. Theoretically, one mol of ligand is required to sequester one mol of the iron. However, each chelator assesses different free electron pairs (i.e. atom numbers) to be donated to the metal to form thermodynamically stable complexes. Therefore, as it was stated in **Table 2-1**, ligand to metal ratio may vary from 1 to 2 (mol/mol) depending on the applied chelating agent (Wubs, 1994). As a representative for the chelating of iron, the molecule scheme of a free EDTA (left) and its complex with iron (right) is illustrated in **Figure 2-6** (Martell, A. E. et al., 1996). Selecting an appropriate complexing agent helps to optimize different parameters like kinetic behavior, long time performance and thus the operation costs of liquid-redox processes. Thus, chelating agent selection criteria will be discussed in detail in section 3.4.2.

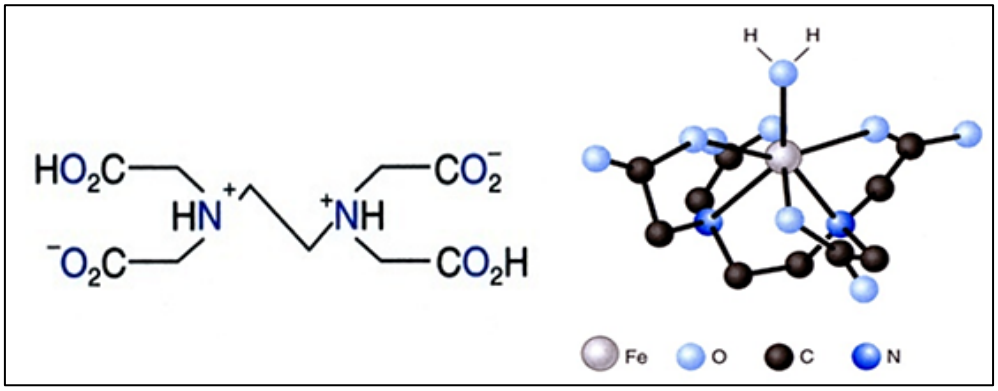

Figure 2-6 Molecular structures of a free EDTA-molecule (left) and an Fe•EDTA-complex (right) (Martell, A. E. et al., 1996)

The reactivity of the suspended iron is claimed to be strongly affected by variations in the method of preparation (Ying, L. et al., 2014). Consequently, the preparation approach must be such that the formation of the most stable form of ferric chelate is favored. This may necessitate use of some additional components as discussed in the following subsection.

2.2.2 Additives

In order to understand the purpose of **co-chelators**, it is important to know that iron-chelates can exist in many different species, depending on the concentration of chelator and iron, the solution pH, the temperature, and the overall ionic strength of the solution (Martell, 2009). The latter, the α_{ion}, can be expressed with Eq.2-3 :

$$\alpha_{ion} = \sum_{i=1}^{n} c_i \cdot z_i^2 \qquad \text{(Eq.2-3)}$$

Where the c_i stands for the concentration (M or mol/L) and the z_i is the charge number of the ions. Especially, keeping the pH of the solution at an optimum is a key feature, as the pH primarily controls the solubility and stability of the different species. In the initial British liquid-redox technology named as C.I.P. (Chelated Iron Process), listed in **Table 1-6**, EDTA was employed to keep the iron in solution. The first application of the process in an oil refinery in Llandarcy (Wales) in 1964, was unsuccessful because of the instability of the chelated iron solution, caused by pH values higher than the reasonable range (Meuly, 1973). Since the complexation approach is an acid-base reaction, the ability of a ligand to form strong complexes depends on the pH of the solution. Chelating agents hold iron ions in different strengths depending on the pH level, and there is a characteristic curve for every chelator. The lower limit should be the hydroxylation point of the chelator above which the iron-chelates start to show reactivity towards H_2S. These minimum pH values for iron complexes are about 6.5 (EDTA), 8.5 (DTPA) and 2.5 (HEDTA) (Martell, 2009). The upper limit should be pH ≈ 10, beyond which metal hydroxide precipitation occurs. **Figure 2-7** shows seven different species of EDTA depending on the solution pH, i.e. deprotonated (Y^n) and protonated molecules (H_xY^n) where the n and the x denote the number of electrons and protons, respectively (Hargis, 1988).

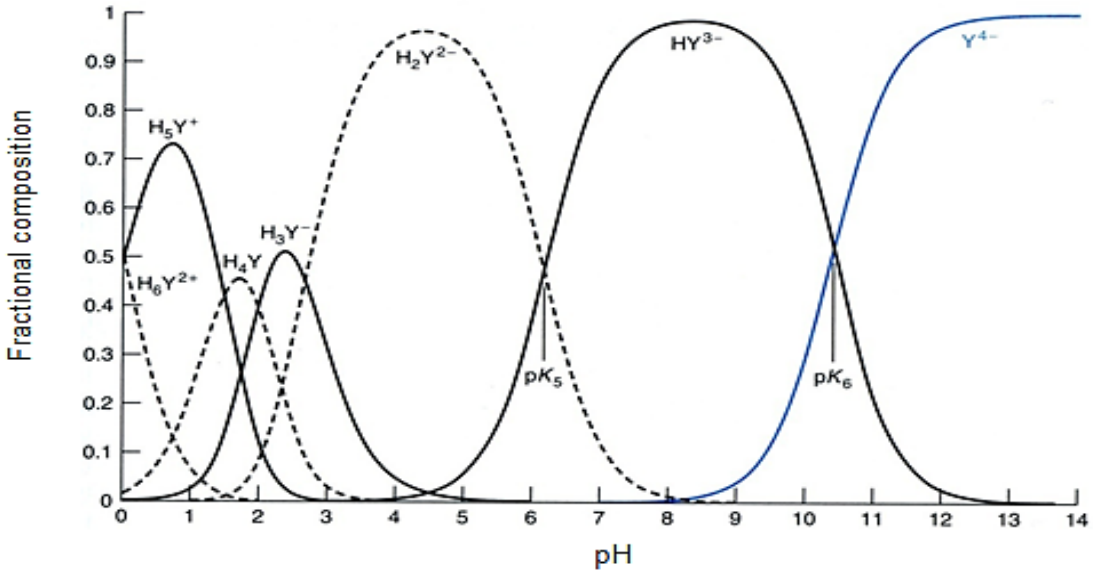

Figure 2-7 Dissociation of EDTA species (Y = EDTA ion) depending on the solution pH at 25°C (influence of pressure can be neglected) (Hargis, 1988)

The most alkaline form of EDTA (Y^{4-}) possesses the highest reactivity towards metal ions in solutions because it offers the highest number of electron pairs (Hargis, 1988). The complex is unstable at pH < 8, since H^+ competes with metal ions for EDTA and thus iron sulfide precipitation would occur (FeS). Although pH > 10 would promote the dissociation of chelating agent into its most alkaline form (i.e. the Y^{4-}), it would lead to $Fe(OH)_3$ precipitation. Therefore, pH > 10 and pH < 8 are regarded as instable regions. In cases where the main chelating agents, e.g. the salts of EDTA, NTA and HEDTA, lose their complexing characteristics, **co-chelating agents** can be added to the mixture to enlarge the stabile pH range of the complex (Martell, 2009).

For this purpose sugar alcohols such as sorbitol, mannitol, xylitol etc. are often used when the desired solution pH is between 8 and 9 (Welch, K. et al., 2002). At higher pH ranges, tri ethanol amine (TEA) is added to avoid precipitation of $Fe(OH)_3$. However, all co-chelators form weaker complexes than the main ligands do. In cases where a higher chelating agent solubility and pH < 8 are envisaged, ammonia salts of chelators can be applied instead of alkali salts, since they are better soluble at lower pH ranges. But operation at low pH values would adversely affect sour gas absorption. Thus, if the solution applied for chemical reasons is not mildly alkaline, liquid redox absorbers should be operated under pressure, thus enforcing gas absorption in the solution.

CO_2-Absorbents: For all iron-chelate systems listed in **Table 1-6,** reportedly, H_2S is absorbed selectively. However, in applications where simultaneous removal of CO_2 is required, glycol ethers can be added to the solutions since they enhance CO_2 absorption without having an adverse effect on H_2S absorption (Winkler, 1978). Winkler identified diethylene glycol mono ethyl ether (DEGEE) as an efficient absorbent, which simultaneously promotes dissolution of NTA.

Surfactants: Sulfur particles may become attached to air bubbles causing them to float on the surface instead of settling. Additionally, heavy hydrocarbons in the sour feed gas may lead to excessive foaming. To counter these problems, surfactants can be added to the process continuously in small amounts. If settling of the sulfur particles is not desired because sulfur separation is achieved by flotation, the addition of the surfactants has to be controlled very carefully and e.g. restricted to a few milligrams per liter solvent. Precipitation of elemental sulfur solids in the contactor is chemically modified with respect to particle agglomeration and sinking by the surfactants listed in **Figure 2-5** (Blytas & Diaz, 1982). Blytas and Diaz proposed that alkenols, alkanols, phosphates and their precursors increase the particle size and thus improve the filterability of sulfur.

Rate modifiers: (Diaz & Blytas, 1982) also proposed that addition of dialcohols (e.g. 2,3-butanediol or 1,4-butanediol) enhances the rate of both absorption and regeneration reactions whereas the use of polymers, for example the poly dimethyl diallyl ammonium chloride (PolyDADMAC), was found to be catalyzing only the absorption reaction (Lampton & Hopkins, 1986).

Degradation inhibitors: Degradation of chelating agents is mainly triggered and enhanced by thermal (decomposition), chemical (radical attack) or biological (bacteria) effects. Whereas thermal degradation can only be minimized by decreasing the temperature, several additives such as radical scavengers and biocides are available to inhibit or to slow it down the aerobic (by free radicals) and anaerobic (by microorganisms) degradation of the chelating agents, respectively. Additives employed for this purpose are discussed in detail in the context of chapter 5 and given in **Table A- 9** in Appendix A-3.2.

Technical differences resulting from the chemical differences of the applied solution systems will be presented by discussing the most frequently implemented iron-chelate systems within the context of the following sections.

2.3 Benchmarking of conventional chelated-iron liquid redox processes

2.3.1 LO-CAT®

The LO-CAT® process has been developed by ARI Technologies in the late 1970s and licensed by Merichem Company. This technology is offered in several configurations tailored to specific applications including, in chronological order:

- LO-CAT® (conventional)
- Autocirculation LO-CAT®
- LO-CAT® II (Heguy, 2003) - offered in both conventional and autocirculation versions.

These LO-CAT® units are employed to remove H_2S from various types of acidic gas streams (off-gases of Amine and/or Selexol plants, sour water strippers) and other overhead gas streams (fuel or sour natural gas). It is reported that the LO-CAT® technique is the process of choice, when the ratio of CO_2 to H_2S in the gas to be treated is greater than 3 and the sulfur removal capacity ranges between 0.5 to 25 LTPD (Merichem Company, 2015). Technical differences of all LO-CAT® versions, their basic chemistry and unique features or bottlenecks will be explained in the following subsections.

2.3.1.1 Basic chemistry

As mentioned in section 2.2.2, the pioneer of LO-CAT® process, the C.I.P., broke down due to chelate instability caused by pH values higher than reasonable (Meuly, 1973). Taking this into consideration, the LO-CAT® absorbent solutions were developed with a dual chelating agent system supplemented with co-chelators. The first LO-CAT® solution employed blends of alkali salts of EDTA and HEDTA as main chelating agents (Thompson, 1980). However, during first implementation of the LO-CAT® technology at the U.S. Oil & Refining Co.´s location in Tacoma, Washington, it was seen that the loss of these chelating agents due to oxidative decomposition turned out to be the most significant and also critical factor affecting the economic feasibility of the large-scale operation (McManus & Kin, 1988). Therefore, the developer of LO-CAT® replaced the mixture of alkali salts of EDTA and HEDTA with alkali salt of NTA. As LO-CAT® processes are operated at pH ranges of 8 to 8.5, sorbitol is added to the solution as co-chelator. Furthermore, the influence of the solution pH on the overall chemistry of these processes i.e. on the absorption and dissociation of process gases (e.g. H_2S and/or CO_2 and O_2) cannot be neglected, as discussed in the following:

- Absorption of the H_2S into the solution and dissolution (refer to reaction Eq.1-6) (Kohl, A. L. et al., 1997)
- Dissociation of the $H_2S_{(aq)}$ into its respective species depending on the pH of the solution as depicted in **Figure 2-8** and expressed in Eq.2-4.

$$H_2S_{(aq)} \leftrightarrow HS^-_{(aq)} + H^+_{(aq)} \leftrightarrow S^{2-}_{(aq)} + 2H^+_{(aq)} \qquad \text{(Eq.2-4)}$$

- Oxidation of the respective specie into elemental sulfur in the absorber (refer to Eq.1-9).

The H_2S in the gas phase is in equilibrium only with its undissociated form in the liquid. As shown in **Figure 2-8**, H_2S dissociation is incomplete when the pH is below 7 whereas almost all of the H_2S is ionized in the solution at a pH value of 9. At higher pH values the amount of dissolved would be only limited by the diffusion of the gas into the bulk of the solution. However, as stated before, above pH 10, $Fe(OH)_3$ precipitates and the solution becomes ineffective.

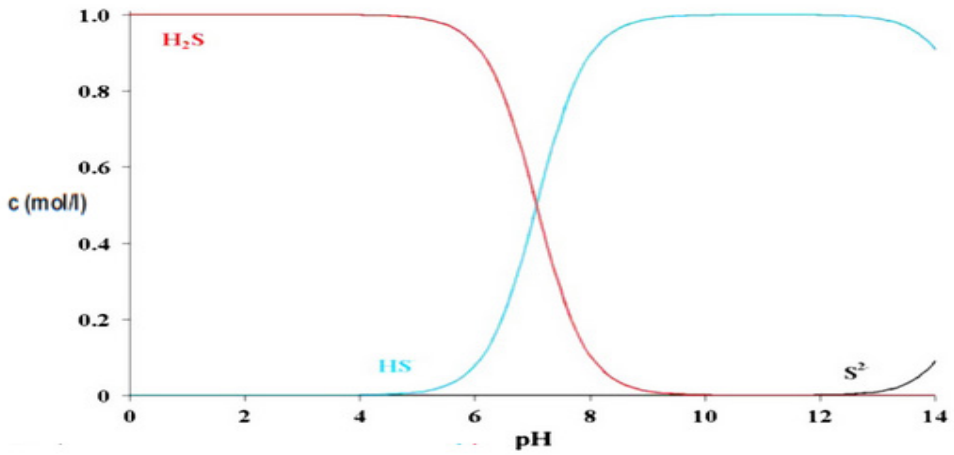

Figure 2-8 Hydrogen sulfide species distribution diagram at 25 °C (influence of pressure can be negleted) (Kohl, A. L. et al., 1997)

Since LO-CAT® processes are operated at pH ranges of 8 to 8.5, most of the H_2S exists as bisulfide (HS^-) in the solution. The HS^- species is being converted to solid sulfur in the absorber according to reaction Eq.2-5[2].

$$2(Fe)^{3+} \bullet Lig_{(aq)} + HS^-_{(aq)} + H^+_{(aq)} \rightarrow S^0_{(s)} + 2(Fe)^{2+} \bullet Lig_{(aq)} + 2H^+{}_{(aq)} \qquad \text{(Eq.2-5)}$$

Regeneration of the reduced iron-chelate is performed in the same way as demonstrated Eq.1-10. However, side-reactions can occur either when unreacted HS^- ions are carried over into the regenerator or when the regenerated solution fed to the absorber contains a large amount of dissolved oxygen. The oxidation of HS^- ions by O_2 instead of (Fe^{3+}) may cause thiosulfate ($S_2O_3^{2-}$) formation. This species can also be further oxidized to sulfates (SO_4^{2-}) as expressed in the following reactions (Yan, 1980).

$$2HS^-_{(aq)} + 2O_{2(aq)} \rightarrow H_2O_{(aq)} + S_2O^{2-}_{3(aq)} \qquad \text{(Eq.2-6)}$$

$$S_2O^{2-}_{3(aq)} + H_2O_{(aq)} + 2O_{2(aq)} \rightarrow 2SO^{2-}_{4(aq)} + 2H^+{}_{(aq)} \qquad \text{(Eq.2-7)}$$

The formation of thiosulfate and sulfate ions according to Eq.2-6 and Eq.2-7, respectively, tends to reduce the pH of the scrubbing solution and consequently, the H_2S removal efficiency (Yan, 1980). If the pH is too low, H_2S absorption is adversely affected. Furthermore, although the solubility of O_2 mainly depends on the operating pressure and temperature as well as on the ionic strength of the solution (α_{ion}), impacts of the pH on the amount of O_2 dissolved in the solution in the absorber should also be taken into consideration (Kohl, A. L. et al., 1997). Kohl stated that the O_2 content will rise if the pH of the solution is shifted above its normal working range (above pH ≈ 8-8.5 in the case of LO-CAT®). Consecutively, $S_2O_3^{2-}$ formation will increase.

Absorption of CO_2, another potential process gas component, is also an issue to regard. Distribution of the $CO_{2(aq)}$ into its respective species depending on the pH of the solution as depicted in **Figure 2-9** and expressed in Eq.2-8.

$$CO_{2\,(g)} + H_2O_{(aq)} \leftrightarrow H_2CO_{3\,(aq)} \leftrightarrow HCO_3^-{}_{(aq)} + H^+_{(aq)} \leftrightarrow CO_3^{2-}{}_{(aq)} + 2H^+_{(aq)} \qquad \text{(Eq.2-8)}$$

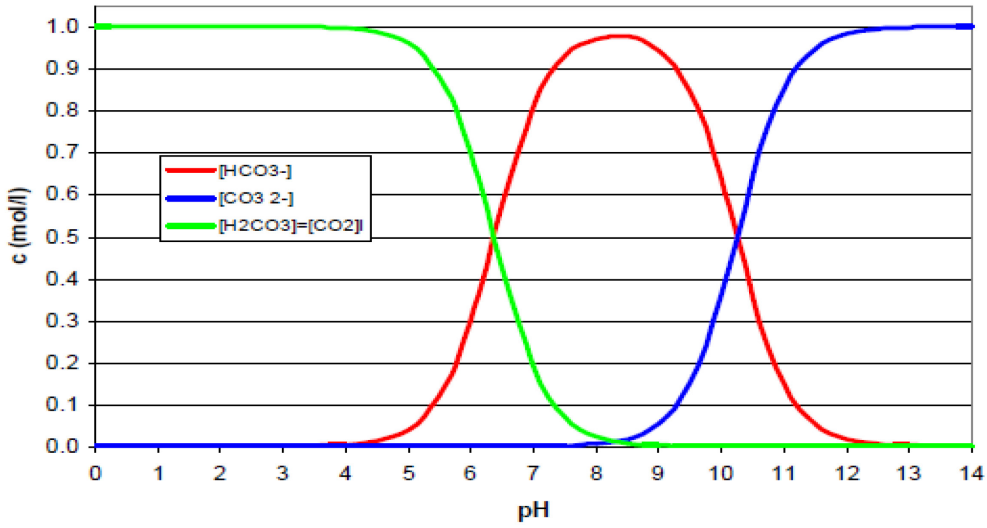

Figure 2-9 Carbon dioxide species distribution diagram at 25 °C (influence of pressure can be negleted) (Carroll, J.J. et al., 1992)

Reportedly, all conventional iron-chelate solution systems are inadequate to remove CO_2 due to low solubility of it. Thus, they are declared to be selective towards H_2S (Hardison & McManus, 1987). When the system is operated at a pH of 8, the solubility of CO_2 in the solution is only approximately the same as in pure water (Hook, 1997).

If simultaneous removal of CO_2 and H_2S from sour natural gas is desired, it is usually preferable to employ an organic-absorbent based solution system. Furthermore, the effect of CO_2 on the pH of the iron-chelate solutions cannot be ignored, since the system is self-enhancing: the higher the pH of the solution, the more CO_2 it will absorb due to bicarbonate (HCO_3^-) and carbonate (CO_3^{2-}) formation, and the more difficult it will be to maintain the desired pH. **Figure 2-9** shows that the concentration of the bicarbonate (HCO_3^-) ions builds up significantly at pH ≈ 8, whereas the concentration of the carbonate (CO_3^{2-}) ions will increase considerably for pH > 9, which is out of the normal range of operation. Presence of bicarbonates/carbonates cause reactions with the cations (K or Na) applied in the washing solution. This results in alkali precipitation in the solution, as well. The increased formation rate of such by-products requires higher blow-down rates and, tends to drive up chemical costs and to impact adversely the operability. To minimize alkali-carbonates and thiosulfate formation as well as chelator loss, the LO-CAT® process is announced to be monitored continuously to ensure that the operation is kept within reasonable pH limits (Merichem Company, 2015).

2.3.1.2 Configurations of LO-CAT® units

As it was indicated in section 2.3.1, four different versions of the LO-CAT® technique are commercially available (Rouleau, 2014). It should be noted that all LO-CAT® versions employ mildly alkaline (pH 8-8.5) solutions containing the same ligand (i.e. the NTA). Thus, the same reactions take place but the units either have different configuration of gas-liquid contactors or different iron (III)-concentrations (c[Fe^{3+}]) depending on the characteristics of the gas to be treated as illustrated in **Table 2-4**. Basically, LO-CAT® systems are suited for handling of relatively high gas flow rates (refer **Table 1-5**), of low or moderate sour gases (as classified in **Table 1-3**).The **conventional version of LO-CAT®** is announced to be economical rather for direct treatment of low sour natural gas up to a certain flowrate (refer **Table 1-5**), while the **autocirculation LO-CAT®** is favourably employed in combination with an amine-Claus unit at higher gas flowrates of low or moderate sour gases (treatment of amine-Claus unit off-gas). **LO-CAT® II** installations, which are available in both conventional and autocirculation versions, have been developed to enable desulfurization of high-pressure gas streams up to 70 bara (Merichem Company, 2012). **Figure 2-10** in **Table 2-4** shows a **conventional LO-CAT®** unit, which is most commonly employed for processing gas streams that are either combustible or must not be contaminated with air prior to absorption, and thus cannot be handled in the combined absorber-regenerator of an autocirculation LO-CAT® unit (Rouleau, 2014). This conventional configuration is applied to treat sour gases with low pressure and very dilute H_2S concentrations. For example, at The Haynesville Shale Converse Central Facility in Mansfield, LA, gas streams of about 3 million standard cubic meters per day (MMSCMD) with 250 ppmv H_2S (approximately 1 LTPD of sulfur) have been processed in 2009 (Merichem Company, 2012). In chelated-iron technologies the ratio of circulated iron to dosed H_2S (Fe^{3+}/H_2S, mol/mol) varies from the stoichiometric requirement of 2 (referring Eq.1-9) to 8, as it was presented in **Table 2-1**. The conventional LO-CAT® version employs dilute iron solutions (500-2000 ppmwt) and is operated with two fold of the stoichiometric iron circulation (Fe^{3+}/H_2S ≈ 4 mol/mol) (Kohl, A. L. et al., 1997). Due to the highly diluted c[Fe^{3+}], a two-step absorption cycle is applied -a venturi scrubber followed by a contactor from the list in **Figure 2-1** (box "H_2S Absorption & Oxidation") - depending on the volumetric gas flow rate and the desired H_2S removal efficiency. As regenerator a conical vertical vessel filled with liquid is employed to minimize plugging risks. The usual approach for the sulfur separation is to combine the settler and the regenerator in one single dual purpose vessel. The settler section is designed as a circular-basin type thickener as illustrated in **Figure 2-10**. Reported drawbacks of this technology are high solution circulation rates and sulfur oxo-anion[4] formation in the regenerator. Reportedly, oxidative degradation of chelating agent turned out to be the most crucial issue in the view of performance.

[4] Sulphur oxo-anions possess either just S-O bonds and or both S-O and S-S bonds.

Table 2-4 Comparison of different LO-CAT® technologies (Nagl, G., 2001) and (Kohl, A. L. et al., 1997)

Process / Parameter	LO-CAT® Conventional	LO-CAT® Autocirculation	LO-CAT® II
Solution system: **pH of the solution**	8-8.5		
Primary components **Additives** **c[Fe^{3+}], ppmwt**	KOH & Fe•NTA (*alkali salts of the ligand) Sorbitol, biocides, surfactant 500-2000	NaOH & Fe•NTA* Sorbitol, biocides 250-500	K_2CO_3 & Fe•NTA* Antifoamer, sorbitol 500-2000
Application fields	Treatment of sour gas stripped from sewer water, coke oven gas, biogas	Amine-Claus tail gas treatment	Direct treatment of high pressure sour gas up to 70 bara
Unique Features	-Fe/H_2S ratio ≈ 4 (mol/mol) -Two-staged absorption → 99.9% H_2S removal efficiencies	-Fe/H_2S ratio ≈ 4 (mol/mol) -Absorption and regeneration in one vessel -Circulation by natural convection, thus reduction in power costs	-Fe/H_2S ratio <2 (mol/mol) -Special regenerator design with staged controlled circulation Reduction of chemical make-up costs to 50$/ton sulfur
Drawbacks	-Sulfur oxo-anion formation (e.g. SO_4 or S_2O_3) -Degradation of chelating agent: high chemical make-up costs i.e. 300 $/ ton sulfur	-Can only be applied to non-combustible gases -S_2O_3 formation higher chemical costs	-Difficulties when treating CO_2-rich gas under pressure →high chemical make up -Plugging of static mixers of absorber→Δp
Process flow scheme	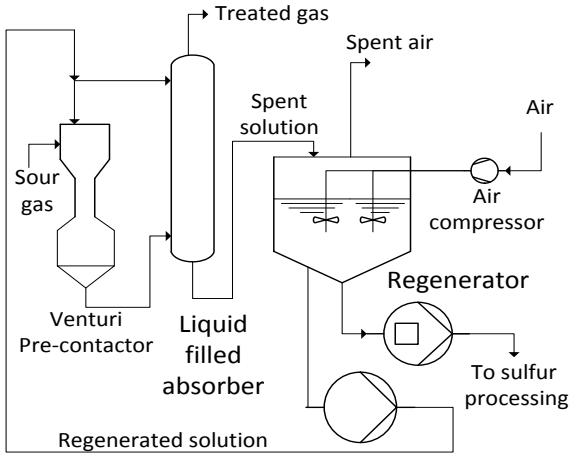 **Figure 2-10** Conventional LO-CAT® technology	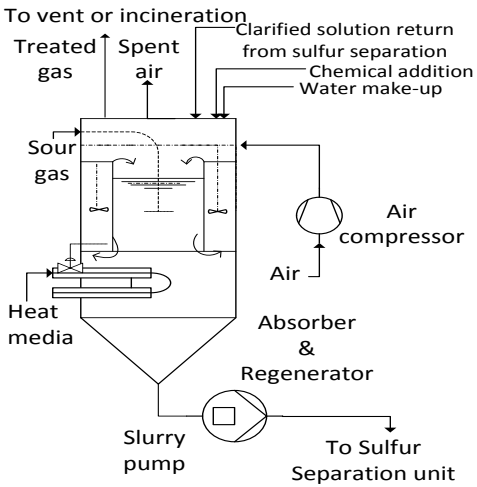 **Figure 2-11** Autocirculation LO-CAT® unit	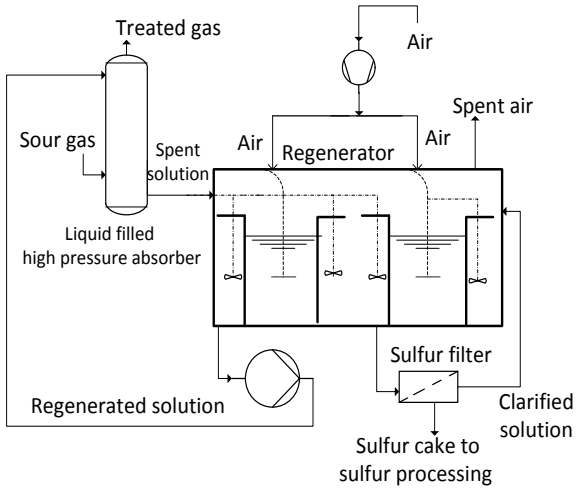 **Figure 2-12** LO-CAT® II technology in conventional version (autocirculation is available as well)

Figure 2-11 illustrates an **autocirculation LO-CAT®** configuration which is favored for the treatment of amine plant acid off-gases and gas streams contain relatively higher H_2S concentrations than those processed in conventional LO-CAT® units (Merichem Company, 2015). The unique feature of this configuration is the combination of the absorber and the regenerator in a single vessel, thus no circulation pumps are required. Solution circulation is achieved by natural convection and through special arrangements of weirs and baffles in the vessel. The sour process gas is bubbled through the chelated-iron solution from a distributor located in the centerwell of the liquid-filled vessel. The H_2S is converted to elemental sulfur in the centerwell, the sulfur particles sink to the conical bottom of the vessel and the slurry is routed from there to the sulfur separation unit. This unit, which is not depicted in the **Figure 2-11** includes e.g. a settler vessel (see **Figure 2-4c**) combined with a vacuum belt filter (see **Figure 2-4h**). Regeneration air is injected into a space between the outside shell of the vessel and the centerwell. The driving force to maintain catalyst circulation is the density differential between the solution in the centerwell and the lighter, highly aerated solution in the space outside of the centerwell. The air flow forces the catalyst solution in the outer space to move upwards. Air and the sweetened gas streams are combined in the headspace of the autocirculation vessel and directed to either an incinerator or directly to the atmosphere. As stated in **Table 2-4**, this version employs a more diluted solution than the conventional version (200-500 ppmwt) which would necessitate significantly higher circulation rates (Kohl, A. L. et al., 1997). However, it is claimed that the special design enables intensive circulation of the dilute solution without the use of pumps minimizing power costs. However, due to the fact that the absorption in these units takes place in O_2 rich environment, sulfur oxo-anion production is promoted. This phenomenon is important because sulfur oxo-anions both tend to reduce the pH of the solution and thus the H_2S absorption efficiency and to attach to elemental sulfur and thus block the precipitation of the formed product.

This impacts the operability and the OPEX adversely due to lower performance and requirement for surfactant addition. Inability of the conventional version to treat high pressure gases and the enhanced thiosulfate formation in the autocirculation version led to the development of the **LO-CAT® II** technology, which is depicted in **Figure 2-12** (Reicher, M. et al., 1999). The unique characteristics of this version are as follows:

(1) Unlike the vertical vessel used in the conventional design shown in **Figure 2-10**, the new LO-CAT® II regenerator is flat-bottomed and rectangular in shape. Staged and controlled air injection is provided by several series of baffled compartments into which the spent solution flows sequentially. This provides better mass transfer than that of conventional version which reduces the air blower head requirement, size of the vessel and by-product salt formation.

(2) Substoichiometric Fe/H_2S ratios (<2 mol/mol) are applied, although the $c[Fe^{3+}]$ is the same as for the conventional version, as given as it is given in **Table 2-4** (Rouleau, 2014). Consequently, the absorption has to be performed under high pressures, reportedly up to 70 bara and the amount of solution flowing through the high-pressure absorber is determined by the kinetics of the absorption reaction (the H_2S-oxidation reaction i.e. the Eq.2-5) and not by the $Fe^{(3+)}/H_2S$ stoichiometry (Hardison & McManus, 1987). Due to operation with substoichiometric iron ratios, HS^- ions are present in the spent solution flowing into the regenerator, which would promote the sulfur oxo-anion formation according to reactions Eq.2-6 and Eq.2-7. However, it is claimed that the special regenerator design allows the mixing up of the spent solution with the chelated $Fe^{(3+)}$ in compartments under absence of dissolved O_2, thus demoting the undesired salt formation.

Although the obstacles of conventional and autocirculation LO-CAT® have been remediated with the LO-CAT® II version, there are some applications where even this improved version is not suitable e.g. high pressure CO_2-rich feed gases (due to limited ability for CO_2-absorption) (Kohl, A. L. et al., 1997). After reviewing the features of the LO-CAT® technologies, the following part of this section gives an overwiew about the characteristics of another well-known liquid redox technology, the SulFerox®.

2.3.2 SulFerox®

The SulFerox® process has been jointly developed and licensed by Shell Oil and Dow Chemical. This technology was introduced to market in 1987 with the aim of achieving smaller footprints together with high H_2S removal capacities and low chelating agent degradation rates (Wubs, 1994). **Table 2-5** gives an overview on the characteristics of this technology. The main process steps are the same as for LO-CAT® units, whereas the significant differences are the iron concentration (ten to twenty fold compared to the upper value for LO-CAT® solutions, i.e. 2 to 4 wt%) and the operation at neutral to slightly acidic pH values (6.5 to 7) (Buenger, 1988). The basic chemistry is comparable to the steps described by the Eq.1-9 and the Eq.1-10. Unlike LO-CAT® technologies, SulFerox® employs ammonium salts of NTA and HEDTA blends instead alkali salts of them since at the given operating pHs the solubility of these chelators with ammonium salts are better than those with alkali salts (Wubs, 1994). Due to the higher c[Fe^{3+}] the SulFerox® solution is claimed to have a much higher H_2S removal capacity per volume of solution which allows lower circulation rates and thus equipment sizes. It is stated that the use of a more concentrated iron solution accelerates the kinetics and uncouples the process from the need to have a pH > 7 for efficient H_2S removal. In turn, operation at relatively low pH of 6.5-7 reportedly takes the process out of the region where the lifetime of HS^- in the solution is reduced (see **Figure 2-8**) and thus the thiosulfate formation is demoted (Yan, 1980). Liquid redox processes are distinguished from each other not only by the chemical nature of the process solution but also the method employed to suppress ligand decomposition. In SulFerox®, ligand degradation has been minimized both by chemical additives (i.e. radical scavengers) and also through the optimization and control of operating conditions. The most important of these are the Fe^{2+}/Fe^{3+} ratio in the circulation solution, the amount of supplied regeneration air, the process temperature (<60°C) both in absorber and regenerator and the solution pH. The SulFerox® process can be used for treating either low or high pressure gas up to 70 bara and has been applied for the desulfurization of sour gas from heavy oil production, amine plant acid gas, Claus SRU tail gas and geothermal non-condensable gas (Al-Mughiery, S. S. et al., 1992). The wide application range of the technology owes to high H_2S selectivity of the process solution, which reportedly does not react chemically with the CO_2. In cases where simultaneous removal of CO_2 is desired it can be achieved either by adding DEEGE to the solution (referring **Table 1-5**) or by removing the CO_2 in an appropriate downstream plant employing a physical solvent, e.g. Fluor's Econamine FG Plus Technology. Despite of the fact that the solubility of CO_2 is very low at the given operating pH (see **Figure 2-9**), and thus the pH is not reduced by dissolved CO_2, small amounts of alkaline make-up buffering agent (typically NaOH) have to be used to maintain the pH. It is reported that the presence of ammonia (NH_3) in the feed gas may be either a drawback (since it would increase the solution pH which may in turn result in enhanced iron precipitation) or a benefit (since it would reduce the amount of make-up for buffering required to control the pH). A schematic flow diagram of a typical SulFerox® plant treating sour gas is shown in **Figure 2-13** fitted in **Table 2-5**.

Absorption: The absorption and the successive oxidation of the H_2S (referring Eq.1-9) take place either in a pipeline contactor or in a bubble column which both are claimed to have non-fouling characteristics (see **Table 2-3**). As it is shown in **Figure 2-13**, the gas-liquid mixture flows from the contactor ("absorber") to a knockout drum ("gas-liquid separator") to separate the treated gas from the spent solution that contains sulfur slurry. The solution is then sent to a flash drum ("degasser") to remove dissolved CH_4 or absorbed CO_2.

Regeneration: The degassed solution is then cooled to remove the heat of reaction and fed to the regenerator. In this unit, the spent solution moves co-currently with the sparged air flow, and thus the inactive iron is oxidized back to its active form (referring Eq.1-10). Regenerated liquor exits the top of the regenerator and flows into the surge settler vessel, where the spent air is vented. The regenerated solution is taken from the side or the middle of the settler and sent back to the absorber by the main circulation pump. Makeup chemicals are typically added to the suction side of this pump to ensure to particle agglomeration and sinking. Regeneration is usually carried out at low pressure (typically up to 2 bara) to minimize regeneration air compression costs.

Table 2-5 Main features of the SulFerox® technology (Wubs, 1994)

Process / Parameter	SulFerox®
Solution system: **Solution pH** **Primary components** **Additives** **c[Fe^{3+}], ppmwt**	 6.5 – 7.0 Ammonium salts of Fe. NTA & Fe. HEDTA DEGEE 20,000-40,000
Application fields	Treatment of associated sour gas (from oil wells), amine plant acid gas, Claus SRU tail gas and geothermal non-condensable gas
Unique features	-High iron concentration in solution due to good solubility of chelators formed with ammonium salts -Suppression of oxo-anion formation (SO_4 and S_2O_3) by operating at relatively low pH -Minimization of oxidative degradation of chelating agent -Absorption under pressure up to 70 bar -Controlled partial oxidation of Fe^{2+} to Fe^{3+} -Versatile design of sulfur processing unit
Drawbacks	-Thermal degradation of chelator during sulfur melting -Chemical make-up costs of up to 200$/ton sulfur
Process flow scheme	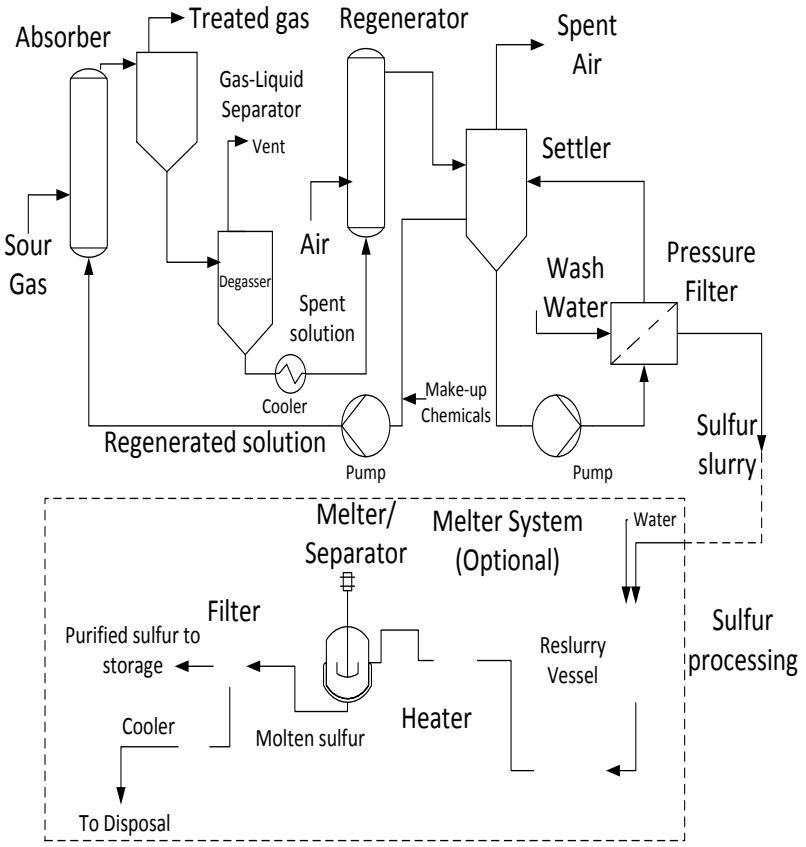 **Figure 2-13** Schematic flow diagram of SulFerox® technology (Buenger, 1988)

At atmospheric pressure, the air volume required to regenerate the SulFerox® solution is typically in the range of 2 to 3 times stoichiometric or 2.5 to 7 times absolute (v/v) (the stoichiometry of the overall reaction calls for a half mol of oxygen or about 2.4 mol of air per mol of H_2S quantity in the inlet gas, see Eq.1-10) (Kohl, A. L. et al., 1997).

Sulfur separation: Sulfur may be recovered as a cake or further processed (melted and purified), depending on the plant size and economics (Buenger, 1988). In order to separate the washing solution content from the thickened slurry, it is fed to a filter press equipped with a cake wash. The recovered process solution flows back to the settler. For purification, a sulfur melter can be added to the process. The sulfur cake is reslurried with water and pumped through a heat exchanger where it is melted using steam. However, this method has reportedly been not preferred, since the sulfur product begins to melt at T = 115 °C, and at T > 60°C chelator-decarboxylation may take place (Martell, 2009) which increases the chemical make-up costs.

Thus now, the other common example of the state of the art liquid redox processes, the Sulfint technology, will be presented in the following part of this section.

2.3.3 Sulfint and Sulfint HP

The **Sulfint** process was developed by Integral Engineering of Vienna, Austria in the late 70's (Rossati, F. et al., 1982) and is currently licensed by Le Gaz Integral Enterprise of Nanterre, France Ten plants using this technology had been built by 1993 to treat sour gases stripped from sewer water and incinerator off-gas (all in Europe) (Kohl, A. L. et al., 1997). All of these units are able to handle only low capacity gases streams at low pressure and with very low H_2S concentrations, leading to a capacity from 0.02 to 0.75 LTPD sulfur. Institute Francaise du Petrole (IFP) in association with Le Gaz Integral (LGI) have developed and licensed an improved version of the Sulfint, named Sulfint HP which can overcome the shortcomings of the conventional Sulfint and thus can be applied to treat sour gas streams with high pressure and high H_2S concentrations such as natural gas (Ballaguet, J.P. et al., 2001). The characteristics of both versions are compared in **Table 2-6**. The catalytic washing solution contains EDTA as the complexing agent for both technologies at a pH range between 7 and 9 (Wubs, 1994). The operation of Sulfint and Sulfint HP is in principal identical to other iron-chelate based H_2S removal processes.

An illustration of the **Sulfint** process flow scheme is shown in **Figure 2-14** (Kohl, A. L. et al., 1997). The H_2S absorption is performed in either venturi or ejector scrubbers, whereas the regenerator and the settling vessels are configured as basin thickeners. The solvent from the outlet of the absorber is forwarded to a block which consists of a regenerator vessel and a settlement tank where the catalytic agent is oxidized and the produced sulfur is withdrawn as slurry, respectively. This slurry is then decanted to further separate the washing solution and the solid sulfur. The wash water is sent to a membrane, where chelated iron is retained and cycled back to the regenerated washing solution, whereas the permeate is sent to waste water treatment. Solid sulfur from the decanter is melted in an autoclave for the further purification; the rest (water) is disposed of. It is stated that the utilization of the decanter in combination with the reverse osmosis to prevent chelating agent loss and the relatively low capital cost are the advantages of this process for low gas capacities. However, the large air requirement which is reportedly twenty fold absolute (v/v) respectively 8 times stoichiometric of the H_2S quantity in the inlet gas or 16 times stoichiometric of the Fe content of the solution, necessitates large regenerator vessels. This turned to a serious issue regarding the footprint of the technology, besides high operating costs for air conveying (Wubs, 1994). The **Sulfint HP** process has been demonstrated under industrial conditions with a pilot plant, operated for more than 6000 hours from 1999 to 2001 by GDF and treating natural gas from an underground storage at Soings en Sologne, France (Ballaguet, J.P. et al., 2001). This process has been designed in order to be able to handle up to 2000 Nm3/h (1.792 MMSCFD) of gas at pressures up to 80 bara at temperatures around ambient, which feature variable concentrations of H_2S between 8 and 5000 ppmv (approximately 100 kg of sulfur/6000 hours). **Figure 2-15** gives a schematic illustration of the employed units.

Table 2-6 Comparison of Sulfint technologies (Kohl, A. L. et al., 1997) and (Ballaguet, J.P. et al., 2001)

Process / Parameter	Sulfint	Sulfint HP
Solution system: **Solution pH** **Primary components** **c[Fe^{3+}], ppmwt**	7.0 – 9.0 Alkali salts of Fe•EDTA In the range of LO-CAT® solutions i.e. 250-2000 (see **Table 2-4**)	
Application fields	Sour gas stripped from sewer water and incinerator off-gas	Underground storage natural gas treatment
Unique features	-Low CAPEX -Mechanical catalyst loss is minimized by decanter plus reverse osmosis	-Absorption under pressure up to 80 bara -Special regenerator design→ Regeneration rate enhancement of factor 30 -Filtration under pressure→pumping costs are minimized
Drawbacks	-Inability to remove CO_2 simultaneously -High air requirement → large regenerator vessels -Inability to treat high pressure gases	Inability to remove CO_2 simultaneously
Process flow scheme	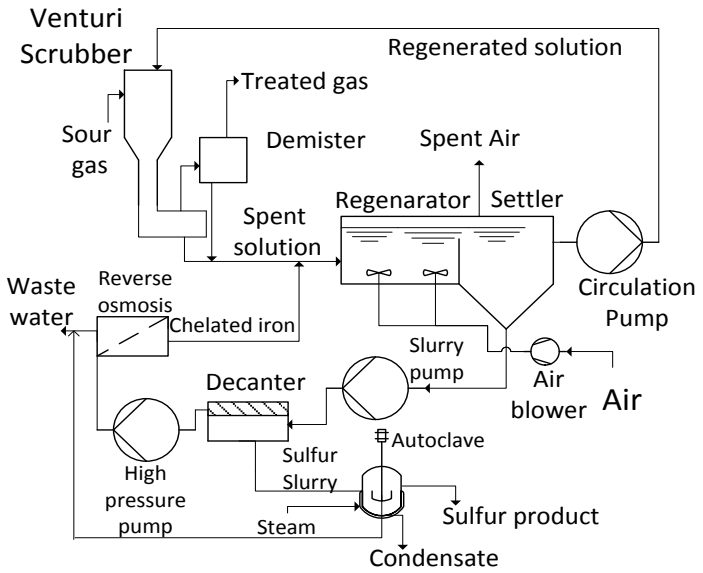	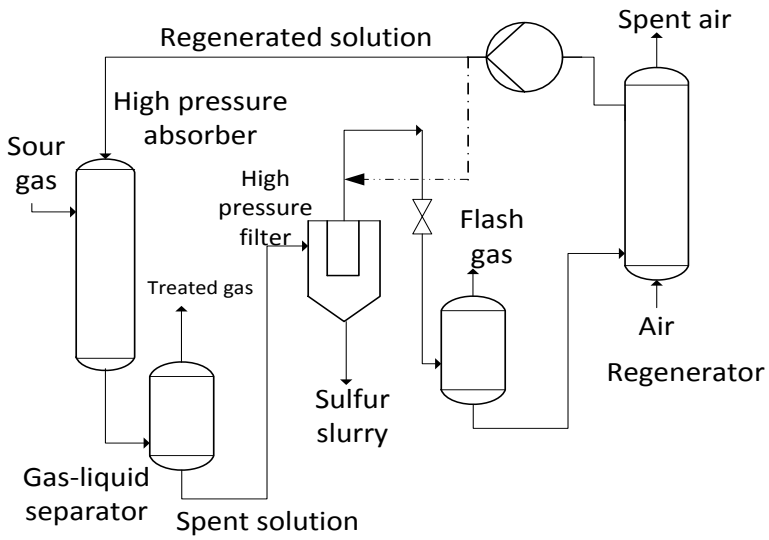

Figure 2-14 Schematic flow diagram of Sulfint

Figure 2-15 Schematic flow diagram of Sulfint HP

The absorber is designed as a co-current gas-liquid contactor filled with static mixer elements. The treated sweet gas is separated from the solution in a high pressure drum. A water wash section (not shown) is included in the upper part of this separator drum, in order to remove any trace of catalytic solution from the treated gas. The spent catalytic solution loaded with sulfur particles is then filtered at high pressure in a pressurized bag filter with proprietary design. The sulfur loaded liquid flows from the outside of the filter cloth through the filtration media and the filtrate is recovered on the inside of the cloth. It is then sent to an expansion valve and from there to a flash drum where the flashed gas is separated. The remaining low pressure solution is then oxidized by contact with atmospheric air in the regenerator vessel operating as pulsating column at co-current upward flow mode. The regenerated solution is then pumped back to the absorber vessel. The solid cake can easily be removed from the filtration cloth by a reverse flow of clear solution, which is applied batchwise (dotted line in **Figure 2-15**). The cloth then expands, thus allowing the solid cake to break into pieces, which will fall to the bottom of the filter vessel and can be withdrawn from there. Reportedly, the regenerator vessel in the GDF pilot plant is designed to have an adjustable volume (i.e. difference in volume is achieved by pulsation) up to 50 liter (Ballaguet, J.P. et al., 2001). It is claimed that a regeneration rate enhancement of factor 30 has been achieved due to the pulsatile operation mode. However, like all other commercial chelated-iron systems, simultaneous removal of CO_2 cannot be performed by both Sulfint versions without other additives. The following section reports about a development initiation in the area of chelated-iron technologies.

2.3.4 GAS/SPEC RT-2

The GAS/SPEC RT-2 technology was developed by Dow Chemical's Oil, Gas & Mining branch for removing H_2S entrained in steam at geothermal power plants (Bedell, S. A. et al., 1987). Reportedly, the HS^- ions present in the condensate from the turbine of the plant were treated with ferric chelates of HEDTA. However, the solid sulfur produced this way is oxidized to water soluble sulfur oxides by reaction with sulfur dioxide in order to prevent fouling of the equipment in the power plant. As for other iron-chelate techniques, also for Dow Chemical´s technology oxidative degradation of the ligand has been an issue. To this end, regeneration of the catalyst is carried out electrolytically under absence of oxygen (Wubs, 1994). This regeneration method is reportedly not further developed due to the significance of power costs. Hence, further researches are focused on the development of appropriate inhibitors against oxidative degradation.

After outlying the potential and the limitations of common iron-chelate technologies, the following section gives an overview about the economics of these which chiefly is affected by the characteristics of their scrubbing solution.

2.4 Cost driving factors for liquid redox processes and their relation to solvent system properties

As studied in the previous sections, general operation principals of all of the state of the art chelated iron technologies are comparable to each other whereas the exact chemical compositions of the solutions are unique. The following issues are important to understand how process variables related to properties of the operating solution interact to affect key parameters of process economics:

Capital expenditures (CAPEX): The capital costs are influenced mainly by the following factors:

- plant size parameters which are impacted by circulation rates and the total solution inventory
- complexity of the whole process (number of equipments) and of the individual units
- material requirements resulting from the chemical nature of the substances handled (corrosiveness)
- design requirements resulting from operating parameters, mainly pressure (thickness of equipment walls)

- other elements of capital investment which are not directly affected by equipment size such as license fee, engineering, procurement services, construction management and commissioning.

Since the complexity and the corrosiveness are comparable for all chelated-iron processes, the operating parameters, especially the solution pump around ratio is the main factor determining the capital cost of plants applying liquid redox approach. The circulation rate is a function of given H_2S concentration of the sour feed gas and the iron content of the scrubbing solution.

Operational expenditures (OPEX): The main elements contributing to the OPEX of chemical plants are:

- Chemicals, utilities, maintenance as well as labor and plant management, etc.

The weighing between these items is individual for each process. For liquid-redox processes, chemicals and utilities are most important, and these two cost groups are the ones which are significantly influenced by the specific technology and the composition of the solvent system. Thus, they will be focused on in more detail, as follows:

Chemical costs: Those are functions of mainly the following factors: iron concentration, chemical loss (oxidative and/or thermal degradation) and mechanical loss through the sulfur separation. Mechanical catalyst loss varies with the sulfur removal method used in the process and can be minimized by applying an appropriate filtration method subsequent to an effective washing. Chemical catalyst loss depends mainly on the oxidative resistance of applied liquid system especially the type of chelating agent. Replacement costs can therefore be reduced by choosing an appropriate chelating agent and advantageous operating parameters (e.g. low temperatures). More concentrated solutions would offer benefits in equipment size (CAPEX), but drawbacks on catalyst loss both mechanical and chemical (OPEX). Therefore, the influences of various iron concentrations of the solutions on the technical as well as economical performance of the process should be investigated.

Utility consumptions: Since most of these processes are operated at temperatures around ambient, there is usually only moderate need of utilizing steam (except for purification of sulfur) or cooling water. The most costly utility is electric power determined by the circulation pumps and the blower or compressor for regeneration air. When a large pressure difference exists between the absorber and the regenerator, pumping costs increase rapidly. To counter this effect, the solution circulation rate can be reduced by increasing its iron-chelate concentration. However, the increasement of the iron-chelate concentration is a challenging process due to solubility constraints and can be improved only to a moderate extent by addition of primary and secondary components to the solvent system (refer to **Figure 2-5**).

Maintaining the pH of the solution at an optimum trade-off is also a key feature with impact on the both CAPEX and the OPEX of these kinds of processes, since pH influences the following phenomena:

- The solubility and stability constraints of chelated-iron solutions → impacts on reaction kinetics of both absorption and regeneration and thus on equipment size (CAPEX)
- Occurrence of side reactions → formation of by-products → necessitation of chemical make-up → (OPEX)
- Solubility of gases → requirement of higher pressures or higher solvent circulation ratios→ higher/larger equipment with thicker walls (CAPEX) and more energy demand→ OPEX
- Corrosion rate → impacts on cost of applied material (CAPEX) and requirement of corrosion inhibitor → OPEX

Addressing the issues mentioned above, various absorbents and chelating agents are to be selected and new formulations of liquid systems containing those chelating agents and/or absorbents will be investigated in order to explore improvement possibilities. These are presented in the following chapter. Detailed economic evaluations on selected formulations will be discussed later in chapter 6.

3 DEVELOPMENT AND SCREENING OF ALTERNATIVE SOLUTIONS FOR LIQUID REDOX TECHNOLOGY EMPLOYING AMINO ACID SALTS (AAS)

3.1 Holistic approach for solvent system development

As it was discussed in detail in chapter 2, the chemical nature of the state-of-the-art-liquid-redox solvent systems causes operational obstacles and stability problems which let them be economically impractical for treating highly variable acidic gas loads - especially for significant fractions of CO_2. Siemens AG has developed a proprietary liquid redox technology to ensure high specific H_2S and CO_2 removal capacity per unit of circulating solution as well as low absorbent and chelating agent degradation rate. Initial technical and economic studies in the early step of the development showed that the energy requirement, and thus, the economics of the technology are closely related to properties of the applied solvent system. This gives the motivation for the investigations on new solvent systems as well as on economic and compact process design.

Within the scope of the rest of this study, the following stepwise, holistic approach for solvent system development has been taken:

- identification and pre-selection of potential candidates for absorbents and chelating agents throughout literature review (section 3.4)
- determination of attractive components (in terms of their oxidative resistance) by screening stability tests (section 3.5):
    - of pre-selected chelating agents, with formulation of blends (each consisting of two chelating agents) as a result
    - of pre-selected absorbents in solvent systems all containing the same metal and the same chelating agent
- formulation of several solvent systems consisting of the most promising components (section 3.5.3),
- technical evaluation of the selected formulations (chapter 4); throughout benchmarking experiments including investigations on regeneration kinetics (section 4) and techno-economic feasibility parameters in continuous operation (section 4.2),
- implementation of detailed degradation studies (chapter 5).

For these investigations, three different test rigs in lab scale were constructed and operated. Deducted from the benchmarking results and serving as consecutive steps for completing the solvent system development, economical evaluations (chapter 6) on the selected formulations will be executed. The results of these studies will reveal the key parameters to achieve the goal of an environmentally friendly, stable and easy operable (technical issues) as well as cost-efficient (economic issues) sour gas treatment process based on the liquid redox method.

As a starting point of the approach given above, a short outline of special features of the Siemens liquid redox technology is presented in the following section. Thereafter, the desired properties of the solvent sytems which can be appropriate to meet the specifications of the technology are highlighted. These will provide a basis for the pre-selection of the components to be screened as presented in the later sections of this chapter.

Parts of Chapter 3 are published as:
Sönmez, H. G. et al. (2015). Investigations on characterization of catalytically activated liquid systems for sour gas treatment. Paper presented at GPA Europe Technical Conference – Gas Treatment and Liquefaction Processes for Natural Gas, Hamburg, Germany, April 22-24, 2015.

3.2 Features of the Siemens liquid redox technology

The technology is intended to be integrated as a sour gas treatment unit into combined and/or open cycle power plants which enables the in-situ treatment of even ultra-high sour gases (H_2S_{in} ≈ 30 vol%; CO_{2in} ≈ 20 vol%) and the direct conversion of the treated gas (H_2S_{out} < 1 ppmv; CO_{2out} ≤ 20 vol%) into electricity on drilling platforms (for the simplified configuration see **Figure 3-1**). The specific targets of the technology are:

- low CAPEX,
- low OPEX,
- small footprint (compact design is of high interest - especially for offshore applications),
- high turn down capacity, and thus, broad applicability.

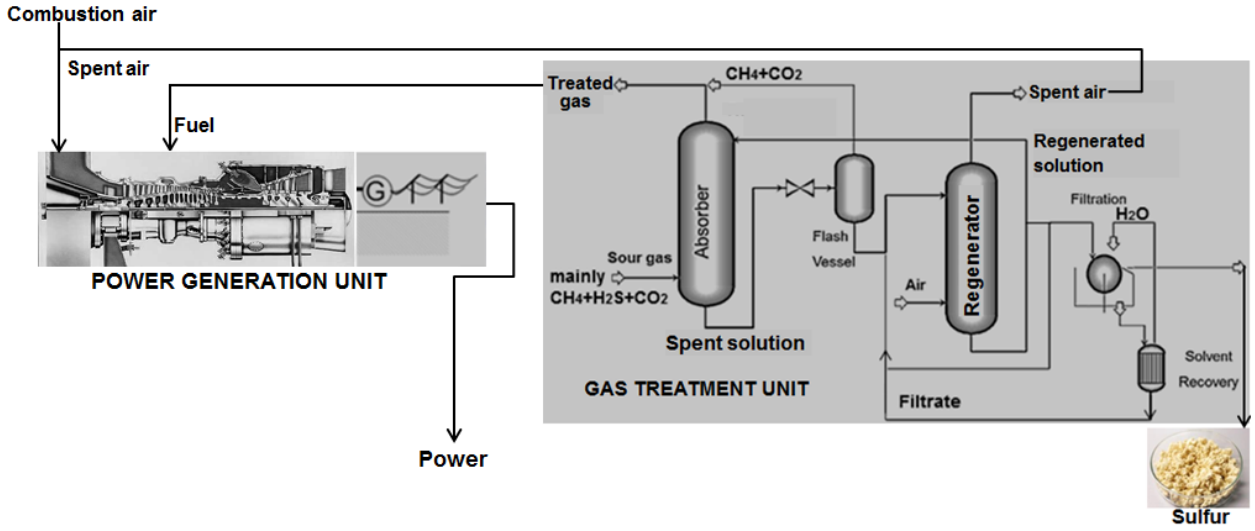

Figure 3-1 Schematic configuration diagram of integrated sour gas treatment technology of Siemens AG (Siemens AG, 2016)

As shown in **Figure 3-1** (Siemens AG, 2016), the gaseous H_2S, a significant fraction of the CO_2, other sulfur contaminants (e.g. RSH, COS, CS_2) and some traces of CH_4 are absorbed from the sour gas in the novel catalytic washing solution (i.e. AAS + chelated metal) in the absorber. The H_2S is oxidized there and converted completely into disposable, non-toxic elemental sulfur in the liquid phase. Absorption is performed at (T_{abs} ≈ 25 to 35 °C) and at a pressure (P_{abs} ≈ 20 to 40 bara) which is higher than the pressure of the combustor of the turbine (P_{com} ≈ 12 to 24 bara dependent on the applied class of Siemens gas turbine) in order to compensate the pressure drop and, thus, to maximize the efficiency of the combustion engine. The treated gas leaves the top of the absorber, the spent solution, which contains elemental sulfur and dissolved gases (CO_2 and some CH_4), is sent from the absorber bottom through an expansion valve into a flash drum, where most of the dissolved gases are flashed at P_{flash} ≈ 2 to 3 bara i.e. separated from the solution and sent to the gas turbine after compression (compression step is not shown in the figure above). Regenerating of the washing solution with respect to CO_2 is achieved in three units of the treatment plant: (1) in the upper part of the absorber by chemical displacement of the CO_2 with the dosed H_2S (2) in the flash vessel by pressure swing (3) in the regenerator by stripping of it with the sparged air, respectively. Following the flash vessel, the spent solution is forwarded to the regenerator where the catalyst is converted back to its regenerated form using oxygen at T_{reg} ≈ 25 to 35 °C and P_{reg} ≈ atm. to 10 bara. The main stream of the regenerated solvent is returned to the absorber. Due to the fact that no heat is required for the regeneration of the process solution (i.e. oxidation of the reduced metal catalyst and CO_2 desorption), and, consequently, no heat exchange equipment is considered as auxilary of the regenerator which thereby provides substantial savings in TOTEX. However, the heat generated from the absorption of acidic gases is to be compensated by a heat exchanger supplemental to the absorber (not shown in the figure). The solid sulfur product is withdrawn by means of a split stream of the regenerated solvent and is

sequestered in a sulfur separation unit which consists of a filter press (automated, enclosed and continuous - refer to **Figure 2-4g**), a cake-washing unit and a solvent recovery unit with complete auxilaries such as feed pumps, storage vessel, vacuum and compressed air systems (not shown in the diagram). The solvent recovered from the sulfur separation unit is refed into the regenerator so that the cycle is completed in the gas treatment unit.

The treated gas streams from absorber and flash vessel containing mainly CH_4 (and some CO_2) and the spent air of the regenerator are fed into the gas turbine after compression up to the required combustion pressure. Here it should be noted that the CO_2 in the treated gas stream does not disturb the operation of the Siemens gas turbine up to a concentration of 10 vol% in the fuel gas (Siemens AG, 2016). The spent air from the regenerator is supplemented by additional air for combustion taken from the environment. The turbine is associated to an AC electric generator which can be a 50 or 60 Hz machine depending on the combustion engine and/or regional grid specifications. The plant is equipped with an inlet cooler to reduce the temperature of the inlet air and to include the selective catalytic reduction (SCR) and a reactor for NO_x reduction (for the descriptions refer to section 1.3) to prevent potential gas emissions.

The typical composition of natural gas (which varies depending on the origin of the gas) was given in **Table 1-1** (Speight, 2013). Accordingly, although the H_2S and the CO_2 are the main acidic components to be removed from the sour feed gas, other contaminants such as RSH, COS and CS_2 may also be present in the sour natural gas streams. There are a lot of different reactions taking place between the applied solvent system and constituents of the gas to be treated. Some of them have been well investigated for the state of the art liquid redox processes employing water-based inorganic absorbents and chelated metal catalysts as solvent system (Kohl, A. L. et al., 1997). However, these reactions are so far largely unknown for all formulations investigated within this study. The known reaction steps between the main acidic gas components and solvent system in the treatment unit can be classified as following:

(1) CO_2 absorption into the absorbent in absorber (referring Eq.2-8; where the absorption reaction taking place differs depending on the type of the absorbent; for AAS see Eq.3-2 and Eq.3-3)
(2) H_2S absorption and its subsequent dissociation by the absorbent in absorber (referring Eq.2-4
(3) Oxidation of the absorbed H_2S into elemental sulfur in absorber by reduction of the chelated catalytic agent (referring Eq.1-9)
(4) Flashing of the absorbed CO_2 to a large extent (≥ 50 vol%) in the flash drum (see **Figure 3-1**) by pressure decrease and to a minor extent in the absorber by chemical desorption per dosed H_2S (Kohl, A. L. et al., 1997) and stripping of it in the regenerator by air sparging
(5) Oxidation of the reduced chelated catalytic agent into its active form in regenerator by using the O_2 from sparged air (referring Eq.1-10)
(6) Consecutive or side reactions of the products emerged from the reaction mechanisms above.

All the above-mentioned aspects of the solvent systems to be developed are depending on the physical and chemical properties of the two main constituents (absorbent and chelating agent) of it. Thus, components with the following properties are of high interest:

- **absorbents** which favor the reactions of mechanisms (1) and (2) and give the system flexibility in terms of CO_2-loading,
- **chelating agents** which promote the reactions of the mechanisms (3) and (5) and help to achieve larger desulfurization capacity by possessing larger complexing capacity for the metal catalyst.

Consequently, **solvent systems**, hindering the undesired side reactions and simultaneously contributing to other desired characteristics from the gas treating point of view in general and from the liquid redox point of view in particular are of high interest. These are presented in the following section.

3.3 Desired solvent system characteristics for the evaluated liquid redox process

An overview of the most important characteristics of solvent systems to be applied for gas treatment is given in **Table 3-1** with the different approaches to investigate them in the scope of this work. The arrow symbol indicates the direction of the change in ascending order (arrow points up, ↑) or in descending order (arrow points down, ↓), both for the desired direction of the characteristic and for the related impacts on corresponding parameters.

Table 3-1 Desired characteristics of solvent systems -compiled from (Mathias, P. M. et al., 2012) and (Hoff, K. A. et al., 2012)

Characteristic (and desired direction)		Function of, (-) Impact on, (➢)	Approach in this study
Stability (↑)	Thermal stability (↑)	-Molecular structure of the constituents -Operation conditions of the process (e.g. temperature, pH, ionic strength, O_2-content and residence time) ➢ Thermal stability (↑), flexibility of process (↑),chemical make-up (↓), OPEX (↓) ➢ Chemical stability (↑), chemical make-up (↓), OPEX (↓)	Screening tests (section 3.5)
	Chemical stability (↑)		Screening tests (section 3.5), stirred cell (batch) and continuous experiments (chapter 5)
Performance (↑)	Mass transfer and reaction kinetics rates for absorption and regeneration (↑)	-Depend on the fluid flow phenomena ➢ Loading capacity (↑), circulation ratios and equipment size (↓) ➢ OPEX and CAPEX (↓)	Stirred cell experiments (batch mode) (section 4.1)
	Loading capacity (↑)	-Composition and concentration of active material ➢ Solution circulation ratio and equipment size (↓) thus OPEX and CAPEX (↓)	Literature and benchmarking experiments (section 4.2.4)
	Regenerability (↑)	-Molecular structure of the constituents ➢ Energy demand for regeneration (↓), OPEX (↓) ➢ Required contact time for regeneration (↓) thus equipment size and CAPEX(↓)	Literature and benchmarking experiments (section 4.2.4)
	Selectivity (↑)	-Molecular structure of the constituents ➢ Required contact time (↓) thus equipment size and CAPEX(↓)	Literature and benchmarking experiments (section 4.2.4)
Viscosity (↓)		-Function of density, temperature and ionic strength ➢ Mass transfer and reaction rates (↑) ➢ OPEX und CAPEX (↓)	Measurements by capillary-tube-type viscometer (see Appendix A-2.3)
Volatility (↓)		-Depends on vapor pressure (↓) ➢ Solvent slip, emissions (↓) ➢ Chemical make-up (↓) and OPEX (↓)	Literature review
Operability (↑)		-Depends on: fouling and crystallization tendency (↓), foaming tendency (↓), corrosivity (↓), viscosity (↓) ➢ OPEX (↓)	Literature, benchmarking and corrosion tests (sections 4.2.5 and 4.2.7)
HSE issues		Flash point ($<<T_{op}$), toxicity(↓), volatility (↓), biodegradability (↑),	Literature (i.e. the MSDS)
Cost (↓) and availability (↑)		Readily available chemicals with reasonable prices are preferred	Literature and communication with diverse vendors

Additional information of the overall process parameters and their associated interactions between the addressed characteristics can help to understand the economic impacts of the solvent system properties in detail. Thus, the supplemental descriptions of the individual characteristics remarked in **Table 3-1** are given in Appendix A-1.1.

Once the required features of the solvent systems to be developed were determined, the most appropriate constituents of it are to be chosen based on literature review, as it is discussed in the next successive sections.

3.4 Pre-selection of potential constituents of alternative liquid redox solvent systems

3.4.1 Absorbent pre-selection

The commercial and/or chemical names of liquid absorbents used for the gas sweetening technologies discussed in section 1.4 are given in **Table A- 1** in Appendix A-1.2 (Younger, 2004). They can be categorized as it is shown in **Figure 3-2** to provide an overview on their chemical nature, and thus, the evaluation of their suitability to the specific targets of the considered technology (see section 3.2) as liquid redox absorbents.

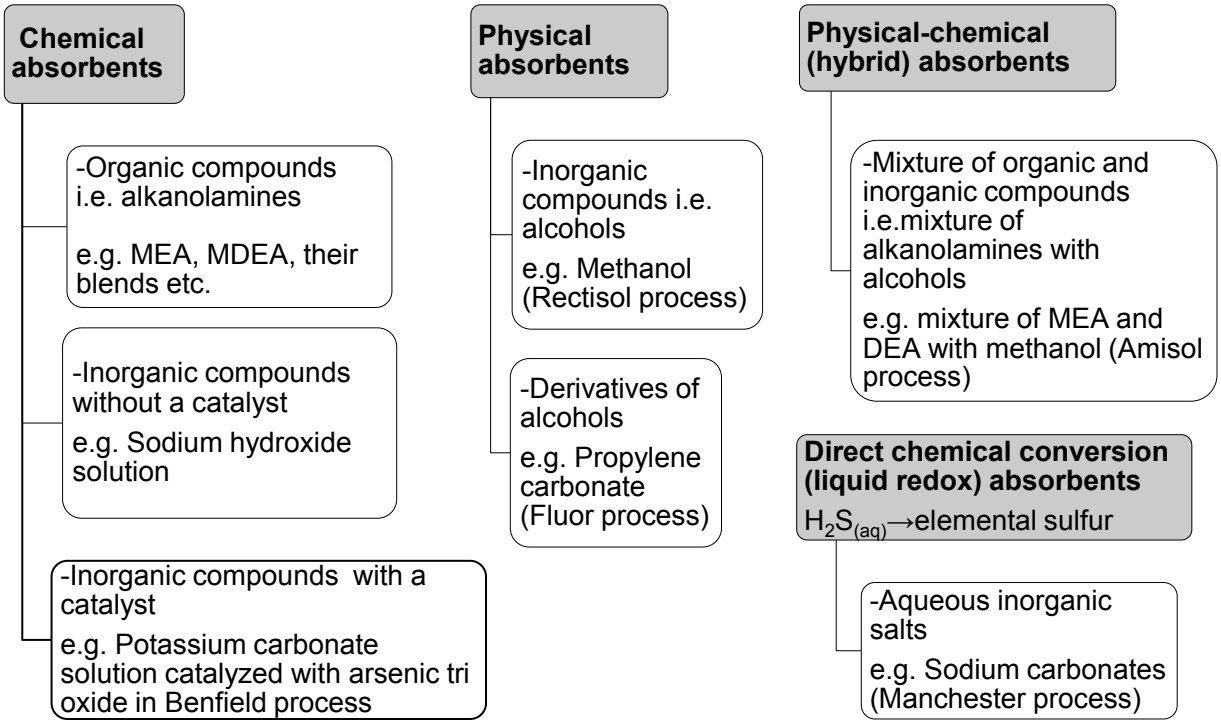

Figure 3-2 Categorization of conventional absorbents for gas sweetening - deduced from (Younger, 2004) and (Kohl, A. L. et al., 1997)

Most frequently used **chemical absorbents** have been alkanolamines, because they are highly reactive towards H_2S and CO_2 (Kohl, A. L. et al., 1997). Nevertheless, they feature some drawbacks such as volatility and solvent degradation due to undesired side reactions, especially with O_2. Besides that, the presence of other gas impurities (such as COS, RSH, etc.) leads to irreversible reactions with amines, thus causing excessive loss of the absorbents or requirement of advanced reclaiming concepts to separate and remove formed salts from the system. Although **physical as well as hybrid absorbents** given in **Figure 3-2** feature higher absorption capacities as well as higher attainable purities than chemical absorbents when applied at elevated pressures, they are reportedly not feasible for the treatment of gases with CO_2 partial pressures lower than 3.5 to 7.5 bara (refer **Table 1-5**) (Younger, 2004). Despite of the fact that **inorganic salts** applied as liquid redox absorbents (the state-of-the-art) may be attractive compared to chemical absorbents regarding the volatility, they are reportedly not capable to remove CO_2

simultaneously. Addition of some organic compounds (see **Figure 2-5**) to absorbent liquid is necessary to ensure (1) maintaining the solution pH in a stable operating range and (2) separation of also CO_2 from feed gas (but still bulk amounts are not reached). Thus, taking the desired characteristics of solvent systems given in **Table 3-1** and above-named obstacles of other absorbents into account, the AASs are worth to be considered as absorbents to be applied in liquid redox technique. The following subsections first give an outline on generic information related to AAS, thereafter, the beneficial properties of AASs when applied for liquid redox technique and consequently presents the pre-selected candidates for the subsequent experimental investigations.

3.4.1.1 Amino acid salts (AAS)

In the scope of this section, first, some general information about the chemical structures of AAS and their reactivity towards acidic gases is given whereafter the selection criteria are lightened from the liquid-redox technique point of view as presented in the subsequent subsections.

3.4.1.1.1 Molecular structures of amino acid salts

The basic chemical structure of amines and amino acids (AA) is similar, and AAs are a subgroup of amines. All amines can be described as derivatives of ammonia (NH_3), by replacing one or more hydrogen atoms (H) with functional groups ($R_{x=1,..,3}$; alkyl[5] or aryl[6]). The main characteristics of an AA is the presence of either a carboxylic (-COOH) or sulfonic acid group (-SOOOH) as part of a functional group attached to an amino group, i.e. the nitrogen (N) (see **Figure 3-3**) (Creighton, 1993).

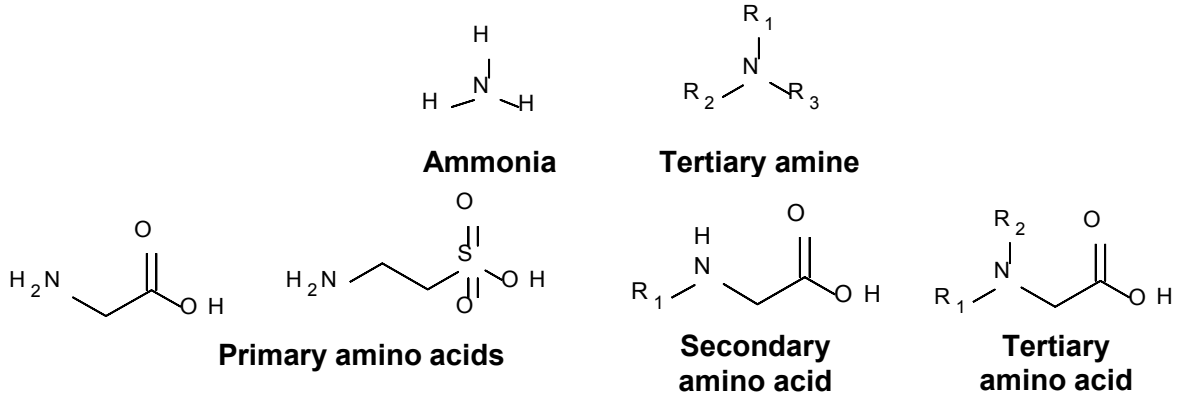

Figure 3-3 Chemical structures of ammonia, tertiary amine and amino acids (Creighton, 1993)

Alike amines, amino acids can be categorized as primary, secondary and tertiary depending on the number of substituents other than hydrogen linked to the (N). In a primary amino acid only one H atom of the ammonia is substituted by a functional acid group. If a second or even a third replacement of H atom with arbitrary side chains takes place, it becomes either a secondary or a tertiary AA, respectively (refer **Figure 3-3**).

Since an AA shows either the functionality of an acid (carboxylic or sulfonic group) or a base (amino group) in aqueous solution at a certain pH (isoelectric point), it is present as a zwitterion (both as cation and anion) (i.e. the form II in reaction Eq.3-1) (Majchrowicz, 2014).

$$\underset{\text{I}}{\mathrm{HOOC-R-NH_3^+}} \underset{+\mathrm{H^+}}{\overset{-\mathrm{H^+}}{\rightleftarrows}} \underset{\text{II}}{\mathrm{OOC^--R-NH_3^+}} \underset{+\mathrm{H^+}}{\overset{-\mathrm{H^+}}{\rightleftarrows}} \underset{\text{III}}{\mathrm{OOC^--R-NH_2}} \leftrightarrow \underset{\text{IV}}{\mathrm{HOOC-R-NH^-}} \qquad \text{(Eq.3-1)}$$

[5] An alkyl substituent is an alkane missing one hydrogen atom (C_nH_{2n+1}).

[6] An aryl can be any substituent which is derived from an aromatic ring.

This compound has no overall electrical charge but it contains separate functional groups, which are positively or negatively charged depending on the pH of the solution and contribute to the overall ionic strength (α_{ion}) of the molecule. In acidic solutions, the amino group of the zwitterion is protonated whereas the carboxyl group is deprotonated (form I in reaction Eq.3-1), vice versa in an alkaline media (i.e. form III in reaction Eq.3-1). This property influences especially the solubility of gases in liquids. In order to form an AA, the acidic side chains (carboxylic or sulfonic group) are neutralized by addition of a proton (cation) to produce the salt of the amino acid (AAS), as it is illustrated in **Figure 3-4**. As cation usually potassium (K) is applied, but also lithium (Li) or sodium (Na).

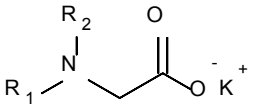

Figure 3-4 General molecular structure of a potassium salt of a tertiary amino acid with carboxylic group (Creighton, 1993)

Each functional group shown in **Figure 3-4** gives the AAS its special characteristics (Hook, 1997):

- the attachment of a cation to the functional groups contributes to alkalinity and thus the absorption capacity of acidic gases into an AAS solution.
- the amino group is the active center for acidic gas uptake.
- the functional groups bond to the amino group (i.e. R_1 and R_2) influence the stability or reversibility of the absorption products (Majchrowicz, 2014).

After giving a short outline on the impacts of the each functional group of an AAS on its characteristics, the possible reaction pathways of an AAS with acidic gas components are to be discussed as illustrated in the following subsection.

3.4.1.1.2 Reaction pathways of amino acid salts

In general, the way a specific AAS reacts with acidic gases depends on many factors including the structure of the amino acid, e.g. primary, secondary or tertiary, steric hindrance and number of amino groups in the molecule. The main reaction steps between the most important acidic gas components (i.e. the H_2S and CO_2) and the solvent system were listed through (1) to (6) in section 3.2. To rephrase them from the liquid-redox-technique point of view:

- In liquid redox absorbers, the H_2S and CO_2 are absorbed into AAS-based solvent systems containing catalytic and chelating agents.

- The reaction of the H_2S in the applied solvent system is instantaneous as long as the required alkalinity is provided. The liberation of the liquid system from ionically bonded H_2S is achieved -also instantaneously- by the oxidation and the conversion of it irreversibly to elemental sulfur with the catalytic agent in the solvent system.

- However, the reactions interacting between the CO_2 and the AAS-based solution system as well as the release of it from the system (i.e. the stability of the reaction products) are different than those for H_2S.

The equilibria between the CO_2, its ionic species and an amine are illustrated in **Figure 3-5** (Fischer, 2013) which is reportedly analog to reaction routes of CO_2 in AAS based solution systems. (Hook, 1997) stated that the redominating reaction route depends on respective parameters such as molecular structure and the concentration of the AAS, the temperature, and the pH-value of the solutions system.

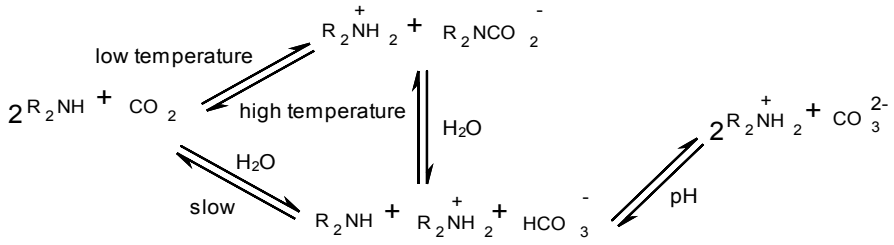

Figure 3-5 Reaction routes for CO_2 absorption in amine based solutions (analog to reaction routes of CO_2 into AAS based solutions) (Fischer, 2013)

Accordingly, the CO_2 absorption reaction pathways of different AAS can be classified into two main groups depending on the bonding between CO_2 and AAS (Majchrowicz, 2014):

(1) **Bicarbonate route:** This type of reaction route consists of **ionic bonding** of the CO_2 with OH^- ions in the aqueous solvent system yielding bicarbonate, HCO_3^- (at low pH) or carbonate, CO_3^{2-}(at high pH) and the deprotonated form of the AAS (representatively shown as an amine in Eq.3-2) where the equilibrium between them depends on the pH of the solution (see **Figure 2-9**). As it can be deduced from the Eq.3-2, one mole of AAS is needed for one mole of CO_2 for absorption via the bicarbonate route, which would allow high carrying capacity. However, this reaction is reportedly slow and thus can be a rate limiting step.

$$CO_{2(g)} + H_2O + R_3 - N \leftrightarrow CO_{2(aq)} + OH^- + H^+ + R_3 - N \leftrightarrow R_3NH^+ + \underset{\text{Bicarbonate}}{HCO_3^-{}_{(aq)}} \qquad \text{(Eq.3-2)}$$

The reaction is simply shown for a tertiary amine but applies to primary, secondary and tertiary AAS, as well. However, it is reportedly predominant for the absorption of CO_2 into tertiary or sterically hindered AASs where the carbamate formation (see Eq.3-3) is not stable or does not even exist (Fischer, 2013) as explained in the following route:

(2) **Carbamate route**: the CO_2 is bonded to the N within the AAS via a **covalent bond** yielding carbamate formation, preferably at low temperatures (see Eq.3-3).

$$\underset{\text{III}}{2\ OOC^- - R - NH_{2(aq)}} + CO_{2(aq)} \underset{\text{fast}}{\Leftrightarrow} \underset{\text{Carbamate}}{OOC^- - R - NH - OOC^-} + \underset{\text{II}}{OOC^- - R - NH_3^+} \qquad \text{(Eq.3-3)}$$

The carbamate undergoes hydrolysis resulting in the appearance of a deprotonated AAS and HCO_3^-/CO_3^{2-} (depending on the solution pH see **Figure 3-5**). The deprotonated AAS can then react with CO_2. As it can be seen from the Eq.3-3, two moles of AAS are required per mole of CO_2 to be absorbed. The carbamate formation reaction is reportedly more rapid than those occuring in the bicarbonate route, where the absorption product is more stable, however. Faster reaction kinetics lead to reduction in absorber size, but the formation of more stable absorption products necessitates higher energy supply to the system to liberate the AAS from absorbed CO_2. The CO_2 reacts with primary AAS mainly via this route.

So the functional groups of the AAS given in **Figure 3-4** are specific to each AAS, they determine main chemical and physical properties of it as well as its reactivity, thus, provide a basis for the selection of the AAS type to be applied as liquid-redox absorbent - as presented in the following subsection.

3.4.1.2 Selection criteria of AAS as absorbents for liquid redox applications

Keeping the abovementioned molecular structures of AASs and their reactivity with the acidic gas components of the high interest (H_2S and CO_2) in mind, the following advantages of them compared to conventional gas-sweetening absorbents given in **Figure 3-2** - making them suitable and promising for H_2S and CO_2 absorption from sour natural gas by liquid redox technique - can be pointed out as:

- robust technical superiority and fast absorption kinetics (both for H_2S and CO_2), compared to all state-of-the-art absorbents (Sönmez, 2014)
- oxidative stability and negligible volatility, compared to alkanolamines (Fischer, 2013),
- applicability for a wide range of partial pressures of acidic gas components, compared to physical as well as hybrid solvents (Hogendoorn, K. J. A. et al., 2008).

Thus, the decisive properties of AAS and their main impacts on the process provide a basis for the selection of the AAS type to be applied as liquid-redox absorbent and can be listed as given in **Table 3-2**.

Table 3-2 Decisive properties of AAS as absorbents and their impacts on the sour gas treatment process -deduced from (Hoff, K. A. et al., 2012)

Characteristic (desired direction)	Impact, (➢ and desired direction)
Base strength (↑)	➢ Reactivity with acidic gas components (↑)
Distance between amino group and side chains (↑)	➢ Oxidative stability (↑), thermal stability (↑) ~ absorbent loss (↓) ➢ Emissions of volatile components (e.g. NH_3) from decomposition (↓) ➢ Corrosivity (↓) ➢ Base strength (↓)
Molecular weight (↓)	➢ Carrying capacity for CO_2 and H_2S (↑) ➢ Circulation ratio (↓)
Water solubility (↑), precipitation (↓)	➢ AAS concentration (↑) ➢ Circulation ratio (↓) ➢ Operability (↑)

Note: Arrows indicate the desired influence direction

- The **base strength** is a function of the molecular structure i.e. the chemical configuration of the amino group and its substituents (Majchrowicz, 2014). The reactivity of an AAS with acidic gases is strongly dependent on its base strength meaning initial absorption rates of the acidic components increase with the rise in the basicity of AAS.

- The **distance between amino group and side chains** also determines the stability (both thermal and oxidative) of the molecule by influencing the accessibility of the amino group. Aliphatic and/or aromatic side chains in the proximity of the amino group shield the nitrogen atom from electrophilic attack. Steric hindrance occurs when bulky substituents adjacent to the amino group are introduced. The size of these groups prevents or delays chemical reactions that are observed in related smaller molecules (Hook, 1997). A trade-off analysis is required to determine the optimal steric hinderance level of the molecule since superior steric hinderance is beneficial with regard to stability of the molecule against oxidative attack whereas low steric hinderance is required for a robust absorption process.

- **Molecular weight** of an AAS is an important criterion since it influences the loading capacity per solution circulation (i.e. mol_{gas}/mol_{sol} or kg_{gas}/kg_{sol}) and thus solvent inventory, required pumping energy and equipment size (Hogendoorn, K. J. A. et al., 2008).

- High **water solubility** of an AAS reportedly creates beneficial conditions regarding the broad window of operation without solid formation (Majchrowicz, 2014). Besides this, AASs possessing high water solubility enable a reduction in the required solution circulation ratio resulting from higher AAS concentrations.

- Reportedly, **precipitation** of certain reaction products of the AAS and CO_2 occurs, either at high concentrations of the AAS or high partial pressures of CO_2 depending on the type of AAS applied (Aronu, E. U. et al., 2013). When the precipitation begins, the CO_2 equilibrium partial pressure above the resulting slurry remains almost constant if also the solid phase under formation is considered as solution loading. It is stated that this might result in higher solvent loadings. However, the precipitation of the AAS is generally considered as a drawback, since such solutions exhibit poor CO_2 desorption potentials. In addition, precipitates will necessitate additional measures from the slurry handling point of view and mechanistic considerations and thus are not desired.

Once the decision for AAS as appropriate liquid redox absorbents had been taken, the pre-selection of potential amino acid candidates was done with a systematic variation in molecular structures, evaluating whether they were primary, secondary or tertiary, sterically hindered or not - depending on the process requirements. All the pre-selected amino acids were neutralized by adding a strong base (KOH) and thus producing potassium salts of them as listed in **Table 3-3**. Primary AASs (e.g. glycinate, alaninate and taurinate) feature high alkalinities and thus the fastest kinetics. However, the reactive nitrogen possesses a good accessibility, which makes them less resistant against oxidative attack than others. Tertiary AASs (e.g. dimethylglycinate) show slower absorption reaction kinetics, but higher stability of the molecule itself. Due to their steric hindrance they are labeled as selective towards H_2S in the presence of CO_2. Secondary AASs (like sarcosinate) exhibit moderately fast reaction kinetics and higher carrying capacities for CO_2 and H_2S when compared to tertiary AASs, however, they require more energy for the regeneration (i.e. the release of CO_2) as the stability of the absorption products (stability of formed bonds between CO_2 and AAS) increase from tertiary to primary AAS.

After the potential candidates for absorbents are determined, the next step is the identification of attractive chelating agents. This is presented in the following section.

Table 3-3 Amino acid salts pre-selected as absorbents for this study and their unique properties- compiled from (Majchrowicz, 2014), (Hook, 1997) and (Creighton, 1993)

Alkalinity(↑), reactivity(↑), stability of bond between CO_2 and AAS(↑)

Thermal and oxidative stability of the AAS (↑)

AAS (Process/Licensor)	Properties	Molecular structure	MW (g/mol)	Cost ($/kg)[7]
Glycinate (GV/Giammarco-Vetrocoke)	-Primary AAS with functional group of ($-COO^-$) and not sterically hindered -Used to promote K_2CO_3 as main absorbent in the mentioned process for bulk CO_2 removal from high pressure gas streams	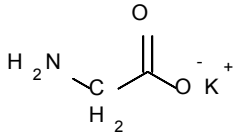	114.17	1-3
Alaninate No commercial application is known	-Primary AAS with functional group of ($-COO^-$) with steric hindrance -Reportedly can be applied for removal of H_2S and/or CO_2 from a variety of gas streams containing other acid impurities such as CS_2	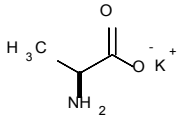	128.19	5-8
Taurinate (CORAL MGA/TNO) (CORAL DECAB/TNO)	-Primary AAS with functional group of ($-SOOO^-$) -Not sterically hindered -Used for CO_2 removal from flue gas streams (MGA process) -Used for CO_2 separation based on the AAS-precipitation-method (DECAB process)	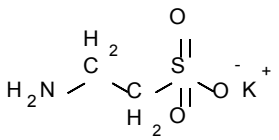	164.24	2-4
Sarcosinate No commercial application is known	-Secondary AAS with functional group of ($-COO^-$) -Not sterically hindered -Reportedly can be employed for CO_2 and/or H_2S absorption	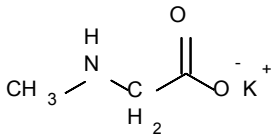	128.19	1.5-3
Solvent-1 and Solvent-2 (PostCap™/Siemens AG)	- Both are secondary AAS with steric hindrance and can be employed for CO_2 and/or H_2S absorption Solvent 1 - Applied for CO_2 capture Solvent 2 - No commercial application yet	n.a.[8]		
Dimethylglycinate (Alkacid-DIK/BASF)	-Tertiary AAS with steric hindrance with functional group of ($-COO^-$) -Selective towards H_2S	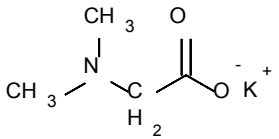	142.22	1-2

[7] Prices (given for technical purity grades 97-99 % and for minimum order quantity of 1 metric tons) were retrieved from http://www.alibaba.com/showroom/bulk-chemical-prices.html on 2nd Feb. 2016.
[8] The data cannot be revealed due to confidentially reasons.

3.4.2 Chelating agent pre-selection

The removal and oxidation of H_2S from sour natural gases to elemental sulfur by the liquid redox technique imposes several requirements towards the chelated metal that is employed as the redox catalyst. As it was mentioned in the section 2.2.1, the chelator does not take part in the redox reactions, but keeps the metal ions dissolved in the solvent system. The reactivity of the metal, however, is highly dependent upon its ligand environment (Martell, 2009). Any change in the environment gives the metal-ligand complex its special characteristics and will affect e.g.:

- **chelating equilibria** between metal and ligand (i.e. thermodynamic influences e.g. formation and stability of the complex)
- **chelator type** (i.e. softer or harder ligand) and molecular structure (i.e. electronic influences e.g. electronegativity etc.)
- **chelator dynamics** (i.e. electron transfer mechanism - steric influences e.g. electron spin state and reduction potential of formed complex etc.)

The choice of an appropriate chelating agent (respectively the combination of chelator and metal) will, therefore, help to optimize the process by:

- promoting kinetics of oxidation of H_2S and regeneration of the reduced metal catalyst → smaller footprint and lower CAPEX of technology
- ensuring long time stability of the applied solvent system → enhancement of performance and reduction in OPEX.

The available technical literature only describes the desulfurization efficiency and stability behavior of the common chelating agents under certain circumstances without referring to a holistic approach on the selection of chelating agents. In the scope of the next section, these issues are addressed.

3.4.2.1 Thermodynamics of the phenomenon of chelating

Before discussing the influences of **chelating equilibria**, **chelator type** and **chelator dynamics** on the chelating phenomenon and the overall process in the next subsections, it must be noted that, in all experimental studies within the context of this work, the same multivalence, monoatomic-transition metal (the Fe), which is highly reactive towards H_2S, was used.

3.4.2.1.1 Chelating equilibria between metal and ligand - thermodynamic influences

In a metal-ligand complex, the ligand forms a coordinated sphere around the metal ions and encases them centrally. The complex formation reaction between the metal ion (Me^{x+}) and the ligand (Lig^{n-}) is expressed with Eq.3-4 and illustrated in **Figure 3-6**.

$$\underset{\textbf{Ligand}}{Lig^{n-}_{(aq)}} + \underset{\textbf{Metal}}{Me^{x+}_{(aq)}} \underset{k2}{\overset{k1}{\rightleftharpoons}} \underset{\textbf{Metal - ligand complex}}{Me.Lig^{x-n}_{(aq)}} \qquad \text{(Eq.3-4)}$$

Figure 3-6 Schematic illustration of the metal-ligand complex formation with EDTA (ligand) and Mangan (metal) taken as example (Welch, K. et al., 2002)

The terms, x^+ and n^- in Eq.3-4, denote the charge of the metal ion (electron acceptor) and the chelator (electron donor), respectively and depend on the type of applied substances. (Welch, K. et al., 2002). The thermodynamic stability of such a complex, referring to the degree of association between the two species involved in the state of equilibrium, is quantitatively determined by the formation constant (K_{ML}) (in other words equilibrium or stability constant) (Clevette & Orvig, 1990) and expressed by the Eq.3-5 where the [Me] and the [Lig] stand for the concentrations of the interacting metal and the ligand, respectively in mol/L, whereas the unit of the term K_{ML} depends on the charges of the respective species which were omitted for clarity.

$$K_{ML} = \frac{[Me \bullet Lig]}{[Lig][Me]} \qquad \text{(Eq.3-5)}$$

$$K_{ML} = f\,(T, c, pH)$$

The thermodynamic characterization of a complex can be obtained from the thermodynamic parameters Gibbs free energy, enthalpy and entropy. They are closely related to K_{ML} which depends on the type and concentration of metal and chelator, the temperature, the ionic strength and the pH of the solution. The larger the formation constant, the more thermodynamically stable is the complex. The logarithm of K_{ML} is directly proportional to the Gibbs free energy of the reaction, which is a criterion to determine whether a certain phenomenon has a tendency to natural occurrence (if the $\Delta G<0$) (Smith & Martell, 1987). The change in the standard Gibbs free energy of the reaction ($\Delta G°$; P~1.0315 bar, T~298 K) and the associated thermodynamic parameters can be expressed by Eq.3-6 where R is the universal gas constant (R= 8.31 J/mol.K).

$$\Delta G° = -RT\ln(K_{ML}) = \Delta H° - T\Delta S° \qquad \text{(Eq.3-6)}$$

An analysis of the interaction between K_{ML} and their component terms reaction heat i.e. enthalpy ($\Delta H°$) and entropy ($\Delta S°$) is essential to develop an understanding of many parameters such as the composition, size, shape, electronic structure of the complex and their dependence on temperature, which influence the stability of a complex (Smith & Martell, 1987). In particular, the entropy term features an enhanced contribution to the chelating phenomenon: The metal-ligand complex formation reaction can be considered as a competitive substitution reaction, where a metal-solvation (hydration) sphere is substituted by a multivalent ligand. Thus, solvation and desolvation of the charged metal species is of fundamental importance in the metal–ligand complexation process. This can account for the increase in entropy since it represents a rise in the disorder of the system, i.e. replacement of the larger hydration sphere around the small metal cation by ligands increases the entropy of the system and favors complex formation. According to Eq.3-6, the higher $\Delta S°$ is, the more negative is the $\Delta G°$ indicating the spontaneity of the chelation process.

In addition to influences of the chelating equilibria on the thermodynamic stability of the complex, also the type of the chelator is of high interest from the reactivity point of view, which is indirectly associated to the thermodynamic stability of the chelated catalytic agent. Therefore, this is presented in the following section.

3.4.2.1.2 Chelator type - electronic influences

As it was discussed in the section 3.2, catalytic agents (metal-chelate complex) promote the conversion of the absorbed H_2S into elemental sulfur (referring the reaction Eq.1-7 in absorber by reduction of the catalytic agent) and the oxidation of reduced catalytic agent (Red^-) into its active form (Ox) (referring the reaction Eq.1-8 in regenerator by using the O_2 from sparged air). In this context, the K_{ML}, which is also a measure of the effectiveness of the formed chelate as oxidizing agent, besides being an indicator of the thermodynamic stability of the formed complex, is a key parameter to be considered in terms of kinetics of the regeneration reaction (Martell, 2009).

The $\Delta G°$ (in joules) can be also expressed as in the Eq.3-7.

$$\Delta G° = -nF\Delta E° \qquad \text{(Eq.3-7)}$$

The term $\Delta E°$ stands for the difference in the standard redox potentials of the two half-reactions (referring the reactions Eq.1-9 and Eq.1-8) (in volts), the term F denotes the Faraday constant (96,500 Joule/Volt.mol) and the n is the number of electrons transferred within the overall reaction (in moles). The criterion leading the reactions Eq.1-9 and Eq.1-8 to proceed is $\Delta G°< 0$, which is equivalent to $\Delta E°>0$. Hence, suitable oxidizing agents are characterized by a high difference in the standard redox potential and vice versa ($\Delta E°>0 \rightarrow \Delta G°< 0 \equiv$oxidative environment; $\Delta E°<0 \rightarrow \Delta G°>0 \equiv$ reductive environment).

After reviewing the impacts of chelator type mainly on the absorption and regeneration reactions, the following section outlines the impacts of chelator dynamics on the chelating phenomenon and indirectly on the regeneration efficiency.

3.4.2.1.3 Chelator dynamics of electron transfer- steric influences

As mentioned in section 3.4.2.1, the value of K_{ML} also depends on the type of the metal ion and its oxidation state, among other factors (Tapscott, R. E. et al., 1969). For instance, the frequently used metal, the Fe, is a first row transition element that can exist in several oxidation states e.g. as Fe(II), Fe(III) and to a minor extent also as Fe(IV). Reportedly, chelates of a metal in its higher oxidation state are more stable than those with the metal in its lower oxidation states. Also different chelators can result in different spin states of the electrons in the same metal, depending on the strength of the ligand field. This dictates whether the electron is transferred by an inner-sphere or outer-sphere mechanism, which controls the reactivity of the applied chelated metal. It seems that in addition to the electronic factors, the geometry and steric of the ligand are also related to the redox potential (E) of the metal complex which is formed. Since one oxidation state of the metal favors a particular geometry, ligands that are better able to accommodate that geometry (due to their steric) will shift the redox potential to a higher redox activity, compared to a ligand that cannot match that geometry.

Taking the brief review on the influences of the equilibria, steric and electronics of the metal-ligand complex on the thermodynamics of the chelating phenomenon and the efficiency of the complex into consideration, the following section describes the selection criteria of the chelating agents contributing to the desired characteristics of a metal-ligand complex described above.

3.4.2.2 Selection criteria of chelating agents for liquid redox applications

For liquid redox applications, a suitable ligand of the metal catalyst has to fulfill several requirements. The factors governing the stabilities (thermodynamic (complex) stability, chemical and thermal stability, i.e. resistance against degradation) of metal chelates and their impacts on process parameters are described in **Table 3-4**.

Table 3-4 Decisive characteristics of chelating agents and their impacts on process parameters- compiled from (Martell, A. E. et al., 1996), (Smith & Martell, 1987) and (Clevette & Orvig, 1990)

Characteristic (and desired direction)	Function of (-), Impact on (➢)
Stability constant (K_{ML}) (↑)	-Type of chelating agent and metal, the c_{ion} and pH of the solution system and temperature ➢ Thermodynamic stability(↑) ➢ Oxidative stability, (↑) ~ however, a thermodynamic stability which is too high may hinder the kinetics of both reduction and oxidation reactions
Electrical charge of ligand	-Type of chelating agent meaning how many electron donating groups it possess ➢ Fast reaction rate of the Fe(III).Lig with H_2S and fast reaction rate of the Fe(II).Lig with O_2 are required
Active pH range (↑~wider range)	-Type of chelating agent and c_{ion} of the solution ➢ Dissociation of the chelating agents (↑)→ Solubility (↑)and thus, kinetics of regeneration reaction (↑)
Nature of donor groups (means either O or N atoms which provide bonds for the metal)	-The alkalinity of the chelating agent and the pH dependence of its dissociation states (see **Figure 2-6)** ➢ More O atoms, solubility of the chelating agents, (↑), chelated catalytic agent concentration (c[Fe•Lig]), (↑) solution circulation ratio for the same acidic gas load (↓) ➢ Oxidative stability of the chelate: ligands containing more N atoms are reportedly more sensitive towards oxygen than those containing mostly O atoms ➢ More O atoms: Oxidative stability, (↑) ~ loss (↓) ~ Corrosivity (↓)
Number of donor atoms bonded to the metal ion (refers denticity of the chelator i.e. monodental, bidental,…,octadental)	- Type of chelating agent ➢ Thermodynamic stability: the most stable complexes will be formed when the number of donor atoms of a chelating agent matches the requirement of the coordination number of the metal ion e.g. the Fe has a coordination number of 6 which can be supplied by a hexadental ligand ➢ Determines the minimum quantity of chelating agent needed (i.e. Lig/Fe ratio (see **Table 2-1**)), thus it influences the cost of the solvent system and the OPEX

Note: Arrows indicate the desired influence direction

Accordingly, to form chelates that are useful as catalysts for the oxidation of H_2S to S, a chelating agent must:

- function in the neutral or mildly alkaline pH range to rapidly absorb the H_2S,
- form sufficiently stable chelates to prevent precipitation of metal hydroxides (e.g. $Fe(OH)_3$ or $Fe(OH)_2$) from alkaline solution,
- provide a low enough difference between the stability constants of the oxidized and reduced form of the chelated metals (referring e.g. K_{ML}(Fe(III)) and K_{ML}(Fe(II)), respectively) to allow reduction of the Fe(III) by H_2S to the Fe(II). If the complexes of Fe(III).Lig are too stable

relative to the complexes of e.g. Fe(II).Lig, the metal ion, e.g. the iron, they prefer to remain in the higher oxidation state and do not oxidize H_2S to S, thus, the catalyst becomes ineffective. Any ligand that produces a difference in the decadic logarithm of the stability constants lower than 4 (see **Table 3-5**) is considered too weak as oxidizing agent (Smith & Martell, 1987).

- Additionally, the stability of the chelates of metals in higher oxidation state (e.g. Fe(III).Lig) must be greater than that of the lower oxidation state (e.g. Fe(II).Lig) to enable the oxidation of the latter by the dissolved O_2 from air. However, a stability of the Fe(III).Lig which is too highmay hinder the kinetics of the regeneration reaction. Chelating agents that stabilize the Fe(II).Lig compared to the Fe(III).Lig are therefore not useful in liquid-redox technique. Although the oxidation of H_2S to S is reportedly instantaneous, the regeneration of the Fe(II).Lig to the Fe(III).Lig has been found as slowest step of liquid-redox processes. The respective regeneration kinetics requires an in-depth experimental study and will be investigated in the scope of section 4.

Chelating agents to be pre-selected must meet the abovementioned chemical and thermodynamic stability criteria and additionally they must be compatible to HSE requirements by primarily not being toxic. The large-scale production costs of chelating agents are also a critical parameter in the overall evaluation of potential candidates. Hence, they should be available in commercial quantities from more than one supplier at moderate cost. Another fundamental criterion relates to the inherent resistance of the chelating agent against degradation by dioxygen reduction products (e.g. superoxide radical, O_2^-) as well as autocatalytical and thermal effects. These conjunctions necessitate a comprehensive experimental study, which will be presented in scope of chapter 5.

Ligands can be divided into two categories:

(1) Soft ligands (neutral charge) with a mixture of nitrogen and oxygen as electron donors. The poly aminopolycarboxylated (APC) ligands are categorized as such since they possess both types of donating atoms i.e. nitrogen in amino groups and oxygen in acetate groups (see **Figure 3-6** and **Table 3-5**).

(2) Hard ligands (negative charge) containing oxygen as electron donor. Examples are more complex organic ligands with heterocyclic structures featuring very basic oxygen atoms such as from hydroxamate, phenolate and catecholate functional groups. They are able to form very stable chelates of Ox (e.g. Fe(III).Lig). This unfortunately leads to very low reactivity toward H_2S, since these Ox-chelates prefer to remain to their original oxidation state (e.g. Fe(III).Lig) rather than to transform into less stable chelates of the Red^- (e.g. Fe(II).Lig) (Martell, A. E. et al., 1996).

The first category is prevailing over the second one because most of the APC ligands are suitable for the oxidation of H_2S under slightly alkaline conditions. Taking this essential information and the K_{ML} values of different chelating agents with the same metal (i.e. the Fe) into account, it seems appropriate to compare the APC chelating agents which are used commercially (e.g. NTA, HEDTA and EDTA) with other members of this group such as imino diacetic acid, diethylene trinitrilo penta acetic acid and trans-cyclohexane-1,2-dinitrilo tetra acetic acid (IDA, DTPA and CDTA, respectively).

Alternative to APCs, some other chelators like the citric acid (from the group of hydroxycarboxylates) and the mannitol (from the group of polyhydroxylated sugars), serve as current hot spots for the formulation of an effective solvent system. They belong to the category of hard ligands and are reportedly highly resistant towards oxygen (due to the lack of amino groups see **Table 3-5**) and also biodegradable and non-toxic.

Thus, **Table 3-5** compares these 8 chelating agents pre-selected for the screening tests.

Table 3-5 Chelating agents pre-selected for this study and their unique properties- compiled from (Smith & Martell, 1987), (Ying, L. et al., 2014) and (Hancock, R. D. et al., 1997)

K_{ML} (↑), thermodynamic stability (↑)

APCs

$LogK_{ML}(Red^{-}.Lig)$[9]	$LogK_{ML}(Ox.Lig)$[9]	Molecular structure and abbreviation	Properties	Cost ($/kg)[10]
5.8	11.3	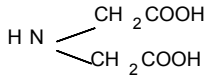 IDA	-Tridental (1 N atom from amino group and 2 O atoms from deprotonated hydroxyl groups of terminal acetate groups - analogical for all APCs) -Small molecular weight (i.e. 133 g/mol)	3-3.2
8.1	15.9	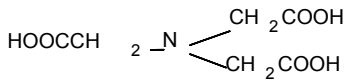 NTA	-Tetradental (1 N atom and 3 O atoms) -A readily biodegradable chelating agent that is not as strong as EDTA but features high temperature stability	2.5-3.2
12.2	19.8	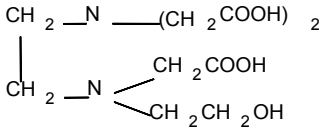 HEDTA	- Hexadental (2 N atoms , 4 O atoms) -A chelating agent with similar efficiency as EDTA. Advantageous with respect to high solubility at low pH and to stabilizing metal ions at high pH.	2.2-2.8
14.3	25.1	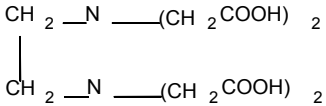 EDTA	-Hexadental (2 N atoms, 4 O atoms) -The most widely used, strong, stable and cost effective agent.	1.55-2
16.4	28.0	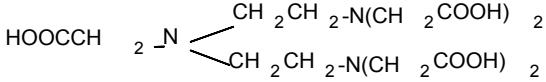 DTPA	-Octadental (3 N atoms, 5 O atoms) -Recommended if high solubility at high pH is sought	2.2-2.8
19.0	30.0	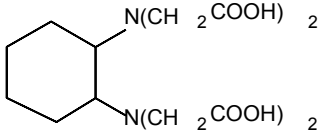 CDTA	-Hexadental (2 N atom and 4 O atoms) -Ring structure makes it reportedly the most stable APC chelator towards free radicals -Highest K_{ML} makes it reportedly the most thermodynamically stable APC chelator -However, the thermal stability of it is unknown	3.6-4.2

[9] K_{ML} values have been taken from literature and measured for the same metal as used in this study (i.e. the Ox is the Fe(III) and the Red^{-} is the Fe(II)) at c~ 0.10 M, T~ 25'C and P~1,01325 bar).
[10] Prices were retrieved from http://www.alibaba.com/showroom/bulk-chemical-prices.html on 15th Feb. 2016 and given for technical purity grades 97-99 % and for minimum order quantity of 1 metric tons.

Table 3-5 (cont´d) Chelating agents pre-selected for this study and their unique properties -compiled from (Smith & Martell, 1987), (Ying, L. et al., 2014) and (Hancock, R. D. et al., 1997)

Oxidative stability (↑)

Without amino group

Log $K_{ML}(Red^{-}.Lig)$[9]	Log $K_{ML}(Ox.Lig)$[9]	Molecular structure and chemical name	Properties	Cost ($/kg)[10]
4.5	8.76	**Carboxylate:** Citric acid 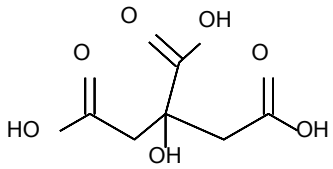	-Tridental (3 O atoms ~ from deprotonated hydroxyl groups with terminal carboxylate groups) -Naturally biodegradable chelator	0.7-1
4.08	9.25	**Hydroxylate:** Mannitol 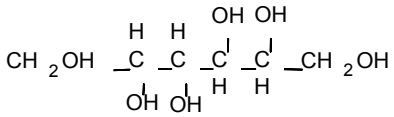	-Tridental (3 O atoms ~ i.e. from 3 adjacent hydroxyl groups) -Mannitol, as hexitol sugar alcohol, forms a very stable complex in highly alkaline media and thus prevents metal-hydroxide precipitation at high pH	1.9-2.2

Once the potential candidates of the chelating agents were determined, the next step is to study the relationship between their molecular structures and stability (oxidative and thermal) in the scope of screening tests (section). After selection of suitable chelating agents, these are formulated with pre-selected absorbents (refer to **Table 3-3**). Then the regeneration kinetics and the desulfurization performance of those were ranked within the context of benchmarking tests (referring section 4 and 4.2 respectively).

3.5 Experimental investigations on stability screening for pre-selected constituents of solvent systems

Selection of the constituents of the solvent system to be developed is an essential step because the solvent system directly influences the energy demand and the environmental impact of the applied liquid redox process. To this purpose, first, the constituents were identified through literature review (see **Table 3-3** and **Table 3-5**). Mastering the stability of pre-selected components under typical operation conditions is prior to their implementation into continuous benchmarking tests, because the advantage of a high performing solvent system should not be impaired by an unreasonable degradation rate, which would lead to high chemical make-up costs up to the degree of non-economical operation of the process. Within the scope of the following subsections, the stability screening tests are explained describing the chemical substances, the experimental set-up as well as the testing procedure and the analytical methods. Subsequently, the results are discussed and the best suited candidates are selected for the benchmarking.

3.5.1 Stability screening of chelating agents

3.5.1.1 Background

Within the scope of this subsection, investigations on both the thermal and oxidative degradation of the pre-selected constituents in aqueous solutions will be addressed. Rapid screening experiments (“stress tests”) have been used not only to acquire first-hand data on the stability characteristics of 8 different chelating agents (referring **Table 3-5**) containing the same metal (i.e. the Fe), but also to obtain the information needed to understand the mechanisms behind different degradation pathways of them.

Decomposition of chelating agents is mainly triggered by chemical (oxidative attack) or to a lesser extent thermal effects (leading to so-called “hydrolytic cleavage” and subsequent break down of C-N bonds) (Martell, A. E. et al., 1975). Typical operation conditions in absorbers and regenerators of the common liquid redox processes are shown in **Table 2-1**. As it can be seen, these kinds of processes are operated at relatively moderate temperatures, since reportedly at elevated temperatures (i.e. higher temperatures than 60°C), **thermal decomposition** may occur i.e. carboxyl groups of chelating agents may cleave. The hydrolytic cleavage of them which is called as decarboxylation consecutively causes the weakening of metal-ligand bonds due to the loss of one electron donor atom (the oxygen) with the respective carboxyl group. Degradation conditions will vary within a gas treatment plant depending on the operating conditions, thus, different degradation mechanisms (for the schematical illustrations of different degradation reaction mechanisms see chapter 5) are involved in different parts of the plant. In other words, the chelator may not undergo hydrolytic cleavage at elevated temperatures but may be attacked and broken throughout dioxygen radicals. Therefore, a degradation setup (“stress test” apparatus) taking both degradation types into account was introduced, where the samples are exposed to both oxidative and thermal degradation conditions in a single system.

Wubs claimed that the **chemical decomposition** of chelators occurs mostly in the regenerator during the oxidation of the redox catalyst by oxygen from air (Wubs, 1994). Thus, in order to prevent misinterpretation and rather to understand the degradation behavior of the solutions during the regeneration of them by air, hydrogen sulfide (H_2S) and other acidic gas components, which are present in real systems, are not applied in the tests. Since solvent degradation in the real plant is a long term effect, hard process parameters had to be chosen in the laboratory experiments to obtain useful data within an acceptable, shorter period of time. The experiments were therefore run under comparably severe conditions (at 60°C under atmospheric pressure with an excessive amount of air sparging through the solutions).

The preparation of the investigated solvent systems, the experimental set up as well as procedure and analytics applied on the taken samples are presented in the following subsections.

3.5.1.2 Preparation of the feed substances

It should be noted that in order to eliminate the cross-matrix influence of AAS on the stability of the respective chelating agent, no AAS was added to the metal-ligand complex solution systems. Thus, their chemical nature is comparable to those of the state-of-the-art-liquid redox solutions, which provides a basis for comparison with the later examined formulated solvent systems (AAS + chelated metal).

Thus, **aqueous solutions of metal-ligand complexes** (see **Table 3-6**) were prepared by:

(1) dissolving precisely predetermined amounts of pre-selected ligands (Na-salts of chelating agents, which are listed in **Table 3-5** were purchased with purities >99% from Sigma Aldrich) in distilled water. The pH of the prepared solutions was adjusted to the same alkaline initial pH level (see **Table 3-7**) with a buffer solution.

(2) then, the appropriate amount of the metal catalyst (the Fe(III) in anhydrous form of its metal-halide, purity >98% from Carl Roth) was added to produce an aqueous chelated-metal solution system. Most ligands form complexes with metals in an equimolar ratio, meaning that at least 1 mol of chelator is required (depending on the denticity of it) to produce 1 mol of complex. In order to ensure the complete complexation of the metal, the same defined excess amount of respective chelator (Lig/(Fe•Lig)) (see **Table 3-7**) was added to the solutions.

The **gaseous substance**, the air (purity>99.5%; 20.9% O_2, N_2>79%), was obtained from Infraserv GmbH.

3.5.1.3 Experimental set up, procedure and analytical method

The stability screening experiments on the aqueous metal-chelate solutions listed in **Table 3-6**, in other words the stress tests of them, were performed in sparged reactors (see **Figure 3-7**) in each of which a defined air stream was bubbled through the thermostated solutions under the conditions given in **Table 3-7**.

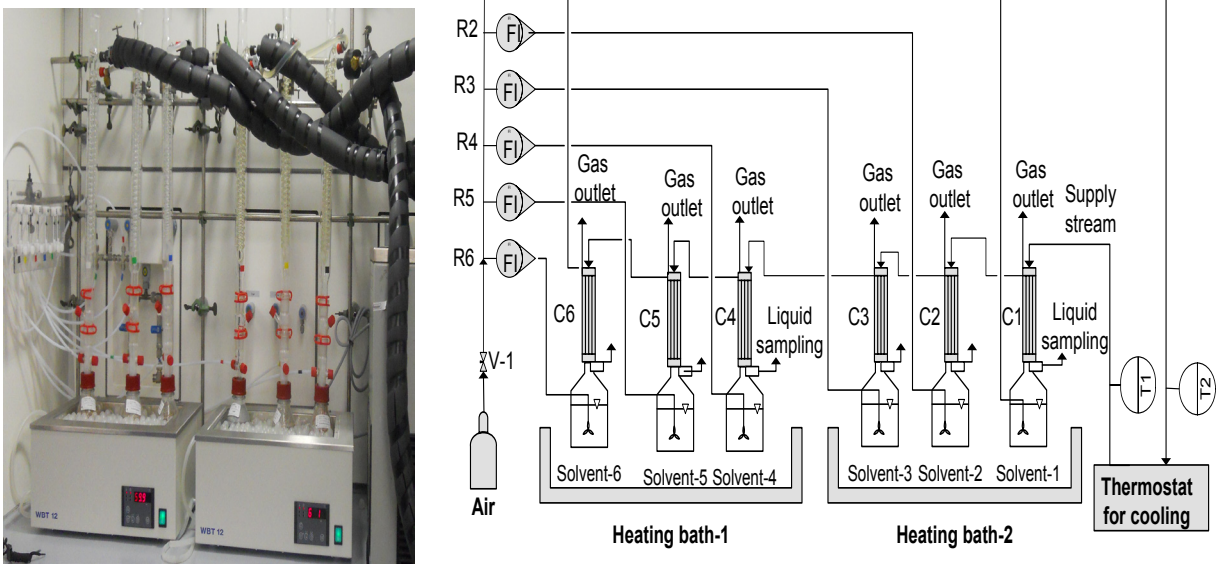

Figure 3-7 Experimental set up (simplified) of the screening tests

Each 500-ml sparged reactor was filled with 250 ml of one solution. The temperature of the heating baths was controlled at 60 °C. The water loss from the sparged reactors was avoided by utilization of an off-gas cooler with recycling of condensate to each reactor.

Although only one thermostat for cooling is shown in **Figure 3-7** for clarity, three thermostats were used in real operation to avoid high temperature differences ($\Delta T = T_2 - T_1$) between return from the cooler of the last reactor and supply to the first reactor. An excess flow of air was used to ensure that a maximum amount of oxygen was absorbed in the solutions and to perform accelerated oxidative degradation during a period of 700 h. For the evaluation of ligand degradation, liquid samples were taken from the fresh solution and after 700 hours.

Table 3-6 Screened chelators

No. of sample	Composition (Fe•Lig complexes)[11]
C1	(Fe•IDA)
C2	(Fe•NTA)
C3	(Fe•HEDTA)
C4	(Fe•EDTA)
C5	(Fe•CDTA)
C6	(Fe•DTPA)
C7	(Fe•Citrate)
C8	(Fe•Mannitol)

Table 3-7 Experimental conditions of screening tests of pre-selected chelators

Experimental conditions, (unit)	
Iron concentration, c[Fe(III)], (mol/L)	0.1
Excess amount of ligand [Lig/(Fe•Lig)],(mol/mol)	1.5
Concentration of respective AAS, c[AAS], (mol/L)	-
Temperature, T, (°C)	60
Pressure, P, (bar)	atm.
Air flow rate, $\dot{V}_{air}$, (L/min)	1
Initial pH, (-)	9.5
Solution inventory, (mL)	250
Duration of experiments,(h)	700

Quantitative concentration measurements of the metal-ligand complexes (the Fe•Lig) were carried out with a UV-Visible spectrophotometer using a method developed for given substances within the scope of this work. During the elaboration of the analytical method, it was seen that neither the non-complexed metal (i.e. the Fe) nor the free chelating agent[12] (i.e. the Lig) that does not take part in the complexation was detected by the UV-Vis method. This means the UV-absorbance recorded during all measurements belongs to respective metal-ligand complexes (the Fe•Lig). Therefore, the concentration of the excess amount of the free chelating agent (the Lig) was determined as follows: An excessive amount of metal catalyst (the Fe) was added to the samples in order to produce metal complexes of free ligands (i.e. the Fe•Lig), thus to make them also visible in UV. Consequently, the samples were reanalyzed. The increase in absorbance revealed the concentration of excessive ligands. The relative Fe•Lig concentrations, the c_r (in %), of the samples were calculated by Eq.3-8. The term c_0 denotes the initial concentration while the term c_t is the remaining concentration after 700 hours.

$$c_r = c_t / c_0 * 100 \qquad \text{(Eq.3-8)}$$

[11] The Fe in all metal-chelate-complexes is in its active form (i.e. the Fe(III)).

[12] It should be noted that all samples were formulated with an excess amount of chelate, as a usual practice for liquid-redox solvent systems, in order to keep the transition metal reliably in the solution.

The UV/Vis spectra of the samples (diluted in the ratio 1:1000) were obtained with a J&M Tidas II UV/Vis-spectrometer, which emits light within a certain spectral range (wavelength 190 – 400 nm). For each sample the value of the absorbance A is different for each wavelength λ, thus yielding characteristic curves as shown in **Figure 3-8**. The concentration of the Fe•Lig in the diluted samples was calculated according to the Beer-Lambert law (referring Eq.3-9) where A denotes the recorded light absorbance at the given wavelength, I_0 is the intensity of the incident light (in W/m^2), I is the intensity of the transmitted light (in W/m^2), c stands for the concentration of the absorbing species (the parameter to be measured), d is the optical path through the cell (in cm) and ε is the extinction coefficient (in L/mol.cm).

$$A(\lambda) = \log_{10}(I_0/I) = \varepsilon(\lambda).\,c.\,d \qquad \text{(Eq.3-9)}$$

For all measurements, standard quartz cells with the same optical path (d=1 cm) were used. The extinction coefficient (ε) is a function of various parameters such as the type of Fe•Lig, the wavelength (λ), the ionic strength (α_{ion}) and the pH of the solution. Therefore, in a first step, the extinction coefficients of each species were identified by measuring the absorbance of the corresponding stock Fe•Lig-solutions of known concentration and calculating ε according to Eq.3-9. A calibration method was established in order to determine the absorbance-to-concentration relationship for each individual specie, since different species generate difference UV-absorbance spectra (generally in the 225-400 nm spectral range). The calibration curves for each Fe•Lig specie were obtained with the following procedure:

- three stock solutions with different concentrations of the Me•Lig were prepared (see **Table 3-8**),
- with each solution, three measurements of the absorbance were performed at T≈ 25 °C and pH ≈ 9.5,
- for each Fe•Lig, the peak value for A appears at a certain wavelength λ, which stays the same for certain concentrations,
- at this λ-value (λ = 250 nm in the case of Fe•DTPA) a mean value for the absorbance was calculated from the three measurements done for a certain concentration.

If the absorbance A_0 of the initial Fe•Lig concentration is known, the concentration c_t can also be derived from Eq.3-9 as it is expressed in Eq.3-9a:

$$\frac{A_t(\lambda)}{A_o(\lambda)} = \frac{\varepsilon(\lambda).\,c_t.\,d}{\varepsilon(\lambda).\,c_0.\,d} \qquad \text{(Eq.3-9a)}$$

Since λ = constant (wavelength at the maximum of the absorbance) and thus also ε(λ), Eq. 3-9a simplifies to:

$$c_t(\lambda) = \frac{A_t(\lambda)}{A_o(\lambda)}.\,c_0 \qquad \text{(Eq.3-9b)}$$

Table 3-8 Conditions and results of calibration measurements performed for Fe•DTPA-complexes

No. of stock solution	c(Fe):c(DTPA) (mol/L:mol/L)	c(Fe•DTPA), mol/L	Wavelength (λ), nm for A=max.	Maximum absorbance (A=max), (-)			Mean value of the max. absorbances, (-)
1	0.06:0.06	0.06	250	0.574	0.599	0.571	0.581
2	0.1:0.1	0.1	250	0.952	0.952	0.960	0.955
3	0.15:0.15	0.15	250	1.290	1.286	1.276	1.284

During the development of the analytical method, almost 100 spectra were recorded for all Fe•Lig species tested (3 measurements for each 3 different concentrations of the stock solutions of 11 different Fe•Lig solutions). As an example of those, only the calibration curves for the Fe•DTPA complexes are shown in **Figure 3-8**.

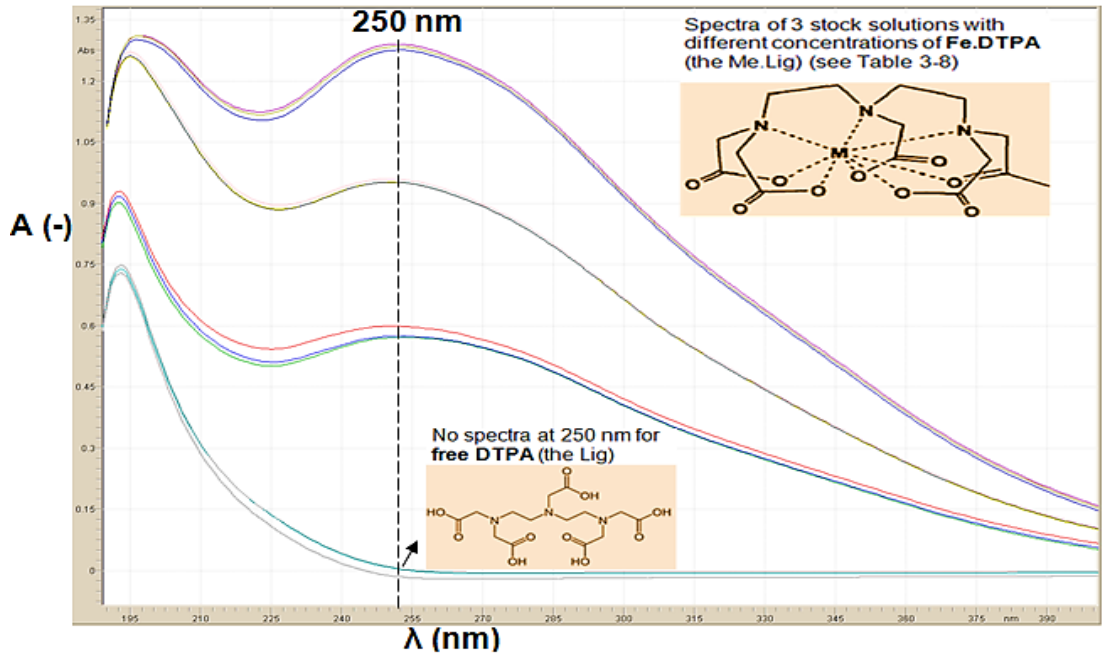

Figure 3-8 Absorbance to wavelength curves of the free DTPA and different concentrations of the Fe•DTPA at 250 nm

For the reproducibility of the measurements and the spectral analysis which was performed with the calibration model for all Fe•Lig solutions see **Table A- 2** given in Appendix A-1.3. The data regression of the calibration measurements for each metal-ligand complex was done by the partial least square data regression (PLSR) model (Wold, S. et al., 2001). The accuracy of the calibration data was assessed by the square of the regression coefficient (R^2) values obtained (R^2= 1-squared deviation between predicted and measured mean concentrations, meaning optimum R^2=1). For all Fe•Lig (or Me•Lig)complexes, the UV absorbances recorded follow perfectly the Beer-Lambert law with molar absorptivities yielding a very accurate linear relation between the concentrations and the absorbance meaning $R^2 \geq 0.95$ for all Fe•Lig (see **Table A- 2**); e.g. R^2=0.99 for Fe•DTPA as it is shown in **Figure 3-9**.

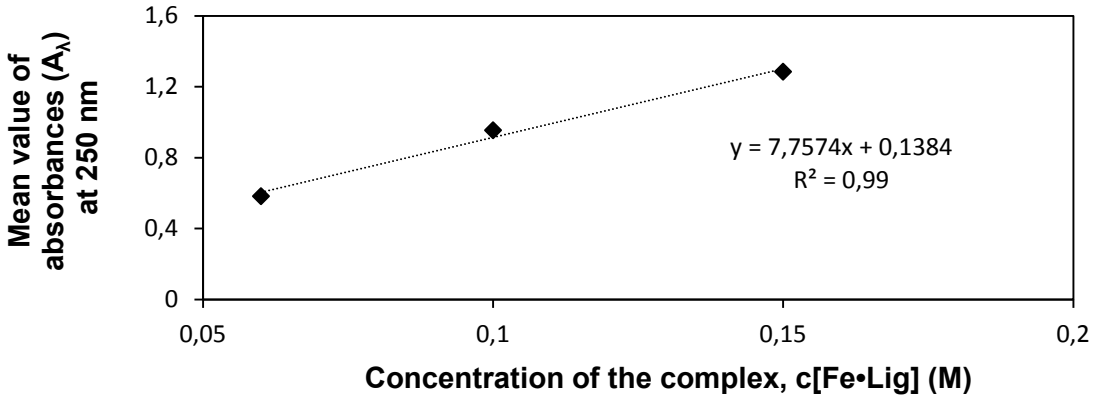

Figure 3-9 Calibration curve and determination of regression - Absorbance to concentration relationships of different concentrations of the Fe•DTPA complex

Taking the maximum value of standard deviation of the regression (±1%), the inaccuracies during the preparation of feed solutions (±3%) as well as the impurity of the chemicals used (±1%) into account, an additive overall accuracy of ±5% was concluded for the analysis by UV/VIS-spectroscopy. The following section presents the results of the conducted stress tests.

3.5.1.4 Results and discussion

The comparison of the relative concentrations of Fe•Lig solutions (thermostated at 60°C and exposed to air) at the beginning and after 700 hours of operation is illustrated in **Figure 3-10**.

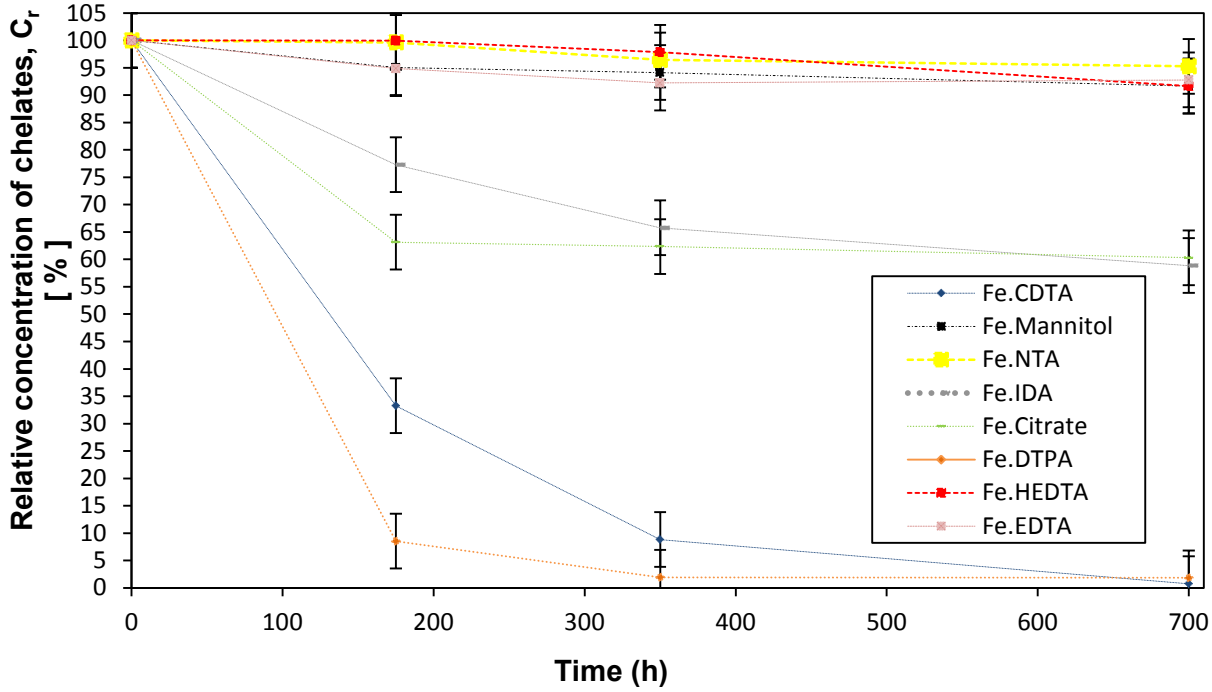

Figure 3-10 Relative concentrations of iron-ligand complexes formed by pre-selected chelators sparged with air at T = 60°C – for additional experimental parameters see Table 3-8 (analytic accuracy ± 5%)

The **Figure 3-10** reveals:

(1) **Stability ranking** after 700 h is as follows: NTA > HEDTA ≥ Mannitol ≥ EDTA > IDA > Citrate > CDTA > DTPA.

The stability can be clustered into 3 groups:

- loss < 10 %: NTA, HEDTA, Mannitol, EDTA
- loss ≈ 40 %: citrate, IDA
- loss > 95 %: DTPA, CDTA

Since for each ligand a specific degradation mechanism dominates, it seems reasonable to analyze each ligand individually in order to achieve a cognitive correlation between their molecular structure and stability behavior (thermodynamic, thermal or oxidative):

Chelators possess an inherent thermodynamic stability which can be evaluated by the comparison of their K_{ML} values, denticities and the nature of donor groups. In particular:

- denticity (↑) → K_{ML} (↑) and thus thermodynamic stability (↑)
- however, denticity (↑) → thermal stability (↓)
- besides these, if number of nitrogen atom (↑) → oxidative stability (↓).

(2) This is consistent with the results obtained, since DTPA as the chelator with highest denticity (most nitrogen atoms - i.e. octadental with 3N atoms see **Table 3-5**) decomposed to a larger extent than all others. The results indicate that the DTPA is not a suitable candidate for benchmarking, since it is broken rapidly under simultaneous thermal and oxidative stress despite its superior thermodynamic character.

(3) The Fe•CDTA also had decreased to a large extent and it seems that the electrostatic bonds appear to become weaker under thermal stress resulting in a decrease in the strength of the ligand field which promotes the decomposition of the CDTA (hexadental) (steric influences see section 3.4.2.1.3). Thus, the CDTA was also eliminated for the further investigations in benchmarking tests.

(4) Comparing the relative concentrations of the remaining APCs with each other gives a stability ranking of: NTA > HEDTA ≥ EDTA > IDA.

This result is consistent with the influence of the ascending number of nitrogen atoms in a chelating agent on its oxidative resistance (with the exception of the IDA see **Table 3-5**). Although the NTA and the IDA both feature the same denticity (tridental) and the same amount of electron donating atom (i.e. 1 N atom), the IDA decomposed significantly more than the NTA. This must be explained by its thermodynamic instability (the lowest K_{ML}), not by oxidative or thermal degradation. Although NTA features a lower K_{ML} and thus a lower thermodynamic stability than HEDTA and EDTA, it showed excellent thermal and oxidative resistance under test conditions. However, HSE issues limit its allowable concentration, since reportedly at concentrations > 1 wt% it may be carcinogenic to human beings (The DOW Chemical Company, 2016). Hence, the NTA cannot be applied as the main chelate for cases where higher Fe•Lig concentrations are required, but its remarkable thermal, oxidative as well as thermodynamic durability under tested conditions makes it a promising candidate for co-chelator.

(5) Comparing the relative concentrations of the non-APCs gives a stability ranking of: Mannitol > Citrate

The mannitol and the citrate had been pre-selected since it was expected that they feature high thermal stability (due to low denticity, i.e. both are tridental) and high oxidative stability (due to absence of nitrogen). The results exhibit that although its K_{ML} value is lower than those of all APCs (see **Table 3-5**), the mannitol showed a comparably high thermal and oxidative stability. Despite its favorable thermal and oxidative resistance, its lower complexation capacity (compared to APCs) prevents the mannitol from further examination in the benchmarking tests as the main chelate, but it is also a promising candidate for co-chelator.

(6) Contrary to mannitol, the citrate showed a lower stability under tested conditions, which can be explained by its thermodynamic instability of the complex. Martell found that the thermodynamic stability of citrate decreases with increasing pH (becoming significant for pH>9). Because of its carboxyl groups, the citrate complexes metals stronger in an acidic environment (Martell, 2009). The thermal and oxidative durability of citrate may be higher in an acidic environment, but this is not enough to label it as a promising candidate, since the absorption kinetics of H_2S are enhanced in alkaline media.

Thus, the promising chelating agents were identified. In addition, from **Figure 3-10**, it can be deducted that IDA featured a significantly high decomposition rate. As it was mentioned above, this lower stability behavior under tested conditions can be explained by its lesser thermodynamic strength. A literature review done on this account gave the following information: Martell et al. suggest either to apply a Lig/Fe•Lig ratio of at least 3 for systems with IDA as Lig or to add a co-chelator to the solution in order to assure thermodynamic stability (Smith & Martell, 1987). In order to verify these promising findings and examine the potentials to improve the stability of chelators labeled as “weak”, some blends of them were formulated and tested again, as presented in the following section.

3.5.1.5 Formulation of stable chelator blends and conclusions

In order to verify the proposal of (Smith & Martell, 1987) given in the previous section, a chelating system was formulated which contains IDA (Lig/Fe•Lig =1.5) and Mannitol (Lig/Fe•Lig=1.5) yielding a dual-chelator system of IDA+Mannitol (with a total Lig/Fe•Lig=3) (main chelator + co-chelator; see section 2.2.2). This system is labeled as C9. In addition, two more combinations of dual-chelator systems were formulated (i.e. the C10 and the C11 given in **Table 3-9**) by merging two individual chelating agents with each other, which were labeled as stable as a result of the

performed test shown in **Figure 3-10**. This was done in order to investigate whether the addition of a co-chelate increases the stability of components which were already categorized as stable even further or not. In this context, the sample C10 was prepared to be a blend of NTA (Lig/Fe•Lig=1.5) and Mannitol (Lig/Fe•Lig=1.5). The composition formula of the sample C11 cannot be stated due to confidentiality reasons but it will be denoted as **Lig2** during the rest of this study.

Table 3-9 Formulated chelator blends to be screened

No. of sample	Composition (Fe•Lig)-complex
C9 (C1+C8)	Fe•(IDA +Mannitol)
C10 (C2+C8)	Fe•(NTA+Mannitol)
C11 (non-disclosed formula)	Fe•(Lig2)

The relative concentrations of co-chelated Fe•Lig solutions at the beginning and after 700 hours of operation tested under the same conditions compiled in **Table 3-7** are given in **Figure 3-11**. To provide a visual comparison basis of the stabilities of blended samples (i.e. C9, C10 and C11) with the stabilities of their non-blended pairs (i.e. the C1, C2; see **Figure 3-10**), the latter are reshown in **Figure 3-11**. With regard to this, it should be noted that the non-blended comparison pair of the sample C11 was not regiven in the **Figure 3-11** in order not to declare its formula.

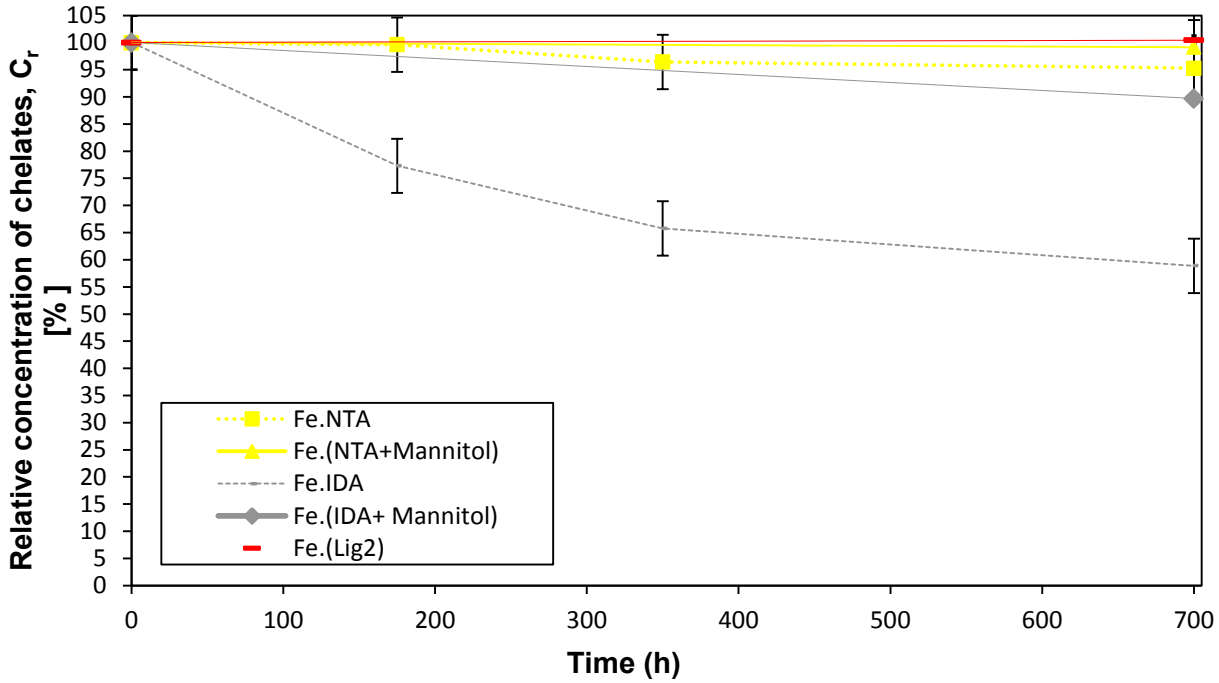

Figure 3-11 Relative concentrations of formulated metal-ligand complexes sparged with air at T=60°C – for additional experimental parameters see Table 3-8 (analytic accuracy ± 5%)

As **Figure 3-11** reveals, chelator blending showed a positive effect i.e. it increased the stabilities of the respective chelate mixtures. The most apparent positive effect occurred for the addition of Mannitol to IDA. This phenomenon can be explained by the thermodynamic stabilization effect of the co-chelators i.e. they provide the main chelate[13] a flexibility in terms of the pH-range in which the bonds between the Me and the Lig are strengthened. Hence, the decomplexation of the respective Me•Lig is suppressed. This fact is in agreement with the study of Piche et al. in which

[13] It is worth to mention that the molar concentration of the co-chelate should be significantly lower than that of the main chelate. However, in this study, the molar concentration of them was kept equal in order to enable a fair comparison of the results with those obtained in the previous experiment given in Figure 3-10.

the synergism of blended chelators to form dual compounded systems was investigated in detail (Piche, S. et al., 2005).

Conclusions:

- By proper choice of the chelator (respectively the blend) and/or the operation conditions (e.g. T and pH), it is possible to stabilize chelators to a certain extent from where on only their inherent stability characteristics (as discussed in section 3.5.1.4 from point (1) to (6)) play a decisive role regarding their durability.

- To keep a safety margin with respect to chelate stability, the sour gas treatment process applying liquid redox technique should be operated at T < 60°C and 9.0<pH<9.5.

- Among the 8 chelators and 3 chelator blends screened (referring **Table 3-6** and **Table 3-9**, respectively), two of them which had turned out as comparatively excellent ligands and ligand systems (in terms of thermodynamic, thermal and oxidative resistance) are determined as the potential chelating agent and blend candidates for benchmarking experiments: (1) the EDTA, (2) the Lig2.

Thus now, the stability screening tests of the solutions containing pre-selected AAS are to be conducted, as described in the following section.

3.5.2 Stability screening of formulated AAS solvent systems containing chelated metal

3.5.2.1 Background

The thermal and oxidative degradation of amino acid salt solutions applied for post combustion capture processes to reduce CO_2 emissions from power plants were studied in detail in (Fischer, 2013). In his work, (Fischer, 2013) found that the AAS solutions are resilient towards thermal stress even up to temperatures of 140 °C. It is also stated that the AAS solutions showed a reasonable oxidative resistance under post combustion capture process conditions. It should be noted that the operation principles and parameters of the post combustion capture (temperatures up to 140°C for regeneration) and the Siemens-liquid-redox (T=20-60°C), are different. In addition, AAS solutions applied in post combustion processes do not contain a chelated-metal[14]. Taking the lower temperatures of liquid redox processes into account, the thermal stress is not the dominating degradation mechanism for the AAS. Therefore, the oxidative degradation behavior of various AAS solutions containing chelated-metal has to be examined by long-term tests in order to characterize the suitability/applicability of them at industrial scale under corresponding industrial operation conditions.

The preparation of the investigated solvent systems, the experimental set up as well as procedure and the analytics applied on the taken samples are presented in the following subsections.

3.5.2.2 Preparation of the feed substances

Aqueous solutions of solvent systems containing AAS as absorbent and chelated metal as catalytic oxidizing agent (referring **Figure 1-4**) were prepared by:

(1) neutralizing a precisely determined amount of pre-selected amino acids given in **Table 3-3** (purity >99% from Chemical Point Company) to AAS with an aqueous KOH solution containing equimolar amount of K. The KOH solution was prepared by dissolving KOH-pellets >96 % from the supplier company, the neoLab, in distilled water to produce the potassium salts of the amino acids (e.g. Glycin+KOH→K-Glycin ~ Glycinate)

(2) in order to eliminate the cross matrix influence of different metal-ligand complexes on the stability of respective AAS, the same metal complex of the same ligand (i.e. the Fe•EDTA), which is labeled as “stable” according to the conducted stress tests (see section 3.5.1), was added to all AAS solutions prepared.

[14] Although the AAS solutions applied for PostCap® processes do not contain a chelated metal, (Fischer, 2013) proposed that trace amounts of metal ions in corroding plant material can catalyze the oxidative degradation of the applied solvent, which can be inhibited by addition of appropriate corrosion inhibitors.

The **gaseous substance**, the air (purity>99.5%; 20.9% O_2, N_2>79%), was obtained from Infraserv GmbH.

3.5.2.3 Experimental set up, procedure and analytical method

The screening of the formulated AAS based solvent systems containing chelated-metal was performed in the same experimental set-up as it was shown in **Figure 3-7** and as described in the section 3.5.1.3, however under the conditions given in **Table 3-11**. The analysis of the AAS-contents in the solvent systems listed in **Table 3-10** was performed using Liquid Chromatography equipped with a mass spectrum (LC-MS) (accuracy of ±10%) (by an external analytic service provider), whereas the concentration of the Fe•EDTA in them was measured with UV-Vis (by a self-developed method) as it was explained in the section 3.5.1.3.

Table 3-10 Screened solvent systems

No. of sample	Composition (AAS+ Fe•EDTA) [11]
A1	(Glycinate+Fe•EDTA)
A2	(Alaninate+Fe•EDTA)
A3	(Taurinate+Fe•EDTA)
A4	(Sarcosinate+ Fe•EDTA)
A5	(Siemens Solvent-1+ Fe•EDTA)
A6	(Siemens Solvent-2+ Fe•EDTA)
A7	(Dimethylglycinate+ Fe•EDTA)

Table 3-11 Experimental conditions

Experimental conditions, (unit)	
Metal concentration, c[Fe], (mol/L)	0.1
Excess amount of ligand [Lig/(Fe•Lig)],(mol/mol)	1.5
Concentration of respective AAS, c[AAS], (mol/L)	1.65
Temperature, T, (°C)	60
Pressure, P, (bar)	atmospheric
Air flow rate, $\dot{V}_{air}$, (L/min)	1
Initial pH, (-)	9.5
Solution inventory, (mL)	250
Duration of experiments,(h)	700

3.5.2.4 Results and discussion

The comparison of the relative concentrations of the AAS solutions containing the Fe•EDTA at the beginning and after 700 hours of operation is illustrated in **Figure 3-12**. Although all of these solutions comprise of an AAS and the chelated metal catalyst (Fe•EDTA), they were expressed only with the name of the AAS for simplification purposes (for example, only glycinate was emphasized instead of glycinate containing Fe•EDTA). It reveals that more than 80% of the glycinate and more than 60% of the alaninate were oxidized and thus destroyed within 700 hours, while the taurinate showed reasonable stability and the sarcosinate, the Siemens-absorbents as well as the dimethylglycinate showed very good resistance to oxidative degradation. This result indicates that the molecular structure of an amino acid salt has an impact on its stability because the two remarkably instable degraded solvents are primary AASs, whereas the others are either secondary or tertiary or sterically hindered.

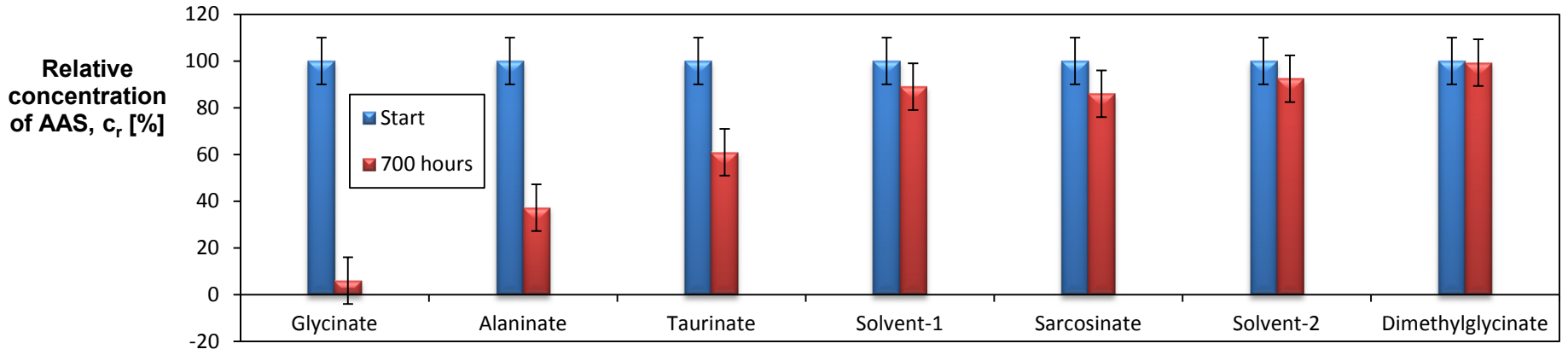

Figure 3-12 Relative concentrations of the AAS solutions containing Fe•EDTA sparged with air at T = 60°C – for additional experimental parameters see **Table 3-11** (analytic accuracy ± 10%)

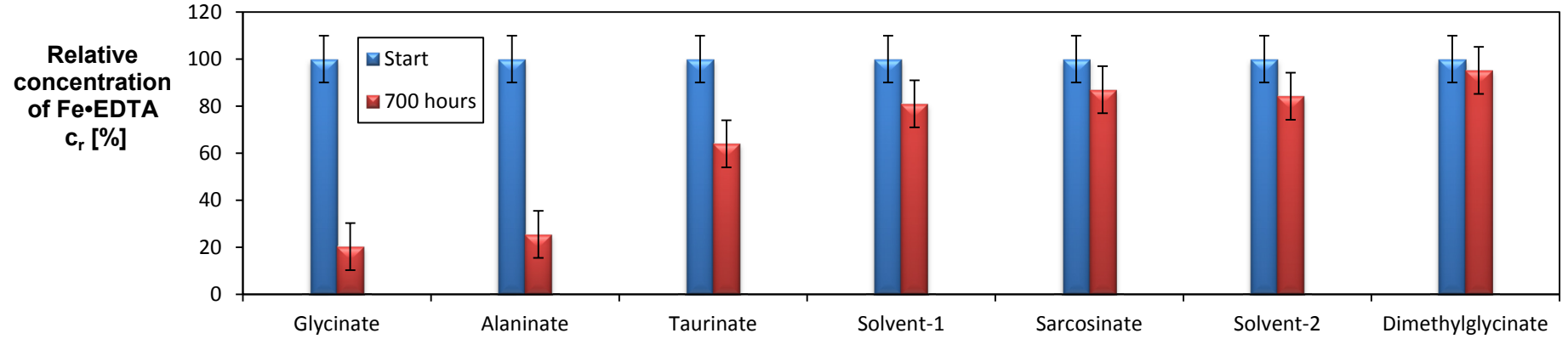

Figure 3-13 Relative concentrations of the Fe•EDTA in formulated AAS solvent systems sparged with air at T = 60°C – for additional experimental parameters see **Table 3-11** (analytic accuracy ± 5%)

- **Stability ranking of the AASs:** tertiary AAS (A7) > secondary AASs (A6>A5>A4) > primary AASs (A3>A2>A1). Although the A1, A2 and A3 are all primary AAS, they showed different resistance towards oxygen, which can be explained by discrepancies in their molecular structure. As it was stated in **Table 3-2**, the distance between a carboxyl and an amino group in an AAS is a decisive criterion, since it affects the accessibility of the amino group. The stability ranking of two primary AAS (Alaninate>Glycinate) is consistent with the fact of accessibility (Sönmez, H. G. et al., 2015), since the alaninate is sterically hindered, whereas the glycinate is not (for the molecular structures see **Table 3-3**). The type of side chain plays a significant role for the oxidative durability of the AAS, since the taurinate, which possesses a sulfonyl group rather than a carboxyl group, showed significantly higher stability (see **Figure 3-12**) compared to the other two primary AAS (i.e. the A1 and the A2). The considerably higher resilience of the dimethylglycinate in comparison to all secondary AASs (the A4, A5 and A6) indicates that resistance against oxidative degradation of an AAS increases with the number of hydrogen substitutions (Sönmez, H. G. et al., 2015).

All solutions with different AAS contained the same initial amount of the same metal-ligand complex (the Fe•EDTA)[11]. The relative concentrations of the chelate (the Fe•EDTA) in the selected absorbent solutions at the start of the experiments and after 700 hours are illustrated in **Figure 3-13**.

- **Stability ranking of the Fe•EDTA complexes in the respective AAS:** in tertiary AAS (A7) > in secondary AASs (A6>A5>A4) > in primary AASs (A3>A2>A1). More than 70% of the EDTA in the glycinate and the alaninate were oxidized and decomposed within 700 hours. This is consistent with the result of the oxidative degradation of the absorbents shown in **Figure 3-12**. The profiles obtained from **Figure 3-13** indicate that the reaction medium is an essential parameter determining the stability of the Fe•Lig, due to the contribution of the solvation/desolvation process as discussed in the section 3.4.2.1.

3.5.3 Conclusions of the screening tests and selection of formulations for technical evaluation

All results presented in sections 3.5.1.4 and 0 reveal the conclusions which are listed in **Figure 3-14**:

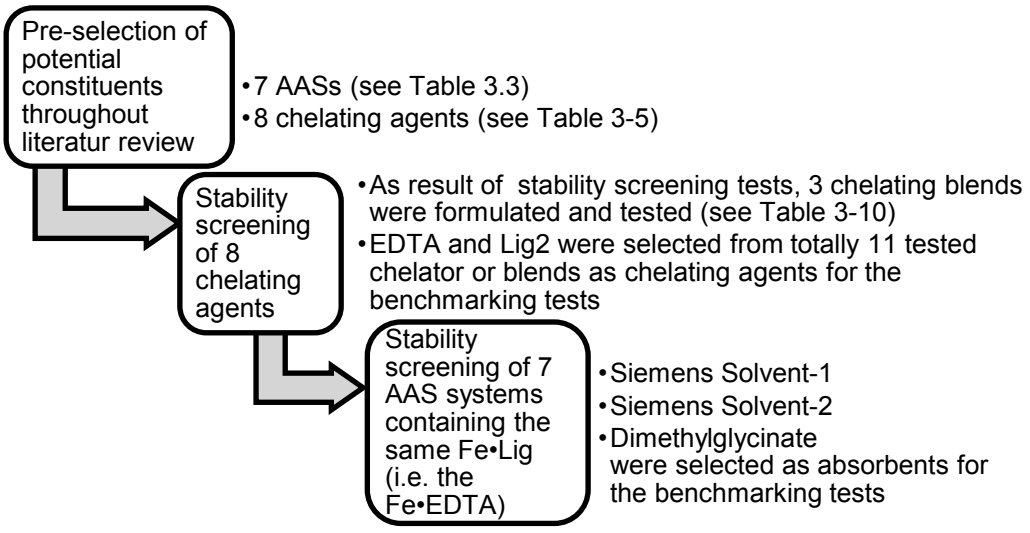

Figure 3-14 Selected components for further experimental investigations

Based on these results, the next steps of the solvent system development procedure, the technical evaluations tests namely the benchmarking tests (regarding the regeneration kinetics and the overall performance in continuous operation of mini lab plant) were carried out with a reduced list of solvent system formulations, which were gained by matching selected absorbents with the selected ligands. They are presented in the following chapter.

4 TECHNICAL EVALUATION OF THE FORMULATED SOLVENT SYSTEMS

When designing a new gas treatment process for H_2S removal by liquid redox technique with the help of utilizing a chelated-metal formulated AAS solvent system, knowledge on optimal operating conditions and key process parameters is required. As it was discussed in section 2.4, performance and economics of such processes depend primarily on the following factors:

1. Solution circulation rate→ equipment capital (CAPEX) and power (OPEX) costs
2. Regeneration air consumption→ equipment capital (CAPEX) and power (OPEX) costs
3. Loss of active material (chemical and/or mechanical) → chemical costs (OPEX)

These factors, especially the solution circulation ratio, are influenced directly by the iron concentration in the solution, which is limited by the solubility constraints and the thermodynamic stability of the applied ligand. The active iron (i.e. the Fe(III)) concentration of the solution is also influenced by the regeneration efficiency of the reduced catalyst (i.e. the Fe(II)) and thus, by the design of the regenerator vessel and the plant operating conditions. Therefore, in the scope of technical evaluation experiments, first, investigations on the regeneration kinetics of the reduced metal catalyst-complex (i.e. the Fe(II).Lig) in respective solvent systems with O_2 from regeneration air were conducted (refer to section 4). Derived from these findins on the regeneration behavior, new solutions were formulated, and thereafter, the overall performance (absorption+regeneration) evaluation of them was performed in the mini lab plant (refer to section 4.2). **Figure 4-1** gives the first hand information about the objectives of the kinetics and techno-economic feasibility experiments which will be studied in detail in the scope of the following subsections.

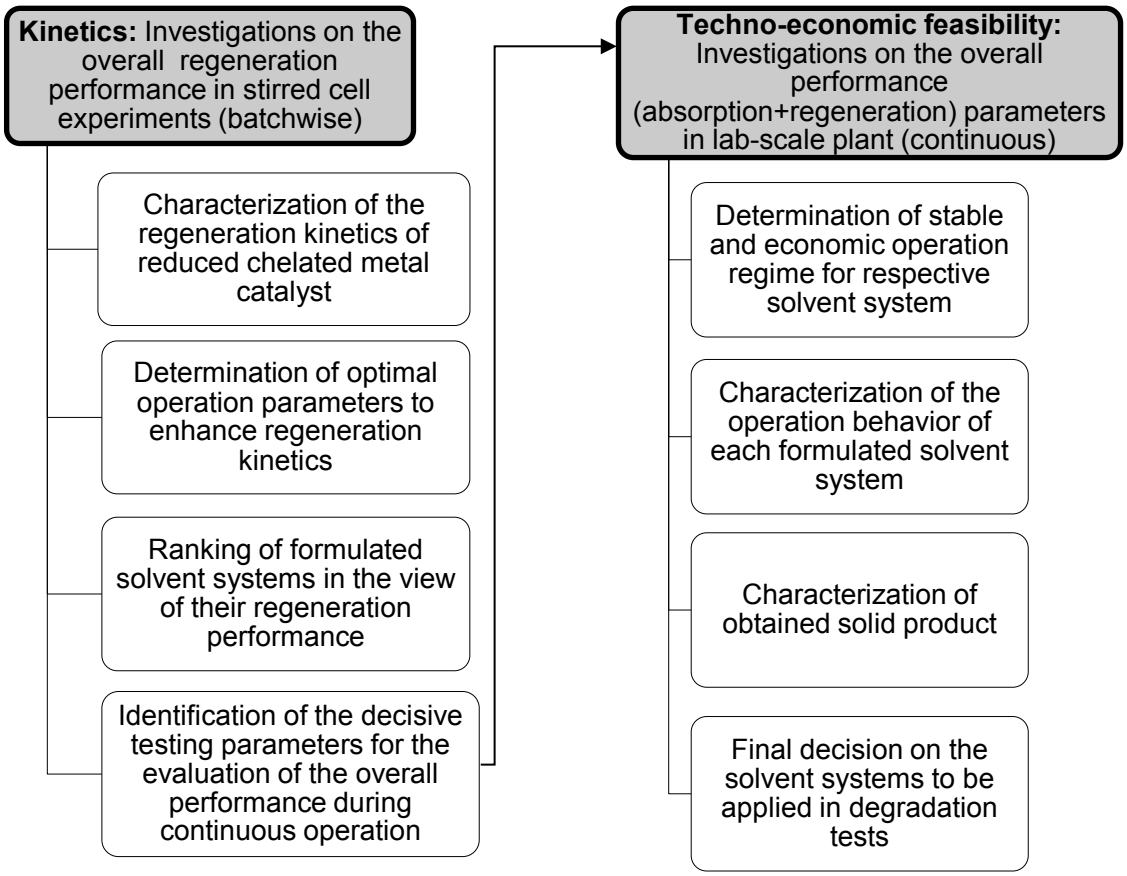

Figure 4-1 Stepwise benchmarking approach

4.1 Experimental investigations on the regeneration kinetics of the chelated metal in formulated solvent systems in batch operation

4.1.1 Background

In general, chelates of Fe(III) with several ligands have been widely used for the removal of:

- H_2S from exhaust of waste water fermentation,
- H_2S from atmospheric emissions of pulp and paper industry,
- NO from flue gas.

The reaction between these chelates and the dissolved O_2 **in water based solutions** has been the object of several studies. Particularly in liquid redox technique, they have been used for the absorption of H_2S including the formation of elemental sulfur with the help of electron transfer from chelated metal. The simultaneous reduction of the active form of the chelated metal to its inactive form is reportedly instantaneous (i.e. from Fe(III)•EDTA to Fe(II)•EDTA, respectively). However, the regeneration of the Fe(II)•EDTA to its active form (the Fe(III)•EDTA), as expressed in Eq.4-1, is the slowest step in the process cycle (Ebrahimi, S. et al., 2003).

$$2(\mathrm{Fe(II)} \bullet \mathrm{EDTA})^{2-}{}_{(aq)} + {}^{1}/_{2}\,\mathrm{O}_{2(aq)} + 2\mathrm{H}^{+}{}_{(aq)} \rightarrow 2(\mathrm{Fe(III)} \bullet \mathrm{EDTA})^{-}{}_{(aq)} + \mathrm{H_2O} \qquad \text{(Eq.4-1)}$$

Thus, design of a H_2S removal plant employing liquid redox technique centers around the regenerator which performs the oxidation, and hence, the regeneration of the reduced chelated-metal catalyst. Therefore, the reaction rate and the kinetics of this step are of high interest. The kinetics of liquid-redox reactions in the liquid phase are basically influenced by:

- Temperature,
- Concentration of interactive species (which in turn is depending on e.g. the mass transfer of species from the gas to the liquid phase),
- Catalysts (to be understood in general and not in the sense of “chelated-metal catalyst”, which do not act as catalysts for the regeneration reaction, but are one of the reaction partners),
- Ionic strength (α_{ion}) and pH of the solution.

Therefore, the operating conditions and regenerator configuration must be such that the regeneration kinetics of the chelated-metal catalyst is accelerated. In this context, several earlier studies applying different ligands, operating conditions and test configurations to investigate the regeneration behavior of the **chelated-Fe(II) in water based solutions (state-of-the-art)** are available in literature. A summary of them is presented in **Table 4-1** together with the approach used in these studies. The aim of this section is not to develop a reaction kinetic model but rather to obtain reliable rate data on the regeneration reaction as well as the appropriate operating window by carrying out experiments **in a batch system** under controlled conditions. Thus, the gap in the literature data on regeneration kinetics of the **Fe(II)•EDTA in AAS based solvent systems (new formulations)** and under conditions relevant to the Siemens liquid-redox-process for sour natural gas treatment (i.e. higher pH, higher Fe(II) and O_2 concentrations) will be covered in the scope of this section.

For this purpose, the following solvent systems were formulated and employed:

(A) Water (without AAS) + Fe(II)•EDTA
(B) Solvent-1 (secondary AAS) + Fe(II)•EDTA
(C) Dimethylglycinate (tertiary AAS) + Fe(II)•EDTA

These solutions were mixed in a such way they have comparable pH and ionic strength values at the end as well as they contain the same amount of Fe(II)•EDTA; but they differ only in the presence and/or type of AAS. Thus, testing their regeneration performance under the same experimental conditions will reveal the influences of the presence and type of the AAS on their regeneration kinetics behavior. In addition, the results will help to understand key parameters for a cost-effective process design leading to successful operation in industrial scale and will determine optimal performance testing parameters for the continuous mini lab plant. It shall be noted that, the findings on the reaction rates and kinetics of the Fe(II)•EDTA can be correspondingly transferred to the Fe(II)•Lig2 (the other chelator labeled as stable; section 3.5.3 and employed

later for the performance tests in the mini lab plant; section 4.2) due to the fact that no significant difference in the diffusivities of these chelating agents under the given experimental conditions is expected because of their comparable sizes (the higher the size of the complex, the more decelerated is the diffusivity of the molecule into the solution). Thus, no reaction kinetics experiments had to be conducted with the Fe(II)•Lig2.

Table 4-1 Overview on key characteristics of experiments performed on the oxidation of the Fe(II).Lig in water based solutions

Study	System [a-b]	Order[d]		T (°C)	pH	Ligand type	Concentration in mol/m³		
		O_2	Fe(II)•Lig				Fe(II)	Ligand	O_2
(Zang, V. et al., 1990)	E-II	1	1-2	15-50	2-7	EDTA DTPA	0.025-20	0.05-20	0.125-1.25
(Brown, E. R. et al., 1987)	A-IV	1	1-2[c]	25	3-7	EDTA DTPA	< 11.5	< 120	0.125-1.25
(Sada, E. et al., 1987)	A-I	1	0.5 0.7	20-60	6-8	EDTA NTA	< 20	< 40	0.018-0.064
(Travin, S. O. et al., 1981)	E-II	1	1	22	6	EDTA	0.1-0.2	0.1-10	0.25
(Purmal´, A. P. et al., 1980)	F-II	1	2-1	22	4.5-9	EDTA	0.05-5	0.055-5	0.125-0.25
(Kurimura , Y. et al., 1968)	C,D-II	1	1	25	2-7	EDTA DTPA NTA HEDTA CDTA	0.008-0.04	< 1.0	< 1.23
(Wubs, 1994)	B-III	1	2	20-60	7.5	EDTA HEDTA	0-100	120	0.125-1.25
This study	B-II, III	1	1-2	30-60	9.5	EDTA	1-200	1.5-300	5-55
a- Experimental set-up b- Method for rate determination		A) Bubble column, B) Stirred cell, C) Quartz cell with oxygen saturated liquid D) Test tube, E) Stopped flow apparatus, F) “Standing-jet” apparatus I) Chemical analysis of ferric ion, II) Photospectrometrical analysis of ferric chelate, III) Oxygen pressure indication, IV) Electropotential measurement							
c- depending on the c[Fe(III)] at t=0 d- empiric orders of the partial reactions of the O_2 and the Fe(II).Lig, respectively									

Before presenting the kinetic experiments conducted in the scope of this study and their results, first the stepwise methodology used is outlined in the following section, which yields the determination of the reaction rate law model to be applied for the evaluation of the results.

4.1.1.1 Methodology for the determination of the rate law model

The reaction rate calculated by using the rate equation model is an important indicator while assessing the kinetics of a certain reaction in different solutions. The rate equation (or rate law) expresses whether, how and to what extent the operating conditions and reaction partners influence the regeneration kinetics of the Fe(II)•EDTA. Thus, the rate law is to be established first, in order to be able to evaluate the results of the kinetic experiments on an equal basis.

In this context, the starting point is the choice of mass transfer model of O_2 into solutions which is discussed briefly in the following subsection.

4.1.1.1.1 Choice of the mass transfer model for O_2

In the kinetic studies cited in **Table 4-1**, various theories have been used to describe the physical mass transfer process of the O_2 from the bulk gas phase into the liquid phase regarding the steadiness of the diffusion and the restraining phase (i.e. the gas or the liquid phase). The driving force of this transfer, referring the Eq.4-2, is the concentration gradient of the O_2 between the gas phase and the liquid phase.

$$O_{2(g)} \leftrightarrow O_{2(aq)} \qquad \text{(Eq.4-2)}$$

In general, mass transfer models can be classified mainly in two groups depending on the steadiness or unsteadiness of the diffusion process of the respective component into the solution. Two common mass transfer models, in which the diffusion is reported to be an unsteady-state-process, are the **penetration theory** of (Higbie, 1935) and the **surface renewal theory** of (Danckwerts, 1951) (see **Figure 4-2**).

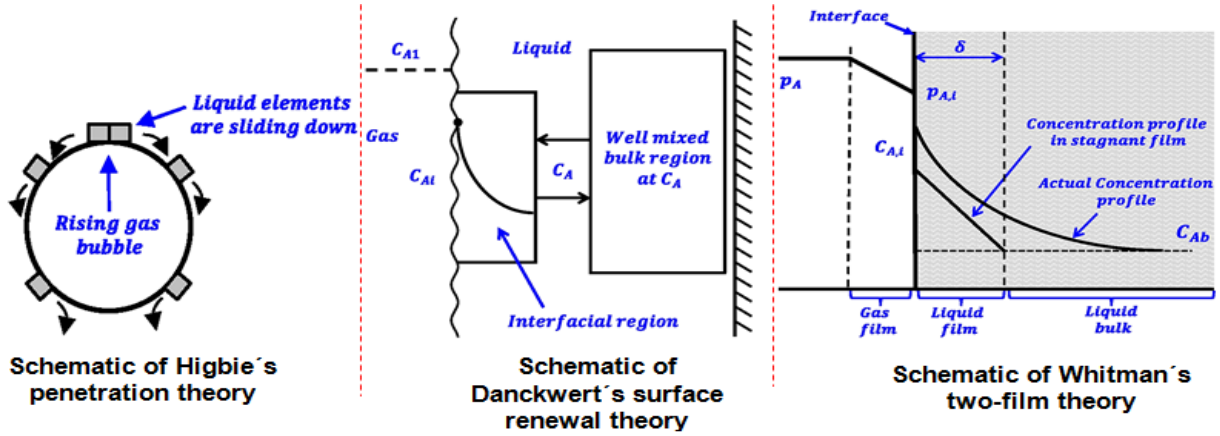

Figure 4-2 Schematics of common mass transfer mode theories - deduced from (Morsi, B. I. et al., 2015)

According to the theories of Higbie and Danckwert, the molecules of the solute are supposed to be in constant random motion, where clusters of these molecules arrive at the gas-liquid-interface and remain there for a period of time: some of them penetrate while the rest mixes back into the bulk of the respective phase. Contrary to these, (Whitman, 1923) proposed the **two film theory** stating that the diffusion is a steady state process and the resistance to mass transfer lies in two films on both sides of the gas-liquid-interface (see **Figure 4-2**).

A detailed experimentally based comparison between these three theories when applied for diffusion processes in the liquid-redox-technique was provided by (Wubs, 1994). Since there is no enforced mixing in the bulk gas phase and at the boundary layer applied in the experiments within this study (refer to section 4.1.3), it was concluded to employ the stationary two film model of (Whitman, 1923). Assuming that the thermodynamic equilibrium is reached at the gas-liquid-interface and the mass transfer resistance of the gas side can be neglected, the mass transfer model for O_2 that is used in this study can be described by Eq.4-3 according to Fick´s second law. It is derived from Fick´s first law and according to the **two film model with neglected gas-side mass transfer resistance**.

$$\frac{dc_{O_{2(l)}}}{dt} = k_{l,O_2} \frac{A}{V_L} \left(c^*_{O_{2(g)}} - c_{O_{2(l)}} \right) \qquad \text{(Eq.4-3)}$$

where the dc_{O2}/dt is the concentration change of the O_2 in the liquid phase within the progress of the time in mol/L.s, the term $k_{l,O2}$ denotes the mass transfer coefficient of the O_2 in the liquid phase in m/s, A is the interfacial area in m^2, V_L is the liquid volume in m^3, the term, $c^*_{O2(g)}$, stands for the

equilibrium concentration of the O_2 at the gas-liquid-interface in mol/L and the $c_{O2(l)}$, denotes the concentration of the O_2 in the liquid phase in mol/L.

After determination of the mass transfer model to be applied, thus now, the derivation of the reaction rate equation from the selected model can be illustrated as given in the following subsection.

4.1.1.1.2 Specification of the rate law

Since the absorption of the O_2 into the solution is accompanied by a chemical reaction consuming O_2, the Eq.4-3 should be redefined for **mass transfer combined with chemical reaction**. Thus, the reaction law of the regeneration reaction taking place in the experiments conducted in this study, Eq.4-1, can be described by Eq.4-4:

$$\frac{\mathrm{dc_{O_{2(l)}}}}{\mathrm{dt}} = \mathrm{k_{l,O_2}}\frac{\mathrm{A}}{\mathrm{V_L}}\left(\mathrm{c^{*}_{O_{2(g)}}} - \mathrm{c_{O_{2(l)}}}\right) - \mathrm{kc^{x}_{O_{2(l)}}c^{y}_{Fe(II)\bullet EDTA}} \qquad \text{(Eq.4-4)}$$

where the term k is the reaction rate constant (the unit of this term depends on the order of interacting components in the respective reaction), $c_{O_2(l)}$ denotes the concentration of the dissolved O_2 in the aqueous phase in mol/L, $c_{Fe(II)\bullet EDTA}$ stands for the concentration of the Fe(II)•EDTA in the aqueous phase in mol/L and the terms x as well as y are the empiric orders of the partial reactions of O_2 and Fe(II)•EDTA, respectively. The mass transfer coefficient of O_2 in the liquid phase ($k_{l,O2}$) given in Eq.4-4 is a function of the temperature, the composition of the liquid phase, the stirrer speed and the geometry of the stirrer and the reactor. Therefore, knowledge of the hydrodynamics in the stirred-cell contactor depending on the process conditions is required to determine the kinetics of the regeneration reaction. In a stirred cell reactor, the mass transfer i.e. the physical absorption rate of the O_2 can be enhanced by an increase in stirrer speed, thus improving the conditions at the gas-liquid contact area and the transport from there into the liquid phase. Hence, the mass transfer can be uncoupled from the reaction kinetics by adjusting the stirrer speed to a value from where on the mass transfer rate cannot be enhanced any more. By doing that, the reaction rate model given in Eq.4-4 can be shortened to Eq.4-5.

$$\mathrm{r} = \frac{\mathrm{d_{C_{O_2}}}}{\mathrm{dt}} = -\mathrm{kc^{x}_{O_2}c^{y}_{Fe(II)\bullet EDTA}} \qquad \text{(Eq.4-5)}$$

Subsequent to identifying the valid reaction law for the kinetic tests done in this study, it shall be specified by determining the respective components of Eq.4-5. Knowledge of the gas solution process and the resulting solubility of O_2 and information on the occurrence of side reactions are required to determine the kinetics of the oxidation reaction. These will be adressed in the following subsections.

4.1.1.1.2.1 Calculation of gas solubility in the liquid redox solvent systems

Before discussing the approach used to describe and calculate the solubility of the O_2 in the liquid phase, the theoretical stoichiometric amount of O_2 (nO_2) which is necessary to regenerate one mol of the Fe(II)•EDTA in the solution should be determined. It can be obtained as 0.25 moles of O_2 for 1.0 mol of Fe(II)•EDTA from Eq.4-6:

$$\frac{1}{4} * \left(\mathrm{n(Fe(II)\bullet EDTA)^{2-}_{(aq)}}\right) = \mathrm{nO_{2\,(aq)}} \qquad \text{(Eq.4-6)}$$

Once the theoretically required amount of O_2 (n_{O2}) for the given amount of Fe(II)•EDTA is determined, the required partial pressure of the O_2 (P_{O2}) and subsequently the required pressure of air to be supplied into the solvent systems (20.9 vol% O_2, >79 vol% N_2), the P_{air}, can be calculated by the ideal gas law as it is expressed in Eq.4-7:

$$P_{air}\ x\ 0.209 = P_{O_2} = \frac{nO_{2\,(aq)}RT_G}{V_G} \qquad \text{(Eq.4-7)}$$

where the V_G (m^3) is the volume of the gas phase, R is the ideal gas constant (J/mol.K) and T_G (K) is the temperature of the gas phase. Subsequently, the dissolved O_2 concentration, c_{O2}, can be calculated using the Eq.4-8 according to Henry's law. The solubility of the gas component, i, in the liquid phase in absence of chemical reaction can be described by the Henry coefficient (bar.L/mol) and is defined as the ratio of the partial pressure of the gas and its concentration in the bulk liquid at equilibrium:

$$He, i = P_i / c_{i(l)} \qquad \text{(Eq.4-8)}$$

For physical absorption of a gas in a respective solvent system in a batch setup, the mass balance gives the following relation for the Henry coefficient[15]:

$$He, i = \frac{P_{i_{t=\infty}} - P_w}{P_{i_{t=0}} - P_{i_{t=\infty}}} \frac{RTV_L}{V_G} \qquad \text{(Eq.4-9)}$$

where the subscripts (t=0) and (t=∞) stand for the initial value at the beginning of the test and final value at the end of the test, respectively. The term w denotes for the water, which accounts for the partial pressure of the aqueous solutions studied in this context. The solubility of gases in pure liquids is significantly different from liquids with already soluted electrolytes. The adverse influence of the charged ions in the solution on the solubility of a gas is called as salting-out effect and lowers the amount of the gas that is to be solved in a liquid. Schumpe proposed a model for the correction of the Henry's constant for a mixture of electrolytes by taking the salting-out effect into consideration: Therefore, corrected Henry coefficients for O_2 in different liquid redox solutions (Solution A to C) calculated from the model proposed by (Schumpe, 1993) can be written as:

$$\log \frac{He, i}{He_w} = \sum_i (h_i + h_G) c_i \qquad \text{(Eq.4-10)}$$

The declinations of the terms used in Eq.4-10 are as following: He,i (bar.L/mol) is the corrected Henry coefficient of the respective component in the electrolyte solution, He_w (bar.L/mol) is the Henry coefficient in pure water, h_i is the ion specific constant in L/mol, whereas the h_G is the gas specific constant in L/mol and c_i stands for the concentration of the species i in mol/L. Furthermore, the model can be extended to a wider range of temperature by the following modification:

$$h_G = h_{G,0} + h_T(T - 298.15) \qquad \text{(Eq.4-11)}$$

where the term h_T is the temperature correction parameter of the gas specific constant in L/mol.K and the term $h_{G,0}$ is the respective value of this constant in L/mol at T = 298.15 K.

In addition to the determination of the solubility of the O_2, the information on other possible O_2 consuming reactions besides the main reaction (Eq.4-1) is also important to find out whether the concentration decrease of the O_2 occurs only due to the consumption of it for the oxidation of the Fe(II)•EDTA or also due to the consumption of it in side reactions. Thus, the real stoichiometric coefficient of iron (ν_B) for the reaction system has to be determined experimentally, as described in the following subsection.

4.1.1.1.2.2 Determination of the real stoichiometric coefficient of iron

As it was expressed in the regeneration reaction, Eq.4-1, the O_2 supplied into the system shall be theoretically used to oxidize the Fe(II)•EDTA to Fe(III)•EDTA with a stoichiometrical ratio of the

[15] The Eq.4-9 is only valid with the assumption that all O_2 in the gas phase is transferred into the liquid phase or that the partial pressure of the O_2 remaining in the gas phase can be neglected.

respective reaction partners, one to four. However, this reaction can run differently in real operating conditions depending on e.g. the occurrence of side reactions. In this case neither the stoichiometric coefficients of the reaction partners nor the type of the reaction products would be known. Thus, the reaction Eq.4-1 can be expressed as Eq.4-12 under real operating conditions.

$$\nu_B(\mathrm{Fe(II)} \bullet \mathrm{EDTA})^{2-}{}_{(aq)} + \mathrm{O_2}_{(aq)} \rightarrow \text{products} \qquad \text{(Eq.4-12)}$$

The real stoichiometric coefficient of the iron, the ν_B, can be calculated with the help of Eq.4-13.

$$c(\mathrm{Fe(II)} \bullet \mathrm{EDTA})^{2-}{}_{(aq)t=t}.V_L = c(\mathrm{Fe(II)} \bullet \mathrm{EDTA})^{2-}{}_{(aq)t=0}.V_L - \nu_B.nO_{2\,(aq)} \qquad \text{(Eq.4-13)}$$

The concentrations of the iron chelates before and after reaction (i.e. the $c(Fe(II)\bullet EDTA)_{t=0}$ and $c(Fe(II)\bullet EDTA)_{t=t}$, respectively) can be analyzed by UV-Vis as mentioned in section 3.5.1.3, while the total number of moles of O_2 absorbed, n_{O2}, can be calculated from the absorption profiles recorded during the decreasing pressure experiments. If the value of the ν_B calculated based on the experimental results differs from 4, it reveals the occurrence of the undesired side reactions. Thus, in addition to the reaction rates, the ν_B is also to be considered as an important indicator of the effectiveness of the different solutions while comparing the regeneration performances of them.

In order to specify the rate of the regeneration reaction, Eq.4-1, first, the solubility of the O_2 must be described whereafter the values of x, y and k must be identified, as presented in the following subsections.

4.1.1.2 Approach for the determination of kinetic data at various process conditions

In the scope of this study, two different approaches were conducted to determine the required kinetic data, i.e. the reaction rate, reaction constant and order of the reactive species. By doing this, the regeneration kinetic behavior of the formulated solutions will be investigated under the pre-determined conditions applied for this study. These two approaches, namely the pseudo order approximation and decreased pressure approach, will be addressed in the following subsections.

4.1.1.2.1 Pseudo-order kinetics by constant pressure experiments

In some studies available in open literature, the regeneration reaction has been stated as first order in Fe(II)•EDTA, whereas a second order dependency is observed in some other studies (see **Table 4-1**). Reportedly, the change in the order in Fe(II)•EDTA is supposed to be a function of the concentration of it. At low concentrations, the reaction seems to be first order in Fe(II)•EDTA, whereas the order changes to 2 at increasing Fe(II)•EDTA concentrations. So that to verify this phenomenon under the conditions applied in this study and to acquire first-hand-information regarding the order dependency of interacting species, determination of the pseudo kinetic data by **constant pressure experiments** was prior to determination of the r in decreasing pressure experiments (section 4.1.1.2.2). Accordingly, the values of x, y and k are found by application of the so-called method of initial rates (Connors, 1990). This method allows the values of these parameters to be found by running the reaction multiple times under controlled conditions and measuring the rate of the reaction in each case ($r=dco_2/dt$). All variables are held constant from one run to the next, except for the concentration of only one reactant (either concentration of the O_2 or the Fe(II)•EDTA). The empiric order of that reactant in the rate law can be specified by observing how the reaction rate, r, varies as the concentration of that reactant is changed. This method is repeated for each reactant until all the orders (i.e. x and y) are determined. At that point, the rate law (i.e. Eq. 4-5) can be used to find the value of k for each experiment. If the temperatures are the same for each test, the values of k should be the same too. The method of initial rates relies upon the assumption that the concentration of each reactant and the temperature do not change significantly over the time interval during that the reaction rate is being measured. This is accomplished by the application of a **pseudo-first-order approximation** proposed by (Turanyi & Tomlin, 2014). In this context, conditions required for a pseudo first order reaction can be fulfilled by manipulating the initial concentrations of the reactants.

If the concentration of one reactant is in excess, its concentration is assumed to remain constant during the reaction because its consumption is small enough the change in concentration becomes negligible. Because of this assumption, the reaction rate law Eq.4-5 is shortened to Eq.4-14 and Eq.4-15 for the cases of excess amount of ferrous chelate and O_2, respectively (see **Table 4-3**). To get pseudo order kinetic data relevant to the Siemens liquid-redox process, the constant pressure experiments were conducted for the solvent system, which is called (B) - containing Siemens Solvent-1+Fe(II)•EDTA - under the conditions given in **Table 4-3**.

Once the background to obtain the pseudo kinetic data for the controlled conditions is given and the behavior of the reaction law towards respective interactive species (meaning Eq.4-14 and Eq.4-15) is understood, determination of the kinetic rate constant by decreasing pressure experiments under given process conditions is the next step, as presented in the following section.

4.1.1.2.2 Reaction rate determination by decreasing pressure experiments

The kinetic data under varying process conditions reveal the functional relationship between concentration and reaction rate as well as whether the amount of a compound speeds up or retards the reaction. Subsequent to determination of the k, the r is calculated (see Eq. 4-5) in each case by using the pre-set values for v_B, x and y. The calculated value is then fitted by adjusting the v_B, x and y and by conducting the least square method (generalized reduced gradients (GRG) non-linear algorithm (Jain, A. et al., 1978)) – until the value of $r_{calculated}$ corresponds to its measured value ($r_{measured}=dco_2/dt$) (e.g. see **Figure 4-9**). **The rate determination** was executed in three different formulated solvent systems (A), (B) and (C) by **decreasing pressure experiments** under variation of the parameters given in **Table 4-4**.

After discussing the background of the kinetic experiments conducted in this study, the preparation of the investigated solvent systems, experimental set up and procedure of all performed tests are presented in the following sections.

4.1.2 Preparation of feed substances

Aqueous solutions of Fe(II)•EDTA are extremely O_2-sensitive, thus all formulated solvent systems were handled in so-called glove boxes under a protective N_2 atmosphere.

The solvent system (A) (chelated metal w/o AAS) was prepared by;
(1) dissolving a predetermined amount of EDTA (Na-salt) purchased from Sigma Aldrich 99% in degassed and double-distilled water. The pH of the prepared solution was adjusted to a value of 9.5 with an alkaline buffer solution.
(2) adding the appropriate amount of the metal catalyst in its lower oxidation state (the Fe(II) in anhydrous form of its metal-halide, purity>98% from Chemical Point Company) to the dissolved EDTA, thus producing an aqueous Fe(II)•EDTA solution.

The solvent systems (B) and (C) (chelated metal with AAS) were each prepared by;
(1) neutralizing a predetermined amount of the amino acid, (dimethylglycine or the Solvent-1 respectively – both >99% from Chemical Point Company) in aqueous solution with KOH-pellets (>96 % from neoLab) to produce its potassium salt (e.g. Dimethylglycine+KOH→K-Dimethylglycine + H_2O ~ Dimethylglycinate)
(2) adding the AAS solution to the already prepared Fe(II)•EDTA solution (both in aqueous solution and in predetermined amounts).

In this context, it shall be noted that all substances were prepared to have comparable values for α_{ion} by applying equal concentrations of the constituents, since different ionic strengths (α_{ion}) and viscosities (μ) result in changes of the solubility, diffusivity and liquid side mass transfer coefficient of the O_2 and thus its absorption rate. The resulting densities of the solutions and the kinematic viscosities were measured.

The results of the measurements given in **Table A- 5** in Appendix A-2.3 showed that they all had comparable densities and viscosities so that also the influence of these parameters on the absorption rate of the O_2 could be ruled out.

The **gaseous substances**, the air (purity>99.5%; 20.9% O_2, N_2>79%) and the N_2 (purity>99.99%) were obtained from Infraserv GmbH.

4.1.3 Experimental set up, procedure and analytical method

All kinetic experiments were conducted in a tempered stirred cell reactor (see **Figure 4-3**) in which the amount of sparged air can be controlled and the amount of consumed O_2 can be determined.

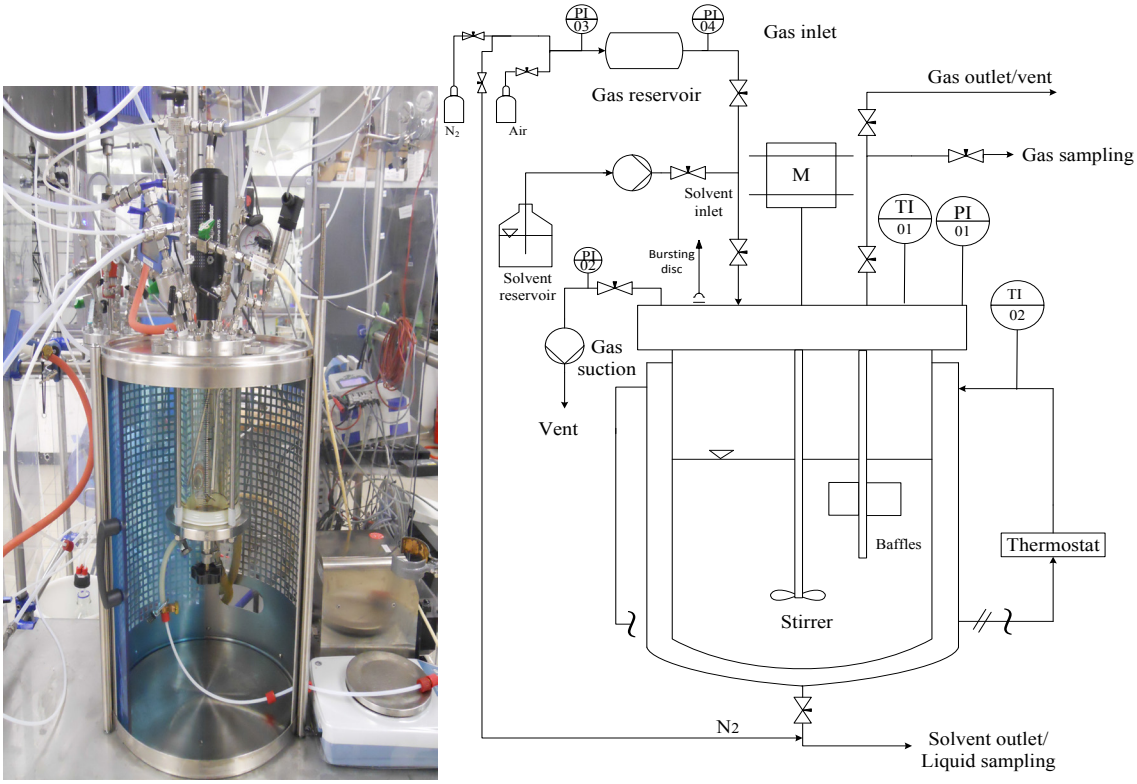

Figure 4-3 Experimental set up of the kinetic tests

The dimensions of the reactor are given in **Table 4-2**.

Table 4-2 Characteristics of the stirred cell reactor

Type	Buechi, Ecoclave 075
Main material	Glass
Diameter, m	0.082
Total volume of reactor, m^3	1.523×10^{-3}
Liquid volume, m^3	0.75×10^{-3}
Liquid impeller type	Three-flat-bladed (tilted 45° to horizontal level) stirrer; diameter of 0.06 m, length of 0.22 m
Allowable operation pressure, bara	6 (in laboratory)
Allowable operation temperature, °C	Up to 100 °C

A three-bladed turbine stirrer was located centrally at a height of 0.04 m (lower end of the agitator shaft) above the reactor bottom. Two symmetrically mounted stainless steel baffles increased the effectiveness of the mixing and prevented the formation of a vortex. The reactor was thermostated with a Huber Ministat-125 thermostat. The temperature and pressure transducers TI01 (BIS Pt100, 0-450°C) and PI01 (GE 5000, 0-6 bar) were connected to a data logger (Ahlborn Almemo

2890-9), thus enabling automatic data collection with the AMR WinControl software, which had been programmed for reactor operation. The pressure of the reactor could be set to the desired values either by evacuating it via a vacuum pump (PI02) or by a pressure release valve (PI01). Additionally, a rupture disc was installed which would protect the glass reactor against cracking in case of pressure exposure of more than allowable working limit (refer to **Table 4-2**).

4.1.3.1 Procedure of the constant pressure experiments

To get pseudo order kinetic data relevant to the Siemens liquid-redox process, the constant pressure experiments were conducted for the solvent system, which is called (B) - containing Siemens Solvent-1+Fe(II)•EDTA - under the conditions given in **Table 4-3**.

Table 4-3 Experimental conditions of constant pressure experiments performed in solvent system-(B)

Solvent system / **Standard experimental parameters**	(B) Solvent-1 + Fe(II)•EDTA
Reaction equation	$2(\mathrm{Fe(II)\bullet EDTA})^{2-}_{(aq)} + 1/2O_{2(aq)} + H_2O \rightarrow 2(\mathrm{Fe(III)\bullet EDTA})^{-}_{(aq)} + 2OH^{-}_{(aq)}$
Stirrer speed, (rpm or min^{-1})	2200 (for determination see section 4.1.4)
pH	9.5
T, (°C)	30
EDTA to Fe(II) ratio,(mol/mol)	1.5
Case1- Fe(II)•EDTA in excess (low O_2 partial pressure)**:**	Parameter variation for the determination of the pseudo reaction order with respect to O_2
Reaction rate equation	$r = \frac{dc_{O_2}}{dt} = -kc^{x}_{O_2}$ (Eq.4-14)
c[Fe(II)], mol/m^3	2Ψ=200
c[O_2], mol/m^3	0.2Φ= 5 (~the O_2 partial pressure, P_{O2}= 0.12 bar at 30 °C)
Case2- O_2 in excess (Fe(II)•EDTA in low concentration)**:**	Parameter variation for the determination of the pseudo reaction order with respect to Fe(II)
Reaction rate equation	$r = \frac{dc_{O_2}}{dt} = -kc^{y}_{Fe(II)\bullet EDTA}$ (Eq.4-15)
c[Fe(II)], mol/m^3	0.01Ψ=1
c[O_2], mol/m^3	1.5Φ= 37.5 (~the O_2 partial pressure, $P_{O2,\ t=0}$= 0.9 bar at 30 °C)

An experimental procedure for the constant pressure experiments described in detail by (Beenackers & Wubs, 1993) was applied. The bulk of the respective solution was fed from the solvent reservoir to the reactor while continuously purging with N_2. The reactor content was heated to the desired temperature by means of the thermostat. Subsequently, a sample of liquid was taken to analyze the initial amount of the Fe(II)•EDTA in the reactor by UV-Vis. Before starting an experiment, the headspace of the reactor was evacuated to remove the enclosed air, until the vapor pressure of water at the respective temperature was established. At this point, air was supplied to the reactor until the calculated desired pressure was reached (for the calculation see section 4.1.1.1.2.1 - Eq.4-7; the desired value was depending on the aim of the experiment – either Fe(II)•EDTA or O_2 in excess see **Table 4-3**). Subsequently, the inlet valve was closed, the stirrer was activated, and the absorption process was started. The O_2 absorbed into the solution and reacting with the Fe(II)•EDTA resulted in a pressure decrease until a minimum experimental pressure was reached, after which extra air was supplied until the initial pre-set maximum pressure (the value was individually pre-set for every pressurization), was reached again.

By repeating this procedure several times, the pressure profile appeared as a saw-tooth-like curve (see **Figure 4-4**).

4.1.3.2 Procedure of the decreasing pressure experiments

The rate determination was executed in three different formulated solvent systems (A), (B) and (C) by decreasing pressure experiments under variation of the following parameters (see **Table 4-4**):

- the AAS type in (B) and (C)
- the concentration of dissolved oxygen, $c_{O2,}$ in mol/m^3) in (A), (B) and (C) by variation of the O_2 partial pressure
- the concentration of the ferrous chelate (c[Fe(II)•EDTA] in mol/m^3) in (B)
- the temperature (T in °C) in (A), (B), and (C).

Table 4-4 Investigated solutions and experimental conditions of decreasing pressure experiments

Solvent system / **Reference conditions**	(A) water (without AAS) + Fe(II)•EDTA	(B) Solvent-1 (secondary AAS) + Fe(II)•EDTA	(C) Dimethylglycinate (tertiary AAS) + Fe(II)•EDTA
Reaction equation	$2(\mathrm{Fe(II)EDTA})^{2-}_{(aq)} + 1/2\mathrm{O}_{2(aq)} + \mathrm{H_2O} \rightarrow 2(\mathrm{Fe(III)EDTA})^{-}_{(aq)} + 2\mathrm{OH}^{-}_{(aq)}$		
Reaction rate equation	$r = \frac{dc_{O_2}}{dt} = -kc^{x}_{O_2} c^{y}_{Fe(II).EDTA}$ (Eq. 4-5)		
Stirrer speed, (rpm or min^{-1})	2200 (for determination see section 4.1.4)		
pH	9.5		
T, (°C)	30		
c[Fe(II)], mol/m^3	1Ψ=100		
EDTA to Fe(II) ratio,(mol/mol)	1.5		
c[O_2], mol/m^3	1Φ= 25 (~the O_2 partial pressure, P_{O2}= 0.6 bar at 30 °C)		
Variations deviating from reference conditions	(A) water (without AAS) + Fe(II)•EDTA	(B) Solvent-1+ Fe(II)•EDTA	(C) Dimethylglycinate + Fe(II)•EDTA
c[Fe(II)], mol/m^3	reference	0.5Ψ=50 and 2Ψ=200	reference
c[O_2], mol/m^3	1.5Φ=37.5	1.5Φ=37.5	1.5Φ=37.5
T, (°C)	60	60	60

The bulk of the respective solvent system was fed from the solvent reservoir to the reactor under continuously purging with N_2. The reactor content was heated to the desired temperature by means of the thermostat. Subsequently, a sample of liquid was taken to analyze the initial amount of the Fe(II)•EDTA in the reactor by UV-Vis. Before starting an experiment, the headspace of the reactor was evacuated to remove the air, until the vapor pressure of water at the respective temperature was established. The pre-determined amount of air was supplied to the reactor until the pressure reached the desired value. At this point, the inlet valve was closed, the stirrer was activated, and the absorption was started. The pressure decrease was measured until it reached a minimum and remained constant, which indicated that the reaction between the interactive species and the O_2 was ended. After the experiment was finished, the solution was drained by opening the respective valve under N_2 atmosphere. Typical pressure profiles obtained with this procedure are given in **Figure 4-7**. The rate of the regeneration reaction is controlled by the diffusion of O_2 in the liquid and its reaction there (see Eq.4-2). The diffusion of O_2 increases with T, solution pH, and the contact time. The dissolved oxygen concentration, c_{O2}, will vary for a given $P_{O2,t=0}$ depending on T, c, pH and the O_2 consumption rate of the solution. If the parameters T, c and the pH are kept constant for a given $P_{O2,t=0}$, the O_2 consumption rate becomes directly related to the conversion rate of Fe(II) to Fe(III). The conversion rate of ferrous chelate (i.e. Fe(II)•EDTA) to ferric chelate (i.e. Fe(III)•EDTA) of the samples taken at the beginning and the end of each experiment was therefore analyzed by UV-Vis as it was explained in section 3.5.1.3.

4.1.4 Results and discussion

Before presenting the results of the applied two approaches, constant and decreased pressure experiments, first, the results of the determination of gas solubilities shall be described: In the study of (Behringer, 2015), where similar solvent systems were tested in the same experimental set up used in this study (**Figure 4-3**), **the agitation speeds of 2200 rpm or min^{-1}** was found to be optimal, since at this speed the highest mass transfer efficiency was reached under conditions comparable to this study. Thus, the influence of mass transfer limitations on the chemical reaction kinetics was eliminated by applying this already determined optimal agitation velocity for the experimental systems used. Furthermore, the physical solubility data of the O_2 from the regeneration air in comparable solvent systems considered in this work were obtained from the study of (Behringer, 2015). Behringer performed physical solubility experiments of air, thus of the N_2 and O_2, in respective solvent systems not containing Fe(II)•EDTA at both 30 °C and 60°C. As an example of these physical solubility experiments, the pressure decrease curve of air in Solvent-1 (without Fe(II).Lig) at 30°C is given in **Figure A- 1** in Appendix A-2.1 providing the required input data for the calculation of $He_{,O2}$ in the given solution by applying Eq.4-9. The results of the calculated $He_{,O2}$ under given conditions are available in **Table A- 3** in Appendix A-2.1. As it was mentioned in section 4.1.1.1.2.1, the obtained Henry coefficients were corrected by applying Eq.4-10 where the $h_{G,O2}$ was calculated inserting the data of h_T, $h_{G,0}$ and h_i taken from (Schumpe, 1993) into Eq.4-11. The values of corrected $He_{,O2}$ (both at 30°C and 60 °C) and the $h_{G,O2}$ calculated for the investigated solutions (i.e. Solution (A) to (C)) and water for the comparison are given in **Table A- 4** in Appendix A-2.2. To sum up, the physical solubility experiments all led to a fast and relatively small pressure decrease. Thus, it was concluded that the pressure decrease observed in the experiments within this study depends practically only on the consumption of O_2 due to the chemical reaction. In consequence, the monitored pressure decrease of the O_2 only reflects the kinetics of the reaction as the the physical absorption and the mass transfer resistance from gas to liquid phase do not have noticeable influence.

4.1.4.1 Results of constant pressure experiments

4.1.4.1.1 Case1 - Determination of pseudo-order kinetic data of O2 with Fe(II)•EDTA in excess

In this experiment, the $c(Fe(II)•EDTA)_{t=0}$ was added in an amount 10 times[16] higher than the initial stoichiometric O_2 requirement in order to meet the conditions for pseudo first-order approximation. As a result of the constant pressure test under the conditions given in **Table 4-3**, the so-called “sawtooth curve (Wubs, 1994)” was obtained and is shown in **Figure 4-4**.

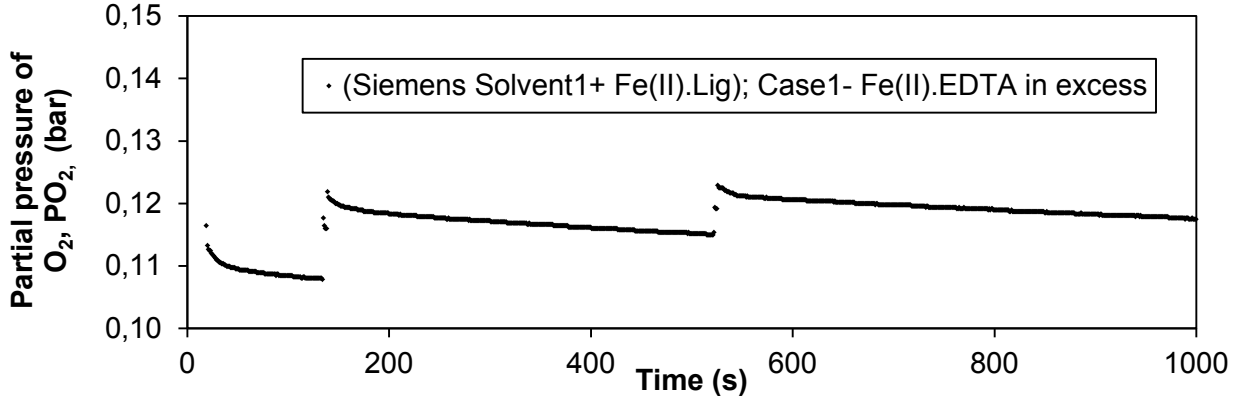

Figure 4-4 Obtained pressure drop profile of solvent system (B) at 30 °C and under conditions for Case-1 as given in Table 4-3

[16] The factor ten emerged from the maximum feasible Fe(II)•EDTA concentration of the solution due to solubility constraints under given conditions.

As it can be seen from the **Figure 4-4**, the condition $\Delta P_{O2(t)} <<< P_{O2(t)}$ was maintained at the second and the third air supply . Thus, the cFe(II)•EDTA$_{(t)}$ during each air-dosing-process can be considered as constant (as it had been added in extensive excess). The natural logarithm of the partial pressure change of O_2, $\ln(PO_{2(t=0)}/PO_{2(t=t)})$, was calculated for all three air-dosing. Plotting $\ln(PO_{2(t=0)}/PO_{2(t=t)})$ versus time followed a linear tendency (see **Figure 4-5**) except for an additional pressure drop at the first air supply caused by co-absorption of the N_2 which was already present in the gas phase due to filling the solution under N_2 purging into the reactor. It was assumed that the solution was saturated with N_2 after the first test.

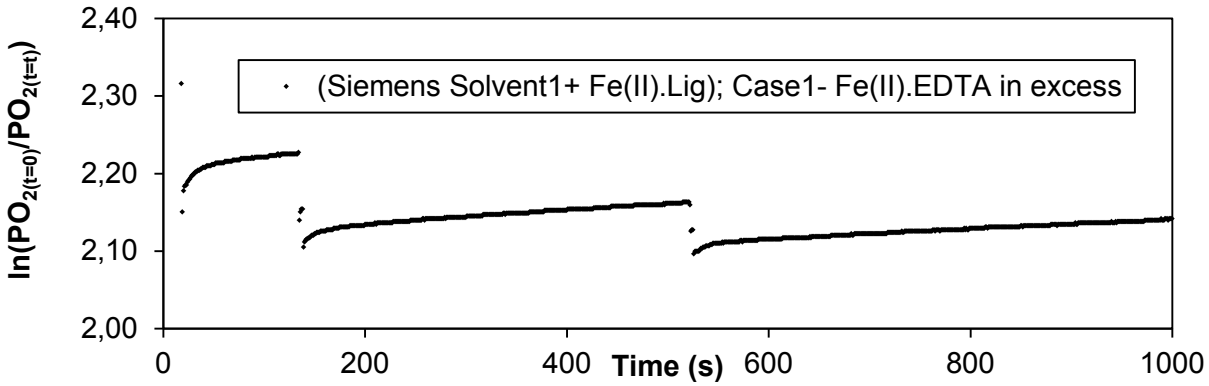

Figure 4-5 Natural logarithm of the pressure gradient of O_2 as a function of time: first-order dependency of the reaction in O_2 under conditions for Case-1 given in Table 4-3

Thus, the reaction rate Eq.4-14 can be described as first order with respect to O_2 which is in a good agreement with the literature results (see **Table 4-1**).

4.1.4.1.2 Case2 - Determination of pseudo-order kinetic data of Fe(II)•EDTA with O2 in excess

In this experiment, 150 times more O_2 than stoichiometrically required for the given c(Fe(II)•EDTA)$_{t=0}$ (see **Table 4-3**) was supplied in order to investigate pseudo first-order behavior of the reaction with respect to Fe(II)•EDTA. The pressure change of the O_2 (which can be assumed as negligible relative to the duration of the measurement i.e. approx. 100 seconds) as well as the natural logarithm of the calculated ferrous-chelate concentration change $\ln(cFe(II)•EDTA_{t=0}/cFe(II)•EDTA_{t=t})$ was plotted versus time and is shown in **Figure 4-6**. At the beginning and the end of the experiment, samples were taken, and the concentrations measured by UV-Vis were compared with the calculated ones – with good accordance.

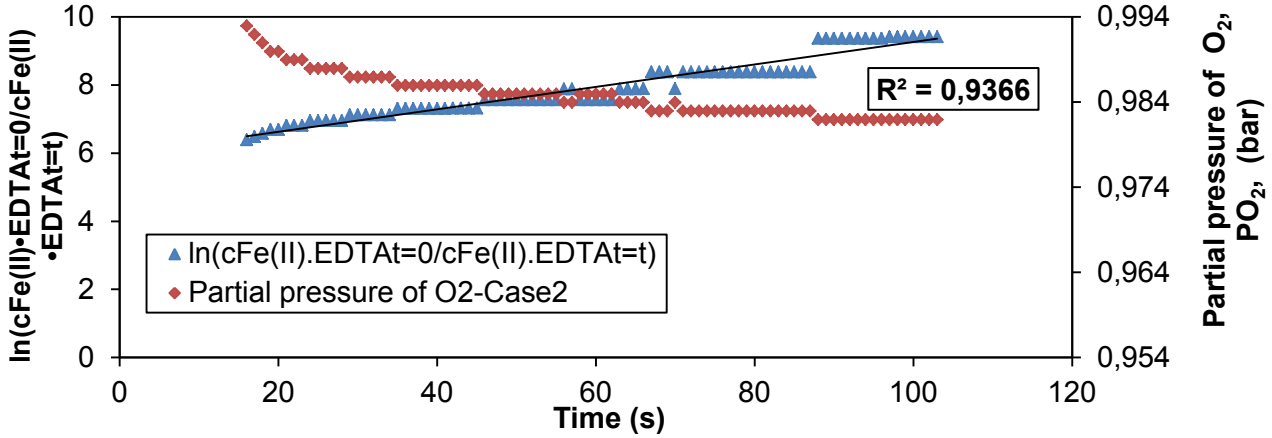

Figure 4-6 Natural logarithm of the concentration gradient of Fe(II)•EDTA: first-order dependency of the reaction in Fe(II) under conditions for Case-2 given in Table 4-3

Similar to the **Figure 4-5**, the plot of $\ln\left(\frac{cFe(II)\bullet EDTAt=0}{cFe(II)\bullet EDTAt=t}\right)$ tends to be a straight line. This reveals that the reaction order with respect to the chelated metal catalyst seems to be 1 for low concentrations (i.e. 0.01Ψ=1 mol/m^3), which is consistent with the literature data (see **Table 4-1**). Also the regression of the natural logarithm of the Fe(II)•EDTA concentration gradient (i.e. R^2= 0.9366 - see **Figure 4-6**) indicated that the measurement enables a fair evaluation. This is important for assessment of the results of investigations on the reaction kinetics by decreasing pressure experiments under industrial conditions, which are presented in the following subsection.

4.1.4.2 Results of decreasing pressure experiments

4.1.4.2.1 Influence of the AAS type on the regeneration kinetics

The experimental procedure for decreasing pressure as described in section 4.1.3.2 was used to investigate the influence of the type of AAS on the regeneration reaction Eq.4-1 at two different temperatures. For comparison, an aqueous Fe(II)•EDTA solution without AAS was applied. The partial pressure decrease curves of O_2 in contact with solutions (A), (B) and (C) under the reference conditions (i.e. T=30°C, c[Fe(II)]~1Ψ=100 mol/m^3, c[O_2]~1Φ= 25 mol/m^3, etc.) given in **Table 4-4** is shown in **Figure 4-7**.

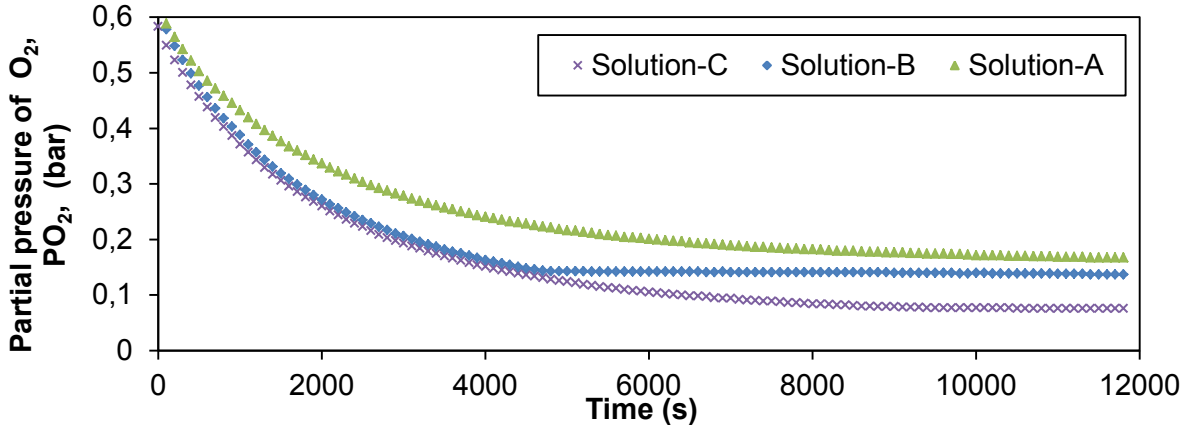

Figure 4-7 Partial pressure gradient (in time) curve of O_2 in contact with all investigated solutions under reference conditions given in **Table 4-4** (T=30°C, 1Φ, 1Ψ)

If all other parameters are kept constant and only the temperature is changed (i.e. T=60°C, c[Fe(II)]~1Ψ=100 mol/m^3, c[O_2]~1Φ= 25 mol/m^3, etc.) the partial pressure curves of oxygen, $P_{O2(t)}$, versus time given in **Figure 4-8** are obtained.

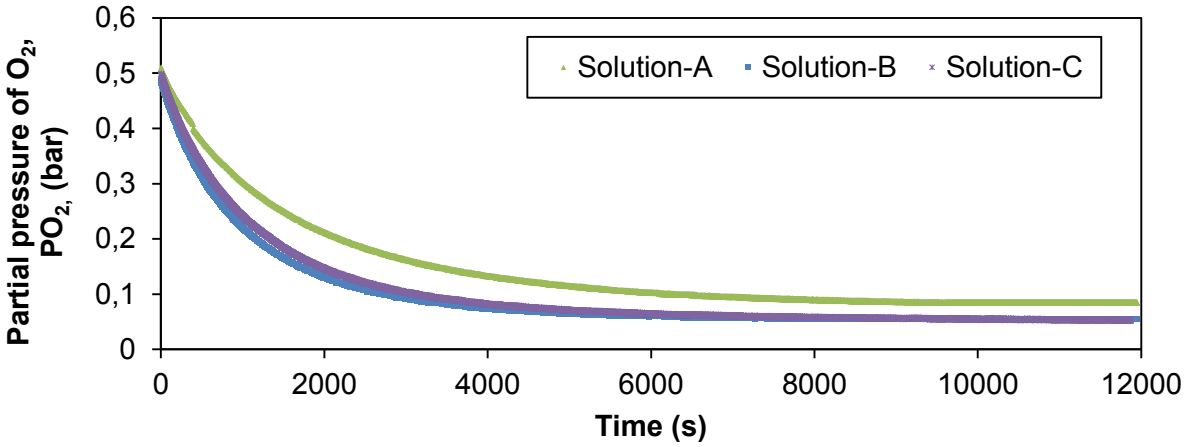

Figure 4-8 Partial pressure gradient (in time) curve of O_2 in contact with all investigated solutions under varied conditions given in **Table 4-4** (T=60°C, 1Φ, 1Ψ)

The change in the solutions' redox potential were also measured offline using a digital meter with multiple probes (accuracy ± 0.02 mV see **Table 4-12**) at the beginning and at the end of the experiment. The results are given in **Table 4-5** for the experiments at 30 °C.

Table 4-5 Redox potential in the solutions before and after the regeneration reaction at 30 °C

Parameter / Solution	Redox potential, E, in mV (before/after) (t=0 / t=12000 s)
Solution-(A)	-350/+55
Solution-(B)	-330/+40
Solution-(C)	-330/+40

As it was mentioned in section 3.4.2.1, the change in the solution's redox potential is a significant indicator for evaluating whether the environment is oxidative (ΔE > 0) or reductive (ΔE < 0). After the regeneration reaction the solutions' redox potential changed from negative to positive, which indicates that the oxidation of the reduced chelated metal catalyst took place. The changes in the redox potential of all solutions are comparable (see **Table 4-5**), which reveals that the degree of conversion of the chelated-metal catalyst is not dependent on the type of AAS.

4.1.4.2.2 Determination of the reaction orders, the kinetic constants and the rate of the regeneration reaction

All solutions listed in **Table 4-4** were tested either for variation on T (30 °C or 60 °C) or on the supplied O_2 amount (1Φ= 25 mol/m^3 or 1.5Φ=37.5 mol/m^3). The chelated metal concentration (1Ψ= 100 mol/m^3), the value of the pH (9.5) and the stirrer speed (2200 rpm) were kept constant. As an example, the resulting graph of the Dimethylglycinate+Fe(II)•EDTA (i.e. Solution-(B)) under reference conditions (T=30°C, 1Ψ and 1Φ etc.) is shown in **Figure 4-9**.

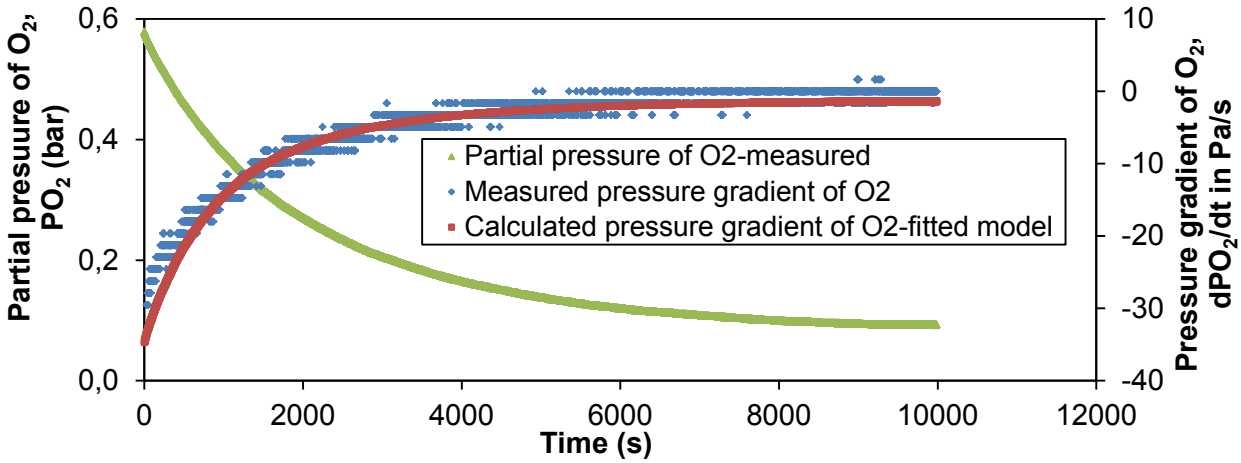

Figure 4-9 Measured partial pressure decrease of O_2 in contact with Solution-(B) under reference conditions given in Table 4-4 (e.g. T=30°C, 1Ψ and 1Φ etc.)

Following the procedure described in section 4.1.1.2.2 and taking the measured partial pressure decrease curves of O_2 in contact with the tested solutions into account, the kinetic data were calculated (i.e. r, k, v_B, x and y) according to the kinetic model of Eq.4-5. The results are compiled in **Table 4-6**.

Table 4-6 Results of decreasing pressure experiments (T= 30 and 60 °C, cFe(II)•EDTA=1Ψ=100 mol/m^3, c_{O2}=1.0Φ=25 mol/m^3 and 1.5Φ=37.5 mol/m^3 and other reference conditions given in Table 4-4

Calculated kinetic data		x (-)	y (-)	k ($L^y/mol^y.s$)[17]	$k_{1.5\Phi}/k_{1\Phi}$ (-)	r (10^{-5} mol/L.s)	$r_{1.5\Phi}/r_{1\Phi}$ (-)	v_B (-)
Varied parameter		**T=30°C**						
Solution-(A)	**1.0 Φ**	1	1.8	3.67	1.01	1.31	1.96	4.0
	1.5 Φ	1	1.8	3.70		2.57		3.3
Solution-(B)	**1.0 Φ**	1	1.8	5.0	0.97	1.58	1.56	3.5
	1.5 Φ	1	1.8	4.88		2.47		3.5
Solution-(C)	**1.0 Φ**	1	1.8	4.14	1.09	1.37	1.73	3.6
	1.5 Φ	1	1.75	4.52		2.37		3.5
Varied parameter		**T=60°C**						
Solution-(A)	**1.0 Φ**	1	1.9	6.50	1.00	1.40	1.93	4.0
	1.5 Φ	1	1.8	6.55		2.68		3.5
Solution-(B)	**1.0 Φ**	1	1.75	9.93	0.99	2.10	1.52	4.0
	1.5 Φ	1	1.8	9.83		3.36		3.5
Solution-(C)	**1.0 Φ**	1	1.8	8.59	1.02	2.73	1.47	3.7
	1.5 Φ	1	1.8	8.78		4.03		3.5

Considering the reaction rate law Eq.4-5, the following relationship between the reaction rates $r_{(1.0\Phi)}$ and $r_{(1.5\Phi)}$ emerges, if all other parameters are kept constant, but only the O_2 concentration is varied and if the reaction is first order with respect to O_2:

$$\frac{r(1.5\Phi)}{r(1.0\Phi)} = \frac{-kc_{O_2}^{x}(1.5\Phi)c_{Fe(II)\bullet EDTA}^{y}}{-kc_{O_2}^{x}(1.0\Phi)c_{Fe(II)\bullet EDTA}^{y}} = 1.5 \qquad \text{(Eq.4-16)}$$

- As it is given in **Table 4-6**, the reaction rate increases linearly with the O_2 concentration for both temperatures and for all three solutions. Thus, the reaction order with respect to O_2 is found to be 1 for each tested solution which is in a good agreement with literature data.

- Since k is a characteristic constant for a reaction, it does not change for the same reaction and the same solution if only the concentrations of the reactants are varied. Each solution showed similar k values for Φ = 1.0 and Φ = 1.5 at both temperatures (with an accuracy of ± 2%; except the test with the Solution (C) at 30 °C which showed an accuracy of ±9% see **Table 4-6**).

- The calculated values of the reaction rate constants and reaction rates at 30 °C for Φ = 1.0 lead to the following ranking, respectively: $\mathbf{k_A<k_C<k_B}$ **and** $\mathbf{r_A<r_C<r_B}$**.** These rankings reveal the ability of AAS to buffer the H^+ ions (one of the reaction partners see Eq.4-1), which shifts the equilibrium of the reaction to the side of the products and simultaneously accelerates the reaction leading to higher r values (secondary AASs have higher buffering capacity).

- Both AAS show comparable results concerning the ratio of the reaction rates. As a conclusion, no influence of the AAS structure on the reaction order with respect to O_2 can be stated for the two AAS which were applied.

- The v_B values were determined using Eq.4-13 for a number of absorption experiments performed with different O_2 partial pressures (0.6 and 0.9 bar) and T values of 30 and 60 °C at a constant $c_{Fe(II)\bullet EDTA}$=1Ψ=100 mol/m^3. The experimentally obtained constants of the reaction

[17] Since the empiric order of the reaction with respect to O_2 was found to be 1 in each experiment, the unit of the k depends on the magnitude of the empiric order of the reaction with respect to Fe(II)•EDTA in this study.

stoichiometry (see **Table 4-6**) differed from the theoretically calculated value of 4 which indicates that side reactions took place. The v_B values ranged from 3 to 4 and are dependent on the supplied amount of O_2. For example, at lower O_2-supply (i.e. for 1.0 Φ) the v_B was close to 4 for Solution (A), indicating that other O_2 consuming reactions either did not take place – or only to a minor extent. With increasing O_2-supply (i.e. for 1.5 Φ), the v_B dropped significantly to a value of 3.3 (see **Table 4-6**) for the same solution.

- The results at 60 °C concerning the reaction order with respect to O_2 and Fe(II)•EDTA are in good agreement with the findings at 30 °C. The reaction rate constants, k, were practically equal for the experiments with different c_{O2} (Φ = 1.0 and Φ = 1.5) and were higher compared to the values at 30°C. The reaction rates r of all solutions (A), (B) and (C) were greater than the corresponding rates at 30 °C. This is expected following the Arrhenius law, which is presented in the next part of this section.

4.1.4.2.3 Determination of the kinetic constant of the regeneration reaction at various temperatures

All experiments were performed under conditions defined as reference (see **Table 4-4**). The temperature was varied to determine the T-dependence of the reaction rate constant, k. In theory, this dependence is exponential and is described by the Arrhenius law (Turanyi & Tomlin, 2014):

$$k = A.\, e^{(-\frac{E_a}{RT})} \qquad \text{(Eq.4-17)}$$

where A is the pre-exponential factor $(L^y/mol^y.s)$[17] and Ea is the activation energy in kJ/mol. Taking the natural logarithm of the Arrhenius law leads to:

$$\ln(k) = -\frac{E_a}{R}\frac{1}{T} + \ln(A) \qquad \text{(Eq.4-18)}$$

The experimentally determined k values at two different temperatures (i.e. 30 °C and 60 °C) are graphically provided in the form of an Arrhenius plot as shown in **Figure 4-10**. For comparison, experimental data of (Wubs, 1994) are added, which were determined at three different temperatures (i.e. 20 °C, 36 °C and 58 °C) for the Fe(II)•EDTA system (pH=7.5; EDTA to Fe(II) ratio=1.2; initial c[Fe(II)]=100 mol/m^3, [cO_2]= 0.125-1.25 mol/m^3 see **Table 4-1**).

Although all other parameters - except the solution pH and the given c_{O2} - are comparable with those applied in this study, the kinetic constants found in (Wubs, 1994) (for natural logarithm of them refer to **Figure 4-10**) are lower than the values calculated by applying the two film model **with** neglected gas-side mass transfer resistance (see **Table 4-6**). These considerable deviations are likely related to the differences in the applied kinetic models and calculation procedures: (Wubs, 1994) employed the film model theory **without** neglecting gas-side mass transfer resistance (the physical solubility of the O_2, as well) to calculate kinetic data which were derived by (DeCoursey, 1974) using the penetration theory of (Danckwerts, 1951). Therefore, the differences in k values seem to be the impacts of the c_{O2} and pH (which are comparably lower than those applied in this study see **Table 4-1**) on the k. The results of (Wubs, 1994), where the plot of ln(k) versus 1/T gives a straight line, can be correspondingly transferred to those found in this study. Thus, in analogy, straight lines were also conducted to fit the data measured at two temperatures in this study. The slopes and the intercepts of the respective line can be used to calculate the Ea and A of the solution by Eq.4-18 as presented in **Table 4-7**.

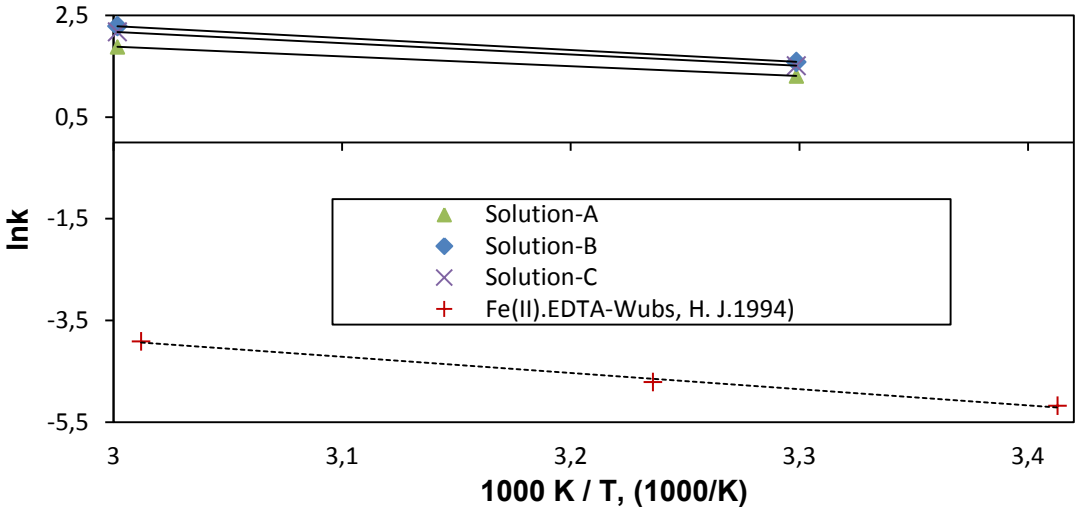

Figure 4-10 Temperature dependence of the rate constants of all tested solutions under reference conditions; solid line: this study; dashed line: (Wubs, 1994) Fe(II)•EDTA system (under conditions given in **Table 4-1**)

Table 4-7 Activation energies Ea and pre-exponential factors of this study obtained from the Arrhenius plot and given in (Wubs, 1994) for a Fe(II)•EDTA system

Parameter / Solution	Ea (kJ/mol)	A ($L^y/mol^y.s$)[17]
Solution-(A)	18.98	2102
Solution-(B)	16.68	11636
Solution-(C)	21.00	7200
Fe(II)•EDTA, (Wubs, 1994)	27.20	1627 ($m^6/mol^2.s$)

The activation energy is also a criterion for the ranking of solutions. In systems, which feature low activation energies, the regeneration reaction would be more feasible, since the energy which has to be provided in order to start the reaction is low. Consequently, a higher energy demand to start the reaction results in slower reaction kinetics. Hence, the activation energy for regeneration should be as low as possible for a solvent used in liquid phase redox oxidation processes. Ranking the investigated solutions depending on their activation energies yields $\mathbf{Ea_B < Ea_A < Ea_C}$. Furthermore, the differences in the values are significant; Ea_B is approx 12 % lower than Ea_A. This makes the Solution-(B) an attractive candidate for further investigations in the continuous lab plant.

4.1.4.2.4 Determination of the kinetic constant of the regeneration reaction under variation of Fe(II)•EDTA concentration

It is reported that the concentration of the metal catalyst has a significant influence on the kinetics of the regeneration reaction. To investigate this, the last group of experiments -with different concentrations of the Fe(II)•EDTA- were conducted in the Siemens-Solvent-1 (Solution-(B)), which had shown advantageous features with respect to the activation energy Ea. The experimental approach as well as the evaluation of the results followed the procedure described for the variation of the supplied O_2 amount (see section 4.1.4.2.2; Eq.4-16). However, the amount of O_2 was pre-calculated for each temperature and kept constant for the different concentrations of the chelated-metal catalyst. Due to the results of the previous investigations, the reaction order with respect to O_2 was set to 1. As variation, however, half (i.e. 0.5Ψ=50 mol/m^3) and twice (i.e. 2Ψ=200 mol/m^3) of the reference concentration of the Fe(II)•EDTA in Solution-(B), (i.e. 1Ψ=100 mol/m^3) at 30 °C were applied in order to investigate the effects of this change on the oxidation kinetics.

As example, the measured O_2-partial pressure ($P_{O2(t)}$) curves and calculated O_2-pressure gradients (dP_{O2}/dt) (T=30 °C, c(Fe(II)•EDTA)=0.5Ψ and 2Ψ) are illustrated in **Figure A- 3** and **Figure A- 4**, respectively in Appendix A-2.4. The results of these experiments are summarized in **Table 4-8**.

Table 4-8 Results of the decreasing pressure experiments (T=30 °C and 60 °C, c(Fe(II)•EDTA)=0.5Ψ=50 mol/m^3 and 2Ψ=200 mol/m^3); cO_2=1.0Φ=25 mol/m^3 and other reference conditions as given in Table 4-4

Calculated kinetic data		x (-)	y (-)	r (10^{-6} mol/L.s)	$r_{2\Psi}$ / $r_{0.5\Psi}$	v_B (-)
Varied parameters		**T=30°C**				
Solution-(B)	**0.5Ψ**	1	1.3	4.2	0.61	3.5
	2Ψ	1	1.8	6.60		4.0
Varied parameters		**T=60°C**				
Solution-(B)	**0.5Ψ**	1	1.3	9.16	0.68	3.5
	2Ψ	1	1.8	13.30		3.5

The influence of the concentration of the Fe(II)•EDTA on its reaction order is different compared to that of the O_2. At lower concentrations of the Fe(II)•EDTA (i.e. 0.5Ψ= 50 mol/m^3) the reaction order was found to be lower (i.e. 1.3) whereas it approximates to 2 at higher Fe(II)•EDTA concentrations (i.e. 2Ψ= 200 mol/m^3). It can be stated that the overall reaction order of the chelated-metal catalyst shows an exponential dependence on its concentration. This observation is fully in agreement with the available literature data (see **Table 4-1**) based on which a concentration-dependency of the reaction order in Fe(II)•EDTA can be proposed. This phenomenon can be explained with the fact that not only the overall reaction determines the reaction kinetics, but different intermediate reactions as well. Based on the references cited in **Table 4-1** including (Butler, J. et al., 1982) and (Cher, M. et al., 1955), the following reaction scheme, which yields to an overall reaction given in Eq.4-23, was proposed to explain this behavior:

$$(\mathrm{Fe(II)} \bullet \mathrm{EDTA})^{-2}{}_{(aq)} + \mathrm{O_2}_{(aq)} \leftrightarrow (\mathrm{Fe(II)} \bullet \mathrm{O_2} \bullet \mathrm{EDTA})^{-2}{}_{(aq)} \quad \text{(Eq.4-19)}$$

$$(\mathrm{Fe(II)} \bullet \mathrm{O_2} \bullet \mathrm{EDTA})^{-2}{}_{(aq)} \rightarrow (\mathrm{Fe(III)} \bullet \mathrm{EDTA})^{-}{}_{(aq)} + \mathrm{O_2^-}_{(aq)} \quad \text{(Eq.4-20)}$$

$$(\mathrm{Fe(II)} \bullet \mathrm{O_2} \bullet \mathrm{EDTA})^{-2}{}_{(aq)} + (\mathrm{Fe(II)} \bullet \mathrm{EDTA})^{-2}{}_{(aq)} + 2\mathrm{H_2O}_{(aq)} \leftrightarrow 2(\mathrm{Fe(III)} \bullet \mathrm{EDTA})^{-}{}_{(aq)} + \mathrm{H_2O_2}_{(aq)} + 2\mathrm{OH^-}_{(aq)} \quad \text{(Eq.4-21)}$$

$$(\mathrm{Fe(II)} \bullet \mathrm{EDTA})^{-2}{}_{(aq)} + \mathrm{O_2^-}_{(aq)} + 2\mathrm{H_2O}_{(aq)} \rightarrow (\mathrm{Fe(III)} \bullet \mathrm{EDTA})^{-}{}_{(aq)} + \mathrm{H_2O_2}_{(aq)} + 2\mathrm{OH^-}_{(aq)} \quad \text{(Eq.4-22)}$$

$$3(\mathrm{Fe(II)} \bullet \mathrm{EDTA})^{-2}{}_{(aq)} + (\mathrm{Fe(II)} \bullet \mathrm{O_2} \bullet \mathrm{EDTA})^{-2}{}_{(aq)} + \mathrm{O_2}_{(aq)} + 4\mathrm{H_2O} \rightarrow 4(\mathrm{Fe(III)} \bullet \mathrm{EDTA})^{-}{}_{(aq)} + 2\mathrm{H_2O_2}_{(aq)} + 4\mathrm{OH^-}_{(aq)} \quad \text{(Eq.4-23)}$$

It appears to be so that at low concentrations of Fe(II)•EDTA, the first step (Eq.4-19) may be the rate controlling one and the third step (Eq.4-21) is still negligible. With increasing concentrations of the chelated metal catalyst, the third step (Eq.4-21) seems to become more and more important, finally overruling the second one, Eq.4-20, because of high concentration of the catalyst. Consequently, with the change of the rate determining step the order changes from 1 to 2. Due to the chemical reaction taking place (i.e. Eq.4-1) the concentration of the reduced form the chelated metal catalyst (Fe(II)•EDTA) decreased during the experiments whereas the concentration of the oxidized form of it (Fe(III)•EDTA) increased. At a certain concentration of Fe(II)•EDTA, the change of the rate determining step seems to have occured. Hence, the overall reaction order in Fe(II)•EDTA would be a combination of the orders of the two different regimes. It can be concluded that, at the lower initial concentration of the Fe(II)•EDTA (i.e. 0.5Ψ = 50 mol/m^3), the critical concentration, where the change of the rate determining step occurs, is reached earlier.

It is worth to mention that the real stoichiometric coefficient, the v_B, (which is given as 3 in the proposed overall reaction Eq.4-22) may differ depending on the chemical nature of the applied solution and the rate of degradation caused by the formed oxidizing species and/or their intermediates (e.g. hydrogen peroxide (H_2O_2) and/or O_2^-) as discussed in section 5.2.2.1.

4.1.5 Conclusions and decisive parameters for the techno-economic feasibility studies

- The results showed that the regeneration reaction appeared to be pseudo first order with respect to O_2 and also pseudo first order with respect to the Fe(II)•EDTA, when the other reactant was in excess, respectively.

- A remarkable, unprecedented step change in the nature of the reaction was observed when the reaction was performed at higher metal concentrations. At low concentrations, the reaction seems to be first order with respect to ferrous chelate, whereas the order changes to 2 at increasing Fe(II)•EDTA concentrations (for Fe(II).EDTA > 100 mol/m^3).

- All kinetic studies performed in the scope of this section imply that the reaction is first order with respect to oxygen, independent of the Fe(II)•EDTA concentration.

- At 60 °C, a considerable excess amount of O_2-consumption was observed for all solutions. Consequently, it can be stated that higher temperatures enhance the O_2-consumption and, hence, the oxidative degradation of the solutions. This statement is in good agreement with the literature where it is reported that the side reactions with the chelating agents increase with temperature beyond 60 °C (Heeres, E. J. et al., 2005); (Beenackers & Wubs, 1993) and (Martell, 2009).

- The ranking of the AAS used in the scope of this study is deducted from the ability to compensate the acidity. Hence, a higher ability to buffer changes in the solutions' pH can be labeled as a very important property for application of the solution in liquid redox processes.

- The stoichiometry differs from the theoretical requirement: In contrary to expectations, the overall reaction stoichiometry was found to be less than 4 which reveals occurrence of side reactions. Generally, the overall reaction stoichiometry was between 3 and 4 which indicates that the oxidation of Fe(II)•EDTA to Fe(III)•EDTA is not the sole O_2-consuming reaction. The extent of side reactions, possibly related to EDTA ligand degradation, is found to be a function of T and of the O_2-concentration (see v_B values in **Table 4-6** and **Table 4-8**). Further studies to gain more insights into the side reactions taking place when treating aqueous Fe(II)•EDTA solutions with air and high temperatures, and particularly those on EDTA degradation, will be reported in chapter 5.

The results of the kinetics experiments give an understanding about the key interacting parameters of the Siemens liquid redox process such as:

- O_2 supply to Fe(II)•EDTA (which in turn depends on the H_2S to Fe(III)•EDTA ratio)
- chelated-metal concentration (which in turn determines the pump around to H_2S ratio)
- buffering ability of the solvent system towards changes in solution pH and in turn the stability of the steoreochemical equilibria of the chelating process (for description refer to section 3.4.2.1) which are connected to the type of AAS used and can be monitored online
- occurrence of side reactions (which is connected to v_B value and can be evaluated by varying the operation conditions).

Taking the deducted aspects of the regeneration kinetics into account, the desulfurization performances of thirteen different solvent formulations, prepared from pre-selected ligands (2) and AAS (3) will be evaluated in the continuous mini lab plant under consideration and/or variation of above listed parameters. This will be presented in the following section.

4.2 Experimental investigations on the techno-economic feasibility of formulated solvent systems in continuous operation

4.2.1 Background

Based on results of screening stability tests conducted in the scope of section 3.5, suitable constituents of an appropriate solvent system were identified (see **Figure 3-14**), whereas the key interacting performance parameters regarding the catalyst regeneration were deducted from the results of kinetic experiments (see section 4.1.5). In addition to these, operational behavior and flexibility of the solvent system in continuous operation are of high interest for the techno-economic feasibility of the process. Stable operation of the solvent system involves a complicated matrix of:

- several different operation parameters such as operation temperature and pressure, gas and liquid hold-up in both reactors, solution inventory, volumetric flow rate of the sour feed gas ($\dot{V}_{sour}$), the H_2S concentration of the sour feed gas (c_{H2S}), the CO_2 concentration of the sour feed gas (c_{CO2}), liquid to gas ratios in both reactors (L/G_{abs} and L/G_{reg}), residence time (t_{abs} and t_{reg}), superficial gas velocity in both reactors (u_{abs} and u_{reg}), the volumetric flow rate of the supplied regeneration air ($\dot{V}_{air}$) and volumetric flow rate of solution circulation ($\dot{V}_{sol}$)

- properties and composition of the washing solution (i.e. ionic strength, concentrations: cFe(III), c(Fe•Lig), c(AAS), chelate to metal ratio, pH value, viscosity, density, etc.).

The flexibility of liquid systems towards changing concentrations of acidic gas components in the sour feed gas is primarily depending on the type and the concentration of the absorbent as well as of the chelated-metal.

Taking all these into consideration, thirteen solvent systems were formulated (see **Table 4-9**), each containing one of the absorbents labelled as stable, one of the stable chelating agents and the same metal (i.e. the Fe) with varying concentrations. A high flexibility in operation with different solvents was provided by the set-up of the constructed test rig (see **Figure 4-11**). As next step, the process behavior of all formulated solutions was studied in the mini lab plant (test rig) with continuous operation mode, under variation of process conditions given in **Table 4-10** and **Table 4-11** and under variation of their constituents such as:

- the chelate to metal ratio i.e. 1.5 to 1 or 1 to 1 (varied only in one test – for the reason see the footnote 12)
- the type of the chelating agent i.e. the EDTA or the Lig2
- the concentration of the ferric chelate (c(Fe(III)•EDTA) = 0.1 M and 0.5 M)
- the AAS type i.e. tertiary, secondary or absent
- the concentration of AAS, (c(AAS) in mol/L= 1.60, 0.80 and 0.40 M).

Some solution systems without AAS were also tested in order to eliminate a potential cross-matrix influence of AAS on the absorption performance, regenerability, robustness and operability of the chelated-metal catalyst. Thus, their chemical nature was comparable to those of the state-of-the-art liquid redox solutions (i.e. formulations without AAS=Sol.1 to Sol.5). This provided a basis for comparison with those later examined (i.e. formulations with AAS= Sol.6 to Sol.13).

Table 4-9 Benchmarked solvent systems and their formulations[3]

Composition / Sol. No	Type of AAS (absorbent)	Type of ligand	c(AAS) (mol/L)	c(Fe)[11] (mol/L)	Lig/(Fe•Lig) (mol/mol)	Varied parameter
Sol.1	-	EDTA	-	0.1	1.5	Formulations **without AAS** (see Figure 3-6) - Ligand type - (Lig/Fe•Lig) ratio - c[Fe][11]
Sol.2	-	EDTA	-	0.1	1.0	
Sol.3	-	EDTA	-	0.5	1.5	
Sol.4	-	Lig2	-	0.1	1.5	
Sol.5	-	Lig2	-	0.5	1.5	
Sol.6	SiemensSolvent-1 (secondary)	EDTA	1.60	0.1	1.5	Formulations **with AAS** (see Figure 1-4) - AAS type - c[AAS] - c[Fe][11]
Sol.7	SiemensSolvent-1	EDTA	0.80	0.1	1.5	
Sol.8	SiemensSolvent-1	EDTA	0.40	0.1	1.5	
Sol.9	Dimethylglycinate (tertiary)	EDTA	1.60	0.1	1.5	
Sol.10	Dimethylglycinate	EDTA	0.80	0.1	1.5	
Sol.11	Dimethylglycinate	EDTA	0.40	0.1	1.5	
Sol.12	SiemensSolvent-2 (secondary)	EDTA	1.60	0.1	1.5	
Sol.13	SiemensSolvent-2	EDTA	1.60	0.5	1.5	

Table 4-10 Standard experimental conditions for benchmarking

Parameter, unit	Value
Total duration of tests per respective solvent system, h	160
Duration of one test run (combination solvent system / gas concentration), h	23
Operation temperature, T_{op} (absorber and regenerator), °C	25-26
Operation pressure, P_{op} (absorber and regenerator), bar	Atmospheric
Initial pH of the solutions, -	9.0
Total solution inventory, L	5.6
Solution inventory in absorber, V_{abs}, L	2.4
Solution inventory in regenerator, V_{reg}, L	3.2
Gas injection depth in both reactors, m	0.06
Sour feed gas flow, l/min	1
Number of sulfur filtration cycles per test run, -	4

Table 4-11 Compositions of sour feed gas with different concentrations of acidic gases

Parameter / Case No.	$\dot{V}_{sour}$, (l/min)	c(H_2S), vol%	c(CO_2), vol%	c(N_2), vol%
Case1	1.00	5	0	95
Case2	1.00	10	0	90
Case3	1.00	20	0	80
Case4	1.00	10	10	80
Case5	1.00	10	20	70
Case6	1.00	10	30	60
Case7	1.00	20	30	50

It shall be stated that the three different concentrations of the AAS and two different concentrations of the metal given in **Table 4-9** resulted of pre-performed solubility, regeneration kinetics and precipitation tests. In this context, the feasible upper concentrations were determined at which no other additives (see **Figure 2-5**) were required to dissolve all constituents of the solvent system and no precipitation occurred if the systems were loaded with CO_2 at the partial pressure of interest. In gas treatment, the concentrations of active constituents are usually given as weight percentages. For a scientific approach, however, molar ratios are essential, thus, the molar concentrations of these species were regarded to provide a fair ranking between the investigated solvent systems. Their performance was evaluated in such a way that for each test run only one of the abovementioned parameters was changed - either the formulation (given in **Table 4-9**) or the gas concentration (given in **Table 4-11**). For each formulation filled into the rig, the gas Cases 1 to 7 were adjusted step by step. All other parameters, the so-called standard testing conditions were kept constant (see **Table 4-10**). More than 2000 operation hours (approximately 160 hours of operation per solution) were performed in order to determine the "stable" and "economic" operation regime for each of the formulated solvent systems. Since 13 formulations (Sol.1 to Sol.13) and 7 gas compositions each (Case1 to Case7) were involved, the total number of 91 test runs was conducted. Each test run (i.e. parameter change) was defined as finished, as soon as stable operation conditions were reached (i.e. no significant changes in pH and redox potential).

With the results generated in the scope of this section, an overview of the overall performance of the respective solvent system will be presented, indicated by the decisive cost driving factors i.e. minimum required solution circulation rate per dosed H_2S (f_{sol}) and minimum required air flow rate per dosed H_2S (f_{air}) for stable operation - in a way that the pH and the redox potential were constant and the H_2S in the treated gas from the absorber was below the detection limit (i.e. 1 ppmv). The method employed here cannot yield exact/absolute numbers for f_{sol} and f_{air}, which are directly transferrable to commercial production, since the industrial scale plant will be operated under high pressure (i.e. $P_{abs} \approx 20$ to 40 bara; see section 3.2), however it is suited for a relative ranking of solvents regarding these two parameters. The experimental results will help to develop an understanding about the behavior of formulated solvent systems in the view of operability, performance and handling. In addition, they will enable the selection of the most promising candidates to be further investigated in terms of their chemical stability under process conditions (see chapter 5) and for the economic evaluation by providing first-hand information for the sizing of various process units of a semi-industrial scale demo plant as presented in chapter 6.

After reviewing the motivation of the techno-economic feasability tests, the preparation of the investigated solvent systems, the experimental set up as well as the procedure and the analytics applied on the taken samples are presented in the following sections.

4.2.2 Preparation of feed substances

Formulations without AAS (i.e. the Sol.1 to Sol.5) were prepared in the same manner as it was explained in section 3.5.1.2.

Formulations containing AAS (i.e. the Sol.6 to Sol.13), were prepared in the same way as it was presented in section 3.5.2.2.

To eliminate the influence of the pH on the absorption of acidic gases, all solvent systems were adjusted with the same buffering solution to the defined pH of 9.0 (±0.02) as given in **Table 4-10**. The used buffering solution (non-disclosed) let the formulations without AAS to be categorized as inorganic absorbents as discussed in section 3.4.1 and shown in **Figure 3-2**).

The sour gas feed (T= 23 C°, P= 1.013 bara) was composed of H_2S, CO_2 and N_2. The H_2S (purity>99.5%, COS<3 ppmv; CH_4<500 ppmv) and the CO_2 (purity>99.7%, H_2O<200 ppmv) were purchased from Air Liquide whereas the N_2 (purity>99.99%) and the regeneration air (purity>99.5%, 20.9% O_2, N_2>79%) were supplied by Infraserv GmbH.

4.2.3 Experimental set up, procedure and analytical method

All evaluation benchmarking experiments were conducted in the mini plant test rig shown in **Figure 4-11**.

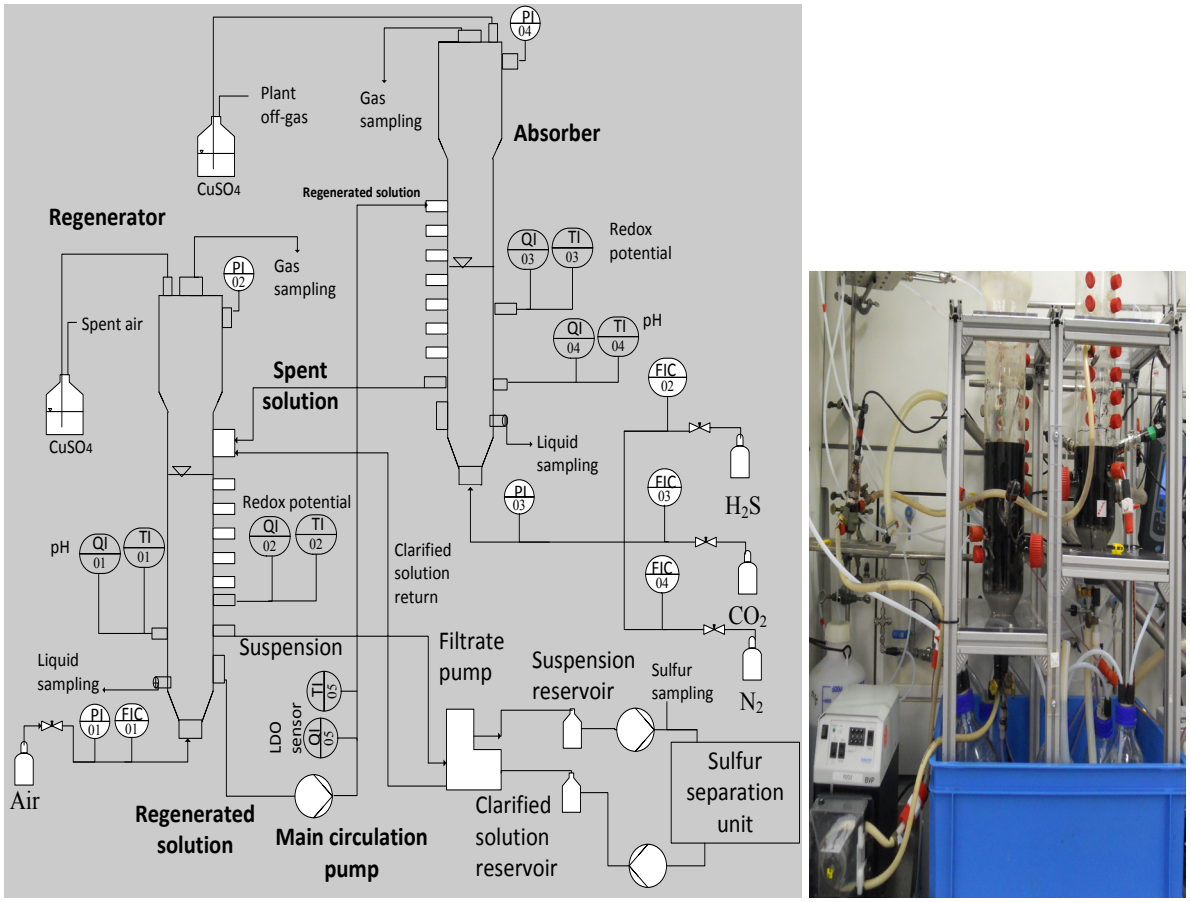

Figure 4-11 Experimental set up (simplified) for the benchmarking tests in continuous operation

The design of this test rig is comparable to those applied in conventional liquid redox processes. The characteristics of the equipment used in the test rig are given in **Table 4-12**. Both gas-liquid contactors (i.e. the absorber and the regenerator) were constructed as bubble columns. Each has a total volume of 9 liters with following sections:

(1) cylindrical section (D= 0.12 m; H=0.44 m),
(2) concentrical enlarged top section (D= 0.16 m; H=0.20) to serve as mechanical device for foam breaking,
(3) conical bottom section (D= 0.08 m; H=0.06 m) to serve as settler for the solid sulfur product.

The contactors were designed to be flexible in terms of mode of operation (i.e. co-, counter- or crosscurrent) and gas loads. The sour gas feed (at atmospheric conditions) was composed of H_2S, CO_2 and N_2. The N_2 was used as inert gas replacing the CH_4 and other hydrocarbons which might be the constituents of the sour natural gas. The flowrates of all process gases (i.e. the H_2S, CO_2, N_2 and air) were controlled by mass flow controllers (MFC), where the set points were kept constant by the Siemens PCS 7-V7 software. The sour feed gas was distributed countercurrently into the washing solution through the bottom of the absorber by a glass frit (for the technical data see **Table 4-12**). Interchangeable pH and redox electrodes with an integrated temperature sensor were used. This allowed recording also the operation temperature in both contactors with the help of digital meter HQ440dmulti, in which all relevant data were stored. During the benchmarking experiments, no heat exchanger was installed in the liquid pump around, since the temperature had been observed to be quite stable due to the considerable liquid hold-up and the homogenization brought about by the gas.

Table 4-12 Characteristics of the main equipment of the lab plant

Equipment	Vendor/Model No.	Specific feature
Contactors: Absorber and Regenerator) (Siemens AG, 2016)	Customized self-design / manufactured by Technion GmbH	- Cylindrical bubble column (D= 0.12 m; H=0.44 m) with concentrical enlarged head section (D= 0.16 m; H=0.20 m) and conical bottom section (D= 0.08 m; H=0.05 m) - Material: glass - Total volume of each contactor: 0.009 m^3
Mass flow controllers (Brooks Instrument, 2016) FIC01-FIC04	Brooks Instrument/ MultiFlo™-GF40	- Principle: Heat conductivity of gases (i.e. the measured ΔT is directly proportional to the mass flow rate of the gas) - Range: 3 sccm - 50 slpm (at T= 5-50 °C and P=10 bara) - Accuracy: 1% of set point - Response time: <1 second - Set points were kept constant by PCS7-software version 7
Main circulation pump	ISMATEC / ISM444B	- Peristaltic pump (positive displacement) - Pipeline external diameters of 12 mm - Liquid flow: 0 to 3.70 L/min - Discharge pressure: 15 m of water column
Pumps for clarified solution return	ISMATEC / ISM834C	- Peristaltic pump (positive displacement) - Pipeline external diameters of 4 mm - Liquid flow: 0 to 0.035 L/min - Discharge pressure: 10.2 m of water column
Gas spargers	ROBU® GmbH/ VitraPOR sintered filters (Por.0 - P250)	- Glass frit made of pure borosilicate glass 3.3 with 160-250 µm pore size
pH-electrode with internal temperature sensor QI01 and QI04 TI01 and TI04	HACH LANGE / IntelliCAL™-pHC101	- Principle: Online measurement of $\log_{10}{}^{(H+)}$ against a reference electrode - Range: 2 to 14 pH - Accuracy: ± 0.02 pH, ± 0.3 °C - Response time: <40 sec
Redox potential electrode with integrated temperature sensor QI02 and QI03 TI02 and TI03	HACH® / IntelliCAL™-MTC101 ORP	- Principle: Potentiometric measurement against a reference electrode - Range: ± 1200 mV - Accuracy: ±0.02mV or 0.05%, ± 0.3 °C - Response time: <40 sec
Dissolved O_2-electrode with integrated temperature sensor QI5 and TI5	HACH® / IntelliCAL™-LDO101	- Principle: Online optical luminescence (cold light) measurement - Range: 0.05 to 20 mg/L - Accuracy: ±0.1-0.2 mg/L, ± 0.3 °C - Response time: <40 sec
Digital meter-processing device for all sensors	HACH / HQ440dmulti	- Continuous data measurement & storage - Automatical transport of entire data log

Procedure:

(1) Each experiment began by filling the same amount of the respective solution given in **Table 4-9** into the rig (i.e. total solution volume of 5.6 L; 2.4 L in absorber and 3.2 L in regenerator). Subsequently, the initial pH, redox potential, and the temperature of the system were recorded.

(2) Step by step, the sour feed gases with different compositions (Cases 1 to 7 shown in **Table 4-11**) were introduced into the respective liquid system. As it can be seen from **Table 4-11**, first the behavior of the respective solution towards varying concentrations of H_2S (i.e. 5 to 20 vol% see Case1 to Case3) without CO_2 was investigated in order to eliminate cross matrix influences of

the CO_2 on the techno-economic parameters. Subsequently, a systematic variation of the CO_2 concentration (i.e. 10 to 30 vol% see Case 4 to Case 7) was performed to examine the possible impacts on the process behavior and the steadiness of the operation. First, the main circulation pump was started, by which "excess" active catalyst circulation in the system was ensured, an "excess" amount of air was supplied and then the sour feed gas flow was initiated. For safety reasons, the test rig was not in operation over the night. Thus at the end of each day, first the gas flows and then the liquid circulation pump were stopped, whereas the solvent inventory was left in the test rig. At the beginning of the next day, the liquid and gas flows in the lab plant were started again as described above.

The H_2S, CO_2 as well as some traces of N_2 and accompanied impurities in the supplied gases (e.g. H_2O, COS, CH_4) were absorbed from the sour gas in the respective washing solution in the absorber (T= 25 °C, P= 1.013 bara). The H_2S was oxidized there in-situ to elemental sulfur by the reduction of the chelated-metal catalyst. This spent solution containing solid sulfur product, the inactive catalyst and dissolved gases (CO_2 and some N_2), was fed from the absorber bottom into the regenerator through an overflow stream. This stream was driven by geodetic altitude of the columns (hydrostatic pressure). The regenerator was also operated countercurrently where the catalyst was converted back to its active form and the greater part of the dissolved gases i.e. CO_2 and N_2 (>50%) were stripped out by dispersed air at atmospheric pressure. Most of the regenerated solution was sent from the bottom of the regenerator to the top of the absorber by the main circulation pump to complete the cycle, whereas a smaller amount of it was withdrawn from the regenerator and transferred to a suspension reservoir by means of a filtrate pump.

The solid product in the suspended solution was separated discontinuously in the sulfur separation unit by vacuum filtration (P~0.3 bara) as filter cake with a moisture content (including AAS, Fe, and Lig) (ranges from 35 to 60 wt% see **Table 4-15**) and the cleaned solution was fed into the clarified solution reservoir shown in **Figure 4-11**. The filtrate pump circulated the suspended solution from the regenerator into the suspension reservoir continuously at the same rate as another pump transferred the clarified solution from the respective reservoir back into the regenerator. Hence, a constant level of solid sulfur (i.e. 5 wt%) in the system was enabled (since the sulfur separation by filtration was virtually 100%). Four sulfur filtration cycles per test run (160 h) were performed. To quantify the amount of residual moisture in the filter cake, the taken solid samples were washed two times with their own weight equivalent of water. The resulting washing water samples and the filter cake were analysed to determine the concentration of the active species (i.e. the AAS, the Fe and the Lig). With these data, the active material loss per filtration process could be quantified. These results gave an understanding about the relation between the applied operation parameters and the active material loss Hence, the chemical make-up requirement per produced sulfur for keeping the solvent properties constant could be estimated (refer to **Table 4-16**) and were used in the economic studies conducted (refer to section 6.2.4.3). A mechanical loss of approx. 1% of the total solution inventory per filtration cycle was determined, which however had no remarkable influence on the results of the conducted experiments.

(3) The pH and the redox potential values were continuously measured and recorded every 30 minutes in order to ensure the regeneration of the metal catalyst as well as to qualify a test run as "stable". The lower the redox potential, the higher is the ratio between the reduced and the oxidized form of the metal component (i.e Fe^{2+}/Fe^{3+}) at constant pH and dissolved O_2 concentration which indicates an infeasible regeneration (Kohl, A. L. et al., 1997). The influence of the O_2 concentration on the redox potential depends of the used ligand, but in general higher O_2 concentrations lead to higher redox potential values. Therefore, the dissolved O_2 concentration was also measured by a so-called LDO sensor, which was located right downstream of the main solution circulation pump (see **Figure 4-11**).

If the redox potential was changed into the positive direction[18], the operation was assumed to be "overstable", meaning that more than "enough" (i.e. "excess") catalyst and air per dosed H_2S were circulated in the system. Therefore, the pump around ratio or the air supply (only one parameter adjusted each time) was reduced till an unstable operation was indicated by the continuous drop of the redox potential and/or the pH value in the absorber or in the regenerator. In case of non-absorbed H_2S in the off-gases from both columns as an impact of infeasible regeneration, the H_2S reacted with $CuSO_4$ to solid copper sulfide (CuS) (which could observed from the discoloration of the $CuSO_4$ solution from blue to black because of the precipitation of CuS) according to Eq.4-24, so that a safe operation without H_2S-emission in the plant off-gas was ensured.

$$H_2S_{(g)} + CuSO_{4(aq)} \rightarrow CuS_{(s)} \downarrow + H_2SO_{4(aq)} \qquad \text{(Eq.4-24)}$$

(4) The latest operating parameters (i.e. pump around ratio and air supply) was defined as the "stable" conditions where no significant drop in the pH and/or redox potential as well as H_2S emission had been observed. These were used to calculate the techno-economic comparison factors of the tested solution (i.e. f_{sol} and f_{air} by Eq.4-25 and Eq.4-26, respectively) for the given gas composition (Case1 to 7 given in **Table 4-11**). Determining these parameters was beneficial to develop a further understanding in the view of industrial process design and thus the economics of the process when utilized for the treatment of different sour gases originating from various sources. In this context, also other important parameters regarding the economic and compact process design such as the L/G ratio, the superficial gas velocity, u, the required filling height, h, and the residence time of the washing liquid in each contactor were calculated using the respective equations given in **Table 4-13**.

Table 4-13 Calculations of the decisive design and performance parameter of the contactors

Parameter, (Unit)	Absorber	Regenerator
Specific performance factor per dosed H_2S, [(l/min)/(l/min)] or (m^3/Nm^3)	$f_{sol} = \frac{\dot{V}_{sol}}{\dot{V}_{H_2S}}$ (Eq.4-25)	$f_{air} = \frac{\dot{V}_{air}}{\dot{V}_{H_2S}}$ (Eq.4-26)
Liquid to gas ratio, [(l/min)/(l/min)] or (m^3/Nm^3)	$L/G_{abs} = \frac{\dot{V}_{sol}}{\dot{V}_{sour}}$ (Eq.4-27)	$L/G_{reg} = \frac{\dot{V}_{sol}}{\dot{V}_{air}}$ (Eq.4-28)
Superficial gas velocity, (m/s)	$u_{abs} = \frac{\dot{V}_{sour} * 10^{-3}}{A_{abs} * 60}$ (Eq.4-29)	$u_{reg} = \frac{\dot{V}_{Air} * 10^{-3}}{A_{reg} * 60}$ (Eq.4-30)
Filling height, (m)[19]	$h_{abs} = V_{abs}/A_{abs}$ (Eq.4-31)	$h_{reg} = V_{reg}/A_{reg}$ (Eq.4-32)
Residence time, (s)	$t_{abs} = \frac{h_{abs} * 10^{-2}}{u_{abs}}$ (Eq.4-33)	$t_{reg} = \frac{h_{reg} * 10^{-2}}{u_{reg}}$ (Eq.4-34)

The overall reaction of the oxidation of H_2S (Eq.1-9) and the regeneration of the catalyst (Eq.1-10) yields one mol of H_2O per mol of absorbed H_2S. Since it would gradually dilute the solution, a mass balance for the formation (as a product of the overall reaction) and the loss of H_2O (caused by stripping with the gases in absorbent and regenerator) was performed by using Eq.A-4.1 (for the assumptions see Appendix A-2.5). Thus, the accuracy of the analytical results was assured by preventing the dilution of the solutions by reaction water and ensuring identical operation conditions. The balance led to formation of approximately 0.2 to 2 g H_2O during the 160 hours of operation for each solution. In relation to approximately 6000 g of the respective solution in the

[18] As a result of the H_2S-oxidation, the Fe^{3+} was reduced to Fe^{2+}. This led to decrease of the redox potential in negative direction i.e. lower than zero.

[19] The cross-sectional areas A_{abs} and A_{reg} were calculated based on the cylindirical body of each contactor. In order to ensure that values of the V_{abs} and the V_{reg} did not change during the experiments, the h_{abs} and h_{reg} was continuously measured with the help of a ruler.

system it was considered as negligible with respect to comparability of the operation condition and the accuracy of the conducted analysis, as decribed in the following:

Analytical methods:

Within the context of the continuous benchmarking experiments, various analytical methods were applied:

a) to determine the characteristics (concentrations and/or compositions) of the process and/or waste streams including gas streams (e.g. treated gas and spent air vented), liquid streams (e.g. washing medium in absorber and regenerator) and solid product (i.e. sulfur-cake)
b) to develop an understanding about the efficiency of the filtration, the chemical make-up and the handling of the wastes the following methods were used:
   - **concentration of the metal-ligand** in liquid samples via UV-Vis method as explained in section 3.5.1.3 (internal method, ±5%)
   - **concentration of the AAS** in liquid samples either by the means of an internal titration method as given in (Fischer, 2013) (±5%) or by LC-MS at an external service provider (±10%)
   - **concentration of metal ions** (e.g. Fe and K) in liquid samples and in filtrated solid product by inductively coupled plasma mass spectrometry method (ICP-MS) according to DIN EN ISO 17294-2 (external, ±5%)
   - **composition of solid product;** determination of total elemental carbon (C), hydrogen (H), nitrogen (N), oxygen (O), sulfur (S) by instrumental methods according to DIN 51732 (external, ±5%)
   - **measurement of particle size distribution** (PSD) using the focused beam reflectance measurement (FBRM) method (internal, ±5%) as described in (Greaves, D. et al., 2008).

Once the preparation of the feed substances, experimental set-up and testing procedure were highlighted, the results of the conducted tests are presented in the following section.

4.2.4 Results and discussion

4.2.4.1 Variation of iron concentration and ligand-to-iron ratio in formulations without AAS

Figure 4-12 shows the impacts of the variation of metal concentration and ligand-to-metal ratio in aqueous Fe•EDTA alkaline solutions (without AAS) on the two decisive performance factors respectively ranking factors (i.e. the f_{sol} and the f_{air}) under one given gas composition[20] (Case2 see **Table 4-11**).

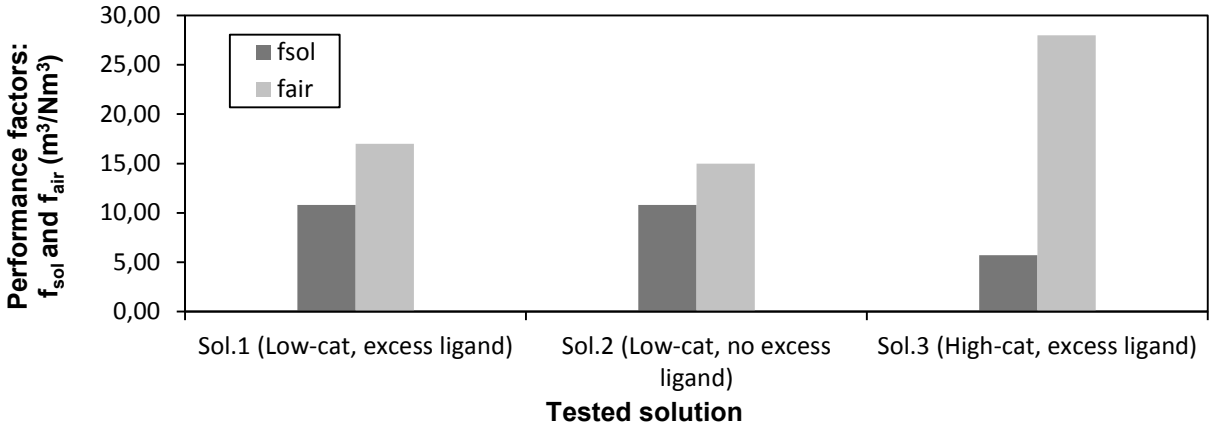

Figure 4-12 Performance parameter comparison for Sol.1, Sol.2 and Sol.3 under Case2 given in Table 4-11

[20] It shall be noted that the results were presented exemplarily only for one given case within the context of this section, however, the given relationships were comparable for the other cases tested.

The **Figure 4-12** reveals:

- When comparing Sol.1 and Sol.2 with each other, it was found that the ligand to metal ratio (i.e. EDTA to Fe) has practically no impact on the required solution circulation ratio per dosed H_2S. Hovewer, presence of the 0.05 M excess free ligand in Sol.1 led to an approx. 12 vol% increase in air demand for the same amount of dosed H_2S and circulated iron in the system. This could be interpreted as occurrence of side reactions between free, non-complexed ligand species and the O_2 of the regeneration air. However, the results of UV-Vis analysis showed that the Fe•EDTA concentration of the two solutions did not change significantly during the operation under Case2 (see in **Figure A- 5** Appendix A-2.6).
- Increasing the Fe concentration from 0.1 M to 0.5 M allowed approx. 50% reduction in solution flow per dosed H_2S flow. However, contrary to expectations, in the case of higher catalyst concentration (i.e. the Sol.3), the air demand for the regeneration increased significantly for the same amount of H_2S dosed. As it was mentioned above, the concentration of the Fe•EDTA had been analysed in order to find out whether chelate degradation took place or not. However, the concentration of the chelated metal remained almost constant during the total operation of 160 h, as well. Thus, the higher air demand of the high-cat solution could not caused by degradation.
- As mentioned in section 2.3.1.1, side reactions tend to form undesirable sulfur oxo-anions as by-products. Therefore, in addition to UV-Vis analysis also the compositon of the produced solid product was analyzed to find out whether elemental oxygen was present in it or not. The concentration of the elemental sulfur in the produced solid product was found to be >99 wt% on dry basis, therefore, also the formation of sulfur oxo-anions was ruled out.
- These findings indicated that in cases of higher iron concentration and/or higher chelate concentration (which result in increased viscosity and density), the mass transfer of the O_2 into the washing liquid had been affected adversely, which necessitated to supply the regeneration gas in higher flow rates to ensure stable operation by increasing the gas-liquid contact area (i.e. higher superficial gas velocities lead to greater turbulence see **Figure 2-3**). For the comparison of densities and viscosities of these solutions (see **Table A- 6** in Appendix A-2.7).

In addition to iron concentration and ligand to iron ratio, also the possible impacts of the applied ligand type in the formulations without AAS on the process performance parameters were investigated. Although Sol.2 showed more advantageous performance regarding the f_{air}, all other formulations were tested with an excess amount of respective ligand (see **Table 4-9**) to avoid the precipitation of Fe as FeS (irreversible) and the thermodynamical stability of the complex which are caused by the absence of excess ligand. Thus, the results excluding the Sol.2 are presented in the following section.

4.2.4.2 Variation of the chelator type and the complex concentration in formulations without AAS

The impacts of the applied ligand type in the formulations without AAS on the process performance parameters were investigated by comparing the performance factors of the Sol.1 with Sol.4 under standard conditions and the Case1 given in **Table 4-10** and **Table 4-11**. During the test runs, it was observed that there was more than one stable operation point for one solution and gas composition. As an example, three stable points per formulation are shown and clustered with dashed points in **Figure 4-13**[20].

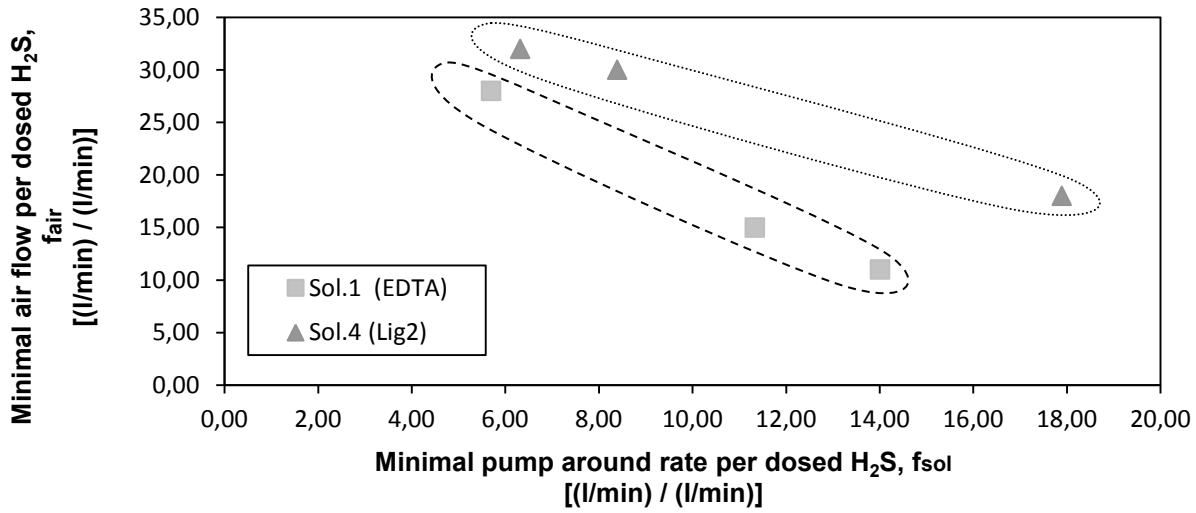

Figure 4-13 Performance parameter comparison for Sol.1 and Sol.4 under Case1 given in Table 4-11

- The **Figure 4-13** indicates that the determination of trade-off curves between f_{air} and f_{sol} are crucial for evaluation of an economic operation, since with an increase in one parameter, the other can be decreased or vice versa.
- From **Figure 4-13**, it can also be deducted that for the same amount of dosed H_2S, the solution containing the Lig2 as chelating system (i.e. the Sol.4) needs to be supplied with higher amounts of regeneration air than the solution system containing the EDTA as chelator (i.e. the Sol.1).
- In order to prevent misinterpretation of higher O_2 consumption and exclude the influences of oxidative degradation (which would lead to higher consumption of the O_2), concentrations of the complexes in both solutions were measured at the beginning and at the end of the operation. The results of UV-Vis analysis showed that the concentration of the active species in Sol.1 and Sol.4 did not change significantly during the operation under Case1 as shown in **Figure A- 6** and **Figure A- 7**, respectively in Appendix A-2.8. A literature review done on this account revealed that the complex of iron with Lig2 (i.e. Fe•Lig2) is present in its dihydroxylated form ($Fe(OH)_2$•$Lig2^{n-}$) at the given pH (i.e. 9.0). Therefore, it seems to be that the proposed mechanism for the regeneration kinetics was affected adversely (see section 4.1.4.2), and thus, a higher O_2 supply was required to ensure steadiness of the operation. The hydroxylation of the chelate also influenced its net charge and the resistance to regenerability (see **Table 3-4**).
- Thus, it can be concluded that, if the iron is complexated by the Lig2, the system should be operated at lower pH values than 9.0 to ensure stable and economic operation. Decreasing the pH would, however, adversely affect the thermodynamic stability of the iron, if the applied chelate is EDTA, since it exists in its protonated form at pH < 8, which is regarded as instable region (see section 2.2.2 and Figure 2-7).

In addition to investigations on the impacts of varying the type of chelator in low-cat solutions w/o AAS (Sol.1 and Sol.4) on their performance under Case1, also investigations on the behavior under variation of the chelated-metal-concentration (i.e. Sol.1 to Sol.5) were performed under the conditions given as Case2 (see **Table 4-11**). The formulation with no excess ligand (Sol.2) was not included in the comparison. The results are displayed in **Figure 4-14**.

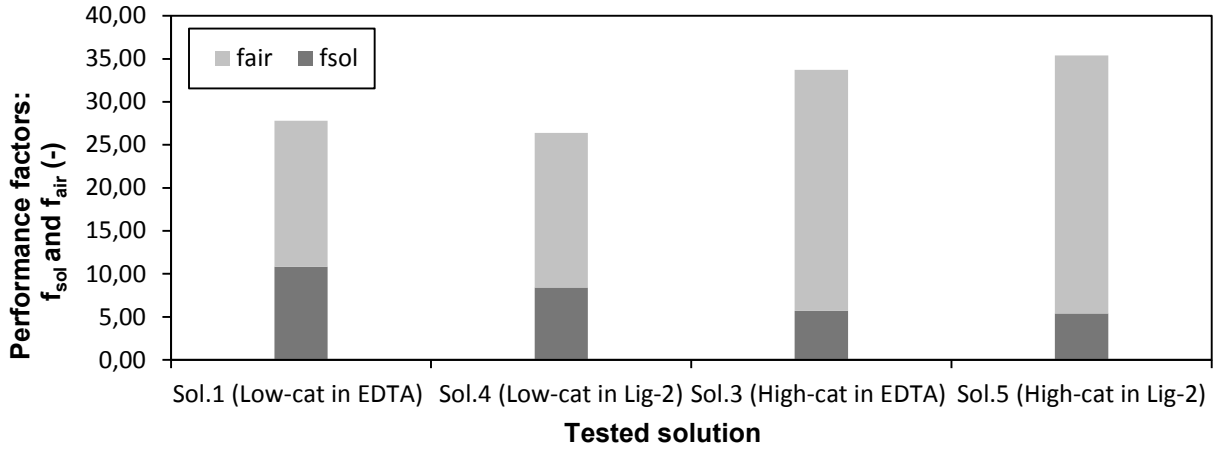

Figure 4-14 Performance parameter comparison for formulations w/o AAS with varying chelated metal concentrations under Case2 given in Table 4-11

- From **Figure 4-14** it was seen that, increasing the chelated-metal concentrations by factor 5 (high-cat solutions: Sol.3 and Sol.5) enabled significant reductions (35 to 48 vol%) in pump around for both solutions under given circumstances. However, it necessitated approx. 40 vol% more air supply to the system to achieve stable operation.
- This fact can be explained as follows: The Fe(II) was produced in the course of the oxidation reaction of the H_2S by the reduction of the Fe(III). The relative amount of the produced Fe(II) to the Fe(III) remaining (i.e. $Fe^{2+/}Fe^{3+}$) was lesser in the solutions with high initial catalyst concentrations (high-cat: Sol.3 and Sol.5) than with low initial catalyst concentrations (low-cat: Sol.1 and Sol.4). The influence of the concentration of the Fe(II)•EDTA on the overall kinetics of the regeneration reaction was studied in detail in section 4.1.4.2, where it was proposed that the reaction (Eq.4-19) may be the rate controlling step at lower Fe(II)•EDTA concentrations. Since the forward reaction of the Eq.4-19 was stated to be slow at lower Fe(II)•EDTA concentrations, the products (Fe(II)•O_2•EDTA)- cannot equilibrate with the (Fe(II)•EDTA)- and O_2 which would slow down the reaction Eq.4-21, and thus, the conversion of the Fe(II) to Fe(III). This proposal is consistent with the observed impact of lower Fe(II)•EDTA concentrations leading to a lower regeneration air demand for the same H_2S amount (see **Figure 4-14**). It is also in good agreement with the results presented in the study of (Demmink, J. F. et al., 1998).

After discussing the influences of the iron concentration, ligand to iron ratio and the chelator type on the performance parameters of the solutions w/o AAS, the results of the investigations conducted with the formulations containing either different concentrations or types of AAS are presented in the next part of this section.

4.2.4.3 Variation of the AAS concentration and type

Keeping the conclusions from the experiments performed with formulations without AAS in mind, the following tests were conducted to develop an understanding what happens in the system if different concentrations (and later on also types) of AASs were added to the solutions to serve as alkaline providing absorbent media.

If the AAS concentration was varied: Figure 4-15 shows a comparison of the design and performance related parameters (for the calculation refer to **Table 4-13**) of the solutions containing different concentrations of dimethylglycinate as absorbent and the same concentration of Fe•EDTA as redox catalyst (for the concentrations refer to **Table 4-9**) under conditions given as Case2 in **Table 4-11**.

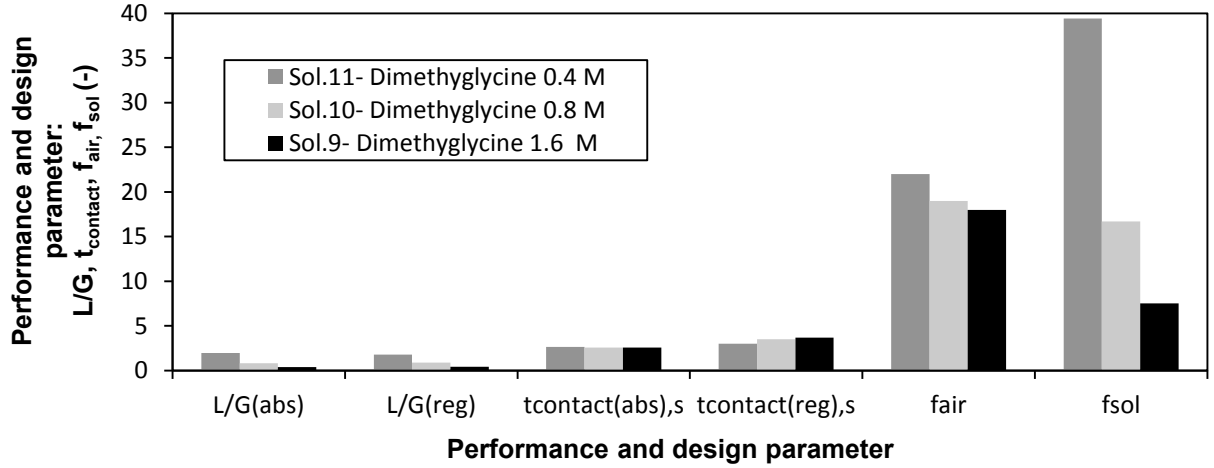

Figure 4-15 Comparison of operational parameters for different concentrations of the tertiary AAS (Sol.9 to Sol.11) under Case2 given in Table 4-11

The **Figure 4-15** reveals that despite the constant concentration of the redox catalyst in all solutions and the same amount of dosed H_2S into them:

- The required pump around ratio is found to be depending on the AAS concentration, which enables a significant reduction in the circulated solution ratio per dosed H_2S and in turn smaller L/G ratios in both contactors. However, the costs for higher concentration of ASS have to be compared with possible savings in the operational costs due to smaller pumping ratios and in the capital costs due to smaller vessels.
- As expected, the air demand was found not to be proportional to the AAS concentration which reveals that the concentration of the AAS does not significantly influence the conversion rate of the ferrous chelate to ferric chelate, as long as the required alkalinity is supplied to the system.
- Furthermore, the processes with this formulation were found not to require relatively long contact times for oxidation, which is beneficial for an industrialization, since if CO_2 is present in the sour gas stream, the relatively long contact time would result in the absorption of CO_2 and the consequential reduction in the pH of the solution and in the efficiency of the system.

If the AAS type was varied: Taking the significant influence of the AAS concentration on the pump-around and low influence on the air demand into account, three different concentrations of a tertiary AAS (Dimethylglycinate) and a secondary AAS (Siemens-Solvent-1) were compared (see **Figure 4-16**) regarding the required solution circulation ratios.

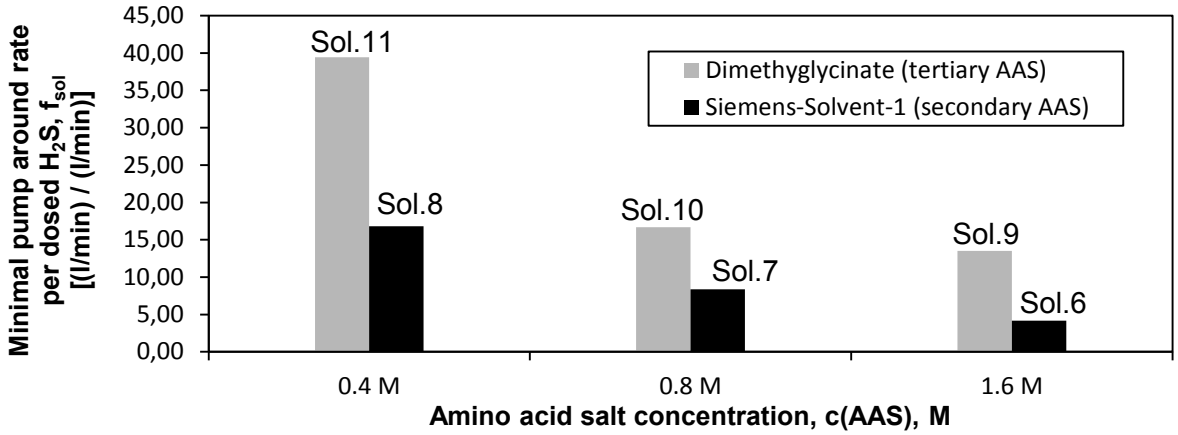

Figure 4-16 Comparison of operational parameters for different concentrations of the tertiary AAS (Sol.9 to Sol.11) and the secondary AAS (Sol.6 to Sol.8) under Case2 given in Table 4-11

The experiments were still conducted without presence of CO_2 in the sour feed gas. **Figure 4-16** indicates that:

- At the same AAS concentrations, a tertiary AAS requires higher pump around ratios (higher OPEX) compared to the applied secondary AAS, which is consistent with the given relation of alkalinity to AAS type in the **Table 3-3**.

Since the used secondary AAS (Solvent-1) was observed to be more beneficial than the tested tertiary AAS (dimethylglycinate) in terms of f_{sol} and f_{air}, the influences of the iron concentrations on the performance parameters of the formulations containing the other secondary AAS (Solvent-2) were investigated and compared with the formulations which contain no AAS. The results are presented in the subsequent section.

4.2.4.4 Impact of the iron concentration for the formulations with and without AAS

Figure 4-17 gives an overview on the changes in decisive comparison parameters if the iron concentration in formulations with (Sol.12 and Sol.13) and without AAS (Sol.1 and Sol.3) is varied:

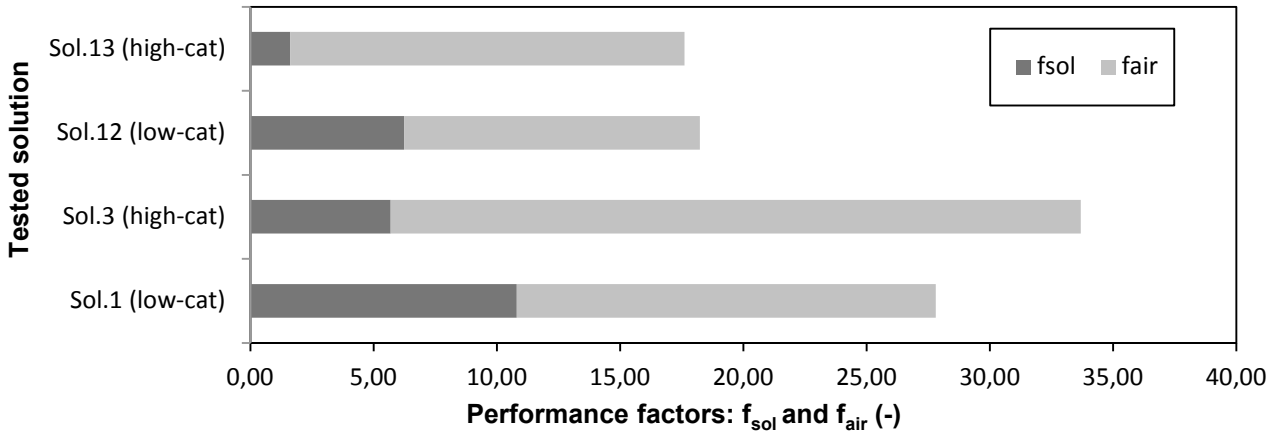

Figure 4-17 Comparison of operational parameters for different iron concentrations in formulations with (Sol.12 and Sol.13) and without AAS (Sol.1 and Sol.3) under Case1 given in Table 4-11

- As it is seen from **Figure 4-17**, increasing the chelated-metal concentrations in the solution containing a secondary AAS as absorbent (the Sol.13 containing 0.5 M complex) by a factor of 5 enabled significant reductions in the pump around ratio by a factor of approx. 4 in comparison to Sol.12 (secondary AAS containing 0.1 M complex), whereas this factor was found to be 2 in the solution containing the same amount of iron but no AAS (i.e. the Sol.3: no AAS 0.5 M complex; see **Table 4-9**). This information is essential and supports the consistency of the expected positive influences of the utilization of the AAS as alternative to inorganic absorbents.
- In addition to this, a fivefold increase in the initial metal concentration led to an increase in air demand required for a stable operation by a factor of approx. 1.7 for the formulations without AAS as it is also shown in **Figure 4-14**. However, the increase in the air demand was lesser in the case of the formulations containing AAS (i.e. approx. 1.3 see **Figure 4-17**), which is consistent with the information gained from the previous kinetic experiments (see section 4.1.4.2): The presence of the AAS helps compensate the influence of H^+ ions produced as a result of the absorption reaction Eq.1-9. It was also deducted from the previous continuous experiments, that for a given gas composition and the solution, there are more than one stable operation point regarding pump around and air demand yielding a stable operation window (refer **Figure 4-13**). This reveals that the presence of the AAS promotes the width of the stable operation window by affecting the rate determining step (refer reactions Eq.4-19 to Eq.4-23), which results in a considerable decrease in requirement for air supply.

As it was mentioned in 4.2.1, the techno-economic feasibility experiments were first conducted without CO_2 in sour feed gas in order to rule out its possible influences regarding the stable operation. However, the sour gas fields generally contain varying concentrations of the both of main acidic gases, H_2S and CO_2. Therefore, the results of the experiments executed with presence of CO_2 and varying acidic gas concentrations in the sour feed gas are to be presented, as discussed in the following section.

4.2.4.5 Influence of the sour feed gas composition on performance parameters of the formulations

If the impacts of CO_2 in the feed gas on the performance of the buffered[21] (with AAS) and non-buffered (w/o AAS) formulations were compared: In order to understand the major effects of the presence of the CO_2 in the sour feed gas on the performance of the solutions w/o AAS and with AAS, one representative solution of each group (i.e. the Sol.3 (non-buffered) and the Sol.13 (buffered), respectively) were operated with a constant H_2S concentration (i.e. 10 vol%) and varying CO_2 concentrations (0 vol%, 10 vol% and 20 vol%; i.e. Case2, Case4 and Case5 see **Table 4-11**). The comparison of them with respect to the decisive performance factors is shown in **Figure 4-18**.

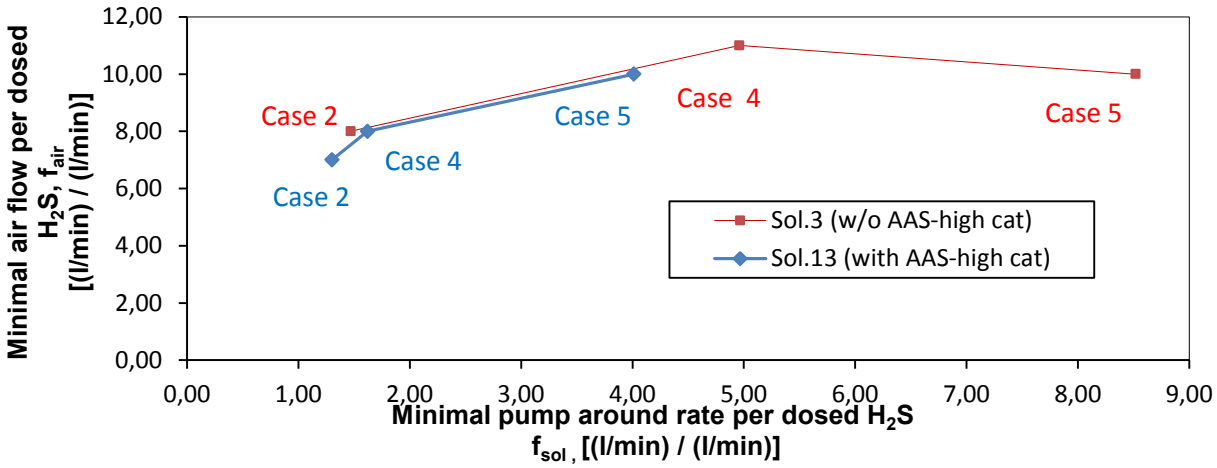

Figure 4-18 Influence of the CO_2 concentration in the sour feed gas on the performance parameters of the high-cat solutions with and w/o AAS (Sol.13 and Sol.3) under variation of Case2, Case4 and Case5 given in Table 4-11

It is found that the presence of CO_2 in the sour gas had two major effects:

- The first effect was lowering the pH of the Sol.3 which was not observed during the operation of the same solution without CO_2 in the feed gas (i.e. the Case2). As it can be seen from the **Figure 4-19**, which shows the dynamic behavior[22] of both sytems, the pH of the solvent system containing a secondary AAS as absorbent (i.e. the Sol.13) was not remarkably affected by the presence of the CO_2 under the conditions of Case4, while the establishment of the equilibrium in Sol.3 took significantly longer than it was in Sol.13. This result was unexpected. The possible reasons for continuous pH drop and the longer time periods needed to reach steady state can mainly depend on the current species distribution and composition of the produced solid reaction products, which in turn influence the chelator dynamics (see section 3.4.2.1). Therefore, the dynamic and steady state behavior of both solutions under long time CO_2 sparging (even at higher partial pressures) shall be investigated in detail.

[21] The notations buffered or non-buffered were used in terms of the chemical nature of the formulations i.e. meaning that no additional buffering agents were added to the formulations with AAS and vice versa.

[22] In the scope of this section, all results, given before and after **Figure 4-19**, represent the behavior of the solutions at equilibrium where they show stabil operation. However, **Figure 4-19** illustrates the dynamic behavior of the solutions presented, since this knowledge is of high importance from the operational start-up point of view.

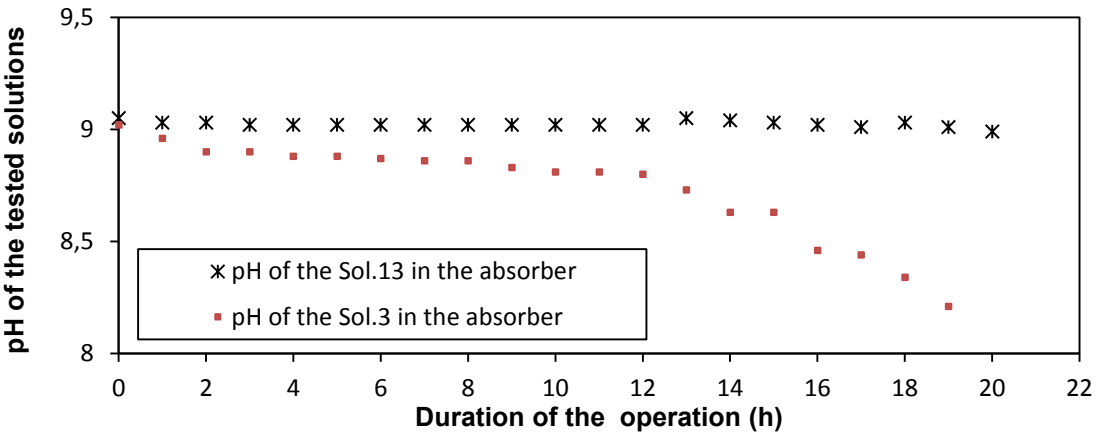

Figure 4-19 Change in pH of the solutions during 20 h operation under Case4 given in Table 4-11

- The second and even more important effect was decreasing the H_2S conversion efficiency until the solutions reached equilibrium - in other words stable operation. The reduction of the pH resulted in a considerably lower reaction rate in the oxidation reaction of H_2S to sulfur unless buffered (in the case w/o AAS). The slowing down of the reaction was measured by the changes in the redox potential of both solutions, which was compensating by increasing either the pump around ratio or the air supply. Comparing the results of the Sol.3 and Sol.13, both solvent systems demanded similar amounts of regeneration air for the same amount of H_2S dosed under given conditions. However, the decrease in the performance of the Sol.3 was more than that of the Sol.13 with increasing CO_2 concentration of the sour feed gas. This required much higher solution circulation ratios (f_{sol}) to the system operated with Sol.3 compared to Sol.13 as illustrated in **Figure 4-18** (comparison of Case4 and Case5). Thus, it can be concluded that the applied AAS (the Siemens Solvent-2 = Sol.13) showed superior performance towards the variation of $c(CO_2)$ in the feed gas than that of the inorganic aqeous alkaline system (i.e. the Sol.3).

If the impacts of CO_2 in the feed gas on the performance of the formulations with changing AAS types (secondary and the tertiary AAS) were compared: To study whether the solution pH and in turn the overall absorption efficiency in the presence of CO_2 in the feed gas is influenced by the type of AAS applied, the Sol. 9 (Dimethylglycinate, tertiary AAS as absorbent) and the Sol.12 (Siemens Solvent-2, secondary AAS as absorbent) were operated under the conditions of Case2, Case4 and Case5 referring **Table 4-11**. The results are given in **Figure 4-20.**

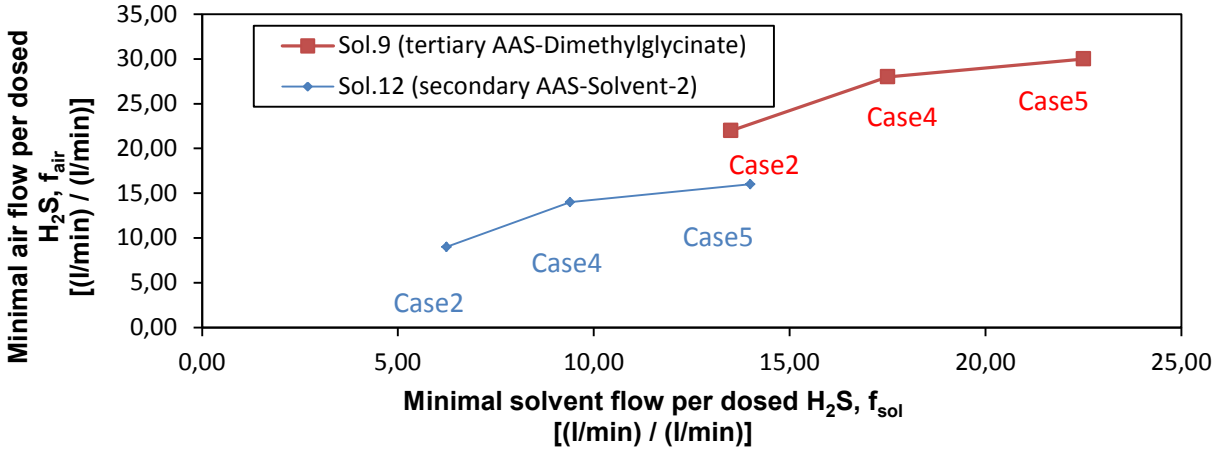

Figure 4-20 Influence of the CO_2 concentration in the sour feed gas on the performance parameters of the solutions with tertiary or secondary AAS (Sol.9 and Sol.12) under Case2, Case4 and Case5 given in Table 4-11

- During the start-up of the operation with solutions, no remarkable changes in their pH were observed as it was also deducted from the initial dynamic behavior of the Sol.13 shown in **Figure 4-19**. However, the increase in c(CO_2) in the feed gas (i.e. Case 4 and Case 5 compared to Case2) necessitated higher f_{sol} and f_{air} ratios for both, Sol.9 and Sol.12 (see **Figure 4-20**). Nevertheless, comparing the Sol.12 and Sol.9, the increasement factors of the two decisive figures (i.e. f_{sol} and f_{air} ratios) were found to be lesser than for the Sol.12, which contains a secondary AAS as absorbent. This is consistent with the fact derived from the **Figure 4-16** that at the same AAS concentrations, a tertiary AAS requires relatively higher f_{sol} factors compared to a secondary AAS.

If the influences of H_2S in the feed gas on the performance of the formulations with changing AAS types (secondary and the tertiary AAS) were compared: Before giving a comparison on the performance parameters, i.e. f_{sol} and f_{air}, for Sol.6 and Sol.9 in Cases 1 to 3, it must be noted that no results of the experiments, which were performed under "ultra-high" (see **Table 1-3**) sour feed gas sparging (i.e. the Case6 and Case7) into the solutions, are shown. This is caused by the fact that these ultra-high sour gas concentrations necessitated much higher volumetric flow rates and circulation ratios for most of the formulations which were not feasible for the given design of the lab plant and thus would not be attractive candidates for an industrial application regarding the process economics. Only the solutions Sol.6, Sol.12 and Sol.13 showed a fairly acceptable performance under the test conditions of Case6 and Case7. However, their performance parameters cannot be declared due to the confidentially of the data.

- As expected, the increase in the required circulation ratio for both, the Sol.6 and Sol.9, was found to be related to the c(H_2S) of the gas as illustrated in **Figure 4-21**. The phenomenon of relatively higher f_{sol} of the tertiary AAS for given H_2S concentrations was observed here again for cases where the sour feed gas did not contain CO_2 for an industrial application but different H_2S concentrations (referring the Case1, Case2 and Case3 given in **Table 4-11**), which can be explained with the higher alkalinity of the applied secondary AAS (Sol.6) compared to the dimethylglycinate (Sol.9) and the higher molecular weight of the dimethylglycinate compared to the non-disclosed AAS (i.e. Siemens Solvent-1) (if the MW(↑), carrying capacity for acidic gases (↓), circulation ratio (↑) referring **Table 3-2**).

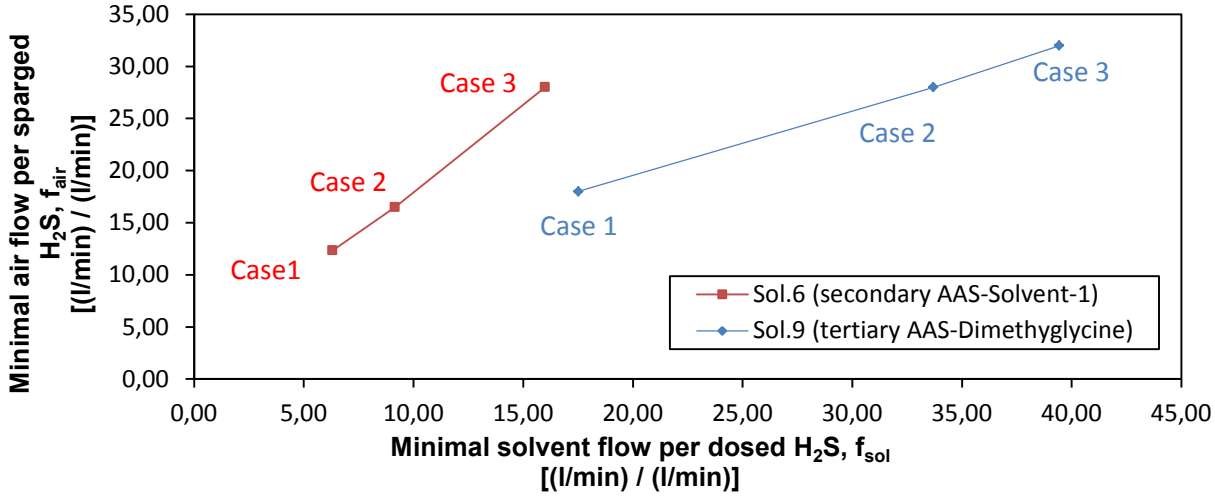

Figure 4-21 Influence of H_2S concentration of the sour feed gas on performance parameters with secondary and tertiary AAS (Sol.6 and Sol.9) under Case1, Case2 and Case3 given in Table 4-11

In addition to the relatively higher circulation ratios, also a significant difference in the air requirement of both systems per dosed H_2S was measured (see **Figure 4-21**). This can be explained with the impacts of the chemical nature of the reaction medium on the contribution of

the solvation/desolvation process of the Fe•EDTA, which in turn influences its regenerability (as discussed in section 3.4.2.1).

After illustrating and discussing the impacts of the variation of important operation parameters on the performance parameters of the solutions with different compositions, their overall performance regarding the operational behavior is presented in the following section.

4.2.5 Evaluation of overall performance parameters for all formulated solvent systems

Figure 4-22 gives an overview on the relative ranking of the formulated solutions based on the decisive performance factors. The most promising ones are clustered.

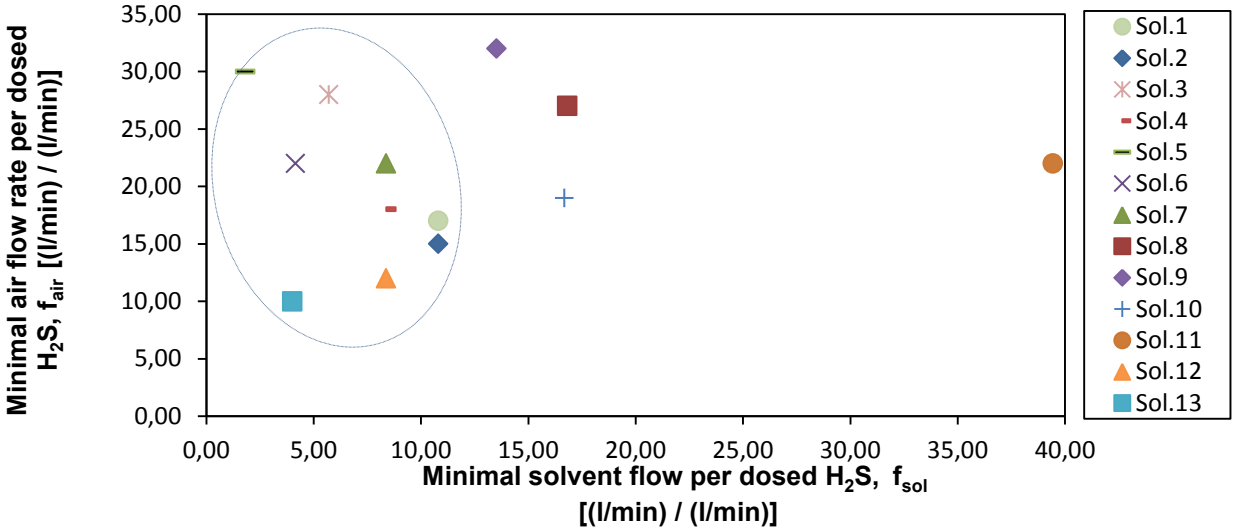

Figure 4-22 Comparison of techno-economic parameters of all formulated solvent systems given in Table 4-9 under Case2 given in Table 4-11

As it was mentioned before and illustrated in **Figure 4-13**, more than one stable operation point could be reached with the same solution for a given gas composition. To enable a fair comparison of all formulated solvents, their performance parameters were compared for Case2 and illustrated in **Figure 4-22**. For this case, only one stable point per tested solution (confirmed by 3 replications of the measurements), which is attractive regarding the process economics for an industrial application, was selected and is shown. The solutions which are not clustered in the bubble drawn in **Figure 4-22** (i.e. the Sol.8, Sol.9, Sol.10 and Sol.11) were considered as infeasible even for moderate H_2S concentration (i.e. 10 vol%) due to high solvent circulations rates f_{sol}>13 at simultaneously high air flow rates f_{air}>18. As it can be seen from **Figure 4-22**, some of the clustered solutions showed superior performance over others in terms of lower circulation ratios for the same H_2S concentration (e.g. Sol.5), which however necessitated the highest amount of air supply for the regeneration. Hence, to develop further understanding on their performance factors, some criteria for the operation behavior of the solvent system shall also be characterized based on the operational observations as given in **Table 4-14**. The criteria of the solutions are ranked with plus and minus, which is referred as beneficial and disadvantageous, respectively. The multiple entries stand for an increase in the degree of the respective property. The arrow symbol in the column of the optimization proposals in ascending order (arrow points up, ↑) indicates the change direction of the related impacts of corresponding parameters on the operational behavior. For example, the arrow up for the response time parameter (i.e. response time↑), means that response of the system towards changes in parameters can be faster, if the corresponding parameter is optimized; however, it does not mean that longer response time is desired.

Table 4-14 Overview on criteria for the operational behavior of the investigated solvent systems

Solution number	Response time	Flexibility	Operability	Sulfur settling behavior F:flotated S:settled	Suggested design modification/ process optimization
Sol.1	+++	+	++	F	1. Settling behavior↑: by replacing the vacuum filtration unit with a sulfur separation unit involving a conventional flotation cell (see **Figure 2-4a**) combined with a thickener (see **Figure 2-4d**) and a belt filter (see **Figure 2-4h**)
Sol.2	+++	+	++	F	
Sol.3	+	++	+	F	2. Operability↑: Installment of an eductor mixer (**see Figure 2-2**) 3. Alternatively applying a pipeline contactor with static mixing elements 4. Settling behavior↑: Modification of the sulfur separation unit (see Item-1)
Sol.4	+++	+	++	F	5. Flexibility↑: Operation at lower pH (7.5<pH<8.0)
Sol.5	+	++	+	F	6. Flexibility↑: Modification of the gas-liquid contactor/distributor and the sulfur separation unit (see Item-1, 2 and 3)
Sol.6	+	+++	+++	S	7. Response time↑: Operation at higher pH (9.5<pH<9.8) 8. Operability↑: Installment of a mechanical foam breaker
Sol.7	++	+	+	S	
Sol.8	++	+	+	S	
Sol.9	+	++	++	F	9. Operability↑: Either application of an air skimming flotation unit instead of a vacuum driven filtration (see **Figure 2-4b**) **-** if bubble columns are used 10. Or use of venture scrubbers as absorber & regenerator (see **Table 2-2**) instead of bubble columns 11. Or increase in absorber height
Sol.10	++	+	+	F	
Sol.11	++	+	+	F	
Sol.12	+++	+++	+++	S	12. To enable a considerable reduction in mechanical catalyst loss: Installment of a hydrocyclone unit upstream of vacuum driven sulfur seperation unit
Sol.13	+	+++	++	S	13. Flexibility↑: Modification of the gas-liquid distributor and/or contactor (see Item-2 and/or 3) 14. Also the Item-8 is applicable

Response time:

The required response time of a solvent system towards changes in the process configuration and/or operation parameters is defined and measured with the time until stable conditions are reached again at the outlets as well as no changes anymore in the pH value and the redox potential. The results of the experiments conducted in the scope of this subsection revealed that the more concentrated solutions (e.g. Sol.3, Sol.5, Sol.13) clearly have benefits in equipment and pump size (CAPEX↓). However, the operational benefits of the more dilute systems are also

important. It was seen that solutions containing lower catalyst concentrations (e.g. Sol.1, Sol.12 etc.) featured faster changes in pH and the E of the solutions (see **Table 4-14**) in comparison to others. They showed also fast response to changes in the sour feed gas composition, which enabled significant reduction in operator attention (OPEX↓) for the lab plant. The solutions with low catalyst concentrations were also beneficial in terms of ensuring higher capacity to solubilize by-products formed during the treatment process (e.g. thiosulfates and/or organic degradation products) as explained in section 4.2.6. In addition to the optimization of the catalyst concentration, an optimization in the solution pH depending on the respective solution composition can result in faster responses and thus give more flexibility to the employed system, as it is remarked under Items-5 and 7 in **Table 4-14**, since the pH directly influences the absorption and oxidation mechanism of the interactive species.

Flexibility (in terms of turn down ratios of CO_2 flow and liquid to gas ratios):

- **Effect of CO_2 concentration in the sour feed gas:** It was deducted that when the sour gas contains higher concentrations of CO_2 than 10 vol%, the H_2S absorption efficiency of some solutions with lower flexibility drops (given as, +, in **Table 4-14**). As it is stated in **Table 4-14** under Item-11, the decrease in the absorption efficiency can be mitigated by a considerable increase in the absorber height.

- **Variation of L/G & contact time:** As discussed previously, more concentrated solutions necessitated higher flow rates of regeneration air which may be explained with mass transfer limitations. Higher gas flow rates resulted in lower L/G and higher superficial gas velocity, which in turn cause coalescence of gas bubbles and development of a turbulent flow pattern in the column (i.e. heterogeneous flow see **Figure 2-3**). This led to a significant decrease in the efficiency and the flexibility of the system towards changing acidic gas concentrations, which resulted in H_2S-breakdown, which was observed by the color changing in $CuSO_4$ solutions. This fact reveals the requirement of modifications to the given set up to enable homogeneous distribution of bubbles for an optimal mass transfer (i.e. homogeneous flow see **Figure 2-3**). In this context, installment of a more appropriate gas distribution device (e.g. an eductor mixer see **Figure 2-2**) can be promising to improve the mass transfer efficiency, while enabling reduction in operational expenses (air compression cost) – if the column type to be applied in industrial scale is a bubble column. Alternative to bubble columns, pipeline contactors with static mixing elements (referring to section 2.1.1.2) can be used, if the more concentrated solutions are employed in the system (Hauke S. , Joh, Sönmez, Nickelfeld, & Schüler, 2016).

Operability:

- **Plugging:** As main circulation pump, a peristaltic pump was chosen, since this type features high flexibility in terms of viscosity of the liquids, flowrates, or a combination of the two. However, during the experiments with some solutions whose operabilities are ranked with, +, in **Table 4-14** (e.g. Sol.3, Sol.5, etc.) difficulties with keeping the liquid circulation were encountered due to sulfur plugging. As design improvement, utilization of so-called closed-impeller single and/or multi-stage centrifugal pumps for pilot plant and industrial applications are recommended since they can also handle varying concentrations of suspensions, besides lower cost compared to positive displacement devices (Heguy, 2003).

- **Foaming:** Besides affecting the response time adversely, high catalyst concentrations led to some operational difficulties such as foaming. The primary corrective measure to combat this situation would be the addition of surfactants (listed in **Figure 2-5**). In this context, pre-experiments had been performed independently from the benchmarking tests with some solutions featuring comparable properties to those called as “high-cat” in the scope of this study (e.g. Sol.3, Sol.5 and Sol.13). The results showed that most of the surfactants given in **Figure 2-5** made the formed solid sulfur tend to adhere to the gas-liquid surface and thus adversely influenced the mass transfer efficiency of the process gases into the respective solution by blocking the gas-liquid interface. Utilization of surfactants adversely impacted the settling behavior of the sulfur

product. Hence, it is recommended to use a mechanical foam breaking device rather than applying a chemical measure as it is given under Item-8 in **Table 4-14**.

Besides operability, flexibility, robustness and performance factors of different liquid system compositions, also the settling behavior and the quality (composition) of the produced solid product were investigated, which are essential for the techno-economic evaluation of the process. The results are presented in the following section.

4.2.6 Effects of the composition (solvent system, sour feed gas) on the sulfur product quality

4.2.6.1 Precipitation behavior of the sulfur product

The desired solid product, i.e. the elemental sulfur, precipitates as whitish-yellowish particles due to its low aqueous solubility (approx. 5 g/L at 293 K (Boulegue, 1978) while it is lower in solutions with high salt fractions). During the operation with different solutions, it was observed that the sulfur either flotated (F) or settled (S) in the respective solution (see **Table 4-14**). The literature review done on this account revealed that the precipitation behavior of elemental sulfur primarily depends on the Fe(III) to Fe(II) ratio in the solution and the rate of the H_2S oxidation reaction (referring to Eq.1-9) (DeBerry, 1997). High initial Fe(III)-concentrations and relatively lower Fe(II)-concentration during operation lead to faster oxidation of H_2S and in turn fast formation of solid sulfur. This results in smaller particle size of the sulfur, more likely floatated. In addition, if the oxidation of the H_2S occurs at very low rates, the undesired formation of by-products is encountered (Kohl, A. L. et al., 1997), which are reportedly composed of small particle size, and thus, flotated. Control of sulfur composition is therefore a key topic from as presented in the following.

4.2.6.2 Composition (quality) of the produced sulfur

The reasons for occurrence of the side reactions were discussed in section 2.3.1.1. Reportedly, formation of by-products (the so-called sulfur oxo anions) like thiosulfate ($S_2O_2^{3-}$) is promoted either if the Fe(II)-concentration is too low or the amount of dissolved O_2 is much higher than needed (DeBerry, 1997). Analyzing the composition of taken solid samples (according to the method mentioned in section 4.2.3) give the information whether and to what extent side reactions occur, which lead to the decrease in concentration of the “desired” product (elemental sulfur) and to increase in “undesired” components such as sulfur oxo-anions. The composition of the sulfur product affects the waste disposal considerations, as well. The results of the analysis of the taken solid samples are exemplified in **Figure 4-23**. Here, the dry compositions of the unwashed solid products formed during the test of the Sol.12 and Sol.13 (representing Siemens-Solvent2 with low-cat (0.1 M) and high-cat (0.5 M)) under Case1 are compared.

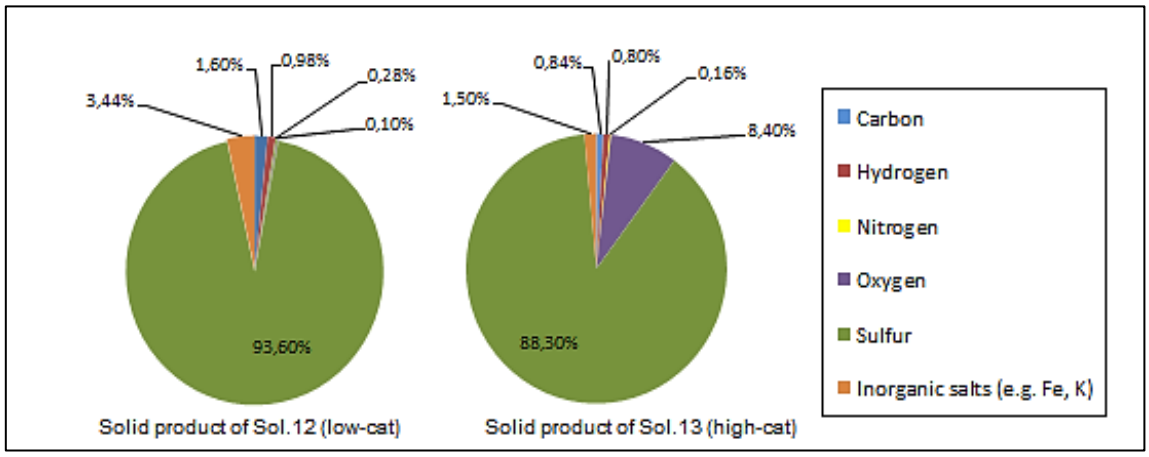

Figure 4-23 Dry composition of the unwashed solid samples taken at the end of the test runs with Sol.12 and Sol.13 under the conditions given in Case1 in Table 4-11 (accuracy ±5%)

The filter cake moisture content (including AAS, Fe and Lig) of both samples before drying at 105 °C (according to DIN 38414 S2) were comparable (see **Table 4-15**). As illustrated in **Figure 4-23**, the unwashed, dried sulfur samples contain:

- Sol.12 (low-cat): 93.6 wt% sulfur (S) with less than 3 wt% of elemental atoms (i.e. C, N, H and O) and <4 wt% of inorganic salts (i.e. Fe and K)
- Sol.13 (high-cat): 88.3 wt% sulfur (S) with ≤10 wt% elemental atoms and less than 2 wt% inorganic salts, respectively.

An increase of approx. 8 wt% in the elemental oxygen concentration of the sulfur cake obtained from the Sol.13 (i.e. high-cat see **Table 4-9**) can be explained by the possible oxidation of H_2S to thiosulfate ($S_2O_3^-$) and further oxidation of it to sulfate (SO_4^{2-}) referring to Eq.2-6 and Eq.2-7, respectively. It seems that the excess regeneration air supply into the solution with higher initial Fe(III)-concentration and relatively lower Fe(II)-concentration during operation (i.e. Sol.13) promoted the formation of sulfur oxo-anions (for the countermeasures to be taken to suppress the formation of sulfur oxo-anions, and thus, to enhance the quality of the solid product refer to section 2.3.1.1).

Improving the quality of the sulfur product by minimizing also the inorganic salt concentration of the sulfur cake requires an efficient purification/washing process as mentioned in section 2.1.2. It must be noted that, during the benchmarking tests in the lab plant, the active materials in the washing water solution (i.e. AAS, Fe, Lig) for the filter cake which had been withdrawn from the sulfur separation unit (see **Figure 4-11**) were not recovered and not re-fed into the solution inventory in the plant. Since, the further treatment/recovering of the spent wash water causes additional operational expenses (OPEX), this processing step is essential to sustain an economically feasible operation in industrial scale. Therefore, the optimal amount of wash water ratio to sulfur was examined in detail (to recover maximum amount of catalyst while using as little wash water as possible). As an example, analysis of the wash water obtained from the sulfur cakes of Sol.12 and Sol.13 is given in **Figure 4-24**, illustrating the influence of the amount of wash water on iron content of the respective sulfur cakes.

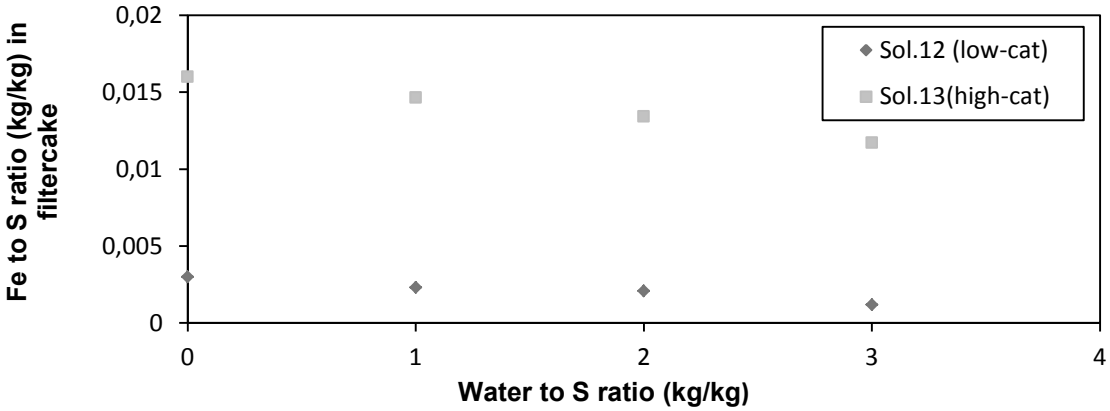

Figure 4-24 Effect of the wash water to sulfur ratio on iron content of the sulfur cakes (residual moistures in the range of 55-60 wt% (±5%) obtained from Sol.12 and Sol.13 (accuracy ±5%)

As **Figure 4-24** indicates, the filter cake residual iron content is decreasing only slowly with increasing water ratios, however it seems to be strongly depending on the initial catalyst concentration of the respective solutions (i.e. 0.1 M in Sol.12 and 0.5 M in Sol.13, see **Table 4-9**). This can be also an indication of the inefficiency of the washing process probably due to the maldistribution/penetration of the water molecules through the presumably dentritic agglomerated sulfur particles or larger channels in the filter cake. A similar observation has also been described by (VanKleeck & Morisse-Arnold, 1990). They stated that the residual iron content in the sulfur cake is a strong function of its moisture content, which is directly affected by the efficiency of

filtration method used and primarily depends on the particle size of the sulfur particle in the cake. For this reason, there is an economic incentive to investigate the particle characteristics (shape and size), hence, to minimize the filtercake moisture content and related iron-chelate losses, as discussed in the following section.

4.2.6.3 Particle characterization of the sulfur product

There are many parameters to characterize particles to specify the downstream processing unit into which they are fed i.e. shape, size, volume or mass of them. Regarding the techno-economic evaluation done in this study, the particle size data of the sulfur cake are of high interest for the design of the filtration unit and thus for an efficient seperation of the sulfur particles from the system. Large particle size means simple solid-liquid separation and in turn low moisture content of the filter cake (thus low chemical make-up ratio and vice versa (see **Table 4-15**). For the characterization of the particle size distribution (PSD) in the respective sulfur cakes obtained from all formulated solutions (Sol.1 to Sol.13 see **Table 4-9**), the focused beam reflectance measurement (FBRM) method (offline) was used. The basics of the measurement are given in (Greaves, D. et al., 2008). The FBRM approach uses a laser beam projected through a window: when the focused rotating laser beam contacts the particle, light is reflected and propagated back through the probe window. The particle continues to reflect light until the rotating focused beam reaches the opposite edge of the particle. Thus, particle size (meaning its diameter) is measured in terms of a chord length (CL) which is defined as the distance between the two edges of a particle. Thousands of chord lengths (µm) are acquired per second and are organized in size intervals. The FBRM software (Mettler Toledo, 2016) allows the user to select different weighting choices of these distributions. The unweighted, square-weighted (surface area) and cube-weighted (mass) distributions provide amplification or deamplification of the particles. The plots of the unweighted CLs (µm) versus relative number of detected particles (%) yielding the so-called CLD curve is computed. As an example, of the unweighted, to 100% normalized differential CLD curve of the sulfur cake obtained at the end of test run with the Sol.2 is shown in the left hand side of the **Figure 4-25**. The unweighted, differential CLD curve presents the frequency of number of particles within a defined size range. However, it is quite common to convert the normalized frequent based CLDs to cumulative mass fraction based PSDs automatically by the software (see the right hand side of **Figure 4-25**), since the PSD rather than the number provides a greater emphasis on more coarse particles. This follows from the simple fact that one large particle has much more mass than a small particle, despite both represent a number distribution of one.

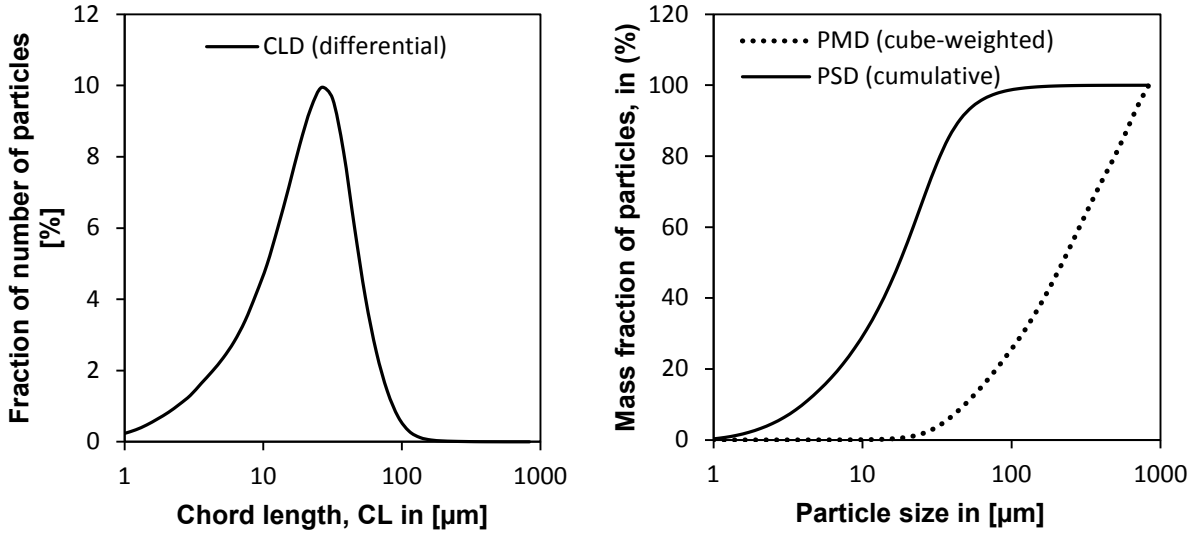

Figure 4-25 The frequent based unweighted CLD (left) , the mass fraction based unweighted PSD and the cube-weighted PDM curves of the sulfur cake obtained from Sol.2

It shall be noted that the obtained PSD must not yield exact numerical values of particle sizes. However, it is assumed that the achieved results allow a fair comparison between the particle

sizes of the analysed sulfur cakes. Subsequently, a mass distribution of particles (PMD) was obtained within a size range generated from the cumulative PSD curve. The conversion of the unweighted PSD to cube-weighted PMD can be achieved by correlating the mass of a single particle with the cube of its measured diameter using the mathematical models given in (Braatz, R. D. et al., 2003) under assumption that particles have a spherical shape and the solid density remains constant throughout measurement. Based on PSDs, the mean particle sizes of the sulfur cakes obtained from all formulations were calculated and are reported in **Table 4-15**. The PMD obtained was characterized by C10 and C90 for the statistical evaluation of the distributions. The terms C10 and C90 present the cube-weightened particle diameter at which 10% and 90% of the total sample mass is below, respectively. The results are also given in **Table 4-15**.

Table 4-15 Particle characterization data of the obtained sulfur cakes at the end of 160 h operation different with solutions (Sol.1 to 13) (accuracy ±5%)

No. of solution	**Mean particle size [µm]**	**C10 [µm]**	**C90 [µm]**	**Moisture content in filter cake** (rounded up to next whole number) **[wt %]**
Sol.1	27.0	40.0	659.9	45 ± 5
Sol.2	27.3	58.4	764.2	45 ± 5
Sol.3	21.5	47.0	809.1	55 ± 5
Sol.4	31.2	41.0	313.3	40 ± 5
Sol.5	20.4	66.8	828.0	55 ± 5
Sol.6	31.3	57.8	784.9	40 ± 5
Sol.7	23.1	42.0	592.6	55 ± 5
Sol.8	21.9	98.1	902.5	45 ± 5
Sol.9	34.3	51.3	436.9	35 ± 5
Sol.10	20.7	31.2	402.6	55 ± 5
Sol.11	29.6	42.5	547.0	40 ± 5
Sol.12	22.5	47.6	683.5	55 ± 5
Sol.13	20.0	79.6	859.3	60 ± 5

Typical particle size distributions for taken samples include particles size ranges from 20 µm to 905 µm. The PMD curve shown in the right hand side of **Figure 4-25** revealed that smaller particles were distributed frequently in the sample of Sol.2, but they have no significant mass due to their smaller sizes. The C10 characterization of the sample Sol.2 done on this account gave the information that particles smaller than 58 µm represent only a small fraction of the entire measured particle size distribution (the 10% of the total sample weight) whereas particles smaller than 765 µm (C90) were accounted for a large range in the measured mass (i.e. 90%) (see **Table 4-15**). This information, that the distributions were in a wide range, is essential since it gives clues for the optimization of the design and thus the efficiency of the filtration unit to be applied. In order to increase the effluent filterability and improve operability of the filtration step by avoiding clogging, the heavy particles (i.e. C90) shall be separated from the lighter ones (i.e. C10) previous to feeding the whole suspension into a single filtration unit. In this context, melting the sulfur cake is not an option, since the ligand decomposes reportedly at T>60°C (see section 2.1.2) (Martell, A. E. et al., 1975). Thus, this should be accomplished by feeding the suspension taken from the treatment plant into downstream unit operations such as settler and/or hydrocyclone (see **Figure 2-4c** and **Figure 2-4e**) where the downstream (heavier ones) can be fed into the main filtration unit while the upstream (lighter ones) can be returned to the treatment plant to enable their growth/agglomeration.The sulfur cakes taken from solutions were found to be made up of particles with mean sizes in the order of 20-35 microns, whereas sulfur entering the regenerator (measured after the filtration of taken liquid samples from the regenerator) was found to have a mean diameter size of 10-15 microns (not listed in **Table 4-15**). This information reveals that sulfur agglomerated during the operation and hence, an induction period is required before inception of colloidal sulfur. In addition to size characterization of particles, also the reflected-light microscopy pictures of all samples were taken for the appraisal of the particle morphology; however, as example, only one picture taken from the sulfur sample of the Sol.12 is shown in **Figure 4-26**.

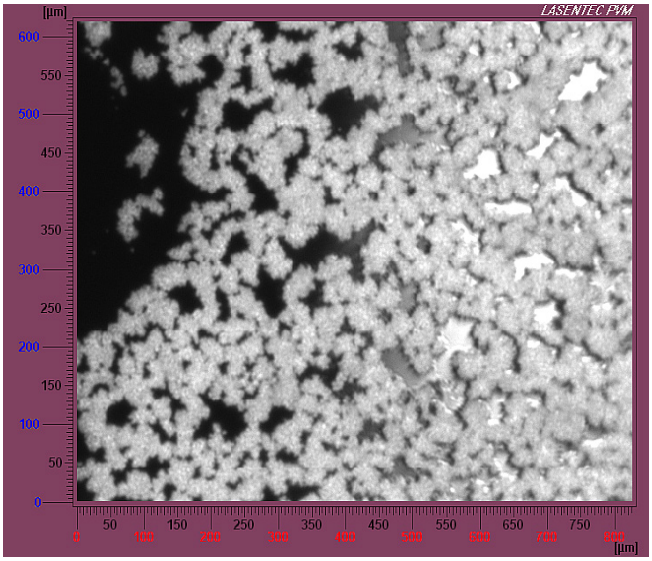

Figure 4-26 Particle morphology of the sample of taken from the Sol.12

Figure 4-26 confirms the assumption on the occurence of the formation of the dentritic-shaped sulfur particles (e.g. see the solid sample of Sol.12) which clarifies the reason of the inefficiency of the washing process mentioned in section 4.2.6.2 (given in **Figure 4-24**). It seems so that the dentritic agglomarates entrapped the solution and thus hinder the solution from being displaced with the washing water. In addition, the mean particle sizes listed in **Table 4-15** were found to be in analogy to the optical appearance determined by off-line microscopy pictures of all samples (for Sol.1 to Sol.13) given in **Figure A- 8** in Appendix A-2.9. The results obtained are in good agreement with literature (typical mean particle sizes of liquid-redox-sulfur from 8 to 45 microns see section 2.1.2) (Quinlan, 1991). As mentioned above, the larger the particles size of the produced sulfur, the lower the moisture content, lower mechanical loss of the solvent system and thus the chemical make-up. Mechanical solution loss by filtration and thus the required chemical make-up ratios to produced sulfur were estimated based on the analysis results, example of these given for Sol.12 and Sol.13 in **Figure 4-23**, are summarized in **Table 4-16**.

Table 4-16 Estimated chemical make-up ratios (kg/kg sulfur) for solutions with low and high catalyst concentrations (accuracy ±5%) *rounded up to next whole number

	Range of chemical make-up ratios for the given component (kg/kg sulfur) *			
Component / **Solution type**	**Fe(III)**	**Ligand**	**KOH** (as alkaline agent for the formulations w/o AAS)	**AAS** (as alkaline agent for the formulations with AAS)
"Low-cat" solutions (c[Fe(III)]=0.1M); Sol.1, Sol.2, Sol.4, Sol.6, Sol.7, Sol.8, Sol.9, Sol.10, Sol.11, Sol.12	0.0018 - 0.003 (for all low-cat solutions)	0.011 - 0.018 (for all low-cat solutions)	0.004 - 0.009 (for Sol.1, Sol.2 and Sol.4)	0.0025 - 0.010 (for Sol.6 to Sol.12)
"High-cat" solutions (c[Fe(III)]=0.5M); Sol.3, Sol.5 and Sol.13	0.010 - 0.014 (for all high-cat solutions)	0.060 - 0.084 (for all high-cat solutions)	0.030 - 0.040 (for Sol.3 and Sol.5)	0.030 (for only Sol.13)

It must be noted that these ratios cover only the mechanical loss (during filtration) when the sulfur cakes (for residual moistures see **Table 4-15**) were washed with a water to sulfur ratio of two and when the chemicals were not recovered from the wash water and re-fed to the process. Thus, the ratios given **Table 4-16** in do not involve the chemical make-up requirement caused by a possible chemical degradation. Some of the investigated solutions promoted the formation of sulfur in smaller mean particle sizes comparably to others (refer to **Table 4-15**), therefore, the chemical make-up ratios were found to be higher than those of others. It shall be noted that, in addition to particle sizes, these ratios vary also for the given operation condition and solvent composition. For instance, if the sour feed gas comprises of both acidic gases (H_2S and CO_2), more potassium hydroxide (KOH) had to be supply to the systems which did not contain AAS in order to maintain the solution pH. However, in the cases of the presence AAS in the formulations (e.g. Sol.13), the interval and amount of alkali supply was significantly lower than those of unbuffered solutions (e.g. the Sol.3).

To complete the techno-economic characterization of the solution systems formulated, corrosivity of them will also be studied as presented in the following section.

4.2.7 Material of construction - corrosion issues

Reportedly, alkaline media containing significant salt fractions are corrosive to the plant equipment because of elevated pH values and operation temperatures (Kohl, A. L. et al., 1997), which necessitate the use of expensive construction material. Thus, industrial applicability of various construction materials must be evaluated through material qualification tests. In liquid redox processes, it is common to use stainless steel material of AISI 316 grade (e.g. DIN No. 1.4571 also known as EN-1088-1 or AISI 316Ti with the composition X6CrNiMoTi17-12-2) (Kohl, A. L. et al., 1997) due to its significant resistance towards alkali corrosion. However, this material is highly cost intensive[23] and has limitations with respect to availability on the world market (Perry, R. C. et al., 1973). Hence, investigations on the corrosion behavior of alternative materials with lower costs[23] and better availiability would sensibly reduce the plant investment costs and enlarge the applicability. In this context, the following two materials were selected based on literature review:

1- Coated case hardening steel DIN No. 1.7139 (EN Standards-X16MnCrS5); (SAE grade-5115)
2- Carbon steel DIN No. 1.0425 (EN Standards-10028-2); (ASTM A285 Grade C).

To evaluate the applicability of them, their weight loss during the exposure time due to corrosive attack was determined at TÜV SÜD Chemie Service GmbH, and the so-called integral corrosion rates (W_{int}) were deducted. Besides that, the samples were examined optically. The W_{int}<0.01 mm/a is known as the allowable limit for the qualification of a material in the construction of an industrial plant, if no corrosion allowances are applied for the wall thickness of the equipment. The tests were conducted on these two different materials according to DIN 50 905 Part 4 and under the conditions given in **Table 4-17**.

Table 4-17 Conditions of corrosion tests

Testing conditions	
Testing medium	Sol.1
	Sol.3
	Sol.12
	Sol.13
pH of the medium	9.0
Temperature, °C	35
Exposure gas	Air (atmospheric)
Exposure time, hours	360

[23] For 1.4571: 1500-3000 $/ton; For 1.0425: 330-410 $/ton and for 1.7139: 6000-1800 $/ton - Prices are given for the minimum order quantity of 5 metric tons and were retrieved from http://www.alibaba.com/trade on 5th October 2015.

Both materials in each of four different solution formulations listed in **Table 4-17** those are containing “low-cat” and/or “high-cat” with and/or without AAS (i.e. Sol.1, Sol.3, Sol.12 and Sol.13 see **Table 4-9**) were exposed to air during 360 hours. It is worth to mention that, these solution samples were taken from the test rig (see **Figure 4-11**) at the end of totally 160 operation hours (see **Table 4-10**). This means the used solution media were already exposed to H_2S and CO_2 during the 160 h operation. The integral corrosion rates of the materials 1.0425 and 1.7139 were not found to be within the permitted range (see TÜV SÜD Chemie Service GmbH official reports in Appendix A-2.10[24]). Thus, the equipment and piping of the pilot plant in contact with the solvent system were planned to be constructed of stainless steel 1.4571. Corrosion test of this material will have to be performed during the experiments in the pilot plant under industrial conditions.

After reviewing the corrosion issues briefly, the conclusions of tests on techno-economic feasibility parameters are drawn as presented in the following section.

4.2.8 Conclusions and selection of formulations for degradation studies

Taking all gained operational and performance behavior of the formulated systems into account, conclusions comprising the three basic unit operations and the transfer to the industrial scale can be presented as follows:

(1) Absorption & oxidation of the H_2S and (2) Regeneration of the operating solution:

- It was found that the ligand-to-metal ratio has practically no impact on the H_2S absorption ratio and thus on the performance parameter f_{sol} (pump around ratio).

- Higher catalyst concentrations enabled significant reductions in pump around. However, it resulted in increased viscosity and density, thus, the mass transfer of the O_2 into the washing liquid had been affected adversely which necessitated to supply the regeneration gas in higher flow rates.

- The required pump around ratio was found to be depending on the type and the concentration of the applied AAS and concentration of chelated iron – lower pump around for secondary AASs with higher AAS and catalyst concentrations. In contrary, the absolute differences in the regeneration air demand for the solutions containing different types of AAS were not that significant. However, it was deducted that secondary AAS buffered the H^+ ions, which are a product of the absorption reaction, more efficiently. This information is essential, since this phenomenon presumably caused changes in the proposed regeneration kinetics behavior (refer to section 4.1.4.2.4).

- Increased CO_2 concentrations of the feed gas resulted in the reduction of the pH. This generated considerably lower rates in the oxidation reaction of H_2S to sulfur (unless buffered; i.e. in the case w/o AAS), resulting in higher f_{sol} ratios.

(3) Separation of produced sulfur:

- Precipitation behavior (i.e. settling or flotation) of the sulfur product was found to be dependent on the chemical composition of the applied solvent system and is favorable for Siemens Solvent-1 and 2. The sulfur cakes were found to be made up of particles with mean sizes in the order of 20-35 microns. The filter cake residual iron content was detected to be not strongly dependent on the wash-water ratio, but to be remarkably depending on the particle morphology and initial catalyst concentration of the respective solutions. To mitigate the inefficiencies in the washing process caused by dentritic agglomarates, it was suggested to feed the suspensions taken from the treatment plant into downstream unit operations such as settler or hydrocyclone to enable their growth/agglomeration.

[24] TÜV-Report No: KO 16 067 from 27.05.2016 and TÜV-Report No: KO 15 159 from 23th October 2015 (in German), respectively.

In addition to the design modification/process optimization suggestions based on the gained operational experience given in **Table 4-14**, the following conclusions can be drawn regarding the **transfer of the results to an industrial scale operation**:

- The process applying AAS as absorbent was found to be able to cope (robust+operable) with variations in the properties of the sour gas to be treated, whereas most solutions without AAS and/or with high catalyst concentrations were characterized as very sensitive (inflexible) towards changes.

- The Sol.9, Sol.10 and Sol.11 (tertiary AAS Dimethylglycinate) were labelled as infeasible even for the desulfurization of “moderately-high” sour gases, whereas the Sol.1, Sol.2, Sol.3, Sol.4, Sol.5, Sol.6, Sol.7 Sol.12 and Sol.13 showed acceptable performance.

- Sol.6, Sol.12 and Sol.13 (Siemens Solvent 1 and 2) were found to be effective even for the desulfurization of “ultra-high” sour gases.

- The non-disclosed Lig.2 (Sol.4 and Sol.5) showed comparable performance to EDTA.

Comparing the two remaining secondary AAS (the Siemens Solvent-1 and Siemens Solvent-2), the Siemens Solvent-2 (Sol.12 and Sol.13) showed a slightly better behavior. The ligand-to-metal-ratio was found to have no practical influence on the performance parameters, however, the impact of it on the chemical stability of the applied ligand under severe conditions is unknown. Thus, the AAS-free solutions with no free ligand (the Sol.2; w/o AAS and EDTA:Fe=1.0) and with excess ligand (the Sol.1; w/o AAS; EDTA:Fe=1.5) will be considered further in the detailed degradation studies. This will also enable a comparison with the AAS based high and low-cat solvent systems (i.e. Sol.12 and Sol.13; with AAS EDTA:Fe=1.5). Hence, the Sol.1, Sol.2, Sol.12 and Sol.13 were chosen for the execution of detailed degradation studies as presented in the following chapter.

5 DEGRADATION STUDIES OF THE FORMULATED SOLVENT SYSTEMS

5.1 Background

As it was mentioned in section 4.2.4, only moderate degradation of formulated solvent systems could be detected during the benchmarking experiments (i.e. 160 hours) in the continuous lab plant under the given conditions. The corresponding results of the analyses available in **Figure A-5** and **Figure A- 6** in **Appendices A-6** and **A-7**, respectively, revealed that degradation of the systems was negligible under the testing conditions (refer to section 4.2.4) but this can still lead to remarkable solvent refill costs during longer periods of operation, depending on the process conditions. If the amount of ligand and/or AAS loss by degradation exceeds the acceptable ranges, this can adversely affect the industrial application of the developed formulations (performance↓; OPEX↑). Therefore, further information is needed to explain why and under what conditions degradation occurs. For this purpose, one representative of each of the promising liquid systems - with/without AAS - containing low or high-cat – with/without excess ligand (i.e. the Sol.1, Sol.2 and Sol.12 and Sol.13) were chosen to execute degradation studies within the scope of this chapter. These solutions were tested under pre-defined and severe conditions with the main goal to describe the degradation behavior of them in detail and to point the ways to further improvements in the process. In this context, the following approach has been taken:

- Firstly, the degradable constituents of the selected solvent systems were determined (i.e. the organic components = AAS and/or chelating agent)

- Subsequently, the common degradation mechanisms proposed for these organic constituents were identified by a detailed review on earlier investigations available in open literature.

- Thereafter, some of them were ruled out, taking the operation conditions of the evaluated process into account, and thus, the possible dominating degradation pathways for the evaluated process were described.

- Accordingly, the decomposition routes were highlighted in order to understand which conditions promote their occurrence.

- After developing an understanding about the corresponding degradation pathways, their consequences on the solution composition (meaning degradation products) were studied.

- Considering the deducted information, the experiments were planned and executed under adequate conditions in order to see whether the respective degradation pathways take place in the formulated solvent systems as proposed in literature or not.

- Consequently, the concentrations of the ligand and AAS were analyzed to acquire first-hand-information regarding the degradation products, which in turn reveals the occurred corresponding pathway.

Since severe experimental conditions were chosen, absolute figures of degradation rates of the tested solutions would not be directly relevant for practical use, and thus it was not the primary goal to determine those. However, the results gained will help to inhibit the possible decomposition of the liquids when operated under process conditions of interest (refer to section 3.2) by taking the corresponding countermeasures, and thus, to assure a flexible operation, an environmentally friendly as well as economically viable treatment process. As the first step of the approach given above, the basic degradation pathways of the degradable constitutents of the selected solvent systems are reviewed in the following section.

5.2 Basic degradation pathways

A representative **solvent system** of the Siemens liquid redox technology contains two organic compounds: (1) AAS as absorbent and (2) Aminopolycarboxylate (APC) chelator (refer to **Figure 1-4**). In this context, as shown in **Figure 5-1**, two possible pathways for the degradation initiation of these components were proposed in literature: thermal and oxidative attacks (Bedell, 2009), (Fischer, 2013), (Rochelle, G. T. et al., 2001), (Motekaitis, R. J. et al., 1993). The latter occurs statedly by two potential oxidation routes: radical induced and autocatalytic oxidation (Martell, 2009).

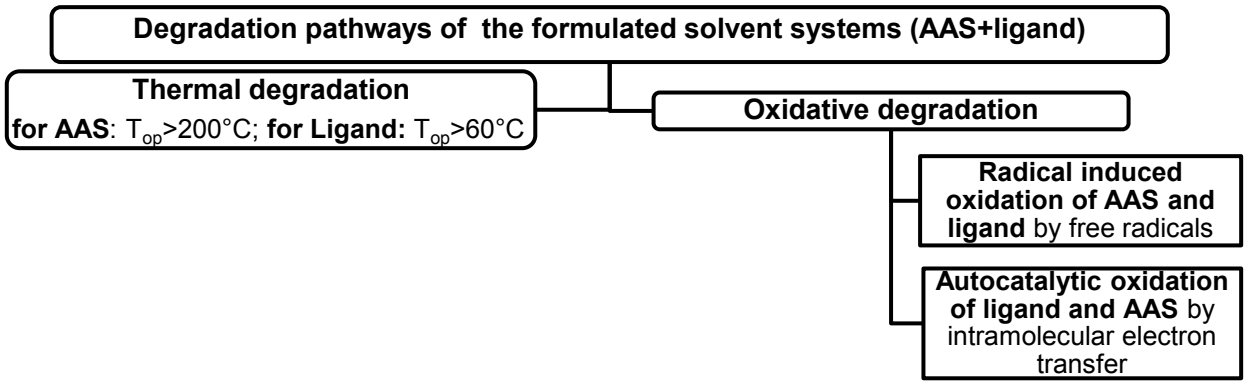

Figure 5-1 Possible degradation pathways of the constituents of the formulated solvent systems

The degradation pathways will be highlighted in the scope of the following sections.

5.2.1 Thermal degradation of the solvent systems

(Rochelle, G. T. et al., 2001), (Bedell, 2009) and (Fischer, 2013) stated that thermal degradation of the amino acids do not take place at T<200 °C. Due to the fact that the liquid redox processes are operated at significantly lower temperatures (20-60 °C - see section 3.5.2.1), thermal stress is not expected to be the dominating degradation mechanism for the AASs applied as absorbents in liquid redox technique under the operation temperature of the evaluated process (i.e. T_{max}=40 °C (Siemens AG, 2016)). Also for the ligands, most studies have shown that thermal degradation is negligible below 60 °C (Martell, A. E. et al., 1975), (Bengoa, 2007). Hence, thermal degradation will not be studied further in the scope of this chapter. However, the presumably dominating degradation mechanism in the liquid redox processes, the oxidative attack, will be covered in detail, as in the following section.

5.2.2 Oxidative degradation of the solvent systems

A literature review on possible reaction pathways causing the degradation of the organic compounds of a representative **solvent system** of the Siemens liquid redox technology (see **Figure 1-4**) revealed two potential oxidation routes: radical induced and autocatalytic oxidation pathways. A basic understanding of distinct differences in these two mechanisms is essential to study, predict and control the oxidative attack in liquid redox systems. They will be presented in the next subsections.

5.2.2.1 Radical induced oxidation - Fenton mechanism

In open literature, it was proposed that trace amounts of metal ions from corroding plant material can catalyze the oxidative degradation of the AAS used as solvent in post combustion carbon capture processes (see the Footnote 14 given in section 3.5.2). (Fischer, 2013) found that EDTA and bicine were effective inhibitors to slow down the oxidative degradation of AAS by sequestering metal ions. As the metal ion is chelated with the ligand in liquid redox processes for H_2S separation, it can be assumed that the complexed iron would not be able to promote the oxidation of the AAS by dissolved O_2 (which forms radicals) in the liquid redox systems. Thus, the radical induced degradation of the applied AAS catalyzed by metal ions can be presumed - as long as enough amount of chelator is available in the solution to protect the AAS.

However, radical induced oxidation of the ligand in long term seems to be inevitable since it is directly linked to the presence of the oxidized form of the iron (i.e. Fe(III) – the reaction partner of the dissolved O_2 in the regenerator. Therefore, only the radical induced degradation of the ligand will be examined for the rest of this study. In this context, it is reported that free radicals are able to abstract H from a C-H bond and initiate radical chain reactions degrading the APC-chelates (Martell, 2009). Taking the NTA as an example of APCs, the radical induced degradation mechanism proposed by (Chen, D. et al., 1995) is illustrated in **Figure 5-2**.

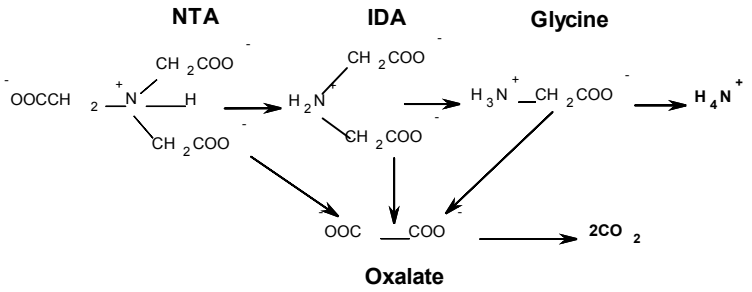

Figure 5-2 Proposed degradation scheme of NTA (Chen, D. et al., 1995) (involved intermediates were not shown)

The main degradation products of NTA identified by (Chen, D. et al., 1995) are iminodiacetic acid (IDA) and glycine (H_2N-CH_2-COOH) (see **Figure 5-2**). These products led to the conclusion that the location of the radical attack is one of the weak locations of the APC-chelates i.e. methylene (-CH_2-) groups, either on the ethylenic bond (C-N) or the side chain acetate (COOH-) groups as shown in **Figure 5-2**. Chen assumed that oxidative attack was initiated by hydroxyl radicals, $HO^{\bullet}$ originating from the so-called Fenton reaction (Fe(II).Lig+H_2O_2; see Eq.5-2) which reportedly takes place during the regeneration of the metal catalyst by air (see Eq.5-1). This triggered the occurrence of successive reactions yielding the formation of intermediates which were not shown in **Figure 5-2**. These reactions proposed by (Chen, D. et al., 1995) are expressed below from Eq.5-1 to Eq.5-7.

Regeneration by air:

$$(\mathrm{Fe(II)} \bullet \mathrm{NTA})^-_{(aq)} + {O_2}_{(aq)} + 2H_2O_{(aq)} \rightarrow 2(\mathrm{Fe(III)} \bullet \mathrm{NTA})_{(aq)} + {H_2O_2}_{(aq)} + 2OH^-_{(aq)} \quad \text{(Eq.5-1)}$$

Fenton reaction – Radical formation:

$$(\mathrm{Fe(II)} \bullet \mathrm{NTA})^-_{(aq)} + {H_2O_2}_{(aq)} \rightarrow (\mathrm{Fe(III)} \bullet \mathrm{NTA}) + OH^-_{(aq)} + HO^{\cdot}_{(aq)} \quad \text{(Eq.5-2)}$$

Hydroxylation of NTA to IDA:

$$R^1R^2N^+HCH_2COO^-_{(aq)} + HO^{\cdot}_{(aq)} \rightarrow R^1R^2N^+H\dot{C}HCOO^-_{(aq)} + H_2O_{(aq)} \quad \text{(Eq.5-3)}$$

Hydrolytic clevage of IDA to aldehyde:

$$R^1R^2N^+H\dot{C}HCOO^-_{(aq)} + H_2O_{(aq)} + (\mathrm{Fe(III)} \bullet \mathrm{NTA})_{(aq)} \rightarrow \quad \text{(Eq.5-4)}$$

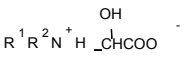

$$+ (\mathrm{Fe(II)} \bullet \mathrm{NTA})^-_{(aq)} + H^+_{(aq)}$$

Conversion of aldehyde to glycine and glyoxylate:

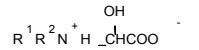

$$\rightarrow R^1R^2N^+H_{2(aq)} + OHCCOO^-_{(aq)} \quad \text{(Eq.5-5)}$$

Oxidation to oxalate:

$$OHCCOO^-_{(aq)} + 1/2\,{O_2}_{(aq)} \rightarrow OOC^- - COO^-_{(aq)} + H^+_{(aq)} \quad \text{(Eq.5-6)}$$

Formation of final degradation products:

$$OOC^- - COO^-_{(aq)} + 2H^+_{(aq)} + 1/2\,{O_2}_{(aq)} \rightarrow 2{CO_2}_{(g)} + H_2O_{(aq)} \quad \text{(Eq.5-7)}$$

R^1=R^2=CH_2COO^-≡ NTA R^1=R^2=H≡Glycin OOC^--COO^-≡Oxalate R^1=H; R^2=CH_2COO^-≡ IDA

For the corresponding molecules denoted as R^1 and R^2 refer to **Figure 5-2**. According to the reaction scheme listed above, the aldehyde formed by hydrolytic cleavage (see Eq.5-4; intermediate was not shown in **Figure 5-2**) subsequent to hydroxylation of NTA (referring to Eq.5-3), is rapidly converted to the corresponding carboxylate (in this case glyoxylate ($OHCCOO^-$); see Eq.5-5) or the oxalate ($^-OOC\text{-}COO^-$) anions (see Eq.5-6). Consequently, the oxidation of these degradation products leads to the formation of CO_2 (see Eq.5-6) and ammonium (NH_4^+) (not given in the reaction equations). This proposal is in accordance with radical induced degradation studies of various APC-chelates in aqeous solutions, which are presented in **Table 5-1** (Deshmukh, G. M. et al., 2012), (Motekaitis, R. J. et al., 1993), (Saelee, R. et al., 2012) and (Schifano, 2004).

Table 5-1 Experimental investigations on the radical induced degradation of APC-chelates and their characteristics

Study[a]	pH	T, °C	Ligand type	Concentration or flow rates of reacting species			Characteristics and findings
				c(Fe(III)) (mol/L)	V_{H2S} at P_{atm} (ml/min)	V_{air} at P_{atm} (l/min)	
(Chen, D. et al., 1995)	8.5	25	NTA HEDTA EDTA	0.018	2	1	2-chambered system[d] Degradation rate: HEDTA>EDTA>NTA
(Motekaitis, R. J. et al., 1993)	5.5 7.0 8.5	25	NTA	0.018	2	1	1-chambered system[e] Degradation rate decreased with increasing pH
(Schifano, 2004)	7.5	25	NTA	0.01	8.3	1.5	1-chambered system[e] H_2O_2 was used as regeneration medium instead of air Degradation rate was found to be lower in the case of regeneration by air
(Deshmukh, G. M. et al., 2012)	6.0	40	NTA EDTA DTPA	0.01	100	1	1-chambered system[e] Degradation rate: EDTA>NTA>DTPA
(Saelee, R. et al., 2012)	7.0	30	EDTA	0.002-0.008	0.4-1	1	1-chambered system[e] Empirical correlations of the degradation rate as f($\dot{V}_{H_2S}$, $c_{Fe_0}{}^b$, $c_{\text{inhibitor}}{}^c$) were found for the given system

a) In all studies solution volume used is 1 liter
b) the c[Fe(III)] at t=0
c)$c_{inhibitor}$: Initial concentration of the radical scavenger
d) Industrially, the process is usually carried out in two chambers, an absorber and a regenerator, so that not the H_2S but the Fe(II) comes into contact with O_2 (air)
e) In 1-chambered systems, H_2S and O_2 are supplied together into the solution system in a single reactor

To prove the existence of free radicals in the solution, (Chen, D. et al., 1995) and (Schifano, 2004) used the so-called spin trapping approach. The spectra of the radicals generated from the reaction of commonly applied spin traps (e.g. 5,5-Dimethyl-1-pyrroline N-oxide (DMPO) and phenyl-tert-butyl nitrone (PBN)) with the $OH^{\bullet -}$ radical were detected by electro spin resonance (ESR) measurements. Various additives that function as radical scavengers have been used to slow

down or prevent radical induced oxidative degradation. The added substances (e.g. chloride ion, imidazole and benzoic acid) react with free radicals, thus preventing them from oxidatively attacking, hydroxylating, and consequently degrading the organic ligand. Another form of the oxidative attack - the so-called **"**autocatalytic oxidation" - will be presented in the following section.

5.2.2.2 Autocatalytic oxidation - electron transfer mechanism

The **"**autocatalytic oxidation" - electron transfer mechanism is proposed to occur in the absence of hydroxyl radicals $OH^{\bullet -}$. The oxidation of APCs by O_2 at low temperatures is reportedly slow and sluggish (Kumar, 1982), however able to cause degradation of the ligand because metal ions may act as catalysts to activate the O_2. Reportedly, direct oxidation of the APCs by the coordinated metal ion (=autocatalytic oxidation) yielding the generation of radicals of chelators can occur even during the preparation of the solvent system independent of the presence/absence of dissolved O_2. (Motekaitis, R. J. et al., 1980) investigated the metal-catalyzed oxidation of EDTA and NTA at temperatures above 100°C in presence and absence of dissolved O_2. They reported that Fe(III) will oxidize the coordinated EDTA at 100-140°C in the absence of O_2 to produce its decarboxymethylated product, i.e. the ED3A, CO_2 and formaldehyde (CH_2O). Statedly, such an intramolecular oxidation reaction involves the electron transfer mechanism shown in **Figure 5-3**, in which reportedly electrons are transferred from one ligand molecule to two Fe(III) ions.

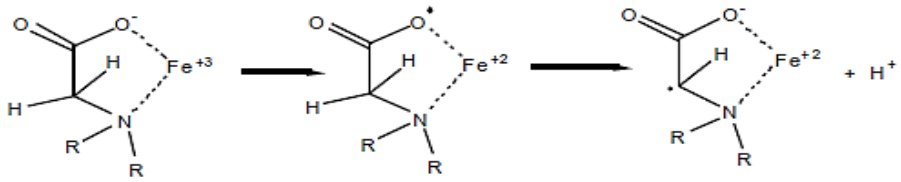

Figure 5-3 Autocatalytic oxidation of the EDTA by coordinated Fe(III) – electron transfer (Motekaitis, R. J. et al., 1980)

The electronic interaction between the metal ion and the ligand leads to a shift of electrons towards the metal ion, which lowers the electrical density in the chemical linkages within the ligand to the extent of atomic abstraction. In the absence of O_2, the reactions Eq.5-8 and Eq.5-9 proceed for a 1.5:1 and 1:1 ligand to metal ratio (mol/mol), respectively. In Eq.5-8, the degradation product (DP) of EDTA was found to be ethylene diamine tri acetic acid (ED3A = lacking an acetate group in comparison to EDTA). As a reaction product of the Eq.5-9, iron oxide, (Fe_2O_3) was detected where the O-atoms presumably came to the iron by the cleavage of the EDTA molecules, thus the molecule denoted as DP in Eq.5-9 lacks 3/2 O atoms and 1 H atom compared to EDTA. In the presence of O_2, the produced Fe(II)•EDTA complex is reoxidized to Fe(III)•EDTA by Eq.4-1 (Martell, 2009).

$$2(\mathrm{Fe(III)} \bullet \mathrm{EDTA})^{-}{}_{(\mathrm{aq})} + \mathrm{EDTA}_{(\mathrm{aq})} \xrightarrow[\mathrm{pH}=9.3]{\mathrm{T=175\,^{\circ}C}} 2(\mathrm{Fe(II)} \bullet \mathrm{EDTA})^{2-}{}_{(aq)} + \mathrm{ED3A} + \mathrm{H}^{+} \qquad \text{(Eq.5-8)}$$

$$3(\mathrm{Fe(III)} \bullet \mathrm{EDTA})^{-}{}_{(\mathrm{aq})} \xrightarrow[\mathrm{pH}=9.3]{\mathrm{T=175\,^{\circ}C}} 2(\mathrm{Fe(II)} \bullet \mathrm{EDTA})^{2-}{}_{(aq)} + {}^{1}/_{2}\,\mathrm{Fe_2O_3} + \mathrm{DP} + \mathrm{H}^{+} \qquad \text{(Eq.5-9)}$$

Autocatalytic degradation of the ligands was also investigated at or near room temperatures. In this context, (Lambert & Jones, 1966) found that hexacyanoferrate(III) (i.e. $Fe(CN)_6^{3-}$) directly oxidizes EDTA in water based solutions even at temperatures lower than 50°C. Thus, it can be concluded that although the reactions Eq.5-8 and Eq.5-9 proceed at slower rates at common liquid redox operating temperatures (i.e. 20-60 °C), they would still contribute to decomposition of the coordinated chelating agent. Since the AAS containing a chelated metal is used for the first time in the Siemens liquid redox technology, which is evaluated in the context of this work, there is no open literature available yet on the autocatalytic oxidation of an AAS under relevant conditions of the process. After identifiying possible dominating degradation pathways and reviewing their corresponding consequences, thus now, these will be examined in detail in the following

experimental part of this chapter in order to confirm whether the respective degradation pathways take place under pre-defined conditions as proposed in literature or not.

5.3 Experimental investigations on oxidative degradation of the formulated solvent systems

5.3.1 Background

Table 5-2 gives an overview on characteristics of the degradation tests performed in three experimental setups with variation of process parameters.

Table 5-2 Experimental conditions of conducted degradation studies in this work

Pathway / Experimental conditions	Radical induced oxidation		Autocatalytic oxidation Study-3
	Study-1	Study-2	
Operation mode	Batch (cyclic)	Continuous	Continuous
Experimental set-up	**Figure 4-3** Stirred cell reactor	**Figure 4-11** Lab test rig with absorber and regenerator	**Figure 3-7** Small sparged reactors in thermostated bath
Investigated solutions (For compositions also see **Table 4-9**)	**Test-1:** Sol.1 no AAS, EDTA as ligand c[Fe] = 0.1 mol/L Lig/(Fe.Lig) = 1.5 **Test-2:** Sol.2 no AAS, EDTA as ligand c[Fe] = 0.1 mol/L Lig/(Fe.Lig) = 1.0 **Test-3:** (Sol.2+$Na_2S_2O_3$)	**Test-1:** Sol.2 no AAS, EDTA as ligand c[Fe] = 0.1 mol/L Lig/(Fe.Lig) = 1.0 **Test-2:** (Sol.2+$Na_2S_2O_3$)	**Test-1 to 3:** Sol.12 Siemens Solvent-2 as AAS, EDTA as ligand c[AAS] = 1.6 mol/L c[Fe] = 0.1 mol/L Lig/(Fe.Lig) = 1.5 **Test-1 to 3:** Sol.13 Siemens Solvent-2 as AAS, EDTA as ligand c[AAS] = 1.6 mol/L c[Fe] = 0.5 mol/L Lig/(Fe.Lig) = 1.5
Parameters kept constant during tests	**Study-1**	**Study-2**	**Study-3**
Solvent volume, V_{sol}, L	0.70	5.6	0.25 each
c(Fe(III)), mol/L	0.1	0.1	Sol.12=0.1, Sol.13=0.5
Fe(III)/H_2S ratio, (mol)/(mol)	2	22	n.a. (no H_2S in feed gas)
EDTA/Fe(III) ratio (M:M)	variable, see below	1	1.5
Initial pH	9.0	9.0	9.0
Temperature, °C	30	25-26	variable, see below
Pressure, bar	P_{air} ≈ 3.9 bar	atm.	atm.
Feed gas flow, l/min	n.a.	1	1
Feed gas composition, %vol	n.a.	c(H_2S) = 10, c(N_2) = 90 (Case2, **Table 4-11**)	variable, see below
Stirrer speed, rpm	2200	n.a.	n.a.
f_{O2} (mol/mol)	1.5	2.25	n.a.
f_{sol} ratio	n.a.	10.81	n.a.
f_{air} ratio	n.a.	22.5	n.a.
Duration of each test, h	approx. 70	70	700

Parameters varied during tests / Test No.	Study-1		Study-2	Study-3		
	EDTA to Fe(III) (mol/mol)	$Na_2S_2O_3$ to EDTA (mol/mol)	$Na_2S_2O_3$ to EDTA (mol/mol)	$\dot{V}_{air}$ (l/min)	T, °C	$\dot{V}_{CO2}$ (l/min)
Test-1	1.5	0	0	1	30	0
Test-2	1.0	0	2.5	1	60	0
Test-3	1.0	2.5	-	0	60	1

With those, the gap in open literature on radical induced oxidation behavior of the ligand (i.e. EDTA) and autocatalytic oxidation behavior of the AAS applied (i.e. Siemens Solvent-2) under conditions relevant to the Siemens liquid redox process will be covered (i.e. higher pH, H_2S, Fe(III) and O_2 concentrations than those given in **Table 5-1**). To this end, the following solvent systems were employed in the scope of three degradation studies performed.

- **Study-1**: On radical induced oxidation mechanism in batch operation: Sol.1, Sol.2 and Sol.2+$Na_2S_2O_3$ as scavenger
- **Study-2**: On radical induced oxidation mechanism in continuous operation: Sol.2 and Sol.2+$Na_2S_2O_3$
- **Study-3**: On autocatalytic oxidation mechanism in continuous operation: Sol.12 and Sol.13

Within each study, two to three tests (**Test-1, Test-2 and/or Test-3**) were conducted with variations of parameters. It must be stated that in order to prevent misinterpretation of the results and rather to understand the occurrence of respective mechanisms, that the other acidic gas component present in real systems (i.e. CO_2) was not applied in Study-1 and Study-2 but it was used in Study-3, as described in the following:

Study-1: In order to investigate the impacts of each redox cycle on the stability of the ligand and the location of the oxidative attack and identification of responsible species, the sequential cycles of the H_2S-absorption&oxidation by Fe(III)•EDTA and regeneration of the Fe(II)•EDTA by air were performed in a stirred cell reactor system under pre-defined process conditions (batch mode). In this context, three sets of experiments (**Test-1 to Test-3**) were conducted:

- Earlier studies on radical induced ligand degradation given in **Table 5-1** revealed that the location of attack of the radicals is stated to be the metal complex (Fe•EDTA) and not the free ligand (EDTA). To verify this, **Test-1** was conducted with an excess amount of ligand (EDTA:Fe(III)=1.5 see **Table 5-2**) under overstoichiometrical air supply (f_{O2}=[(O_2:Fe(II))$_{supplied}$/(O_2:Fe(II))$_{stoichometric}$]=1.5) - as the liquid redox processes usually are operated with an excess amount of air to ensure sufficient regeneration.
- The results were compared with those of **Test-2** which was executed with no excess amount of EDTA but equimolar to the metal catalyst (EDTA:Fe(III) =1 see **Table 5-2**) and under same amount of excess air supply (i.e. f_{O2}=1.5).
- The **Test-3** was performed under utilization of sodium thiosulfate ($Na_2S_2O_3$; an effective radical scavenger) to prove the existence of free radicals in the solution. If the result of the Test-3 shows that the degradation is inhibited by addition of $Na_2S_2O_3$ to the system, this will reveal that radicals are responsible for possible ligand degradation. As reported in (Saelee, R. et al., 2012), the amount of thiosulfate was calculated so that at least one molecule of $Na_2S_2O_3$ is present per N atom of the ligand yielding the ratio of $Na_2S_2O_3$ to EDTA of 2.5 (The EDTA features two N atoms see **Table 3-5**).

Study-2: As it was shown in **Figure 4-12**, the stable performance parameters for continuous experiments in the lab plant were found to be f_{sol}=10.81 (solution circulation ratio) and f_{air}=15 (air demand per dosed H_2S) for Case2 (shown in **Table 4-11**: sour gas feed= 1 l/min; c[H_2S]= 10 vol% and c[CO_2]= 0 vol%). Under these conditions practically no ligand degradation in Sol.2 was detected in continuous lab plant operation over a period of 160 h. Therefore, the operation conditions for the degradation studies on the radical induced oxidation mechanism in continuous operation were set to values which were more severe than those labelled as stable in the benchmarking experiments. This means, the respective solutions were sparged with an amount of excess air 1.5 fold compared to that required for a stable operation, yielding a f_{air} of 22.5 during 70 hours (the f_{sol} was kept constant at the value of 10.81 as given in **Table 5-2**).

- Two tests were performed with fresh solutions of Sol.2 with and without $Na_2S_2O_3$ addition to it (**Test-1 and Test-2,** respectively). Comparing the results of Test-1 with Test-2 will reveal the impacts and/or effectiveness of $Na_2S_2O_3$ on a possible degradation in continuous operation. The results of Study-2 enable a fair comparison with Study-1, which would provide the information whether the degradation behavior and possible degradation products of Sol.2 differ in continuous operation from batch experiments.

Study-3: As it was mentioned, there are no investigations on the autocatalytic oxidation behavior of the AAS containing chelated metal when applied in liquid redox technique. To this end, two solvent systems, the Sol.12 and Sol.13 (the Siemens Solvent-2 (secondary AAS) with the same AAS concentration but with low and high catalyst concentrations, resp.) were selected because they showed superior performance during the benchmarking experiments (refer to section 4.2.5). They were investigated in an experimental setup that was uncoupled from redox cycles:

- In order to rule out the formation of radicals and investigate the influences of the operation temperature on autocatalytic oxidation behavior, the samples were not sparged with H_2S, but with 1l/min air stream at two different temperatures, 30 or 60 °C (i.e. **Test-1 and Test-2**, respectively) over a longer period of time (i.e. 700 hours) and under the additional conditions given in **Table 5-2**.
- In order to examine the occurrence of autocatalytic oxidation also in the absence of air, the solutions were sparged with an equal amount of the other process gas, i.e. the CO_2 (1 l/min), the presence of which does not promote the occurrence of Fenton type mechanism during catalyst regeneration – contrary to H_2S. Investigating the Sol.12 (low-cat with Siemens-Solvent-2 as AAS) and the Sol.13 (high-cat with Siemens-Solvent-2 as AAS) would provide the information whether higher catalyst concentrations promote the occurrence of reaction Eq.5-9, thus the autocatalytic oxidation, or not.

After discussing the background of the degradation studies conducted in the scope of this chapter, the preparation of the investigated solvent systems, experimental set up and procedure of all performed tests are presented in the following sections.

5.3.2 Preparation of feed substances

Solvent systems without AAS (i.e. the Sol.1 and Sol.2) and with AAS (i.e. the Sol.12 and Sol.13) were prepared in the same way as it was explained in section 3.5.2.2. In Test-2 of Study-1 and Test-2 of Study-2, the pre-determined amount of sodium thiosulfate ($Na_2S_2O_3$) (anhydrous, purity>99%, Carl Roth; solubility 701 g/L in water at 20 °C) was dissolved in the respective fresh solvent systems without further purification.

The gaseous substances were used to compose gas feeds of desired composition: H_2S (purity>99.5% and specification of COS<3 ppmv; CH_4<500 ppmv) and CO_2 (purity>99.7% and specification of H_2O<200 ppmv were purchased from Air Liquide. The N_2 (purity>99.99%) and the regeneration air (purity>99.5% and specification of 20.9% O_2 and N_2>79%) were supplied by Infraserv GmbH. Where applicable, mixing of gaseous components occurred according to the approach described in section 4.2.2.

5.3.3 Experimental set up, procedure and analytical method

This section gives an overview on the applied analytical methods, experimental set up and the procedure for each test of the three degradation studies stated in **Table 5-2**, respectively.

Analytical methods:

In all degradation studies presented in the scope of this chapter, the following analytical methods were used:

- The concentration of the Fe•EDTA in liquid samples was measured via UV-Vis method as explained in section 3.5.1.3 (internal method, accuracy ±5%)
- The concentration of the AAS in liquid samples was determined either by the means of an internal titration method as given in (Fischer, 2013) (±5%) or by LC-MS at an external service provider (±10%).
- Ion chromatography with mass spectrometer (IC-MS) (accuracy of 10%) was applied for the identification of the main degradation products such as organic compounds by the external analytic service provider company (Siemens AG, 2016).

5.3.3.1 Cyclic radical induced degradation tests in a stirred cell reactor system (Study-1)

The sequential redox cycles were performed in the stirred cell reactor system shown in **Figure 4-3**. This set-up was already used for kinetic experiments (for the dimensions of the reactor and the characteristics of the experimental set up see **Table 4-2** and section 4.1.3, respectively). The related process parameters that were held constant and varied are summarized in **Table 5-2**. The implementation of the cyclic radical induced degradation tests was principally identical with the procedure of the "decreasing pressure experiments" described in section 4.1.3.2 -except for an additional step of sparging H_2S into the respective solvent system. The major difference to the kinetic experiments was that the fresh solution now did not contain Fe(II)•EDTA, but Fe(III)•EDTA. This was converted to Fe(II)•EDTA by H_2S sparging. One modification to the set- up was an additional three-way valve upstream of the gas reservoir which was connected to the outlet of H_2S-gas cylinder (not shown in **Figure 4-3**) and enabled to fill the gas reservoir with the respective gas, e.g. H_2S or air.

The bulk of the respective fresh solvent system was fed from the solvent reservoir to the reactor and the temperature was kept constant at 30°C by means of the thermostat. Subsequently, a sample of liquid was taken to analyze the initial amount of the Fe(III)•EDTA in the reactor by UV-Vis. Before starting an experiment, the headspace of the reactor was evacuated to remove the air, until the vapor pressure of water at 30°C was established. The amount of H_2S was calculated to be stoichiometric to the amount of Fe(III) in the tested solution (Fe(III):H_2S = 2:1, see Eq.2-5). This presumably resulted in complete conversion of Fe(III)•EDTA to Fe(II)•EDTA. Thus, it was assumed that from the complete absorption of one mole of dosed H_2S, two moles of Fe(II) were generated. The pre-determined amount of H_2S was supplied to the reactor gas phase until the pressure reached the desired value. At this point, the inlet valve was closed, the stirrer was activated, and the absorption was started. The absorption of the H_2S into the solution and the reaction of it with Fe(III)•EDTA were observed to be instantaneous at the given pH. Hence, the pressure in the reactor did not decrease during this process step. Once it was ensured that all of the provided H_2S was absorbed, the stirrer was stopped and the required amount of air (i.e f_{O2}=1.5 see **Table 5-2**) was inserted into the gas phase of the reactor. The ratio of air to regenerate the produced Fe(II)•EDTA, and thus, the necessary pressure were determined according to the procedure given in section 4.1.1.1.2.1 applying equations Eq.4-6 to Eq.4-11. An example of the calculation and the results are available in **Table A- 7** in Appendix A-3.1. Subsequently, the stirrer was activated. The pressure decrease was measured until it reached a minimum and remained constant, which indicated that the reaction between the interactive species and the O_2 was ended. This was repeated 20 times yielding 20 redox cycles and totally round about 70 h of operation for each tested solution. An exemplification of pressure drop curves of air during the first two redox cycles in Test-1 is given in **Figure A- 9** in Appendix A-3.1. From this, the physically absorbed amounts of N_2 and the chemically consumed amount of O_2 were calculated. The results are shown also in **Table A- 7** and **Table A- 8** in Appendix A-3.1. Liquid samples of 5 mL were taken every two cycles after the regeneration step to analyze the actual amount of the Fe(III)•EDTA in the respective solvent system in the reactor by UV-Vis. After one test run (20 redox cycles) was finished, the solution was drained by opening the respective valve under N_2 atmosphere. All of the three test runs (i.e. Test-1 to Test-3) were implemented in the same way - they differ solely in the solvent composition applied (see **Table 5-2** e.g. at the beginning of the Test-3 the pre-determined amount of $Na_2S_2O_3$ was added to the fresh solvent).

5.3.3.2 Continuous radical induced degradation tests in a lab plant (Study-2)

Both tests were conducted in the lab plant which is shown in **Figure 4-11** according to the procedure described in 4.2.3. Distinctly, during the degradation studies, the sour gas feed composition was not changed. At the beginning of each test, the bulk amount of fresh respective solution (i.e. 5.6 L given in **Table 4-10**) was fed into the plant. Subsequently, a sample of liquid was taken to analyze the initial amount of the Fe(III)•EDTA in the reactor by UV-Vis. The pump around ratio (f_{sol}) and regeneration air demand (f_{air}) for the given sour gas composition (refer to **Table 5-2**) were set to 10.81 and 22.5, respectively. Each test (Test-1=Sol.2 without $Na_2S_2O_3$; Test-2=Sol.2 with $Na_2S_2O_3$) was run for 70 hours. To compare the results of Study-2 with those

obtained from the batch experiments (Study-1), one redox cycle is equalized to the time during which the entire amount of metal catalyst is reduced and reoxidized in the continuous tests using Eq.5-10.

$$t_{redox-cycle} = \frac{(V_{sol} * c_{Fe(III)})}{2 * \left(\dot{V}_{H_2S} / V_{M,air}\right)} \qquad \text{(Eq.5-10)}$$

Applying the Eq.5-10, one redox cycle took approximately 1 hour, in the case of a H_2S-feed of 0.1 l/min and 5.6 liters of solvent inventory (V_{sol}) in the plant with a Fe(III) concentration of 0.1 mole per liter as well as the molar volume of air at respective temperature (e.g. $V_{M,air}$ = 25.04 l/mol at 22°C). Liquid samples of 5 mL were taken every two cycles after the regeneration (i.e. every 2 hours) to analyze the end amount of the Fe(III)•EDTA in the reactor by UV-Vis.

5.3.3.3 Autocatalytic oxidation tests in a stress test apparatus (Study-3)

During Test-1 to Test-3 of Study-3, a defined air or CO_2 stream (i.e. 1 l/min) was bubbled through the thermostated solutions Sol.12 and Sol.13. This was performed in the experimental set-up shown in **Figure 3-7**. The tests were conducted as described in the section 3.5.1.3. Standard conditions of experiments and the varied parameters per each test are presented in **Table 5-2**. For the evaluation of ligand and AAS degradation, three liquid samples of 5 mL of each solvent system were taken from the respective solution: at the beginning of the tests, after 350 hours of operation and at the end of the test (t= 700 h), they were analyzed as explained in section 5.3.3.

5.3.4 Results and discussion

5.3.4.1 Results of Study-1

Figure 5-4 compares the results of Test-1, Test-2 and Test-3 regarding the relative concentrations of the Fe(III)•EDTA complexes[25] during the 20 redox cycles of the respective solution system.

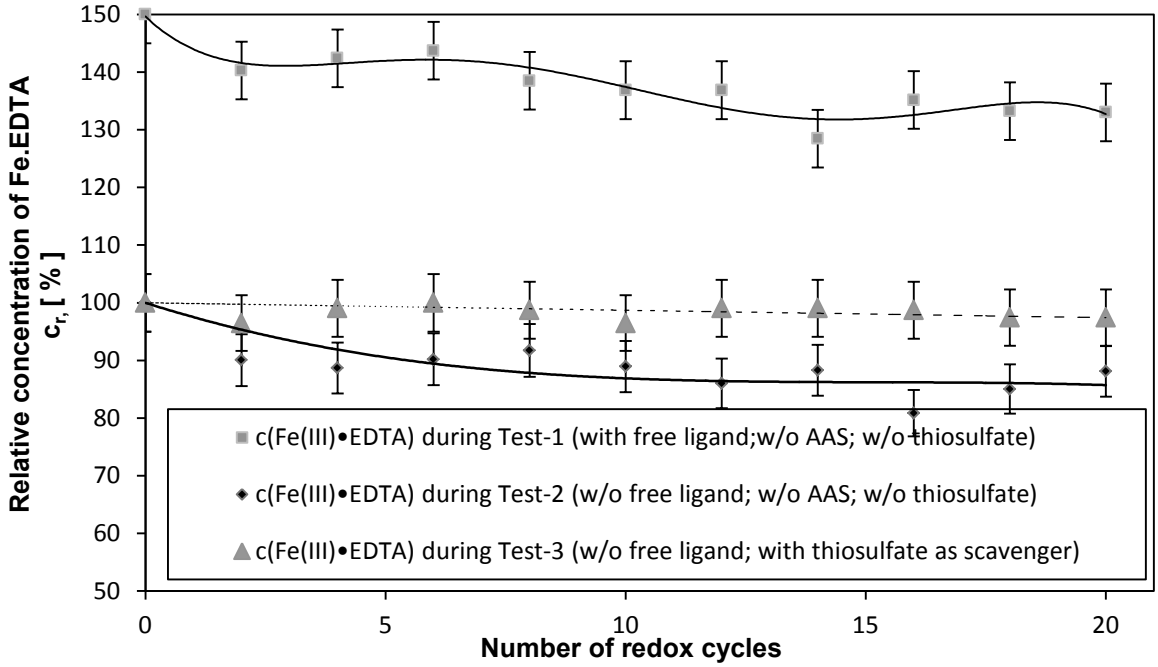

Figure 5-4 Results of Study-1(stirred cell reactor): Relative concentrations of Fe•EDTA complexes in tested solutions without AAS at T = 30°C and f_{O2}=1.5 – for additional experimental parameters see Table 5-2 (analytic accuracy ± 5%)

[25] For the relative concentrations of the chelated iron c_r= $c(Fe(III)•EDTA)_{t=t}$ /$c(Fe(III)•EDTA)_{t=0}$ (in %) refer to Eq.3-8.

Figure 5-4 reveals:

- **ligand degradation occurs not on the uncoordinated, free EDTA but on the EDTA which is directly coordinated to Fe in the complex (Fe•EDTA)**: From **Figure 5-4**, it was deducted that the Sol.1 with an excess of the ligand (i.e. EDTA to Fe = 1.5 mol/mol→Test-1) degraded at the same rate as the Sol.2 which contains equimolar chelated-metal (i.e. EDTA to Fe = 1.0 mol/mol→Test-2). Both tests were run with excess stoichiometrical air sparging (f_{O2}=1.5). As deducted from section 3.5.1.3 the free, excess chelating agent (i.e. the EDTA) in the Sol.1 in Test-1 did not take part in the complexation and thus could not be detected by the UV-Vis method. Therefore, the concentration of the uncoordinated amount of EDTA was determined by addition of an excessive amount of Fe(III) to the sample in order to produce metal complex of it (i.e. Fe(III)•EDTA), thus to make it also visible in UV. By doing so, it was observed that the concentration of the already complexed Fe(III)•EDTA remained constant during Test-1 (not shown in **Figure 5-4**).
  - Hence, it can be concluded that the degraded chelate in the complex was readily replaced with free, uncomplexed ligand molecules. This is a possible indication for the fact that the degradation is initiated on the complex itself and not on the uncomplexed, excess chelator, as the free ligand is not preferably degraded.
- **involvement of radical induced oxidation by Fenton type mechanism:** As shown in **Figure 5-4**, the relative decrease in the initial Fe(III)•EDTA content of the Sol.2 reduced to 2.5% with the addition of thiosulfate (Test-3) compared to the approx. 10% decrease in the Test-1 and Test-2 after 20 redox cycles. This shows the effectiveness of thiosulfate as inhibitor which in turn implicates that radicals and/or H_2O_2 are responsible intermediates for the oxidative attack on the EDTA. These findings are consistent with the proposal of (Chen, D. et al., 1995) discussed in section 5.2.2.1.
  - This result, however, was not demonstrating the type and source of the radical interacting - meaning whether the hydroxyl radical, $HO^{\bullet}$ or the superoxide radical, $O_2^{\bullet-}$ or a combination was responsible for the degradation. In earlier studies (e.g. (Schifano, 2004)), the spin trap method and ESR measurements have been used to determine the type of the interacting radical. Alternative to a proof of the existence of these radicals, the formation of H_2O_2, which is statedly the source of such radicals, can be checked. In order to confirm the formation of the H_2O_2 as a product of the regeneration reaction of the metal catalyst by air, the catalase enzyme (≥11 700 U/mg, Carl Roth) was used in this study. Catalase was chosen because it reportedly destroys H_2O_2 by disproportion of it to ½ O_2 and H_2O. By doing this, it was deducted that addition of catalase slowed down the degradation by presumably preventing the formation of radicals. So that, it was verified that the H_2O_2 was the responsible intermediate for the radical induced ligand degradation. Thus, the proposal done is in a good agreement with the earlier studies given in **Table 5-1** in all of which the occurrence of Fenton type mechanism reactions was proven.
- **EDTA degradation in the solutions without AAS is comparable to that in solutions with AAS:** According to Eq.4-1, the theoretical stoichiometric coefficient of iron is four in the regeneration reaction. However, as it was mentioned in section 4.1.1.1.2.2, the real stoichiometric coefficient of iron (v_B) has to be determined experimentally by applying Eq.4-13 in order to determine the amount of excess O_2-consumption, which contributes to the degradation of the ligand. Taking the Fenton reaction Eq.5-2 into consideration, one mole of O_2 reacts with one mole of $HO^{\bullet}$ according to reaction Eq.5-3, which in turn initiates the degradation of one mole of ligand. The values of v_B for Test-1 and Test-2 calculated from the pressure drops ranged between 3.2 and 3.6 (e.g. for the v_B of Test-1 see **Table A- 7** in Appendix A-3.1), respectively (as an example of the the calculated values of O_2-consumption during Test-1 see **Table A- 8** in Appendix A-3.1). These findings are in a good agreement with the results of regeneration kinetic tests presented in section 4.1.4.2, where the values of v_B were in the range between 3 and 4 also for the AAS based solutions containing chelated EDTA (for v_B values see **Table 4-6** and **Table 4-8**). Thus, it can be concluded that the radical induced degradation behavior of the ligand is comparable with the solutions containing also AAS.

- The proposal that the ligand degradation is comparable in the solutions with and without AAS is important, since it reveals the fairness of the assumption done in 5.2.2.1 that radical induced oxidation of the organic constituents of the solvent system seems to be dominating for the ligand not for the AAS as long as the Fe is held in complex, and thus, it is not able to promote the oxidation of the AAS by dissolved O_2 in the liquid redox systems.

Furthermore, **the concentrations of the major ionic degradation products of EDTA** in the investigated solutions were measured at the end of Test-1, Test-2 and Test-3 by the IC-MS method. The detected amounts of the ionic DPs (i.e. oxalate, formate and acetate) are plotted in **Figure 5-5**.

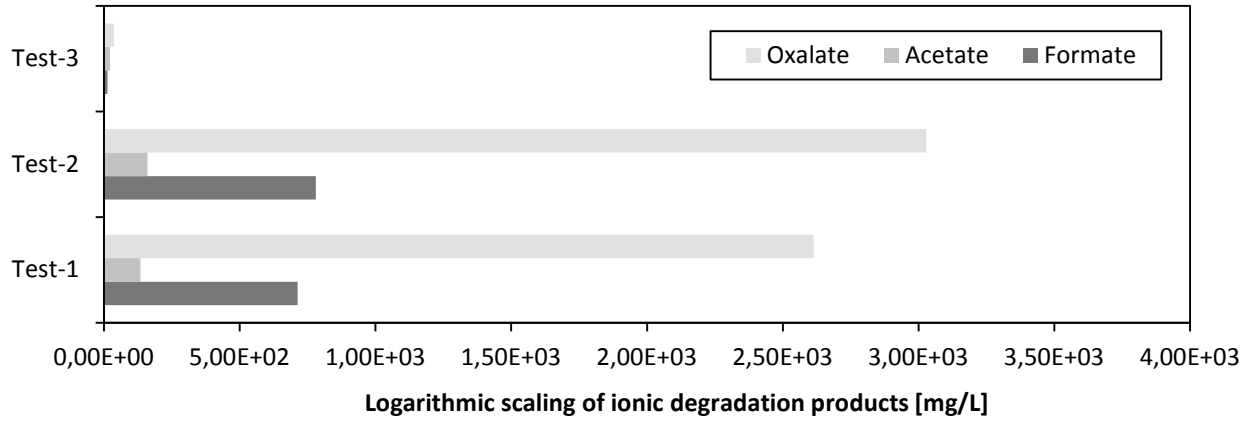

Figure 5-5 Identified major ionic degradation products of EDTA in the investigated solutions (analytic accuracy ± 10%)

Taking the molecular structures of formate, oxalate and acetate into account (Butler, J. et al., 1982), the involvement of radical induced mechanisms can be verified again by assuming peroxyl radical formation as the initial step due to the introduction of excess amount of O_2. Thereafter, the radical oxidation of the side chains of the ligands (as mentioned in section 5.2.2.1) leads to the formation of volatile organic compounds (e.g. acetaldehyde) as primary degradation products (DP). These products undergo oxidization reactions further (e.g. acetaldehyde is oxidized to acetate). This is in good agreement with the reaction mechanism proposed by (Chen, D. et al., 1995). However, it seems that the ionic degradation products (e.g. acetate) do not participate in secondary reactions causing further degradation of the ligand. This would result in weakening of the bonds between them and the metal ions and hence in precipitation of metal oxides.

Keeping the indications of the Study-1 in mind, the following section gives an overview on the results of the Study-2, and then both studies are compared.

5.3.4.2 Results of Study-2

Within the Study-2 (see **Table 5-2**), two series of tests were performed in the continuous lab plant without and with the addition of thiosulfate to the solutions, Test-1 and Test-2, respectively. As it was mentioned above, applying the Eq.5-10, one redox cycle in the continuous lab plant took one hour under the given experimental conditions. In order to enable a fair comparison of the decrease in the relative ligand concentrations in the solutions tested in batch and continuous operation, also during the Study-2 the samples were taken every two hours (equivalent to 2 redox cycles) and analyzed. The results of the relative EDTA-concentrations are displayed in **Figure 5-6**.

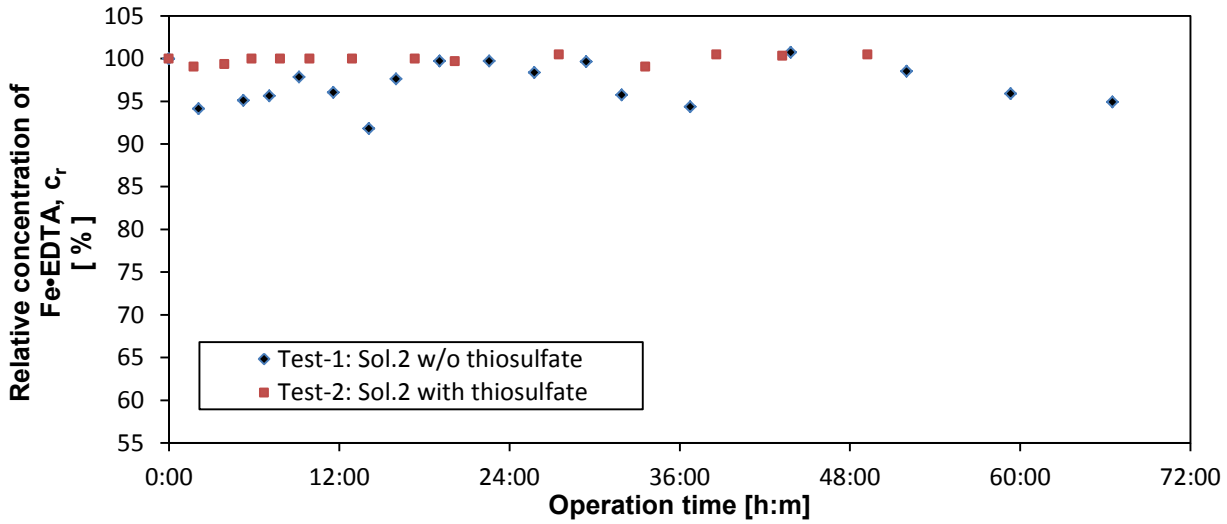

Figure 5-6 Results of Study-2 (continuous lab plant): Relative concentrations of Fe•EDTA complexes in tested solutions w/o AAS; with and without thiosulfate at atmospheric conditions -for additional experimental parameters see Table 5-2 (analytic accuracy ± 5%)

Figure 5-6 reveals:

➢ **the effectiveness of thiosulfate as chelate stabilizer:** in the case of no added thiosulfate (i.e. Test-1), the relative concentration of the Fe•EDTA showed a slight decrease (0-10%) in general. However, a significant fluctuation of the measured data was observed. Furthermore, the ligand seemed to be recovered again after an initial decrease. Contrary to this, with the addition of thiosulfate (i.e. Test-2), almost no fluctuation in the measured concentrations of the chelated-metal catalyst was detected. This means, thiosulfate serves not only as inhibitor but also as so-called chelate-stabilizer by enhancing its thermodynamic stability (refer to section 3.4.2.1).

Comparison of results from Study-2 (continuous lab plant) with Study-1 (batch stirred cell reactor):

➢ During the cyclic tests with the Sol.2 w/o thiosulfate in the stirred cell reactor (i.e. the Test-2 in Study-1), the decrease in the Fe•EDTA concentration came to the amount of approx. 0.94 mol% per redox cycle (refer to section 5.3.3.1). However, during the 70 hours of the continuous experiment, respectively 35 redox cycles, no permanent chelate degradation in the Sol.2 without thiosulfate could be detected, only temporary decrease occured - despite fluctuations in the measured data within the specified accuracy range (i.e. ±5%). For the Test-2 with thiosulfate, the degradation was negligible for all samples. Since all other experimental parameters (i.e. the solution composition as well as concentration, the H_2S flow, and the ratios Fe(II)/Fe(II) and f_{O_2}) were kept comparable, and only the operation mode and the design of the reactor systems were different, the conclusion can be drawn with caution that the mass transfer process of the O_2 influences the effectiveness of air-liquid contact significantly. Hence, it promotes the oxidative degradation of the liquid system. Analyzing the differences in the mass transfer properties of these two systems (i.e. a bubble column - **Figure 4-11** and a stirred cell reactor - **Figure 4-3**), it can be concluded that the presence of the stirrer in the batch system significantly minimized the mass transfer resistance on the liquid side, thus increasing the liquid side mass transfer coefficient (i.e. the $k_{l,O2}$ referring the Eq.4-4) by accelerated the mixing, which results in the promotion of the secondary reactions between the excess O_2 and the ligand. These findings are also in good aggrement with the degradation study given in (Hessler, 2015).

5.3.4.3 Results of Study-3

The results of the autocatalytic oxidation tests performed under air sparging at 30 °C as well as 60 °C (i.e. Test-1 and Test-2) are visualized in **Figure 5-7** and **Figure 5-8** regarding the relative concentrations of:
-the applied AAS (c_r=c(AAS)$_{t=t}$/c(AAS)$_{t=0}$, in % see Eq.3-8)
-the Fe•EDTA in Sol.12 and Sol.13 (c_r=c(Fe(III)•EDTA)$_{t=t}$/c(Fe(III)•EDTA)$_{t=0}$, in % see Eq.3-8).

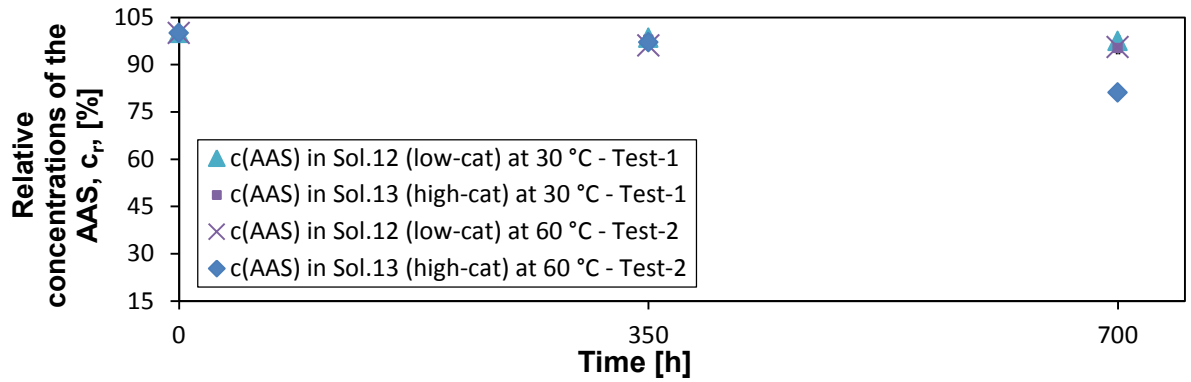

Figure 5-7 Results of Study-3 (sparged reactors): Relative concentrations of the AAS of Sol.12 and Sol.13 during Test-1 and Test-2 of Study-3 (at 30 °C and 60°C under air sparging) - for additional experimental parameters see Table 5-2 (analytic accuracy ± 5%)

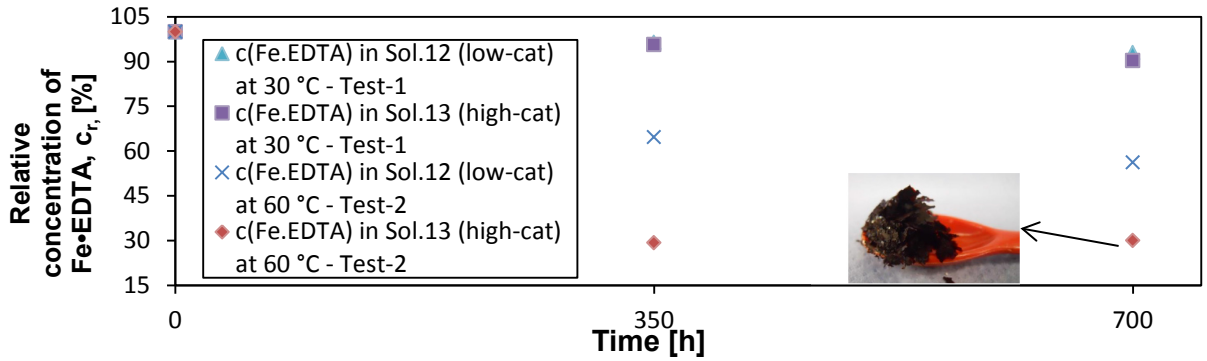

Figure 5-8 Results of Study-3 (sparged reactors): Relative concentrations of the Fe•EDTA of Sol.12 and Sol.13 during Test-1 and Test-2 of Study-3 (at 30 °C and 60°C under air sparging) -for additional experimental parameters see Table 5-2 (analytic accuracy ± 5%)

Figure 5-7 shows that:

- **the relative AAS concentration decreases at 60 °C in high-cat solution:** From **Figure 5-7**, it was deducted that the oxidation of the applied AAS in both solutions at 30 °C was insignificant and not dramatically influenced by the increased metal concentration ($c_{r,AAS}$ in Sol.12 = 96% and $c_{r,AAS}$ in Sol.13= 95%, accuracy ± 5%). However, the $c_{r,AAS}$ in Sol.13 at 60 °C was detected to be 81% whereas the concentration of the AAS in Sol.12 at 60 °C remained in the range of 96% (accuracy ± 5%) at the end of the test (after 700 h).

Figure 5-8 reveals the:

- **significant influences of temperature on autocatalytical degradation of EDTA:** As it can be seen from **Figure 5-8**, the higher metal concentration and temperature (i.e. the Sol.13 in Test-2; c[Fe]=0.5 M and 60 °C) led to a decrease of 70 % in the relative EDTA concentration (already observed after 350 h). This 70% decrease in $c_{r,Fe•EDTA}$ resulted in a EDTA-to-Fe-ratio of 0.08 M whereas the minimal required EDTA:Fe ratio for the chelation is 1 M (see Footnote 12 in section 3.5.1.3). This caused precipitation of iron from the complex at t=700 h (displayed also in **Figure 5-8**). The free, non-complexed iron seems to oxidize the AAS (metal catalyzed

oxidation of the ASS). The precipitation did not occur in Sol.12 at 60°C. At the end of the 700 hours of operation, 56% of the initial EDTA concentration remained in the Sol.12 which comes to an EDTA-to-Fe-ratio of 1.06 M, meaning there was still excess amount of some ligand. This indicates, that the degradation products of the EDTA can also keep iron sequestered in the complex, and hence avoid the precipitation of it; thus preventing it to catalyze the oxidation of the AAS.

Since the autocatalytic oxidation of the applied organic compounds were found to be insignificant at 30°C, the occurrence of the electron transfer mechanism in the absence of air but in the presence of only CO_2 were investigated in both solutions (Sol.12 and Sol.13) at 60 °C. The results of the **Test-3 in Study-3** are given in **Figure 5-9**.

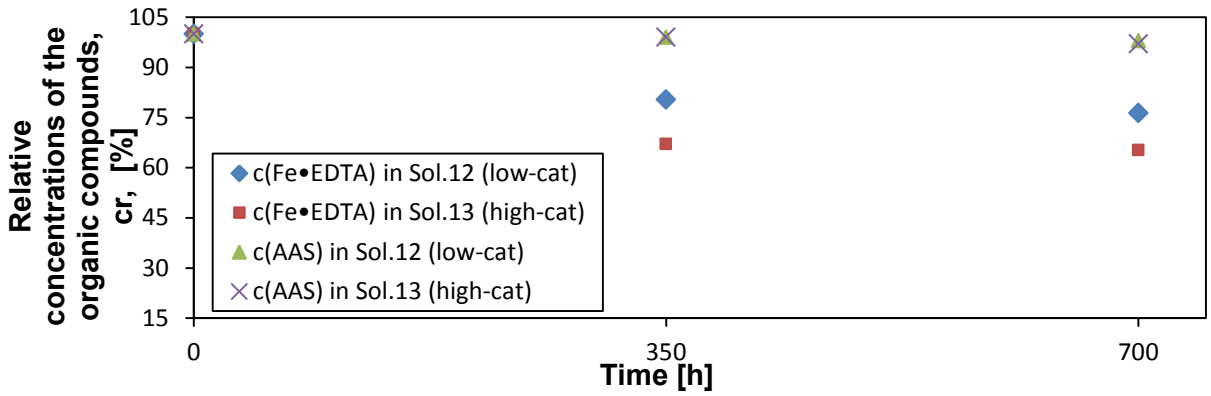

Figure 5-9 Results of Study-3 (sparged reactors): Relative concentrations of the AAS and Fe•EDTA in Sol.12 and Sol.13 during Test-3 of Study-3 (60°C, exclusion of O_2, but CO_2 sparging) - see Table 5-2 (analytic accuracy ± 5%)

According to **Figure 5-9**:

- The decrease in the relative EDTA concentration in the tested solutions shown in **Figure 5-9** verifies the occurrence of the metal catalyzed oxidation of the EDTA by Fe(III) even in the absence of O_2. Comparing the decreases in the EDTA-concentrations of the solutions in the low-cat and the high-cat solution (i.e. $c_{r,Fe•EDTA}$ in Sol.12 = 76.33% and $c_{r,Fe•EDTA}$ in Sol.13= 65.22%, respectively) reveals that autocatalytic oxidation of the EDTA under CO_2 sparging is influenced by the metal concentration –but much lesser than in the presence of air (see **Figure 5-8**). As it can be seen from **Figure 5-9**, the decrease in the $c_{r,Fe•EDTA}$ of both solutions remained stable from the half-time of the tests till the end of operation, even with continued CO_2 loading (i.e. from 350 hours till 700 hours). This implies strongly that there is a pH effect and not a CO_2 specific reaction.

- The proposal by (Motekaitis, R. J. et al., 1980), that the autocatalytical oxidation of the EDTA continues until the ligand becomes exhausted, could not be observed under given experimental conditions for the Test-3 of the Study-3 (see **Table 5-2**). It seems as if reaction Eq.5-8 proceeded twice. This can be explained by the hydrolyzation of the complex during the oxidation of the EDTA which in turn results in an increase in pH and therefore renders it inert to further autocatalytic oxidation (Martell, 2009).

- No significant decrease of the AAS was observed in both solutions. This is consistent with the theory that as long as the iron is kept complexed by EDTA, the proposed electron transfer process would take preferably place from the EDTA to the Fe(III), not between the AAS and the Fe(III).

Taking the gained understanding on the degradation behavior of the formulated systems into account, conclusions yielding proposals to inhibit/slow down the possible degradation of the solvent system are presented in the following section.

5.3.5 Conclusions and proposals to minimize degradation

Table 5-3 summarizes the outcomes of the performed degradation studies in this work with the proposals to minimize the occurrence of the respective degradation pathway. The varied parameters of every experiment are shown in bold letters and the influence of the change on the ligand degradation rate is indicated by the direction of the arrows. An upwards pointing arrow stands for a rising degradation rate and vice versa.

Table 5-3 An overview on the degradation behavior of tested solutions and proposals to minimize degradation

Parameter	Radical induced degradation of the EDTA in solvent systems without AAS		Autocatalytic degradation of EDTA and AAS in solvent systems with AAS
	Study-1	Study-2	Study-3
EDTA:Fe,(M:M)	**1:1** ; **1.5:1**→	1:1	**1.5:1**→
c(Fe(III)), (mol/L)	0.1	0.1	**0.1** ↓**; 0.5** ↑
Temperature, (°C)	30	30	**30** ↓**; 60** ↑
Process gases present	H_2S and air	H_2S and air	**Air** ↑; **CO_2** ↓
$Na_2S_2O_3$:EDTA (mol/mol)	**0; 2.5** ↓	**0** ; **2.5** ↓	0
Outcomes	The fact that thiosulfate greatly decreased the degradation rate led to the interpretation that the free radical ions are the responsible species that attack the EDTA. The Fe(II,III)•EDTA system was found to degrade through the formation of weaker chelating agents whereas the ionic degradation products identified were mainly formate and oxalate. The formation of H_2O_2 was proven as one of the reaction intermediates, since the catalase enzyme (which decomposes the H_2O_2) reduced the EDTA-degradation. The excess, uncomplexed ligand was found to be inert to the radical induced degradation. Hence, the selective and consecutive oxygenation of hydrocarbon substrates during the regeneration of the metal catalyst seemed to occur via the Fenton pathway. This is consistent with the reaction scheme proposed by (Chen, D. et al., 1995) and shown in **Figure 5-2**.		Autocatalytic oxidation of the ligand was promoted by elevated temperatures, metal concentrations and presence of dissolved O_2. The autocatalytically oxidation of EDTA, even under exclusion of O_2 but CO_2-sparging, seems to be inevitable: since it was seen that lowered pHs promote the autocatalytic degradation. The precipitated solid was analysed and found to be Fe_2O_3. This is in agreement with the reaction scheme proposed by (Martell, 2009) indicating the autocatalytic oxidation of EDTA is catalyzed by Fe(III) involving an electron transfer mechanism. The AAS was found not to be autocatalytically oxidized by the Fe(III) - as long as the iron is kept complexed by EDTA. Thus, it can be concluded that the proposed electron transfer process took place preferably between Fe(III) and the EDTA.
Proposals to control the decomposition	**By controlled regeneration:** Combining the control of redox potential and dissolved O_2 concentration by online sensors enables a minimum O_2 supply and thus would reduce degradation. **By inhibitor addition:** Inhibitor addition to the solvent system shall be done previous to commissioning of the plant. The suggested inhibitor (e.g. thiosulfate) amount per N atom of the ligand is two. For alternative inhibitors and inhibitor to Fe ratios refer to **Table A- 9** in Appendix A-3.2.		**By optimization in solvent formulations:** • If the ligand to be applied is EDTA, the suggested solution pH is 9.0<pH<9.5 • Trade-off analysis in c(Fe(III)) required; suggested concentration: 0.1 M<c(Fe(III)<0.3 M **By optimization in process conditions:** Operating the system at 30°C<T_{op}<60°C can minimize the overall degradation of the ligand and the AAS -if the process is run at atmospheric pressure.

Since it was seen that the experimental set up and the operation mode, and thus, the air-liquid-contact efficiency significantly influenced the degradation behavior of the tested solvent systems under given conditions, investigations on long time stabilities of the solution in a pilot plant under industrial process operation conditions (i.e. at T_{op}≈ 35 °C and under high pressure; P_{abs}= 20 to 40 bara; P_{reg} ≈ atm. to 10 bara) are recommended as next steps. This will enable to determine the absolute amounts of the ligand and AAS degraded per amount of sulfur produced and in turn the rate of reasonable inhibitor addition based on the Fe-content in the complex.

After screening and selecting the constituents of the appropriate liquid redox solvent systems (chapter 3), conducting technical evaluations of the formulated solutions (chapter 4) and investigating the degradation behavior of the selected solvent systems (chapter 5), the technical evaluation of the Siemens liquid redox process is completed. Thus now, the economic analysis of the process based on experimental findings is presented in the chapter 6.

6 ECONOMIC ANALYSIS OF THE EVALUATED SOUR GAS TREATMENT PROCESS

6.1 Background

As mentioned in section 3.2, the evaluated technology developed by Siemens AG is intended to be integrated as a sour gas treatment unit (see **Figure 3-1**) into gas-fired power plants, which enables the in-situ separation of the acidic content of the sour gases and the direct conversion of both the sulfuric components into elemental sulfur and the treated gas into electricity. The major constraints for the viability of the utilization of the abundant sour natural gas reserves for direct electricity production are the economics and the footprint of the technology. Mainly the following factors, which are significantly influenced by the composition of the solvent system, are to be considered to sustain cost-effectiveness:

- Low CAPEX (primarily dependent on complexity, size and material of the equipment)
- Low OPEX (mainly dependent on solvent system make-up requirement and power costs)

The individual items of CAPEX and OPEX were discussed in section 2.4. Most of these factors are functions of the techno-economic feasibility parameters - primarily the solution circulation ratio (f_{sol}) and the regeneration air supply (f_{air}) per H_2S content of the sour gas to be treated.
The last but very important measure that makes the intended technology practical for the direct power generation e.g. especially on an offshore drilling platform is:

- small footprint of the plant as a result of low solution circulation ratio and in turn small equipment.

To adress the issues mentioned above and to explore their improvement possibilities, the impacts of the composition of the applied solvent system on process performance and design were investigated by testing thirteen different formulations (section 4.2). The technical feasibility of all developed formulations was proven in continuous operation of the test rig (see **Figure 4-11**) in lab scale. The performance of these was indicated by the decisive cost driving factors i.e. minimum f_{sol} and f_{air} required for stable operation. Deducted potentials as well as limitations of all were reviewed in section 4.2.5. Based on these experimentally obtained data, the most promising solutions were identified (see section 4.2.5). Thus now, the next step is to consider the economics of the process in detail. The experimental investigations assessing the techno-economic feasibility showed that secondary AASs with high concentrations of the AAS and chelated iron enabled significant reductions in the pump around ratio (f_{sol}). Hence, the Sol.13 (refer to **Table 4-9**: Siemens Solvent-2; secondary AAS with high iron concentration) was chosen as key component for the economic analysis in order to obtain the economic figures of the technology. Since Siemens liquid redox is currently in the pre-industrial phase, an appropriate demo plant size (approx. 40 MW of power produced) was chosen for the investigation, which is also feasible for future commercial applications at small gas fields. The evaluation was based on the cost of the main product i.e. the electricity produced from the treated sour natural gas including both the sour gas treatment costs and the actual electricity generation costs. To this end, the total revenue requirement (TRR) method given in (Tsatsaronis, Bejan, & Moran, 1996) was used, out of different economic analysis methods discussed in the literature (Holland & Wilkinson, 1997), (Seider, Seader, & Lewin, 2010), (Woods, 1975), (Peters, Timmerhaus, & West, 2003) and (Smith R. , 2005). Evaluation of the economics of the technology was done by determining the levelized cost of electricity (LCoE, ct/kWh) resulted from the utilization of various alternative solvent systems. A further evaluation of the commercial aspects of utilization of treated sour natural gas in gas turbines was done by comparing with the LCoE obtained from the combustion of sweet natural gas. The results gathered from the economic analysis and evaluation studies will enable to:

- determine the anticipated LCoE resulting from the utilization of the selected solvent system (the Sol.13)
- assess the economic feasibility of the LCoE produced from treated sour gas compared to that generated from sweet gas
- identify the main cost drivers of the LCoE of the plant employing the Sol.13
- assess the economic performance of alternative solvent systems (different than Sol.13) and thus identify potential cost reduction measures

- provide basic input for the sensitivity analysis of the LCoE towards the determined cost drivers
- make proposals for the economic and technical optimization of the evaluated technology.

To this purpose, first, a short outline of the TRR method is presented. Thereafter, a brief review of design and cost estimate base with the financial assumptions is given. Subsequent to these, the approach to determine the LCoE is illustrated. Consequently, analysis and evaluation of the major cost drivers of the obtained LCoE will be presented.

6.2 Determination of the levelized cost of electricity (LCoE) by the total revenue requirement method

For an economic analysis of a process or a plant the battery limits have to be specified clearly at first. Then, the financial assumptions yielding the determination of the incurred costs have to be compiled.
To this end, the following tasks will be highlighted in the content of this section:

- overview on key terminology (written in bold)
- scope of the economic analysis
  - performance, design and cost estimation base
  - financial assumptions
- approach associated with the total revenue requirement (TRR) method to determine the levelized cost of electricity (LCoE)
  - estimation of capital and operational expenses (CAPEX and OPEX)
  - levelization of these
  - calculation of LCoE.

6.2.1 Terminology

The **total revenue** is the revenue required to recover all costs of a project owner to build and operate a plant (EPRI, 2011). These are categorized as the capital-related charges (carrying charges, CC), operational expenses (fixed expenses e.g. plant overhead, labor, fixed operation and maintenance costs (OMC), etc. as well as variable expenses e.g. fuel and chemical costs, FC and C_C). Thus, the **total revenue requirement (TRR) method** (Tsatsaronis, Bejan, & Moran, 1996) attempts to determine the necessary price of the main product of a plant with the purpose to study whether the plant is capable to compensate all outgoings of the operating company within a given period of time through the sale of the main product, which in this study, is the electrical energy. Hence, the **cost of electricity (CoE, ct/kWh[26])** produced from the gas-fired "integrated plant" (for description refer to section 6.2.2) represents the per-kWh costs of erecting and operating the plant over an assumed financial life time and duty cycle. The TRR, the cost components of which may vary significantly within the assumed economic life time of the plant, is the key input to calculate the CoE. In general, carrying charges decrease (if the depreciation is progressive) while fuel and maintenance costs increase with increasing years of operation. In addition, the cost components include non-uniform monetary values (i.e. the CC in $ are upfront costs whereas the OMC in $/a are periodic). Therefore, levelized annual values for all cost components shall be used in the evaluation to get an equivalent series of constant payments year-by-year (the so-called **annuities**) (Tsatsaronis, Bejan, & Moran, 1996). Hence, the **annual levelized total revenue requirement (TRR_L, $/a)** is defined as the sum of the **levelized carrying charges (CC_L, $/a)**, and the levelized expenses such as **levelized fuel costs (FC_L, $/a)** (including all other variable expenses) as well as **levelized operating and maintenance costs (OMC_L, $/a)** (including all other fixed expenses) (refer to Eq.6-32). Dividing the TRR_L with the annual net electricity production (ANEP, MWhe/a) of the plant yields the so-called **levelized cost of electricity (LCoE, ct/kWh)** (see Eq.6-35), which represents an annualized cost of generating electricity over the lifetime of the plant along with financing terms. The approach deducted from (Tsatsaronis, G., & Yang, Y., 2014) and (Tsatsaronis, G., & Morozyuk, T., 2013) was applied in this work to estimate the individual cost items of the TRR_L (i.e. CC_L, FC_L, OMC_L) to determine the

[26] All costs given in the context of this study are based on US dollars.

LCoE (see section 6.2.4). Before presenting the approach, the specific technological characteristics of the evaluated process and financial characteristics of the conducted economic analysis will be presented in the following subsections.

6.2.2 Technology specific data for the economic analysis of integrated plants

As it has been emphasized in the previous sections, the main purpose of the treatment process developed by Siemens AG is to remove the H_2S content of sour gases in order to enable the utilization of them in gas turbines to generate power. The operation procedure of the integrated plant was described in section 3.2. The schematic diagram of the integrated plant shown in **Figure 3-1** is included in **Table 6-1** for illustration. In the scope of this chapter, the term **integrated plant** is used for the combination of a **treatment block** (with three basic unit operations: absorption, regeneration and sulfur separation) with a **power generation block** (combustion unit with turbine and generator including all auxiliaries). Since the specific technological and regional characteristics of a project as well as the performance and cost estimate bases directly affect the CAPEX and OPEX, these are summarized in the **Table 6-1**. Before illustrating the technology specific data, it is important to note that the scenario established below does not reflect any actual investment decision of the developer company (i.e. Siemens AG), it will rather be used only for the purpose to conduct the economic analysis in the scope of this work. The estimate base case scenario yielding the technological data for the economic analysis includes the following steps:

I. As a starting point, the possible location of the integrated plant was determined:
   Middle East (as most of the proven sour gas reserves are located there (EIA, 2016a)).

II. Thereafter, the gas field where the sour gas is to be tapped from was selected:
   The Hail Gas Field in an offshore area west of Abu Dhabi (as the gas producers in the region have been reportedly looking for solutions to utilize the sour gas (Matsumoto, 2013)).

III. The capacity and composition of the sour natural gas of the Hail field was taken from (Matsumoto, 2013):
   Reportedly, approx. 535 MMSCFD sour gas (597,380 Nm^3/h) can be produced from the field which is estimated to contain 10 vol% H_2S and 10 vol% CO_2. Assuming that the gas is at H_2O saturation and does not embody other by-products (e.g. particulates, heavy metals) yielded a dry gas composition of 80 vol% CH_4, 10 vol% H_2S and 10 vol% CO_2.

IV. The cost analysis can be conducted for any desired dimensions of plants (Peters, Timmerhaus, & West, 2003): In this work, the analysis will arbitrarily be executed for a demo integrated plant in semi-industrial phase which would be high of interest and errected after a successful completion of the piloting (the technology is currently in pre-industrial phase).

V. The capacity of the treatment demo plant was adjusted to the capacity of the turbine which is employed in the power generation demo plant: In this context, one of the common industrial gas turbines of Siemens, the SGT-750, was chosen from the Siemens gas turbine portfolio available in open literature (Gas turbines catalogue, 2016), since it is reportedly an excellent choice of industrial gas turbine for power generation - especially for oil and gas industry.

After establishing the scenario, the equipment design and operating parameters of the power generation and treatment plants are to be determined individually, as presented in the following subsections.

6.2.2.1 Design base case for the power generation demo plant

The available fuel input to the turbine was assumed to be equivalent to the CH_4 content of the sour gas treated, since CO_2 is not combustible. It should be noted that the CO_2 in the treated gas stream does not disturb the operation of the Siemens gas turbine up to a concentration of 10 vol% (Siemens AG, 2016) but it lowers the heating value of the fuel (LHV_{fuel}). According to technical data sheet of SGT-750 published in (Gas turbines catalogue, 2016), the plant produces 38.1 MW

of electricity using a single natural-gas-fired SGT-750 industrial gas turbine with a gross efficieny (η) of 40.2 % and at a capacity factor (CF) of 1.00[27] (see **Table 6-1**). Thus, the required fuel input at turbine inlet to obtain 38.1 MW power output (PO, MW) was calculated to be approx. 94.77 MW by using Eq.6-1. Dividing it with the LHV_{fuel}, in this case with the LHV of pure CH_4 (LHV_{CH4}=50 MJ/kg (CER, 2008)), the mass flow rate of the fuel, pure CH_4 ($\dot{m}_{fuel}$) at turbine inlet was calculated to be 6824 kg/h by Eq.6-2. The volumetric flow rate of CH_4 at turbine inlet and normal conditions ($\dot{V}_{CH_4}$) was determined to be nearly 9557.7 Nm^3/h by Eq.6-3 considering the molecular weight of CH_4 ($M_{CH4=}$16 kg/kmol).

$$\eta\,(\%) = \text{Fuel input (MW)} \,/\, \text{Power output (MW)} \qquad \text{(Eq.6-1)}$$

$$\dot{m}_{fuel}(\text{kg/s}) = \text{Fuel input (MW)} \,/\, \text{LHV}_{fuel}\ (\text{MJ/kg}) * 3600\ (\text{s/h}) \qquad \text{(Eq.6-2)}$$

$$\dot{V}_{CH_4}(\text{Nm}^3/\text{h}) = \dot{m}_{CH_4}(\text{kg/h}) / \text{M}_{CH4}\,(\text{kg/mol}) * 22{,}4\,(\text{Nm}^3/\text{kmol}) \qquad \text{(Eq.6-3)}$$

The turbine was considered to be associated in simple-cycle mode to an AC electric generator with 60 Hz. The system was assumed to include a dry, low NOx combustion device capable of realizing <15 ppmvd at 15 vol% O_2 at full load (refer to technical data sheet in (Gas turbines catalogue, 2016)). The plant was regarded as being equipped with an inlet cooler to reduce the temperature of the turbine inlet air. The pressure ratio of it is 23.8, while the exhaust temperature is 458 °C. It must be noted that the cost estimate did not include the cost of selective catalytic reduction (SCR) and carbon monoxide (CO) reactor for NO_x and CO reduction (for the descriptions refer to section 1.3) or any treatment costs for potential gas emissions (e.g. CO_2), waste water or solid waste. The equipment of the treatment demo plant was designed by customizing it to the capacity of the demo power plant as presented in the following section.

6.2.2.2 Design base case for the gas treatment demo plant

The required fuel input at turbine inlet corresponds to the CH_4 content of the sour gas to be treated which comprises of 80 vol% CH_4, 10 vol% H_2S and 10 vol% CO_2. Thus, firstly, the volumetric flow rate of the sour feed gas to be treated at normal conditions ($\dot{V}_{sour}$, Nm^3/h) was calculated using the Eq.6-4. Accordingly, the treatment plant will process a sour gas capacity of 11,947 Nm^3/h. Thus, the amount of sour gas to be treated corresponds to nearly 2% of the capacity of the Hail gas field (refer to **Table 6-1**).

$$\dot{V}_{sour},(\text{Nm}^3/\text{h}) = \dot{V}_{CH_4}(\text{Nm}^3/\text{h}) / 0.80 \qquad \text{(Eq.6-4)}$$

Taking the 10 vol% H_2S content into account, the sour gas fed to the treatment plant contains nominally 41.4 LTPD of sulfur.

[27] Hypothetically, the turbine could operate at full capacity for every hour of the year without interruption. However, no generating unit can run all of the time; thus, the CF of the unit is always less than 1.00. The difference between actual and theoretical maximum output is caused by planned maintenance, mechanical breakdowns (forced outages), and any instances in which the plant is backed-down from maximum output due to lack of load (Boyce, 2012).

Table 6-1 Performance and design base case of the integrated plant for the economic analysis

Integrated plant (Treatment plant + Power generation plant)					
Cycle type			Simple (open) cycle		
Location			Hail gas field, Middle East		
Capacity of the gas field, Nm^3/h			597,380		
Typical sour gas (fuel) composition in the field[a], (dry) vol%			$c(CH_4)$= 80, $c(H_2S)$= 10, $c(CO_2)$= 10		
Economic life of demo plant			10 years with 7000 h/a at full load		
Treatment plant (absorption unit + regeneration unit + sulfur separation unit)			**Power plant (combustion unit+generator+aux.)**		
Sour gas capacity of the pilot treatment plant [b]	**11,947 Nm^3/h**	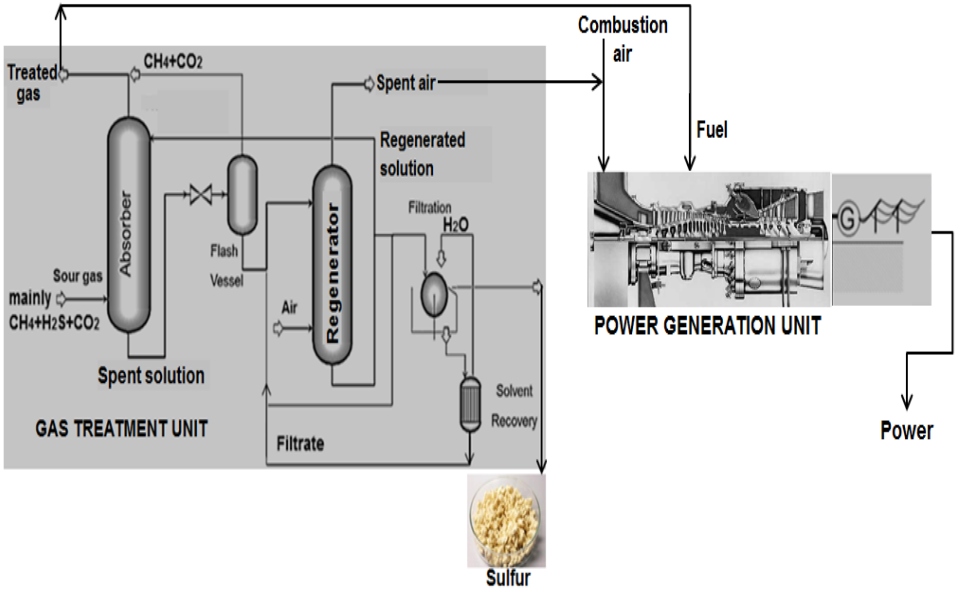	Type of the Siemens turbine/ Model no[f].	**Industrial gas turbine/ SGT-750**	
H_2S content (nominal sulfur)	**41.4 LTPD**		Fuel composition[e] (treated natural gas)	**94.12 vol% CH_4 and 5.88 vol% CO_2**	
Operation temperature (T_{abs} and T_{reg})	**35 °C**		Mass flow rate of CH_4 at turbine inlet [e]	**6824 kg/h**	
Absorption pressure Flashing pressure Regeneration pressure	**25bara** **2 bara** **1.013 bara**		LHV of CH_4[e]	**50 MJ/kg**	
Volumetric flow rate of the sour gas at operation conditions, $\dot{V}_{sour}$	**546.28 m^3/h**		Power input[e]	**94.77 MW**	
Applied solution (see **Table 4-9**)	**Sol.13**		Gross efficiency[f], η	**40.2 %**	
H_2S separation rate	**99.99 vol%**		Pressure ratio[f]	**23.8 : 1**	
CO_2 desorption rate	**50 vol%**		ISO power output, PO[c,f]	**38.1 MW**	
CH_4-slip rate	**<0.1 vol%**		Frequency[f]	**60 Hz**	
			Exhaust temperature[f]	**458 °C**	

a) Sour feed gas composition corresponds to the Case4 given in **Table 4-11**. Assumption: H_2O is at saturation and by-products in the gas were not considered in process design **b)** Calculated by Eq.6-4 **c)** With simple cycle power generation
d) Assumed and given as decimal rates **e)** Calculated as explained in section 6.2.2.1 **f)** Retrieved from open literature (Gas turbines catalogue, 2016)

Table 6-2 summarizes the main equipment of the three basic unit operations (absorption, regeneration and sulfur separation units), into which the treatment plant was split up for the cost estimations.

Table 6-2 Main equipment of the three basic unit operations of the treatment plant

Quantity	Equipment description	Cost scaling (sizing) factor	Unit
1	Absorber (bubble column)	Volume in m^3	Absorption unit
1	Regenerated solution pump with its electrical drives (centrifugal pump)	Power in kW	
1	Flash reactor (process vessel)	Volume in m^3	
1	Air compressor with its electrical drives (axial, turbo)	Power in kW	Regeneration unit
1	Regenerator (bubble column)	Volume in m^3	
1	Filtrate vessel (process vessel)	Volume in m^3	Sulfur separation unit with auxiliaries
1	Sulfur filter (pressurized filter)	Filter area in m^2	
1	Suspension withdrawal pump		
1	Filtrate pump		
1	Vacuum and air compression system for filter		

The capital and operating costs of the treatment plant are specific to the key operating conditions of the process given in the left hand side of **Table 6-1**. Absorption was performed at $P_{abs} \approx 25$ bara which is higher than the pressure of the combustor of the turbine ($P_{com} \approx 23.8$ bara (Gas turbines catalogue, 2016)) in order to compensate the pressure drop, and thus, to maximize the efficiency of the combustion engine. Since the absorber was designed to be operated at T=35 °C, P=25 bara, the sour gas fed into the absorber was calculated to be 546.28 m^3/h under operation conditions. As the acidic gas content of the sour feed gas (i.e. 10 vol% H_2S and 10 vol% CO_2) corresponds to tested gas composition (the Case4 given in **Table 4-11**) experimentally obtained data of the selected solution (Sol.13) for this case were used. Based on the lab results, the decisive performance parameters (f_{sol}, f_{air}, etc.) of the selected solution (Sol.13) were defined for the Case4 and a mass and energy balance of the process was elaborated. In this context, also other important parameters regarding the economics and compact process design such as the L/G ratio, the superficial gas velocity, u, the required filling height, h, and the residence time of the washing liquid in each contactor were calculated using the respective equations (Eq.4-25 to Eq.4-34) given in **Table 4-13** and experimentally found data for each equipment. Then, the sizing calculations of the process equipment given in **Table 6-2** were performed. It must be noted that the costs incurred for the valves, the compressor of the flash gas and the heat recovery/exchange units (were not illustrated in **Table 6-1**) as well as the wash water recovery unit (auxiliary of sulfur separation unit) were not calculated separately but estimated to be almost 8% of the fixed capital investment (see auxiliaries (spares) and contingencies shares of the fixed capital investment given in **Table A- 19**). The Appendix A-4 consists of the tables **Table A- 10** to **Table A- 24** and contains the results of all calculations and/or supplementary informations regarding the economic analysis conducted in the scope of this chapter. Considering the corrosivity of the handled solution (refer to section 4.2.7), stainless steel (of AISI 316 grade e.g. DIN No. 1.4571 also known as EN-1088-1 or AISI 316Ti with the composition X6CrNiMoTi17-12-2) was chosen as construction material. The results of the sizing and design calculations of the treatment unit and its components i.e. the absorber, the regenerator, the flash reactor, the sulfur separation unit and pump as well as the air compressor are available in **Table A- 11** to **Table A- 15**, respectively. The performance factors of the treatment plant given in **Table 6-1** (the separation rate of H_2S ≥99.99 vol%, desorption rate[28] of CO_2≈50 vol% and the CH_4-slip rate <0.1 vol%) (Siemens AG, 2016) yielded a treated gas

[28] Equivalent to the CO_2 absorption rate; all CO_2 initially absorbed from the sour gas stream is desorbed (in absorber + flash vessel + regenerator), and thus, in the end forwarded to the gas turbine.

capacity of 10,155 Nm^3/h (see **Table A- 16**) comprised of 94.12 vol% CH_4 (~9558 Nm^3/h) and 5.88 vol% CO_2 (~597 Nm^3/h) at normal conditions.

After giving the required technical input for the cost estimation, a review of the economic and financial parameters is presented in the following section.

6.2.3 Suppositions of the economic analysis

The implementation of the economic analysis by the TRR method is associated with suppositions for economic and financial parameters. The methodology used in the scope of this study can be categorized into two parts:

(1) economic assumptions for the estimation of capital and operational expenses and
(2) financial assumptions done for the levelization of these as presented below:

Economic assumptions for the estimation of CAPEX and OPEX:

- The study-type estimate method given in (Seider, Seader, & Lewin, 2010) was used for the estimation of CAPEX and OPEX based on the established scenario given in section 6.2.2 and the results obtained from the operation of the test rig in lab scale (refer to section 4.2.4). Since the technology is in pre-industrial phase yet, the accuracy of the design and cost estimation was determined to be ± 30% (according to Class 4 of the cost estimate classifications system recommended by (AACE, 2003)).

- Hot spares respectively capital spares at the warehouse are included.

- The main equipment will be erected as outdoor installation.

- The design standards are; ISO for equipment and ASME/ANSI for piping.

- The plant is fully automatized with distrubuted control system (DCS).

- A country factor for the Middle East region is used.

- Licence costs are included.

- The construction period was committed to be started on 2016, which was regarded as the first year of the capital expenditure period and called as “base-year” for the economic analysis. The start date of commercial operation of plant was set to 2018.

- Cost estimates presumed that the plant is operated as designed.

- All capital costs were supposed to be incurring during the capital expenditure period (i.e. 2 years) and to be including all costs up to start of operation.

- Operational life time of the plant was expected to be 10 years with 7000 h/a total annual time of system operation at full load (as typical figures for a demo plants).

- Electricity generation costs calculated do not include transmission and distribution costs. The costs associated with treatment of wastes or residual emissions – including greenhouse gases – were not included in the costs estimated for the plant and, therefore, are not reflected in the generation costs calculated in this study.

Financial assumptions for the levelization of CAPEX and OPEX:

- The developer of the treatment plant technology was defined as the investor, and thus, the technology was assumed to be a so-called investor-owned utility (IOU) - meaning, the plant will be 100% financed by investor (NETL, 2011). It must be noted that this assumption was used only for the economic analysis conducted in this study. In a commercial investment case, the technology

owner and the gas producer might set-up a joint venture or the gas producer might be the owner of the investment. In these cases, the technology owner would request a licence fee from the plant operator/ utility owner. Thus, there is no contractual liability of the Siemens AG regarding the costs of the technology estimated in the scope of this study.

- The capital cost components of the TRR, the carrying charges, consider the influences of subsidies (i.e. the debt to equity ratio, the return on equity and return on debt) as well as taxation (income taxes and insurance). These vary significantly depending on the local or national laws and are key factors that play an important part in the cost estimate (Woods, 1975). The levelized carrying charges (the CC_L) reflect the costs calculated using tax depreciation schedules consistent with permanent tax law, which vary by technology. By considering these, the so-called "weighted averaged cost of capital (WACC)" approach can be used. An overview of the WACC descriptions, assumptions and methodology can be found in (EIA, 2014). However, as literature and common usages support reporting the LCoE both with and without tax credits, the tax-related components of the CC_L such as the minimum return on investment (ROI), income taxes (ITX) and insurances were excluded in the scope of this study.

- Depreciation was incorporated by applying the so-called capital recovery factor in which both interest rate and price escalation rate are embedded as given in (NETL, 2011).

The costs estimated were reflected in current dollars by adjusting the costs for the effect of inflation by using the real escalation and interest rates (for comparison of the approaches "current-dollar" with "constant-dollar" refer to (Tsatsaronis, Bejan, & Moran, 1996)). The financial suppositions of the economic analysis such as inflation, real interest and real price escalation rates for both plant components as well as operation and maintenance expenses are given in **Table 6-8**.

- It was not intented to estimate the selling price of the electricity produced using developed integrated technology, but rather, to determine the LCoE providing a basis for the evaluation of the economic feasibility of the technology and the solvent systems. Thus, the LCoE calculated in the scope of this study excluded the influences of the cost learning curve and additional volatile costs such as new technology and policy changes.

Once the technical and financial scope of the economic analysis was reviewed, an overview of the approach associated with the TRR method to determine the LCoE and obtained results is given in the following section.

6.2.4 Approach and results of the economic analysis

The determination of the LCoE starts with the estimation of the CAPEX[29] and OPEX[30], which were obtained as percentages of the so-called **delivered bare module costs** ($C_{BM,del}$ in $) of the plant equipment (Seider, Seader, & Lewin, 2010) as described in the following subsection.

6.2.4.1 Estimation of delivered bare module costs

In this study, the so-called **bare module method** (Seider, Seader, & Lewin, 2010) accounting for all direct and indirect costs for each piece associated with purchased equipment was applied. Accordingly, to receive the $C_{BM,del}$ of the plant equipment, the **purchased equipment cost** (C_P, $) are to be determined first. For the estimation of C_P of various equipment types, detailed methods are compiled in (Smith R. , 2005), (Seider, Seader, & Lewin, 2010), (Peters, Timmerhaus, & West, 2003) and (Turton R. et al., 1984). The characteristic cost scaling (sizing) parameter of the each plant equipment given in **Table 6-2** (e.g. power requirement for the pump) was considered in the cost estimation. The applied specific sizing formula, the required input and the results of the sizing calculations of all equipment are available in **Table A- 11** to **Table A- 15** and **Table A- 18** in

[29] The term CAPEX refers to term TCI for the rest of this chapter.
[30] The term OPEX refers to term OMC for the rest of this chapter.

Appendix A-4. The C_P of the respective equipment for the calculated size was either obtained from published cost graphs (Ulrich & Vasudevan, 2004) or diverse vendors. If the costs of equipment could not be directly obtained from the charts given in (Ulrich & Vasudevan, 2004), because they were not available for the required equipment size, the C_{ref}, (the purchase equipment cost of the equipment known for a reference capacity (Q_{ref})), was correlated by applying the given equipment-specific cost exponents (or degression coefficient (α)) and using Eq.6-5 to obtain the C_P for the required size.

$$C_P = C_{ref} * (\frac{Q_P}{Q_{ref}})^{\alpha} \quad \text{(Eq.6-5)}$$

The C_p was also corrected with the so-called **bare module factor (F_{BM})**. This was performed by multiplication of all factors differing from the base case (e.g. the material of construction (F_M) and the design pressure (F_P)). The F_{BM}, which was plotted versus F_P*F_M, was read off on the graphs available in (Ulrich & Vasudevan, 2004). This yielded the so-called **bare module costs (C_{BM} (f.o.b))**[31] as expressed in Eq.6-6.

$$C_{BM}(f.o.b) = C_P * F_{BM} \quad \text{(Eq.6-6)}$$

If the C_{BM} (f.o.b) obtained was not up to date to the estimation base year (2016), it was corrected using appropriate cost indexes. In the scope of this study, the adjustment was done by the means of the annual **Chemical Engineering Plant Cost Index (CEPCI)** obtained from (DoL, 2015). Since the CEPCI for the year 2016 was not available in any open literature, it was determined by modeling the past values and projecting them to the future (refer to **Figure A- 10** and **Table A- 17** in Appendix A-4, respectively). This yielded a CEPCI of 644.4 for the year 2016. After determining the up-to-date C_{BM}(f.o.b) of all equipment, 10% of it was taken as allowance in order to consider transport and delivery costs and thus estimate the total delivered bare module costs $C_{BM,del}$ as expressed in Eq.6-7.

$$C_{BM,del} = C_{BM}(f.o.b) * 1.1 \quad \text{(Eq.6-7)}$$

Consequently, the $C_{BM,del}$ of the treatment plant was estimated to be **3.21 M$** and is given in **Table 6-3** (for the calculation results of the each equipment refer to **Table A- 18** in Appendix A-4).

Table 6-3 Results of estimation of total delivered bare module costs of the treatment plant

Equipment \ Bare module costs		C_{BM}(f.o.b), (M$)
Treatment plant (TP)	Absorber	1.22
	Regenerator	0.14
	Flash vessel	0.11
	Regenerated solution circulation pump	0.57
	Air compressor	0.61
	Sulfur separation unit	0.27
Cost components of $C_{BM,del}$		**Value**
Sum of all the C_{BM}(f.o.b), (M$)		2.92
Delivery costs, (M$)		0.29
Total delivered bare module costs, $C_{BM,del}$ (M$)		**3.21**

It must be noted that, the bare module approach described above was used only to estimate the equipment costs of the treatment plant. For power plant equipment costs, it is common to apply the so-called demand charges of the individual modules of the power plant (P_{DC}) given by the vendor in $/kWe (EIA, 2016b). However, the demand charge (P_{DC}) data of the SGT-750 and the other units of the power plant (e.g. combustion unit) cannot be obtained from the vendor

[31] The purchased equipment costs (C_P) are generally the free-on-board (f.o.b) costs, meaning the purchaser pays the freight.

(Siemens) due to confidentiality reasons. Therefore, the P_{DC} of individual units of power plant (expectedly yielding a power output of 38.1 MWe at full load) and in turn the FCI of it was determined using the cost functions available in open literature (IUTA e.V., 2002). Accordingly, the demand charges of turbine module, combustion module and auxiliary units can be calculated using Eq.6-8, Eq.6-9 and Eq.6-10, respectively.

$$P_{DC,\text{turbine module}}\ (\$/\text{kWe}) = 4207.6 * \text{PO}\ (\text{kWe})^{-0.2826} \quad \text{(Eq.6-8)}$$

$$P_{DC,\text{combustion module}}\ (\$/\text{kWe}) = 32.083 * \text{PO}\ (\text{kWe})^{0.1826} \quad \text{(Eq.6-9)}$$

$$P_{DC,\text{auxilary units}}\ (\$/\text{kWe}) = 993.02 * \text{PO}\ (\text{kWe})^{-0.2388} \quad \text{(Eq.6-10)}$$

Since the P_{DC} of each module was obtained using the functions given for the year 2002, adjustment of each for the estimation base year, 2016, was done by using Eq.6-11 and the CEPCI data given in **Table A- 17** in Appendix A-4.

$$\frac{P_{DC}\text{ in }2002}{P_{DC}\text{ in }2016} = \frac{CEPCI_{2002}}{CEPCI_{2016}} \quad \text{(Eq.6-11)}$$

Consequently, the total P_{DC} of the power plant was estimated to be **836.75 $/kWe** and is given in **Table 6-4**.

Table 6-4 Results of estimation of total demand charge of power plant equipment

Demand chargeof plant equipment / Equipment		P_{DC}, ($/kWe)
Power plant (PP)	Turbine module (incl.turbine+generator+gear shaft)	347.8
	Combustion module (incl. fuel supply system)	358.6
	Auxilary units (e.g. water injection system, cooler etc.)	130.3
Total demand charge of power plant equipment, $P_{DCtotal}$, ($/kWe)		**836.75**

Once the total $C_{BM,del}$ (in M$) of treatment plant and total P_{DC} of the power plant (in $/kWe) had been determined, thus now, the capital expenses (CAPEX) referring the total capital investment (TCI) of both plants could be estimated using these cost data. The respective approaches and the results are presented in the following section.

6.2.4.2 Estimation of capital expenses

The **total capital investment (TCI, $)** of a new plant is generally defined as one-time expense for the design, construction and start-up of it (Smith R. , 2005). The TCI comprises of the **fixed capital investment** (FCI in $; investment for purchase and installation) and **working capital investment** (WCI in $; investment for start-up e.g. initial solvent fill). In this study, it was confined to apply the **multiple factor approach** in which the $C_{BM,del}$ of the treatment plant is multiplied with the factors given in (Seider, Seader, & Lewin, 2010) to consider equipment installation as well as other disciplines such as piping, EI&A, engineering and thus to convert the equipment hardware costs into the FCI of the treatment plant (FCI_{TP}). The sum of the percentages of $C_{BM,del}$ yielded to a factor of 4.0 (for the individual elements of the FCI_{TP} and factors see **Table A- 19** in Appendix A-4). Thus, the FCI_{TP} was calculated to be **12.85 M$** by applying Eq.6-12.

$$FCI_{TP} = C_{BM,del} * 4.0 \quad \text{(Eq.6-12)}$$

As a rule of thumb, the WCI is estimated to be 15% of the TCI (Smith R. , 2005). However, assuming the WCI of the treatment plant (WCI_{TP}) to be the 0.15 fold of the TCI_{TP} would lead to a high inaccuracy of the capital costs of the treatment plant due to the large differences in the chemical (constituents of the respective solvent system) costs. Thus, the incurred WCI_{TP} was calculated as a function of the applied solution type using Eq.6-13 to reduce the uncertainity in estimating the TCI_{TP}.

$$\mathrm{WCI_{TP}} = \mathrm{HU_{total}} * \mathrm{C_{sol}} \quad \text{(Eq.6-13)}$$

In Eq.6-13, the term HU_{total} in kg denotes for the hold-up requirement for both reactors whereas the C_{sol} refers to the costs of the applied solution per kg ($/kg). However, the absolute values of these solution specific data can not be revealed due to the confidentiality of them. The WCI_{TP} employing Sol.13 was calculated to be **0.63 M$** using Eq.6-13.

Thus now, the TCI_{TP} can be obtained using Eq.6-14.

$$\mathrm{TCI_{TP}} = \mathrm{FCI_{TP}} + \mathrm{WCI_{TP}} \quad \text{(Eq.6-14)}$$

Once the TCI_{TP} was determined, the FCI of the power plant (FCI_{PP}) had to be estimated first in order to receive the TCI_{PP}. The FCI_{PP} was calculated by multiplying the total P_{DC} ($P_{DCtotal}$ see **Table 6-4**) with the electrical power output of the generator (PO) in kWe and capacity factor, (-) as expressed in Eq.6-15 (Boyce, 2012).

$$\mathrm{FCI_{PP}\ (M\$)} = \mathrm{P_{DCtotal}(\$/kWe)} * \mathrm{PO(kWe)} * \mathrm{CF} * (10^{-6}) \quad \text{(Eq.6-15)}$$

The FCI of the power plant (FCI_{PP}) was found to be **31.88 M$**. Taking the rule of thumb into account, FCI_{PP} corresponds to be 85 % of the TCI_{PP} (see Eq.6-16), whereas the WCI_{PP} accounts for 15% of the TCI_{PP} (refer to Eq.6-17). Thus, the TCI_{PP} and WCI_{PP} were calculated to be **37.50 M$** and **5.62 M$**, respectively.

$$\mathrm{TCI_{PP}} = \mathrm{FCI_{PP}}/0.85 \quad \text{(Eq.6-16)}$$
$$\mathrm{WCI_{PP}} = \mathrm{TCI_{PP}} * 0.15 \quad \text{(Eq.6-17)}$$

The results of the estimations of WCI, FCI and TCI for both parts of the integrated plant are given in **Table 6-5**. It must be noted that all the cost components were expressed in “base-year” dollars (i.e. 2016). Thus, the finite escalation beyond the start of operation (i.e. 2018) was not included yet.

Table 6-5 Results of estimation of capital costs of the integrated plant

Capital costs of the plants / Cost component	Capital costs of the treatment plant (TP), (M$)	Capital costs of the power plant (PP), (M$)
Fixed capital investment, FCI	12.85	31.88
Working capital investment, WCI	0.63	5.62
Total capital investment, TCI_{2016}	**13.48**	**37.50**

Once the TCI (CAPEX) for both parts of the integrated plant was calculated, the operational expenses (OPEX)[30] of the plants are to be estimated using the approach presented in the following section.

6.2.4.3 Estimation of operational expenses

In the scope of this study, the OPEX, namely the operational and maintenance costs (OMC) were divided into two categories:

1. As **Fixed OMC**, the costs, which are independent from the amount of the electricity produced and operating life time of the plant, were considered. The individual components of fixed OMC of the treatment and power plants are given in **Table A- 20** and **Table A- 21**, respectively, in Appendix A-4.
2. **Variable OMC** are those costs tied directly to power production and dependent on the actual production capacity, the operating life time (years) and work load (h/a) of the plant. These can be classified as operating labor costs (C_{OL}), cost of utilities (C_U), costs for the required

chemical make-up (C_C) and fuel costs (FC). However, it must be noted that the following assumptions were made in the scope of calculation of the variable OMC:

- The fuel costs (FC) were excluded from the variable OMC and considered separately as it is presented in the section 6.2.4.4.
- The C_C given in the following table represent the chemical costs by the mechanical loss resulting from the filtration of the sulfur product. Thus, the C_C did not include the chemical make-up requirement necessited due to chemical loss (degradation) of the solvent system. Even though the absolute degradation ratios are still to be determined in the pilot plant during the long term tests, the chemical loss resulting from a possible degradation of solvent system was considered to be 5% of the "Operating supplies" component of the variable OMC and is contained in this cost element (refer to **Table A- 20**) in order to reduce uncertainity in the cost estimation. The C_C was calculated by multiplying the costs of the constituents of the solvent system (these can not be revealed due to confidentiality reasons) with the experimentally determined chemical make-up ratio of them for the Sol.13 (see **Table 4-16**).
- The C_{OL} was estimated using the labor requirement and cost data obtained from the operator company (Siemens AG, 2016). The input and approach for the calculation of the C_{OL} is given in **Table A- 22** in Appendix A-4.
- The wash water recovery part of the sulfur separation unit necessitates the utilization of steam. In addition, the heat recovery or exchange units demand the utilization of cooling water. These both utility requirements were not calculated separately but considered to be 0.05 fold of "Operating supplies" and are contained in this cost element (refer to **Table A- 20**). Besides steam and cooling water demand of the auxiliary units, electricity is required mainly for the operation of the pump and the compressor. However, the cost of electricity utilized, in this case called as C_U, was not individually added to variable OMC estimated, since the electricity required for the operation of all machinery, e.g. for the pumps and compressors, was assumed to be completely originating from the electricity produced in the power generation plant. Even though no C_U is shown here, the annual power consumed (APC) in MWhe/a within the battery limits of the sour gas treatment plant was calculated (see **Table A- 23**) and substracted from the electricity generated to obtain the annual net electricity production (ANEP in MWhe/a) to finally come to the LCoE (see section 6.2.4.6).

The results of the estimations are shown in **Table 6-6**.

Table 6-6 Results of estimation of operation and maintenance costs

Cost component		**Operational expenses of the TP, (M$/a)**	**Operational expenses of the PP, (M$/a)**
Fixed OMC (OMC without C_{OL} and Cc)		3.38	3.55
Variable OMC	Operating labor costs, C_{OL}	1.89	1.04
	Chemical make-up costs, Cc	4.99	-
OMC_{2016}		**10.26**	**4.59**

Thus now, the fuel costs are to be estimated as described in the following section.

6.2.4.4 Estimation of fuel expenses

As it was indicated before, the CH_4 content in the treated sour natural gas was considered to be the fuel input to the gas turbine. The amount of the sour gas treated (80 vol% CH_4, 10 vol% H_2S and 10 vol% CO_2) was given as 546.28 m^3/h at 25 bar and 35 °C (see **Table 6-1**). Taking the CO_2

desorption (50 vol%) and methan slip rate (<0.1 vol%) given in the **Table 6-1** into consideration, the resulting treated gas stream (10,155 Nm^3/h) consisted of 9557.7 Nm^3/h CH_4 (c_{CH4}=94.12 vol%) and 597 Nm^3/h CO_2 (c_{CO2}=5.88 vol%). As it was described in section 6.2.2.1, the volumetric flow rates of the respective gas components were expressed in mass flows, 6824 kg/h CH_4 and 1173 kg/h CO_2 applying Eq.6-3 (for M_{CH4}=16 kg/kmol and M_{CO2}=44 kg/kmol, respectively). Thus, the mass flow rate of the fuel, ($\dot{m}_{fuel}$) at turbine inlet came to the amount of 7997 kg/h. Since the LHV of the pure CH_4 is given as 50 MJ/kg and the CO_2 is not combustible (CER, 2008), the LHV of the treated gas (LHV_{fuel}) comprising 85.13 wt% CH_4 (x_{CH4}) was calculated to be 42.66 MJ/kg using Eq.6-18.

$$\mathrm{LHV_{fuel}} = (\mathrm{LHV_{CH_4}} * \mathrm{x_{CH_4}}/100) \qquad \text{(Eq.6-18)}$$

Taking the $\dot{m}_{fuel}$ as well as the LHV_{fuel} and the 7000 h/a operation time into account, the annual fuel input into the turbine was obtained as 55,977,145 kg/a. As the sour natural gas abundant in the Middle East is reportedly not tradable on the world market yet and thus can only be used for domestic energy demand in Middle East, where the plant is assumed to be constructed, the domestic price of it was obtained as 0.71 $/GJ for the year 2006 (ECRA, 2006). This price was escalated up to 2016 using the given price escalation rate for the sour natural gas and applying Eq.6-21 ($r_{r,sour}$=0.0056 refer to **Table 6-8**). Results of the fuel cost estimation are shown in **Table 6-7**.

Table 6-7 Results of estimation of fuel (treated sour natural gas) costs

Parameter	**Unit**	**Values for the determination of fuel costs (treated sour natural gas)**
Treated gas input to turbine per operation hour	kg/h	7997
CH_4 input to turbine per operation hour	kg/h	6824
Annual operation hours	h/a	7000
Annual fuel input to turbine	kg/a	55,977,145
Lower heating value of the fuel	GJ/kg	0.04266
Annual fuel consumption of the turbine	GJ/a	2,388,358
Fuel price on year 2016	$/GJ	0.75
Annual fuel costs, FC_{2016}	**M$/a**	**1.79**

After calculating the capital costs (see **Table 6-5**), estimating the operational expenses (see **Table 6-6**) and the fuel costs (see **Table 6-7**), the next step is the levelization of these prior to calculation of the LCoE, as shown in the subsequent section.

6.2.4.5 Levelization of the expenses

As it was stated in section 6.2.1, the estimated investment costs, operating and fuel expenses are to be levelized in order to get an equivalent series of constant payments year-by-year on an equal basis over the economic life time of the plant (i.e. 10 years). However, it must be noted that the costs estimated in the previous sections are called “overnight” costs and were expressed in “base-year” (2016) dollars. This means, these costs incurring during the capital expenditure period did not include the impact of escalation and interest during construction. Thus, the scaling of the estimated TCI, OMC and FC of both plants up to start of operation date, to 2018, using the real price escalation rates, must be performed prior to levelization of them. Therefore, they were levelized taking the financial assumptions stated in section 6.2.3 and the suppositions given in **Table 6-8** into account and escalated by applying the Eq.6-19, Eq.6-20 and Eq.6-21, respectively.

$$\mathrm{TCI_{2018}} = \mathrm{TCI_{2016}} * \left(1 + \mathrm{r_{r,gen}}\right)^{\mathrm{t}} \qquad \text{(Eq.6-19)}$$

$$\mathrm{OMC_{2018}} = \mathrm{OMC_{2016}} * \left(1 + \mathrm{r_{r,gen}}\right)^{\mathrm{t}} \qquad \text{(Eq.6-20)}$$

$$FC_{2018} = FC_{2016} * \left(1 + r_{r,sour}\right)^{t} \quad \text{(Eq.6-21)}$$

The term t denotes for the capital expenditure (construction) period and is 2 years, whereas the $r_{r,gen}$ stands for the real price escalation rate for both TCI and OMC and the $r_{r,sour}$ is used for the cost scaling of the FC (for the calculation and resulting values refer to **Table 6-8**). Consequently, the escalated costs (for the results see **Table 6-9**) include the construction material costs of the equipment, the installation costs of them as well as the technological advances and gas prices at the date of commissioning.

Table 6-8 Suppositions of the economic analysis

Parameter		Symbol, (unit)	Value	Notes, (References)
Inputs	Estimation base year	(-)	2016	Known also as investment year
	Capital expenditure period	t,(years)	2	Usual construction period
	Operation start	(-)	2018	Estimation base year + t
	Operating life of the plant	a,(years)	10	Usual period for demo plant
	Workload	WL,(h/a)	7000	Annual operation time
	Capacity factor	CF,(-)	1.0	(refer to footnote 27)
	Average general inflation rate (nominal)	r_i,(-)	0.025	(NETL, 2011)
	Annual nominal price escalation rate	$r_{n,gen}$,(-)	0.10	For TCI and OMC (NETL, 2011)
	Annual effective interest rate	i_{eff}, (-)	0.08	(EPRI, 2011)
	Real price escalation rate of sweet natural gas	$r_{r,sweet}$,(-)	0.03	(NETL, 2011)
	Real price escalation rate of sour natural gas	$r_{r,sour}$,(-)	0.0056	(ECRA, 2006)
Calculated values	Real interest rate (Known also as discount rate)	i_r,(-)	0.054	(Eq.6-22): $i_r = \frac{1 + i_{eff}}{1 + r_i} - 1$
	Real price escalation rate	$r_{r,gen}$,(-)	0.073	(Eq.6-23): $r_{r,gen} = \frac{1+r_{n,gen}}{1+r_i} - 1$
	Capital recovery factor	CRF,(1/a)	0.132	(Eq.6-24): $CRF = \frac{i_r*(1+i_r)^a}{(1+i_r)^a-1}$
	k-Factor for operational expenses	k_{OMC},(-)	1.019	(Eq.6-25): $k_{OMC} = \frac{1+r_{r,gen}}{1+i_r}$
	k-Factor for sour gas	k_{sour},(-)	0.954	(Eq.6-26): $k_{sour} = \frac{1+r_{r,sour}}{1+i_r}$
	Constant escalation levelization factor (in this case for OMC)	$CELF_{gen}$,(-)	1.460	(Eq.6-27): $CELF = \frac{k_{gen}*(1-k_{gen}{}^a)}{(1-k_{gen})} * CRF$
	Constant escalation levelization factor for fuel (sour gas) costs	$CELF_{sour}$,(-)	1.029	(Eq.6-28): $CELF_{sour} = \frac{k_{sour} * (1 - k_{sour}{}^a)}{(1 - k_{sour})} * CRF$

A more detailed description of all the financial parameters given in **Table 6-8** can be found in (NETL, 2011). After scaling the costs up to the date for start of operation, the conversion of the present value of the TCI at the first year of the operation (TCI_{2018}) into a stream of equal annual payments over the economic life time of the plant (10 years) at a specified discount rate (interest rate i_r=0.054 see Eq.6-22 given in **Table 6-8**) - in other words the levelization - was done. Multiplying the TCI_{2018} with the so-called capital recovery factor (CRF) - see Eq.6-24 in **Table 6-8** - yielded the levelized carrying charges related to capital costs, the CC_L[32], as expressed in Eq.6-29.

$$\mathrm{CC_L} = \mathrm{CRF} * \mathrm{TCI_{2018}} \quad \text{(Eq.6-29)}$$

The levelized carrying charges of the treatment plant ($CC_{L,TP}$) were calculated to be **2.05 M$/a** while that for the power plant $CC_{L,PP}$ was calculated to be **5.69 M$/a** as presented in the **Table 6-9**.

Subsequent to the calculation of the CC_L, the FC and OMC estimated for the beginning of the first year of operation (2018) were levelized by multiplying them with the so-called constant escalation levelization factors (CELF). The $CELF_{gen}$ and $CELF_{sour}$ calculated by Eq.6-27 and Eq.6-28 (see **Table 6-8**) were used to express the relationship between the value of the expenditures at the beginning of the first year and their respective annuity. Thus, the OMC_L and FC_L could be determined:

$$\mathrm{OMC_L} = \mathrm{OMC_{2018}} * \mathrm{CELF_{gen}} \quad \text{(Eq.6-30)}$$

$$\mathrm{FC_{L,sour}} = \mathrm{FC_{2018}} * \mathrm{CELF_{sour}} \quad \text{(Eq.6-31)}$$

After estimation of all levelized costs considered in the scope of this study, the levelized total revenue requirement (TRR_L) of the power plant ($TRR_{L,PP}$) was calculated using the Eq.6-32.

$$\mathrm{TRR_{L,PP}} = \mathrm{CC_L} + \mathrm{FC_L} + \mathrm{OMC_L} \quad \text{(Eq.6-32)}$$

Since the fuel costs were taken solely as the expenses of the power plant, the levelized total revenue requirement of the treatment plant ($TRR_{L,TP}$) was calculated using the Eq.6-33.

$$\mathrm{TRR_{L,TP}} = \mathrm{CC_L} + \mathrm{OMC_L} \quad \text{(Eq.6-33)}$$

The summation of both yielded the total revenue requirement for the integrated plant ($TRR_{L,TP+PP}$) as expressed in Eq.6-34.

$$\mathrm{TRR_{L,TP+PP}} = \mathrm{TRR_{L,TP}} + \mathrm{TRR_{L,PP}} \quad \text{(Eq.6-34)}$$

The results are shown in **Table 6-9**. It should be stated that with the approach described in this section, the $TRR_{L,TP+PP}$ represents the same value within every year of the plant life time.

[32] It must be stated that TCI includes both depreciable (fixed capital investment: FCI) and non-depreciable capital costs (working capital investment: WCI). However, both escalation and interest rates (r_i and i_r) during construction are embedded in the CRF (see Eq.6-24). Thus, it is computed assuming that all capital is depreciable. This simplification meaning not to consider the present value of the FCI (PV_{FCI}) but the TCI, introduced only a negligible amount of error into the resulted carrying charges. If this simplification is not acceptable for the depreciation schedule to be applied in any other economic analysis, the "discounted cash flow analysis tools" given in (NETL, 2011) can be used to calculate the CC_L as CC_L= PV_{FCI} *CRF instead of the simplified equation expressed as (Eq.6-29).

Table 6-9 Cost components of the levelized total revenue requirement

Cost component	Unit	Treatment plant, TP	Power plant, PP
TCI_{2016}	M$	13.48	37.50
TCI_{2018}	M$	15.53	43.20
OMC_{2016}	M$/a	10.26	4.59
OMC_{2018}	M$/a	11.81	5.29
FC_{2016}	M$/a	-	1.79
FC_{2018}	M$/a	-	1.81
FC_L	M$/a	-	1.87
CC_L	M$/a	2.05	5.69
OMC_L	M$/a	17.24	7.72
TRR_L	**M$/a**	**19.29**	**15.28**
$TRR_{L,TP+PP}$	**M$/a**	**34.57**	

Thus now, the levelized cost of electricity can be calculated considering the obtained $TRR_{L,TP+PP}$, as presented in the following section.

6.2.4.6 Determination and analysis of the LCoE

Since the LCoE represents the per-kilowatthour cost of building (carrying charges) and operating (operational and fuel expenses) the integrated plant over its assumed economic life and duty cycle, it can be calculated using Eq.6-35.

$$\mathrm{LCoE} = \frac{\mathrm{TRR_{L,TP+PP}}}{\mathrm{ANEP}} \quad \text{(Eq.6-35)}$$

The term ANEP in Eq.6-35 denotes the annual net electricity production in MWhe/a. As it was mentioned in the section 6.2.4.3, the electricity required for the operation of all machinery, e.g. the pumps and compressors was assumed to be completely provided by the power generation plant. Thus, the ANEP was calculated by subtracting the annual power consumed by plant equipment (APC, MWhe/a) from the annual power produced (APP, MWhe/a) as expressed in Eq.6-36.

$$\mathrm{ANEP} = \mathrm{APP} - \mathrm{APC} \quad \text{(Eq.6-36)}$$

The derivation of the APC is available in **Table A- 23** in Appendix A-4. The APP was calculated by Eq.6-37 considering the given duty cycle (WL=7000 h/a; PO=38.1 MWe at CF=1.0).

$$\mathrm{APP} = \mathrm{PO} * \mathrm{CF} * \mathrm{WL} \quad \text{(Eq.6-37)}$$

To sum up, the electricity generated from the integrated plant, in which 11,947 Nm^3/h sour gas (80% CH_4, 10%H_2S and 10% CO_2) was treated by using the Sol.13, resulting in a treated gas stream (10,155 Nm^3/h comprised of 94.12 vol% CH_4 and 5.88 vol% CO_2) with a LHV of 42.66 MJ/kg was combusted yielding 38.1 MW power output. Taking the technical (see **Table 6-1** and section 6.2.2) and financial (see **Table 6-8** section 6.2.3) assumptions into account, the LCoE was determined to be **13.12 ct/kWh** and is given in **Table 6-10**.

Table 6-10 Levelized cost of electricity produced (integrated plant with Sol.13 for sour gas treatment)

Parameter	Unit	Value
Economic life time of the plant	years	10
Annual full load hour, WL	h/a	7000
Turbine power output, PO	MWe	38.1
Capacity factor, CF	-	1.0
Annual power production, APP	MWhe/a	266700
Annual power consumption of the treatment plant, APC	MWhe/a	3117
Annual net electricity production, ANEP	MWhe/a	263583
Levelized cost of treatment and power generation plant, $TRR_{L,TP+PP}$	M$/a	34.57
Levelized cost of electricity produced, LCoE	**ct/kWh**	**13.12**

Even though this value estimated (13.12 ct/kWh) is very preliminary and subject to significant development, it provides a basis to examine the economic feasibility of the evaluated technology compared to gas-fired power generation plants of the same capacity utilizing "sweet" natural gas, which therefore exclude the treatment plant. In this context, (ECRA, 2006) reported that the domestic levelized electricity production cost for a "sweet" natural gas-fired power plant, which has a power output of 283.9 MW (PO_1) and is located in the Middle East, is 2.2 ct/kWh ($LCoE_1$). Scaling this value for the 38.1 MW (PO_2) capacity of the integrated plant given in this study with a degression coefficient of α=-0.6 yielded an LCoE of 7.35 ct/kWh ($LCoE_2$) by Eq.6-38 given in (EIA, 2016b).

$$\mathrm{LCoE}_2 = \left(\frac{\mathrm{PO}_2}{\mathrm{PO}_1}\right)^{\alpha} * \mathrm{LCoE}_1 \qquad \text{(Eq.6-38)}$$

However, the value obtained (7.35 ct/kWh) is not conclusive yet to compare the competitiveness of the evaluated technology, since (ECRA, 2006) did not report the basic assumptions on the LCoE calculations regarding future unit operations, operating costs, fuel prices, financing terms, and inflation. The knowledge, whether the estimate was in constant or current dollars, if it was on an overnight cost basis or including escalation and whether it considered site specific costs or was a generic estimate is the key for being able to accurately compare costs. Thus, the economic analysis of the LCoE of the sweet-gas-technology is to be conducted by using the same approach given in this study to make the LCoE of each technology comparable on a fair and equal basis. This is presented in the following section.

6.3 Evaluation of LCoE by analyzing alternative fuel and solvent systems

6.3.1 LCoE for power plants fueled with sweet natural gas

It has to be analyzed, whether the "inexpensive" sour gas recovers the cost of "high-sulfur" gas treatment compared to the production of electricity by "expensive" sweet natural gas. For the latter, there is no need to construct an additional gas treatment unit. For the latter, there is no need to construct an additional gas treatment unit. To this end, the TRR of power plants utilizing sweet gas was estimated. With the changing fuel type, the capital and operational expenses were assumed to remain constant while only the fuel costs were supposed to be different than for the case of sour gas utilization (see **Table 6-9**). The price of the sweet gas for the Middle Eastern region and its escalation rate were taken from (IGU, 2015) and (NETL, 2011), respectively. Choosing another fuel type does not only impact the fuel price but also the lower heating value of the fuel and in turn the fuel consumption of the turbine (see section 6.2.4.4). Herefore, the possible influences of changing fuel type (and thus the LHV_{fuel}) on Wobbe Index (WI) and the overall thermal efficieny of the turbine were considered to be negligible yielding the assumption that the efficiency of the turbine remains constant (refer to section 1.3). Thus, based on the assumptions made and considering given annual operation hours, capacity factor, gas price,

escalation rate and the LHV of the fuel to be utilized, the fuel costs for the base-year (2016) were estimated and are presented in **Table 6-11**. For reasons of comparison, the results of the estimated sour natural gas parameter shown in **Table 6-7** are regiven on the third column of **Table 6-11**.

Table 6-11 Results of estimation of fuel costs (treated sour natural gas vs. sweet natural gas)

Parameter	Unit	Treated gas	Sweet gas
Real price escalation rate of natural gas ($r_{r,sour}$ and $r_{r,sweet}$)	-	0.0056	0.03
k-factor, (k_{sour} and k_{sweet})	-	0.954	0.978
CELF ($CELF_{sour}$ and $CELF_{sweet}$)	-	1.029	1.166
Capital recovery factor (CRF)	1/a	0.132	
Capacity factor, CF	-	1.0	
Power input to turbine	MW	94.77	
Lower heating value (LHV_{sour} and LHV_{sweet})	GJ/kg	0.04266	0.0500
Fuel input to turbine per operation hour	kg/h	7997	6824
Annual operation hours	h/a	7000	
Annual fuel input to turbine	kg/a	55,979,411	47,769,098
Annual fuel consumption of the turbine	GJ/a	2,388,358	
Fuel price on year 2016	$/GJ	0.75	3.0
Annual fuel cost, FC_{2016}	**M$/a**	**1.79**	**7.17**

As it is seen from **Table 6-11**, the annual fuel costs (sweet gas) at the base year of the estimation (2016) was determined as **7.17 M$/a**. Thereafter, these costs were first escalated up to 2018 and then levelized, using Eq.6-39 to Eq.6-42 given below, as described in the section 6.2.4.5.

$$\mathrm{FC}_{2018} = \mathrm{FC}_{2016} * \left(1 + \mathrm{r}_{\mathrm{r,sweet}}\right)^{\mathrm{t}} \quad \text{(Eq.6-39)}$$

$$\mathrm{k}_{\mathrm{sweet}} = \frac{1 + \mathrm{r}_{\mathrm{r,sweet}}}{1 + \mathrm{i}_{\mathrm{r}}} \quad \text{(Eq.6-40)}$$

$$\mathrm{CELF}_{\mathrm{sweet}} = \frac{\mathrm{k}_{\mathrm{sweet}} * \left(1 - \mathrm{k}_{\mathrm{sweet}}{}^{\mathrm{n}}\right)}{\left(1 - \mathrm{k}_{\mathrm{sweet}}\right)} * \mathrm{CRF} \quad \text{(Eq.6-41)}$$

$$\mathrm{FC}_{\mathrm{L,sweet}} = \mathrm{FC}_{2018} * \mathrm{CELF}_{\mathrm{sweet}} \quad \text{(Eq.6-42)}$$

After estimating of the levelized fuel costs and considering the already deducted levelized carrying charges and operational expenses given in **Table 6-9**, the levelized total revenue requirement (TRR_L) of the sweet-gas-fired power plant ($TRR_{L,PP}$) was calculated using Eq.6-32. For the power plant utilizing sweet natural gas, the whole electricity generated can be sold without consumption for the operation of the treatment plant (meaning APC=0). Thus, the ANEP is equal to the APP (see Eq.6-37). Consequently, the LCoE was calculated using Eq.6-35, and for the case sweet gas the $TRR_{L,TP+PP}$ is equal to the $TRR_{L,PP}$. The results are presented in **Table 6-12**. To make the comparison simple, the results of the estimated $TRR_{L,TP+PP}$ for the integrated plant utilizing treated sour gas and shown in **Table 6-9** are regiven in the third and forth columns on the left hand side of the **Table 6-12**.

Table 6-12 Components of the LCoE as a function of the used fuel type (sour gas vs. sweet gas)

Cost component	Unit	Integrated plant (treated-sour-gas-fired)		Power plant (sweet-gas-fired)
		TP	PP	PP
FC_{2016}	M$/a	-	1.79	7.17
FC_{2018}	M$/a	-	1.81	7.25
FC_L	M$/a	-	1.87	8.45
CC_L	M$/a	2.05	5.69	5.69
OMC_L	M$/a	17.24	7.72	7.72
TRR_L	**M$/a**	**19.29**	**15.28**	**21.86**
		34.57		
APP		266700		266700
APC		3117		-
ANEP		263583		266700
LCoE	**ct/kWh**	**13.12**		**8.20**

The LCoE for the case of sweet gas utilization was estimated to be **8.20 ct/kWh**. This is comparable with the LCoE data obtained from (ECRA, 2006) (see section 6.2.4.6). The cost analysis under the assumptions made and using the technical data obtained from the lab scale investigations and equipment costs taken from literature indicates that the technology utilizing sour gas is more cost intensive than the one applying sweet gas. To identify the main cost drivers of the LCoE for both, the LCoE was broken down into its components which are given in **Table 6-12**, as shown in **Figure 6-1**.

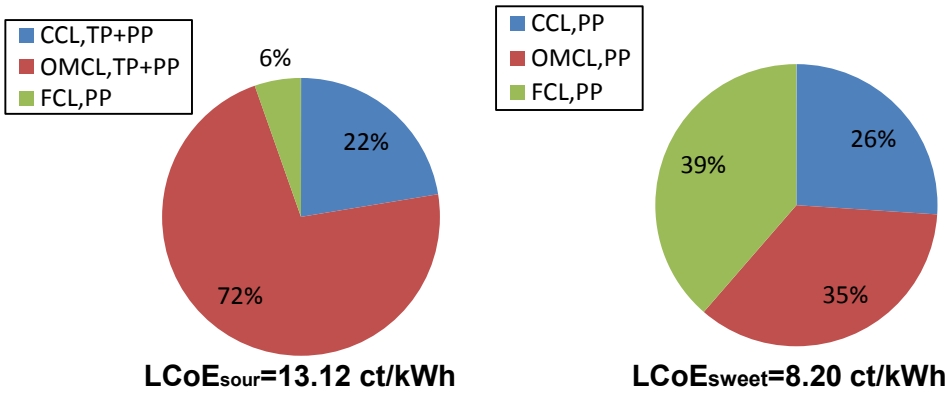

$LCoE_{sour}$=13.12 ct/kWh **$LCoE_{sweet}$=8.20 ct/kWh**

Figure 6-1 Breakdown of the LCoE into its cost components (the integrated plant utilizing treated sour natural gas on the left; the power plant utilizing sweet natural gas on the right)

Figure 6-1 reveals that:

- With a share of 6%, the fuel costs ($FC_{,PP}$ in ct/kWh) represent the smallest part of the LCoE for producing power from the treated sour gas by applying the "integrated plant" technology. While investment costs ($CC_{L,TP+PP}$ in ct/kWh) correspond to approx. 22%, the major driver are the operational expenses ($OMC_{L,TP+PP}$ in ct/kWh) by accounting for 72% of the LCOE.
- Contrary to this, the largest share on the LCoE for power plants utilizing sweet natural gas stems from the fuel costs which represent nearly 40%, making it the main cost driver. It is followed by the $OMC_{L,PP}$ which account for the 35% of the LCoE, while the smallest share (still with 26 %), originates from the $CC_{L,PP}$ for constructing the power plant.
- The LCoE for the integrated plant (with sour gas) are strongly predominated by the OMC_L (72% - mainly chemical costs), whereas in the case of power plants fired with sweet gas the

cost elements are more evenly distributed. Besides that, the absolute value of the LCoE for the sour gas is higher, which further emphasizes the impact of the $OMC_{L.}$

By conducting the economic analysis with the sweet gas, it was acknowledged that changes in the fuel type have a significant impact on the value of LCoE, which is mainly driven by the price of the fuel. In this context, the compilation given in (IGU, 2015) revealed that the natural gas prices vary significantly depending on the region. Accordingly, the cost of natural gas in the Middle East has fallen dramatically roughly within the last decade as a result of sour gas exploitation. Reportedly, Abu Dhabi (where the integrated plant is intented to be built) has subsidized natural gas prices (≤ 3 $/GJ see **Table 6-11**), which are among the lowest in the world and even in the Persian Gulf region while elsewhere in the world the cost of sweet gas remains relatively higher values (i.e. 5 to 12 $/GJ). To deduct and evaluate the impacts of the volatile sweet gas prices on the LCoE, the gas price given for "sweet gas" for the Middle Eastern region (i.e. 3 $/GJ) was considered as base-case and the LCoE was calculated as a function of the price range on the world market (i.e. 5, 8 and 11 $/GJ). The results are shown in the **Figure 6-2**.

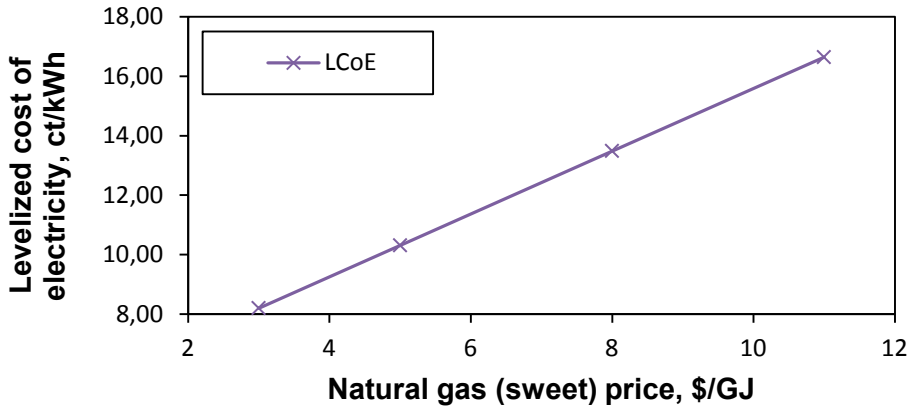

Figure 6-2 Sensitivity of the LCoE for power plants fired with sweet gas to the changes of the fuel price

Figure 6-2 reveals that:

- When the sweet natural gas price changes from 3 $/GJ to 11 $/GJ (based on the oil prices (IGU, 2015)), the LCoE changes linearily from 8.20 ct/kWh to 16.65 ct/kWh, respectively. Thus, the LCoE is very sensitive to the projected prices of the used natural gas.

To sum up, the main cost driver of the sweet-gas-fired-technology was found to be the FC_L, while for the treated-sour-gas-fired-integrated-technology the costs are predominated by the sum of the operational expenses of the treatment and power plants i.e. the $OMC_{L,TP+PP}$ (see **Figure 6-1**). In order to see which part of the integrated plant drives the high OMC, the LCoE for power produced from the treated sour gas (13.12 ct/kWh) was presented as percentages of the levelized total revenue requirement of the each plant in **Figure 6-3**.

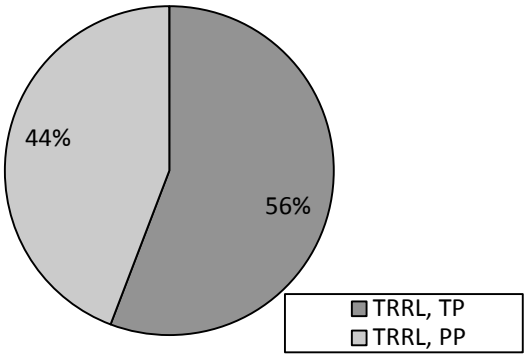

Figure 6-3 Shares of TRRL of the treatment and power plants on the LCoE

As it can be seen, 44% of the LCoE stems from the TRR_L of the power plant - depending on the fuel prices which are volatile, regulated by authorities subject to the world market, and thus can hardly be influenced. Contrary to this, 56 % of the LCoE was found to be caused by TRR_L of the treatment plant, which are directly related to the properties of the solvent system applied in the plant, and thus can be improved. Hence, an analysis of the influence of alternative promising solvent systems on the $TRR_{L,TP}$ is to be conducted to explore optimization potentials. This will be presented in the following section.

6.3.2 Evaluation of the effectiveness of alternative solvent systems for integrated plants

As it was mentioned in section 6, the experimental investigations assessing the techno-economic feasibility of 13 different formulations showed that secondary AASs with higher chelated-iron concentrations resulted in lower pump around ratios (f_{sol}). Thus, the LCoE analysis was firstly conducted with the Sol.13 (secondary ASS; iron concentration: 0.5 M, refer to **Table 4-9**).The per-kilowatthour costs obtained for the integrated plant applying Sol.13 was found to be 13.12 ct/kWh (i.e. the LCoE see **Table 6-10**). Comparing this value with the domestic electricity production costs in the Middle East revealed the cost-intensiveness of the technology which was found to be mainly driven by the $TRR_{L,TP}$ in other words the TOTEX of the treatment plant (see **Figure 6-3**). This necessitated further economic analyses with other solvent systems labeled as promising: As it was mentioned in section 4.2.4.4, high iron concentrations were found to affect the mass transfer of the O_2 into the washing liquid adversely which led to increase in f_{air} (i.e higher flow rates of regeneration air). Thus, the Sol.12 (secondary ASS with low-iron concentration: 0.1 M; see **Table 4-9**) was selected as an alternative to Sol.13 for the economic analysis to be conducted in the scope of this section. To provide a basis for the comparison of formulations with an ASS and a chelated metal with the state-of-the-art liquid redox solutions (w/o ASS, chelated-metal), the economic evaluation studies were carried out also with Sol.1 and Sol.3 (see **Table 4-9**: Fe•EDTA without AAS, with low (0.1 M) and high (0.5 M) iron concentration, respectively). The LCoE can be used as a screening tool when evaluating the impacts of different solvent systems on the economics of the integrated plant. However, this parameter alone is not enough to come to final conclusions, since the effectiveness of a solution to be employed was defined to be made up of low CAPEX (~TCI), low OPEX (~OMC) and low footprint, the latter is of high interest for offshore applications (see section 6). Thus, the comparison shall rather be done based on all three parameters. To this purpose, firstly, the levelized cost components of the solutions were determined and compared based on the resulting respective LCoE. Thereafter, the not levelized costs (TCI and OMC) were compared yielding an analysis of the pros and cons of each solution. This will be presented in the following subsections.

6.3.2.1 Impact of the solvent system on the LCoE

The capital and operating costs are specific to the composition of the applied solvent system and the operating conditions during the experiments in the test rig (see section 4.2). Thus, firstly, the key performance parameters of the selected solutions (Sol.12, Sol.1, and Sol.3) were defined based on the lab results (as described in section 6.2.2.1). Then, the sizing calculations for various process equipment were performed (see section 6.2.2.1) and their estimated costs were determined by the approach given in section 6.2.4. All other technical and financial suppositions of the economic analysis were held constant. Finally, the LCoE as a function of the applied formulation was calculated using Eq.6-35, as it was described in section 6.2.4.6. The results are shown in **Table 6-13**. For comparison purposes, also the results already obtained for Sol.13 (base-case; see **Table 6-1**) are added.

Table 6-13 Components of the LCoE depending on the applied solution type (ASS low and high cat vs. w/o ASS low and high cat)

Case / Component		Costs of treatment plant (TP)				Costs of power plant (PP)
		High-cat with AAS (base case)	**High-cat w/o AAS**	**Low-cat with AAS**	**Low-cat w/o AAS**	
		Sol.13	**Sol.3**	**Sol.12**	**Sol.1**	
C_{BM}(f.o.b) of absorber, M$		1.22	1.77	2.24	2.33	Turbine module (SGT-750) with generator: 347.8 $/kWe Complete combustion unit: 358.6 $/kWe Auxiliaries:130.3 $/kWe
C_{BM}(f.o.b) of flash, M$		0.11	0.14	0.32	0.35	
C_{BM}(f.o.b) of regenerator, M$		0.14	0.22	0.51	0.58	
C_{BM}(f.o.b) of sulfur separation unit, M$		0.27	0.28	0.33	0.34	
C_{BM}(f.o.b) of main pump, M$		0.57	0.64	1.01	1.03	
C_{BM}(f.o.b) of air compressor, M$		0.61	0.51	0.85	0.96	
Total C_{BM}(f.o.b)		2.92	3.56	5.26	5.58	
Delivery costs		0.29	0.36	0.53	0.56	
Total C_{BM}(del), M$		3.21	3.92	5.79	6.14	
$FCI_{(2016)}$, M$		12.85	15.69	23.15	24.57	31.88
$WCI_{(2016)}$, M$		0.63	0.86	2.03	1.97	5.62
$TCI_{(2016)}$, M$		13.48	16.55	25.17	26.54	37.50
$TCI_{(2018)}$, M$		15.53	19.06	28.99	30.56	43.20
CC_L, M$/a		**2.05**	**2.51**	**3.71**	**4.03**	**5.69**
Fixed OMC (OMC without C_{OL} and Cc), M$/a		3.38	3.66	4.39	4.53	3.55
Variable OMC	Operating labor costs, C_{OL}, M$/a	1.89	1.89	1.89	1.89	1.04
	Chemical make-up costs, Cc, M$/a	4.99	7.83	1.11	0.62	-
Total $OMC_{(2016)}$, M$/a		10.26	13.38	7.38	7.03	4.59
Total $OMC_{(2018)}$, M$/a		11.81	15.41	8.50	8.10	5.29
OMC_L, M$/a		**17.24**	**22.50**	**12.42**	**11.82**	**7.72**
Fuel costs, $FC_{(2016)}$, M$/a		-				1.79
Fuel costs, $FC_{(2018)}$, M$/a		-				1.81
FC_L, M$/a		-				**1.87**
Component		**Costs of integrated plant (TP+PP)**				
$TRR_{L,TP}$,M$/a		19.29	25.02	16.13	15.85	
$TRR_{L,PP}$,M$/a		15.28	15.28	15.28	15.28	
$TRR_{L,TP+PP}$, M$/a		**34.57**	**40.30**	**31.41**	**31.13**	
ANEP, MWhe/a		263583	263260	255843	254673	
LCoE, ct/kWh		**13.12**	**15.31**	**12.28**	**12.23**	

In order to identify the main drivers of the LCoE of the integrated plant utilizing one of these solutions, the levelized cost components of the respective LCoE (e.g. CC_L in M$/a) were divided by the corresponding ANEP (MWhe/a) to receive these costs in ct/kWh, and in turn, their shares on the LCoE were determined as percentages (%). These are shown in **Figure 6-4**. It shall be noted that the cost components related to the power plant (i.e. $CC_{L,PP}$, $OMC_{L,PP}$ and $FC_{L,PP}$) are independent from the applied solution type (see **Table 6-13**), hence, no conclusions will be drawn based on the influence of these on the respective LCoE. However, they were also shown in **Figure 6-4** for entirety purposes.

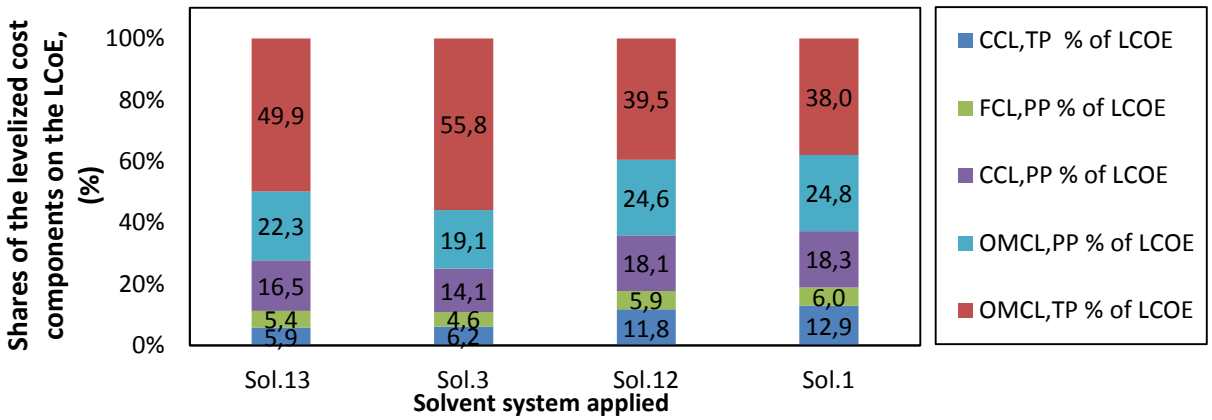

Figure 6-4 Breakdown of the LCoE into its components depending on the applied solution

Excluding the assessment of the shares of the power plant cost components on the LCoE, **Figure 6-4** reveals that:

- The OMC of the treatment plant, ($OMC_{L,TP}$), was found to have the biggest influence on the LCoE independently from the applied solution type, which however varies in the range of 38 to 50 % from low to high-cat solutions.

- The $CC_{L,TP}$ employing both high-cat solutions (either Sol.13 or Sol.3) have the lowest shares on the LCoE. This seems not to depend on the presence or absence of the AAS, as both values for the $CC_{L,TP}$ are very comparable (5.9% vs. 6.2%).

- However, both $CC_{L,TP}$ obtained for low-cat solutions (Sol.12 and Sol.1) are approx. the 2.0 fold of those of the high cat solutions Sol.13 or Sol.3. Nonetheless, the presence of the AAS seems to enable reductions in the carrying charges for low-iron concentrations (see the $CC_{L,TP}$ of Sol.1 vs. $CC_{L,TP}$ of Sol.12 from **Figure 6-4**; 12.9 % vs 11.9 %, respectively).

Since neither the decrease in the carrying charges ($CC_{L,TP}$) nor the increase in levelized operational costs of the treatment plant ($OMC_{L,TP}$) can be clearly related to the presence of the AAS or to high iron concentration, the analysis of the drivers of the individual components of those costs shall be conducted. The CC_L and OMC_L reflect future costs including inflation and escalation and levelization factors. Thus an evaluation of the elements of the CAPEX (or TCI) and OPEX (or OMC) given for the base-year 2016 (see **Table 6-13**) was executed to identify optimization potentials in capital and operational expenses in terms of “today´s” costs (without escalation and inflation). In this context, assessment of capital-cost-effectiveness which indirectly indicates the benefits in the footprint of the technology is prior to the evaluation of the elements of the OMC, as presented in the following subsections.

6.3.2.2 Impact of the solvent system on capital costs and footprint

In order to make the evaluation of the capital costs clearer, the bare module costs (C_{BM}(f.o.b)) of the equipment of the treatment plant were plotted depending on the applied liquid system, since the capital costs were estimated as percentages of these equipment costs (for the approach see section 6.2.4.2; for the absolute values of the C_{BM}(f.o.b)) of the respective equipment refer to **Table 6-13**). This is shown in **Figure 6-5**.

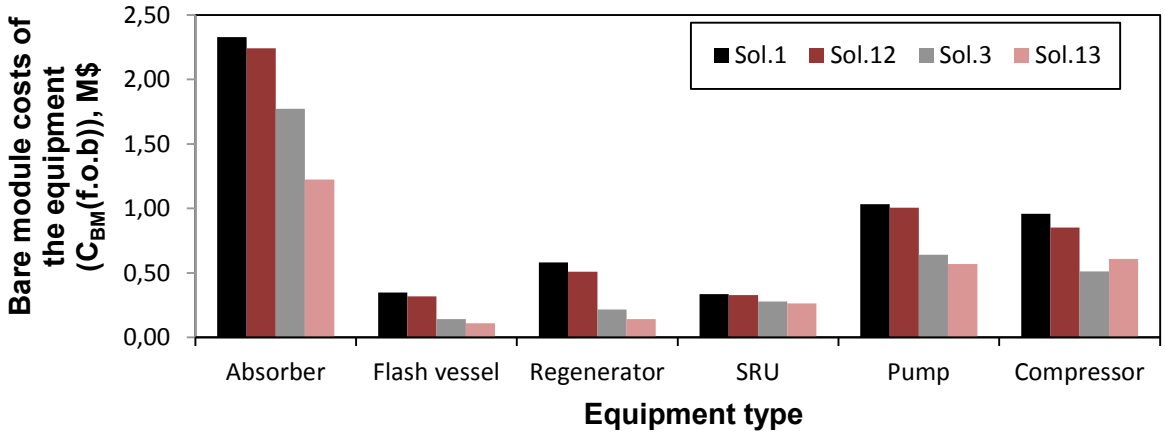

Figure 6-5 Bare module costs of the treatment plant equipment depending on the applied solution

Figure 6-5 indicates that:

- The absorber is by far the most costly equipment for all solutions, followed by the circulation pump and the compressor.

- In comparison to low-cat (Sol.12 and Sol.1), the high-cat solutions (Sol.3 and Sol.13) have benefits in the costs of all equipment (see the TCI_{2016} in **Table 6-13**) whereas the presence of the AAS (Sol.13) was seen clearly to be effective on the cost of the absorber which is the major cost driver of the equipment costs.

Beside the capital costs, the footprint of the plant is of high interest in cases where it is to be constructed directly on an offshore drilling platform. In this context, **Figure 6-5** shows not only the capital-cost-effectiveness of the Sol.13 but indirectly also its contribution to the lower footprint of the technology: the lower the C_{BM}(f.o.b), the smaller the equipment size - resulting in lower footprint. In addition, the size of the equipment is also a significant indicator for the requirement of solution inventory (or hold-up, HU). Determining the HU enables to evaluate the cost-effectiveness in terms of the WCI, one of the main constituents of the TCI (see section 6.2.4.2). Thus, the size of the major equipment of the plant and the amount of HU were identified based on the experimentally obtained data. These are compiled in **Table A- 24** in Appendix A-4 as supplemental to solvent system specific data and costs calculations. Considering all evaluated data, the Sol.13 was found to be the leading solvent system in terms of the investment capital-effectiveness as well as the footprint-effectiveness of the evaluated technology. However, the low-cat solutions Sol.12 and Sol.1 are advantageous in terms of the OMC, leading to a so far lower value for the LCoE (see **Table 6-13**). Thus now, investigations on the drivers on the operational expenses of the solvent system will be presented in the following section.

6.3.2.3 Impact of the solvent system on operational expenses

It was deducted from **Figure 6-4** that; the levelized operational expenses of the treatment plant, $OMC_{L,TP}$, have the highest share on the respective LCoE of each solution. As stated above, the OMC_{2016} was used for the assessment of the benefits of the solutions in terms of plant operation costs, instead of the levelized “future” costs (i.e. OMC_L). Thus, the OMC in M$/a (fixed and variable) was splitted into its individual cost elements (C_C, Fixed OMC and C_{OL} in %) using the

data given in **Table 6-13** (for the calculation of cost components of the OMC_{2016} refer to section 6.2.4.3). The results shown in **Figure 6-6** will enable to explore the reduction potentials in OMC, and thus, to carry out optimization.

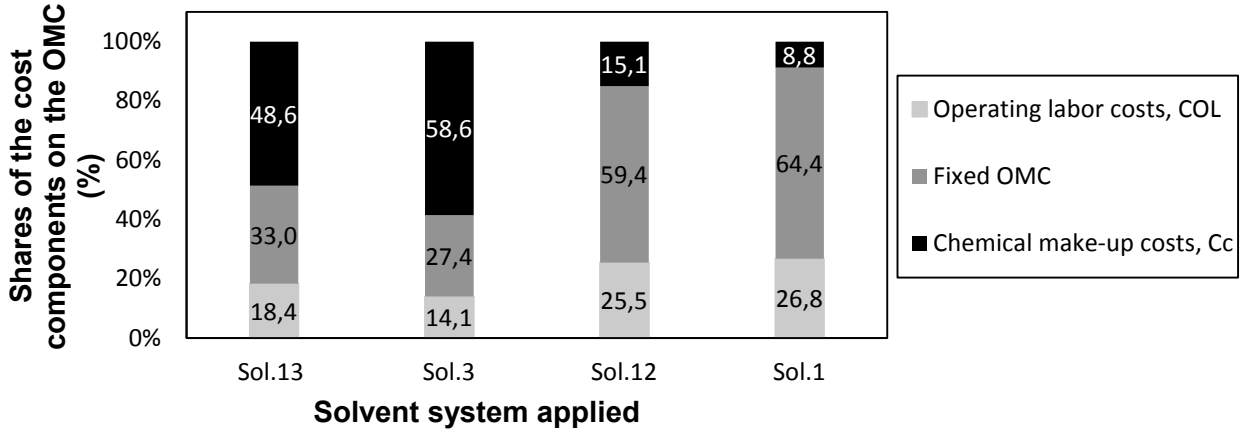

Figure 6-6 Shares of the individual cost components on the OMC_{2016} as a function of the applied solution

Figure 6-6 shows that:

- Speaking for the high-cat solutions (Sol.3 and Sol.13), the operating labor costs (C_{OL}) have the smallest share on the OMC_{2016} with 14.1 % to 18.4 %, respectively. The C_{OL} are followed by the fixed OMC in the range of 27 to 33 %. The chemical make-up costs (C_C), however, account by far for the biggest contribution to the OMC_{2016} representing between 48% and 59% - thus making it the main driver of the OMC_{2016} for both high-cat solutions.
- Contrary to this, for solutions with low iron concentration, the chemical make-up costs, C_C, have the smallest share causing around 15 % and 8 % of the OMC_{2016} when applying Sol.12 and Sol.1, respectively.

From **Figure 6-6** it was deducted that the dilute solution systems are more beneficial in terms of chemical make-up costs[33], which were found to be the dominant component of the OMC_{2016} and in turn for the LCoE of the high-cat solutions. Thus, in order to find out to what extent the LCoE of the high-cat solutions can be improved by reducing the chemical costs, a sensitivity study shall be conducted, in which first the parameters those influence the C_C are to be identified, and thereafter the sensitivity of the LCoE to these parameters is to be examined. This will be presented in the following section.

6.4 Sensitivity analysis of the LCoE

Taking the deductions from the investigations on the sulfur product properties (see section 4.2.6) into account, it can be stated that the characteristics of the sulfur particles, the composition of the solvent system as well as design and operation conditions of the plant strongly influence the chemical make-up costs. In order to identify the major figures related to the sulfur separation and impacting the C_C the following parameter (written in bold) were reviewed:

I. **Iron concentration**: High iron concentrations lead to faster precipitation of the sulfur resulting in smaller particle sizes (DeBerry, 1997) (see section 4.2.6.1)

II. **Particle size**: Smaller particles entrap more solution into them (see section 4.2.6.3).

III. **Particle shape**: Dentritic particles build channels in which the captured solution is held strongly, thus the washing efficiency is influenced adversely (see section 4.2.6.2).

[33] As it was mentioned before, the chemical make-up costs were assumed to be resulted from the mechanical solution loss during the filtration conducted with equipment in lab scale. Thus, the parameters impact the chemical costs which would emerge from degradation of the solution system were not reviewed hereby.

IV. **Filtration efficiency:** If the efficiency of the applied filtering unit is not good enough, the solution entrapped in the filter cake can not be recovered which leads to higher chemical costs to compensate the mechanical catalyst loss.

Hence, favorable conditions to reduce catalyst loss can be either achieved by adjusting the solvent composition (e.g. addition of sulfur thickening agents) or design modification (e.g. increasing the filtration efficiency and/or by placing a thickener upstream of the filtration unit). However, making assumptions on the changes in solvent compostion leads to interactions with high uncertainities as it was deducted that the capital costs (mainly equipment costs) of the treatment plant are highly sensitive to changes in solution composition. Thus, the investigations were focused on increasing the filtration efficiency by design modification/supplementation – without changing any other parameter – since it was concluded that this would enable to decrease the solution content of the filter cake, and in turn woul lead to reductions in chemical make-up costs. To this end, a sensitivity analysis is carried out encompassing the most critical variable of the C_C, the residual moisture of the filter cake, in order to explore the improvement potential of the LCoE, as presented in the following subsection.

6.4.1 Sensitivity of the LCoE to the residual moisture of the filter cake

Chemical make-up costs (C_C in M$/a) of the Sol.1, Sol.3, Sol.12 and Sol.13 (see **Table 6-13**) were calculated by considering the analytically obtained residual moisture data of the sulfur cakes and the chemical make-up ratios for the solutions given in **Table 4-15** and **Table 4-16**. Thus, the base values of the LCoEs determined for Sol.1, Sol.3, Sol.12 and Sol.13 (see **Table 6-13**) have been established with these values. In the context of the sensitivity analysis, the LCoEs were recalculated for cases assuming that the residual moisture of the filter cakes varies from 60 wt%, 40 wt%, 20 wt% to 0 wt%. Doing that, the sensitivity of the LCoE as a function of the selected system to residual moisture was obtained and is shown in **Figure 6-7**. The assumption, that more concentrated slurries can be achieved without the expenditure of extra capital (i.e. for additional equipment of the sulfur separation unit), is implied in the curves.

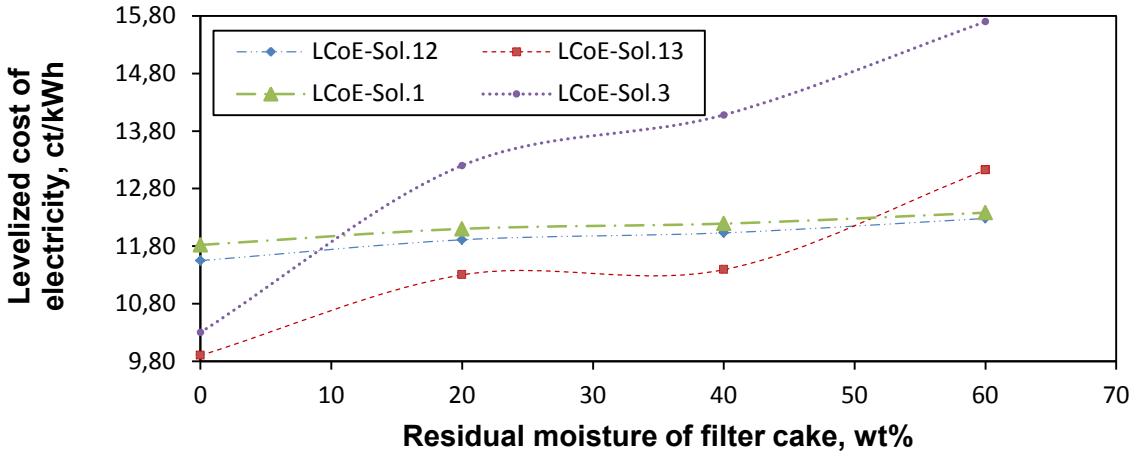

Figure 6-7 Sensitivity of the LCoE to the residual moisture of the sulfur cake of different solutions

Figure 6-7 reveals that:

- The differential in the LCoEs of the solutions decreases as the residual moisture values decrease from 60 wt% to 0 wt%.
- In high-cat solutions (Sol.13 and Sol.3), the differential is more magnified, indicating the respective LCoE is very sensitive to the solvent content in the filter cake. If the residual moisture is reduced from 60 to 0 wt%, this results in decreases of about 25 and 35 % in

the LCoEs of the Sol.13 and Sol.3, respectively (e.g. the LCoE of Sol.13 is cut down from 13.12 to 9.90 ct/kWh while the LCoE of the Sol.3 decreases from 15.70[34] to 10.30 ct/kWh).

- For Sol.13, the LCoE decreases significantly for a reduction of the residual moisture from 60 to 40 wt%, for lower values there is much less influence. For Sol.3, the LCoE decrease is more or less linear between 60 and 0 wt% residual moisture. A moisture reduction from 60 to 40 wt% can be achieved with much better justifiable technical efforts than further decrease.
- In contrary, the changes in the LCoEs of the low-cat solutions (Sol.1 and Sol.12) are nearly identical making it difficult to distinguish between the two lines. The decrease of the residual moisture from 60 to 0 wt% results in an averaged LCoE reduction of about only 5% implicating that the LCoE is relatively insensitive to the moisture content of the filter cake.

Thus, it can be deducted that:

- The insensitivity of the LCoE of the low-cat solutions towards the residual moisture content is consistent with the analysis result of the costs components of the OMC, from which it was seen that, it was not dominated by the chemical-costs but rather by the fixed OMC (see **Figure 6-6**). Thus, the optimization of the LCoE employing one of these solutions seems to be hardly influenced by reductions only in OMC.
- The sensitivity of the LCoE of high-cat solutions (Sol.3 and Sol.13, especially the Sol.3), appears to be high not mainly because of the unfavorable particle characteristics and design conditions, but rather due to the composition of the solution which can be related indirectly to the presence of the AAS, meaning: Since the economic analysis was conducted for a sour gas composition of 10 vol% CO_2 and 10 vol% H_2S, an alkali agent (e.g. KOH) had to be supplied to the system to maintain the solution pH. For the cases with AAS in the solution (e.g. Sol.13), the interval was longer and the amount of alkali supply was significantly lower than for an unbuffered solution, i.e. Sol.3, (refer to section 4.2.6.3). This explains the higher overall sensitivity of the LCoE to the catalyst loss in the filter cake for Sol.3 compared to Sol.13.

It shall be stated that the residual moisture in the filter cake is not only of high interest regarding the chemical costs, but also important for the produced elemental sulfur which, can be a very valuable raw material for the chemical industry. Decreasing the residual moisture content of the filter cake to the levels of pure sulfur (0 wt%) promotes the sale opportunities, which provides an additional revenue to the benefits from the main product, the electricity. The revenue stemming from the sales of sulfur was not yet considered in the economic analysis, since it is not the objective of this study. However, it was stated in a report on the Middle Eastern energy policy, that the economic feasibility of sour gas treatment projects has been greatly affected by sulfur prices (Matsumoto, 2013). Thus, a sensitivity analysis of the LCoE considering potential sales of sulfur is also conducted, as presented in the following subsection.

6.4.2 Sensitivity of the LCoE to the sulfur price

As it is stated in (Lockhart, T. et al., 2007), the elemental sulfur produced from sour gases represents an economic resource which partially offsets the electricity production costs –unless there is an imbalance between demand and supply in the market making sulfur prices uneconomic and leading to large stores of unsold sulfur products. (Sulfur Information Services, 2016) reported that it is extremely hard to predict if and when and to what extent the sulfur prices change in the market. For many years, Canada has been the world´s largest exporter of sulfur. Thus, the f.o.b. price of solid sulfur from the city of Vancouver, British Columbia, has been taken as the market benchmark. However, recently, the sulfur prices (in US $/ton) are reported to be strongly influenced by two other market players, China (the biggest sulfur importer - due to the growth in

[34] The experimentally determined residual moisture of the sulfur cake obtained from Sol.3 is 55 wt%. The LCoE for 55 wt% residual moisture was obtained as 15.31 ct/kWh, as presented in **Table 6-13**.

demand) and the Middle East (the biggest sulfur producer - due to abundant sour hydrocarbon sources). Substracting the revenue for the sales of sulfur (in M$/a by Eq.6-44) from the total revenue requirement for the integrated plant leads to a corrected LCOE value, called as $LCoE_{sulfur}$, as expressed in the Eq.6-45.

$$P_{sulfur\ (ton/a)} = \frac{P\ (ton/day)}{24\ h/day} * 7000\ h/a \quad \text{(Eq.6-43)}$$

$$R_{sulfur\ (M\$/a)} = P_{(ton/a)} * C_{(\$/ton)} * 10^{-6} \quad \text{(Eq.6-44)}$$

$$LCoE_{\ sulfur\ (ct/kWh)} = \frac{(TRR_{L,TP+PP}) - R_{sulfur}}{ANEP} \quad \text{(Eq.6-45)}$$

The annual sulfur production (P_{sulfur} in ton/a by Eq.6-43) corresponds to the ton/day equivalence of the sulfur capacity calculated for the gas composition considered in this study (i.e. 10 vol% $H_2S \rightarrow$ 41.4 LTPD see **Table 6-1**). The term C in Eq.6-44 denotes the f.o.b price of the sulfur in $/ton. In order to find out the sensitivity of the LCoE to the sales price of sulfur, two different sulfur prices in two dominating markets were taken as base: Due to large production in the Middle Eastern region, the sulfur prices are subsidized and projected to be around 100 $/ton (f.o.b), while it is predicted to be 140 $/ton (f.o.b) in China for the year of 2018 (the first-year of the operation). No inflation and escalation rates were included in the revenue of sulfur, since the forecasts of (CRU Group, 2016) state that price levels will remain stable at current values in the near term. The LCoEs calculated for different solvent systems by considering the total revenue (but not including the benefits from the sulfur sales (refer to Eq.6-35) and given in **Table 6-13** were taken as comparison basis (sulfur price = 0 $/ton). For the sensitivity analysis, the LCoEs were calculated considering the revenue resulting from the sulfur sales both for Middle-Eastern and Chinese market prices, as plotted in **Figure 6-8**.

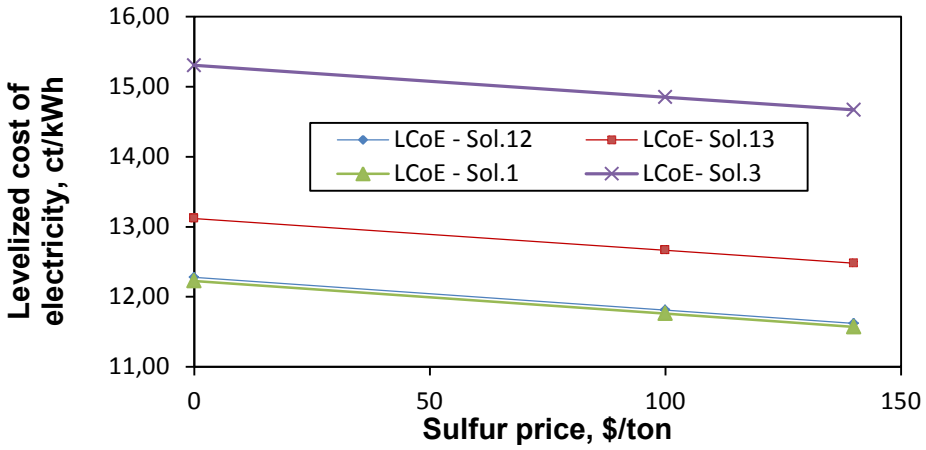

Figure 6-8 Sensitivity of the LCoE to the sulfur price

Figure 6-8[35] indicates that:

- The increase in sulfur prices from 0 $/ton (without selling sulfur) to 100 $/ton (Middle Eastern price) and to 140 $/ton (China price), results in an averaged LCoE decrease of about only 4 % and 6 %, for all solutions. This implicates that the LCoE is relatively insensitive to the achievable sulfur prices, which were assumed to remain stable over the operational period of the plant.

By summing up the economic analyses and evaluation studies carried out in this chapter and by taking the gained understanding about the economics into account, conclusions are presented in

[35] The changes in the LCoEs of the low-cat solutions (Sol.1 and Sol.12) are nearly identical, thus, these two lines are overlapped.

the following section yielding proposals for further optimization of the evaluated technology in terms of technical and economic aspects.

6.5 Conclusions and recommodations for economic improvement

Economic feasibility analyses and evaluations of the new liquid-redox technology for sour gas treatment process were carried out in this chapter, considering the established scenario, influences of various parameters and using the LCoE as a feasibility indicator. The latter was calculated by the TRR method (see section 6.2). The following conclusions can be drawn from these studies:

- The LCoE was calculated for power produced using an integrated-plant to be constructed in the Middle East. It was assumed that 11,947 Nm3/h of sour natural gas (80% CH_4, 10% H_2S and 10% CO_2) were treated by using Sol.13 (Siemens Solvent-2 as AAS, high catalyst concentration c_{Fe} = 0.5 mol/L), and the resulting gas stream (10,155 Nm^3/h: 94.12 vol% CH_4 and 5.88 vol% CO_2) was combusted in a SGT-750 unit yielding a power output of 38.1 MW. The technical data used for the calculations were explained (section 6.2.2) and were justified with financial assumptions (section 6.2.3).
  - Taking all these into account, the LCoE for the case of Sol.13 was determined to be **13.12 ct/kWh** (section 6.2.4.6).

- The LCoE for a power plant of the same capacity utilizing sweet gas was determined based on prices for the Middle East Region (section 6.3.1) in order to examine the competitiveness of the developed technology (profiting from subsidized domestic sour natural gas prices in the Middle East). For sweet gas, there was no requirement on a sour gas treatment unit any more. The higher LHV of the sweet gas compared to sour gas (after treatment) resulted in lesser fuel consumption of the turbine. Keeping all other parameters constant and applying the same approach, the LCoE produced from sweet gas was found to be **8.20 ct/kWh** and mainly dominated by the **fuel costs with a share of approx. 40 %.** Thus, a sensitivity analysis of this technology to the sweet gas prices in the world energy market was done. From this it was seen that:
  - If the sweet gas prices increase in the future and the domestic prices of the sour natural gas remain economically viable, the new “integrated plant” technology (which also enables the direct electricity production on offshore drilling platforms) can be competitive and even cheaper than the utilization of sweet gas. The influences of potential technological improvements which would impact the capacity factors of the power plant equipment as well as improve the capital costs of the treatment plant were not considered while doing this statement.

- Since **56 %** of the LCoE produced from the treated sour gas by applying the Sol.13 was found to be caused by the levelized total revenue required for the treatment plant, the most important cost components (capital and operational expenses which are directly related to the properties of the solvent system applied in the treatment plant) were analyzed to determine the most effective solution system. Three other solutions (Sol.1 and Sol.3 without AAS, Sol.12 with Siemens Solvent-2 but lower iron concentration c_{Fe} = 0.1 mol/L) were integrated in the analysis. All other parameters were held constant (e.g. gas composition and flow), except for those which were directly calculated from the solution-specific character (e.g. f_{sol}, f_{air}, liquid density, section 6.3.2). Herefore, the footprint of the technology influenced by the performance parameter of the selected solution was also considered since this can directly impact the economic viability of the intended technology especially for offshore applications. Thus, the least costly solution with lowest footprint will be considered as the most effective solution.
  - The LCoE of high-cat solutions (Sol.13 and Sol.3) were found to be higher than for solutions with low-cat (Sol.1 and Sol.12); however the plant footprint is significantly smaller for high-cat solutions.

- $OMC_{L,TP}$ was found to be the main cost driver for all solutions. Chemical make-up costs account for the largest contribution to LCoE for high-cat solutions indicating that there is a significant optimization potential in the costs of the high-cat solutions.

- The chemical costs (C_C) are mainly caused by the physical loss of solution during the filtration of the slurry. This is significant to the LCoE especially for the high-cat solutions (Sol.3 and Sol.13).

- In contrary, it was found that the OMC of the low-cat solutions were not driven by the C_C but rather by the fixed OMC, which indirectly were affected by the capital costs. The latter were dominated by the cost of absorber. Thus, it was concluded that optimization of the cost-effectiveness of the treatment plant employing low-cat solutions can hardly be achieved by reductions in OMC unless the performance of low-cat solutions can be enhanced. In addition, low-cat solutions were found to possess high footprint of the technology which is not desired.

- As a result of the sensitivity analysis, it was seen that the LCoE of high-cat solutions can be significantly reduced by decreasing the residual moisture in the filter cake of the sulfur separation units.

- Taking all into consideration, the Sol.13 was found to be effective (low CAPEX, low footprint) and promising (significant optimization potential in OMC) to be tested and optimized further in the pilot plant. With an appropriate filter design, the amount of residual solvent in the filter cake can be reduced to concentrations <20 wt% with much lesser technical efforts than further reductions. However, some additional capital costs will incur in this case and these must also be considered in the estimation of the LCoE. Thereafter, a cost trade-off must be done in order to reproduce the profitability of this optimization potential. Enhancing the filter efficiency in a cost-effective way will not only enable reductions in the LCoE by reducing catalyst losses but also increase the salability of the produced sulfur by decreasing its moisture content and thus contribute to the revenues and further decrease the LCoE.
  - This indicates that modifying the sulfur separation unit is a central part of improving the attractiveness of the evaluated H_2S removal method in the next phase of the development, namely the piloting of the technology.

- Although the LCoE was not found to be that sensitive to the current sulfur prices as it was to the residual moisture content, the decreases of all LCoEs with sulfur sales shown in **Figure 6-8** implicate that if the sulfur prices would rise extremely in the future (e.g. due to potential demand exploitation in the sulfur market), the LCoE would be affected more significantly.
  - Thus, the activities in the sulfur market should be object to much more attention as they can directly impact the promotion or hindrance of the economic viability and the profitability of the evaluated H_2S removal process for sour gas treatment.

Consequently, the studies intented, in the scope of this thesis, namely the selecting and screening the constituents of the appropriate liquid redox solvent systems for the removal of H_2S (chapter 3), the technical (chapter 4 and chapter 5) and the economical evaluation (chapter 6) were completed. The following chapter reviews the deductions from the addressed issues and highlights future perspectives.

7 SUMMARY AND OUTLOOK

Forecasts of the U.S. Energy Information Agency (EIA) indicate that conventional gas resources will not be able to cover the increasing global demand for electric power beyond a period of a few decades. After studying constituents, classification and global reserves of natural and sour gases, it became obvious that sour gas fields are getting more and more interesting for power generation - especially for countries which have abundant domestic reserves. A review done on the parameters of the natural gas specification for the upstream (i.e. pipelines) and downstream (e.g. gas turbine) applications showed that the combustion of sour gases (containing mainly H_2S and CO_2) without treatment can be extremely detrimental to environment (e.g. SOx emissions) and to gas turbine life and operation due to corrosion (e.g. hot gas path), erosion and fouling of the blades, sulfur deposition on the gas control valves (and thus NOx emissions), etc.. Despite the fact that the CO_2 is not toxic (unlike H_2S) it contributes to a lower heating value and obstructs the compression of the gas to the desired pressure. The viability of the development of lying untapped sour gas reserves and their usability for power production are directly connected to the economics of the treatment processes. Analyses of the features of commercially available sour gas sweetening technologies revealed that the processes applying the liquid redox technique can be favorable compared to the most common sweetening approach i.e. the Amin-Claus technology (employing organic alkanolamines as absorbents) in the case of small gas capacities (<10 MNm^3/d) and/or low acidic gas fractions (e.g. <<10 vol% H_2S and CO_2), since Amin-Claus is in those cases very capital expensive. In turn, Amin-Claus is suitable for ultra-sour gases (H_2S>25 vol%) and for installations with large capacities and footprint. However, the state of the art chelated-iron liquid redox processes are infeasible to remove high fractions of H_2S and CO_2 both from small and large gas capacities due to the chemical nature of their inorganic absorbent solutions (employing poor buffering capacities with respect to the pH value).

To cope with those limitations, Siemens AG has developed an **integrated liquid redox technology** by which the sulfuric components of the sour gas are converted directly into elemental sulfur in the liquid phase, the CO_2 is partially removed (treatment plant) and the treated gas is combusted to generate electricity on gas production sites (power plant). The treatment plant employs a solvent system comprising of an amino acid salt (AAS) as absorbent and a chelated iron as oxidation catalyst. Since this formulation is used for the first time in the developed technology, the impacts of its properties on the techno-economics of the treatment process have to be understood and optimized. The focus of the present work was, therefore, development and evaluation of new liquid systems for the liquid redox technique in order to achieve superior technical performance (i.e. stable, efficient for even high acidic gas fractions and easy operable) and an economic sour gas treatment process (low costs, small footprint), thus to propose solutions enabling the viability of the sour gas fields in power generation.

Firstly, configurations, formulations as well as niche and benefits of **state of the art iron-chelate liquid redox technologies** were studied thoroughly with the aim to gain a deep understanding of the key parameters influencing the effectiveness. The basic chemistry of all is comparable, but there are significant differences in their costs, sizes, efficiencies and application ranges resulting from the chemical nature of the applied solvent system: the solutions are generally mildly alkaline (pH 7 to 8.5), while the iron is held in solution by different ligands (Lig, e.g. EDTA) and serves as oxidizing agent. As absorbents, mainly aqueous inorganic alkali components (e.g. KOH) are used. In the first step, the H_2S (and some CO_2 to a minor extend) is absorbed from the gas into the liquid phase and directly oxidized there to elemental sulfur ($S^0\downarrow$) by the reduction of the chelated iron ((Fe(III)•Lig) to (Fe(II)•Lig)). Regeneration is performed in a second apparatus utilizing O_2 from air. The iron concentration in liquid redox solutions is limited by the solubility constraints and the thermodynamic stability of the applied ligand. This affects directly the solution circulation ratio required per H_2S contained in the sour gas stream. The thermodynamic stability of the ligand (referring the strength of the association between the chelating agent and the metal) does not only influence the soluble amount of the Fe(III), but also the regenerability of the reduced metal-ligand-complex (Fe(II)•Lig) to its active form in the solution (Fe(III)•Lig) as well as oxidative stability of the

liquid system. Whereas the H_2S is chemically converted and does not influence the pH of the solution, the CO_2 absorbed from the sour gas will account for a decrease in the pH in the absence of suitable buffering agents. However, the absorption of acidic gases into alkaline solutions (acid-base reaction), the complexation approach and the oxidation of the reduced form of the chelated-metal catalyst (redox reaction) are controlled by the pH of the solution. Above a certain pH maximum (pH > 10), the bond between the chelator and the Fe(III) is weakened, which leads to undesired precipitation of ferric hydroxide ($Fe(OH)_3$) and catalyst loss. Below a pH minimum (pH < 8) H^+ competes with Fe(II) for bonding to the chelating agent resulting in unsoluble iron sulfide precipitation (FeS↓), which leads to catalyst loss as well. Thus, the low pH-buffering capacity of the common liquid redox solutions containing inorganic absorbents is a challenging issue. Therefore, it can be concluded that selecting dedicated absorbents and complexing agents, which provide a favorable pH-buffering capacity, an efficient complexation process and in turn high iron concentrations, is crucial to assure a techno-economic feasibility of the liquid redox process.

Keeping the essential information deducted in mind, theoretical and experimental approaches were used within the content of this work for the **development of alternative aqueous liquid redox solvent systems** for the evaluated technology. During **pre-selecting of absorbents**, the highlighted features of the Siemens liquid redox technology, the reviewed pros and cons of the most common gas sweetening absorbents (e.g. organic: alkanolamines or inorganic: KOH) as well as desired specifications of a "suitable" solvent system for gas treatment (e.g. performance, stability, cost and availability) were followed. This put AAS into a position of potential commercial interest having advantages like low CH_4 solubility, low oxidative degradation potential as well as significant pH-buffering capacity even at high CO_2 contents. Different molecular configurations give AASs their special characteristics. Base strength (which influences alkalinity and loading capacity) and the accessibility of the amino group referring the steric hinderance (which impacts stability and the ease of regenerability) are decisive selection criteria. The alkalinity of an AAS and the stability of the absorption products formed in it decrease from primary via secondary to tertiary AAS, whereas the oxidative stability increases. Thus, the following AASs were identified as potential absorbent candidates for the stability screening.

- 3 primary AASs: glycinate (with carboxyl group, no steric hinderance), alaninate (sterically hindered with carboxyl group) and taurinate (sulfonyl group)
- 3 secondary AASs: sarcosinate and two other non-disclosed Siemens-absorbents (denoted as Siemens-Solvent1 and 2)
- 1 tertiary AAS: dimethylglycinate

Potential chelating agents were chosen based on the reviewed thermodynamic characteristics of the complexation phenomenon like steric interactions (referring to the coordination bonds between metal and chelator) and electronegativity (referring to the charge of the chelator). In this context, the stability constant of the metal-ligand-complex (K_{ML} – measured individually for the reduced and the oxidized form) and the nature of the donor groups of the chelating agent (either N or O atom or containing both) are decisive selection criteria. The K_{ML} is a measure of the reactivity of the initial Fe(III)-complex as oxidizing agent, besides being an indicator of the thermodynamic stability of the formed Fe(II)-complex. If the thermodynamic stabilizing ability of the Fe(II)•Lig is too high, it hinders the occurrence of the regeneration reaction; in turn, if the stability of Fe(III)•Lig is too high, it blocks the reaction of it with the dissolved H_2S – both makes the catalyst ineffective. Any ligand that features a difference in the decadic logarithm of the K_{ML} of Fe(II) and Fe(III) <4 is considered too weak as oxidizing agent. The chelators containing more N atoms than O atoms in comparison to other chelating agents are reportedly more sensitive towards oxidative attack. Based on these findings, the following chelating agents were chosen for the stability screening.

- 6 alkali salts of poly aminopolycarboxylate (APC) chelators: NTA, HEDTA, EDTA, IDA, DTPA and CDTA
- 2 alkali salts of non-APC chelators (containing no amino group): citrate (hydroxycarboxylate) and mannitol (polyhydroxylated sugar).

The stability screening of all pre-selected chelating agents in iron-complexes (Fe•Lig) was mastered under severe conditions (t=700 h; T=60 °C; P=atm.; c(Fe•Lig)= 0.1 mol/L; Lig:Fe=1.5 mol/L and 100 mol% excess air sparging) in a "stress test" sparged cell apparatus where the samples were exposed to both oxidative and thermal degradation conditions in a single system. Quantitative concentration measurements of the metal-ligand complexes (the Fe•Lig) were carried out with a UV-Vis spectrophotometer using a method developed within the scope of this work. Their stability ranking after 700 h was: NTA > HEDTA ≥ mannitol ≥ EDTA > IDA > citrate > CDTA > DTPA. For each ligand a specific degradation mechanism dominates (thermodynamic, thermal or oxidative), there is a cognitive correlation between their molecular structure and stability behavior. To enable the utilization of oxidatively and thermodynamically stable APC-chelators, which however are inresilient towards thermal attack (like DTPA), the process shall be operated at T<<60°C. In order to protect the thermally and oxidatively stable chelators (e.g. citrate, mannitol and CDTA) from thermodynamic decomposition, the pH of the solution shall be kept between 9.0<pH<9.5. To explore the improvement of the inevitable oxidative sensitivity of the some weak APC-chelators, (like IDA), the mannitol can be added as co-chelator yielding a dual chelator system (e.g. IDA+mannitol). The screening tests of 3 chelating blends of that kind showed that the oxidative stability of even weak APC-chelators can be enhanced by addition of one or more non-APC co-chelates to them. From 8 chelators and 3 dual chelate systems, 2 chelators had turned out as comparatively excellent ligands in terms of thermodynamic, thermal and oxidative resistance. One of them (Lig2) was encrypted for the rest of this study due to confidentiality reasons.

- the EDTA and the Lig2 were labelled as attractive chelators for the technical evaluation tests.

The stability screening of the pre-selected AASs - all containing the same amount of Fe•EDTA complexes - was executed in the already mentioned stress test setup under the same severe conditions with the addition of 1.65 mol/L of the respective AAS to the 0.1 mol/L Fe•EDTA solutions. The analysis of the AAS-contents of the solutions was performed by an external analytic service provider using LC-MS. The type of side chain and molecular structure of an AAS plays a significant role for the oxidative durability of it. The taurinate (primary AAS), which possesses a sulfonyl group rather than a carboxyl group, showed significantly higher stability (< 40 % decomposed) compared to the other two primary AAS (>60% of both alaninate and glycinate, were destroyed within 700 hours). The higher resilience of the dimethylglycinate (tertiary AAS, (< 5 % decomposed) in comparison to the three secondary AAS (< 15 % decomposed) indicates that the resistance against oxidative degradation of an AAS increases with the number of hydrogen substitutions. Thus all primary AASs (e.g. taurinate) in the end degraded much more rapidly than the others and were therefore ruled out. Consequently,

- dimethylglycinate and 2 non-disclosed secondary AASs (Siemens-Solvent 1 and 2) were labeled as most suitable absorbents in terms of thermal and oxidative resistance for technical evaluations tests.

For technical evaluations different solvent systems were formulated each containing iron complexed with one of the chelators as well as one the AASs selected in the previous section - with varying concentrations. Since the AAS-based chelated-iron solutions are used for the first time in the Siemens liquid redox technology, the technical data concerning the regeneration kinetics and the desulfurization performance of the developed formulations are so far absent in open literature.

The first aim was to gain a deeper understanding of the functional relationship between concentration/type of the species and reaction rate as well as orders. Thus, the kinetics of the reaction of the O_2 from the regeneration air with the Fe•EDTA were determined in three formulated solutions

(1) Fe•EDTA aqueous (w/o AAS),
(2) Fe•EDTA in a secondary AAS,
(3) Fe•EDTA in a tertiary AAS (dimethylglycinate)

with a variation of the process conditions (pH=9.5; T=30 and 60 °C; c_{ligand}=1.5-300 mol/m^3; cFe(II)=1-200 mol/m^3; c_{O2}=5-55 mol/m^3) using a stirrer cell reactor in batch mode operation. For the O_2 absorption rates, the stationary two film mass transfer model with neglected gas-side mass transfer resistance of Whitman was used, which was derived by Fick´s first law. The findings on the **reaction rates and regeneration kinetics** of the Fe(II)•EDTA can be correspondingly transferred to those of Fe(II)•Lig2 (the other chelator selected in the previous chapter) due to the comparable chemical structure and properties of both chelates. Therefore, no kinetic experiments were conducted with it. Under the variation of the process parameters given above, the regeneration reaction of Fe(II)•EDTA to Fe(III)•EDTA was found to be of first order related to O_2 in all three solutions even at higher dissolved O_2 concentrations and temperatures. However, an unexpected order change (from 1 to 2) with respect to Fe(II)•EDTA was observed resulting from the change in the rate determining reaction step when the reaction was performed at higher Fe(II)•EDTA concentrations (> 0.1 mol/L). The forward reaction of the rate determining step is apparently slow at lower Fe(II)•EDTA concentrations. This reveals that the regeneration process shall be operated at least with the critical Fe•Lig concentration, i.e. 0.1 mol/L, from where on the nature of the regeneration reaction changes. This step can be controlled by online monitoring of the pH (9.0 < pH < 9.5) and the redox potential values in the solutions. The redox potential is connected to the pH value, but strongly influenced by the concentration of oxidational species, and it indicates the feasibility of the regeneration. The temperature dependence of the kinetic constants obtained for all solutions followed the Arrhenius law. However, activating energies (E_a) were found to have the highest values for the regeneration of the Fe(II)•EDTA in the tertiary AAS (dimethylglycinate) solution. This indicated that the AAS type (secondary or tertiary) affects the steoreochemical equilibria of the chelating agent which resulted from buffering the H^+ ions formed at different capacities. Application of secondary AAS leads to a favorable stereogeometry of the complex and makes the regeneration easier. At higher c_{O2} and 60 °C, the oxidation of Fe(II)•EDTA to Fe(III)•EDTA is not the sole O_2-consuming reaction. The calculated stoichiometric coefficients of iron (v_B) in all solutions reveal that the extent of side reactions is connected to the presence of the EDTA (which is coordinated to iron) and not to the respective AAS. Thus, it can be concluded that the amount of O_2 supply, the chelated-iron concentration, the AAS type (in turn pH) and the temperature are key performance parameters for the viability and efficiency of the regeneration.

Considering these perceptions, 13 new solutions were formulated with varying compositions and concentrations of the constituents (AAS type: secondary or tertiary; chelate type: EDTA or Lig2; c[Fe(III)]=0.1-0.5 mol/L, Fe:EDTA=1-1.5, c(AAS)= 0.4-1.6 mol/L). In industrial gas treatment processes, the concentrations of active solvent constituents are usually given as weight percentages. For a scientific approach, however, molar ratios are essential, thus the molar concentrations of these species were regarded to provide a fair ranking between the investigated solvent systems, which can be categorized into two major groups:

(1) aqueous formulations with low and high iron-chelate concentrations without AAS (and thus comparable to the state of the art liquid redox solutions);

(2) aqueous formulations with low and high iron-chelate concentrations with AAS (either secondary or tertiary AAS in different concentrations; 0.4, 0.8 or 1.6 mol/L).

Since it was deducted that 0.1 mol/L is the critical Fe-concentration from where on selectivity and speed of the regeneration reaction changes, all “low-cat” solutions were formulated with 0.1 mol/L Fe•Lig-concentration, whereas all “high-cat” solutions contained the maximum soluble Fe•Lig amount of 0.5 mol/L. **Their overall efficiency, i.e. desulfurization and subsequent regeneration,** was examined during more than 2000 operation hours (approx. 160 hours per solution) in a test rig containing bubble column contactors (representing the absorption and the regeneration step of a treatment plant) in continuous operation with different gas compositions (c(H_2S)= 5-20 vol%; c(CO_2)=0-30 vol%) at T=25°C, P=atm. and pH=9.0. Consequently, design modification/process optimization proposals were accomplished based on the operational behavior of each investigated solution. The stable, efficient and economic operation regime of each formulation was indicated by the decisive cost driving factors: the required solution pump around ratio (f_{sol}) and the regeneration air demand (f_{air}) per dosed H_2S. More diluted solutions (low-cat w/o AAS vs. high-cat w/o AAS) are easier to operate (no foaming) and give faster

response towards the variation in the process conditions (faster stabilizing of the pH and the redox potential). However, they are only feasible for low H_2S loads (up to 10 vol%) and small CO_2 fractions (up to 5 vol%). All high-cat solutions with an excess amount of EDTA provided beneficial f_{sol} independent from the presence or absence of an AAS or of CO_2 in sour feed gas, but led to an increase in the viscosity and density of the solutions. Thus, they necessitated higher f_{air} ratios in comparison to low-cat solutions for the same amount of H_2S supply. Based on analytic results oxidative degradation (which would also lead to higher air consumption) could be ruled out. It can be concluded that the higher f_{air} ratios solely resulted from the adversely affected (decelerated) mass transfer of the O_2 into the more concentrated liquids. The establishment of the pH-steady-state in all solutions w/o AAS took significantly longer than in those containing AAS, which necessitated alkali supply to them. If CO_2 is also contained in the gas, the solutions formulated with both AAS, either secondary or tertiary, featured higher turn down capacities in terms of acidic gas contents. In comparison to dimethylglycinate based solutions, the formulations with secondary AAS required a shorter residence time in both contactors which can be explained with the higher buffering capacity and easier regeneration. The type of both organic molecules, ligand and AAS, influences the regeneration air demand per dosed H_2S as well as the optimal regeneration rate by possessing different provisions for the oxidation of the Fe(II) to Fe(III). One secondary AAS with high-cat concentrations (named “Sol.13”) led to a low f_{sol} by enhancing the loading capacity with a high separation efficiency (i.e. H_2S_{out} ~1 ppmv) even for ultra-sour gas compositions (H_2S= 20 vol% and CO_2= 30 vol%). The “Sol.13” is also beneficial for the thermodynamic equilibria of the Fe•EDTA by stabilizing the overall ionic strength of the solution (and thus steric and electric influences in the ligand) resulting in beneficial f_{air} ratios which in turn minimize the occurrence of possible degradation.

The composition of the solvent system and the sour feed gas does not only affect the f_{sol} and f_{air} but also the precipitation behavior, the composition (quality) and the particle characterization of the solid produced. According to elemental analyses of all obtained solid cakes (DIN 51732), they were confirmed to be elemental sulfur (>88 wt%, dry). High initial Fe(III)-concentrations and relatively low Fe(II)-concentrations during operation lead to faster oxidation of H_2S and in turn fast formation of sulfur. This results in smaller size particles, which tend to be flotating on the gas-liquid interfacial area. In addition, if the Fe(II)-concentration is too low or the amount of sparged air and in turn dissolved O_2 is much higher than needed, components such as sulfur oxo-anions are formed. The shape characterization and statistical evaluation of the distributions (size and mass) of the solid sulfur particles according to the FBRM method used for analyzing revealed that they were made up of dentric particles with mean sizes in the order of 20-35 microns. On the other hand, the sulfur produced at the beginning of each test run had a mean diameter size of 10-15 microns, so the operation time influences the particle size/growth. The dentric morphology of the particles can adversely affect the distribution of the water molecules through larger channels in the filter cake. Thus, to increase the effluent filterability and to improve the operability of the filtration step by avoiding clogging, the suspension taken from the treatment plant shall be fed into downstream unit operations such as settlers and/or hydrocyclones. By enabling the growth of particles, recovering the maximum amount of catalyst can be achieved while using as little wash water as possible. Fe(III)-concentrations and O_2 supply rates which are too high shall be prevented, the induction period for the agglomeration of the sulfur particles shall be envisaged while designing the unit operations for large scale. In addition, since alkaline media containing significant salt fractions can be corrosive, it is recommended to use the stainless steel construction material of AISI 316 grade (e.g. DIN No. 1.4571) for all plant parts in contact with the solvent system.

Although the degradation detected during the 160 hours of the technical evaluation tests was negligible for all formulations and had no observable adverse impact on their performance, long-term projections can lead to remarkable solvent refill costs, depending on the process conditions. A literature review on so far available **degradation studies** revealed two potential degradation routes of the AAS and/or the ligand under the process conditions of interest: radical induced and autocatalytic oxidation. Experiments were planned and conducted under respective conditions

(T=30-60 °C; EDTA:Fe=1-1.5 mol/L; c(Fe•EDTA)= 0.1-0.5 mol/L; c(AAS)=1.6 mol/L) in order to verify the occurrence of the potential degradation routes in the selected solvent systems. **The radical induced oxidation** of the EDTA follows a Fenton type mechanism in which H_2O_2 is formed and free radicals are generated. Major ionic degradation products detected are formate and oxalate. Thiosulfate is an effective radical scavenger and chelate-stabilizer. **Autocatalytic oxidation** refers to electron transfer from the organic constituents (e.g. EDTA, AAS) to the metal, independent from the presence of radicals or dissolved O_2. This route is promoted by elevated temperatures (T>30°C) and metal concentrations (>0.1 mol/L) even under the exclusion of O_2 but with CO_2 loading. This implies strongly that there is a pH effect and not a CO_2 specific reaction. The autocatalytic oxidation of the EDTA involving the electron transfer mechanism is inevitable since it is directly linked to the presence of the oxidized form of the iron (i.e. Fe(III)), the reaction partner of the dissolved O_2 in the regenerator, but it can be minimized by providing optimal operation conditions. As long as the iron is kept complexed by EDTA, the electron transfer process takes place preferably between the EDTA and the Fe(III) and, and thus the AAS can be protected and is not autocatalytically oxidized by electron transfer to the Fe(III). In addition, if there is not enough excess EDTA available to keep the iron complexed, the iron precipitates as Fe_2O_3 and further oxidizes all available organic species. To conclude, controlling of the excess air supply via the redox potential value (-300 < E(mV) < -200), addition of thiosulfate solution (e.g. at least 1:1 molar to EDTA) at the beginning, operation at T < 60°C and always with an excess chelator ratio (e.g. 1.2<Lig:Fe<1.5) are recommended for future applications to provide a safety margin for the suppression of the degradation of the employed solvent system.

As a result of the technical evaluations, “Sol.13” (Siemens-Solvent2, c_{Fe} = 0.5 mol/L), which showed the best performance even at ultra-high gas acidic gas fractions in the sour feedgas (H_2S = 20 vol% and CO_2 = 30 vol%), was chosen for the **economic analysis** to obtain commercial aspects of the evaluated process for a semi-industrial demo phase. The established scenario (location and capacity of the plant to be constructed) is used only for the purpose to conduct the economic analysis in the scope of this study and does not reflect any actual commercial investment decision made by the developer company (i.e. Siemens AG). Thus, there is no contractual liability of the Siemens AG regarding the costs obtained in the scope of this study. The Levelized Cost of Electricity (LCoE) was calculated by applying the Total Revenue Requirement (TRR) method for power produced in an integrated plant (treatment plant + power plant) to be constructed in the Middle East. It was assumed that 11,947 Nm^3/h of sour natural gas (80 vol% CH_4, 10 vol% H_2S and 10 vol% CO_2) were treated by using “Sol.13”, and the resulting gas stream (7997 kg/h = 10,155 Nm^3/h, 94.12 vol% CH_4 and 5.88 vol% CO_2) was combusted in a Siemens gas turbine SGT-750 unit yielding a power output of 38.1 MW. Using technical data obtained from the operation of the lab plant (especially solution pump-around ratio and regeneration air per H_2S contained in the sour gas) and conventional financial assumptions, the LCoE for the case of “Sol.13” was determined to be 13.12 ct/kWh. Since 56% of this LCoE (when applying “Sol.13”) was found to be caused by the treatment plant, the important cost components (capital and operational expenses which are directly related to the properties of the solvent system applied in the treatment plant) were analyzed to determine the most effective solution system. Three other solutions (“Sol.1” and “Sol.3” without AAS and “Sol.12” with Siemens-Solvent2 but lower iron concentration c_{Fe} = 0.1 mol/L) were integrated in the analysis. All other parameters (e.g. gas composition and flow as well as financial assumptions of the established scenario) were held constant, except for those which were directly obtained from the solution-specific character (e.g. f_{sol}, f_{air}, liquid density). Herefore, the footprint of the technology influenced by the performance parameters of the selected solution was also considered, since this can directly impact the economic viability of the intended technology especially for offshore applications.

The operational expenses of the treatment plant were found to be the dominating component for all solutions. The chemical make-up costs resulting from mechanical losses during the separation of the sulfur product, based on the moisture contents obtained under lab conditions (simple filtration process), account for the largest contribution to the LCoE for high-cat solutions indicating that there is a significant optimization potential in the costs by optimization of the filtration step.

The sensitivity analysis showed that for “Sol.13” even only a slight improvement in the moisture content of the sulfur cake, which can be accomplished easily by applying an industrial, advanced filtration technology in the piloting phase (efficient washing, pressing and air blowing) will give a clear cost advantage. In contrary, it was found that the operation and maintenance costs (OMC) of the low-cat solutions were not driven by the chemical costs, but rather by the fixed OMC, which were affected indirectly by the capital costs. The latter were dominated by the costs of absorber and pumps. Thus, it was concluded that an optimization of the cost-effectiveness of a treatment plant employing low-cat solutions can hardly be achieved by reductions in OMC unless the performance of low-cat solutions can be enhanced. Besides this, low-cat solutions were found to cause high footprint of the technology which is unfavorable.

In addition, the LCoE for a power plant of the same capacity utilizing sweet gas was determined to be 8.20 ct/kWh based on prices for the Middle East Region in order to examine the competitiveness of the evaluated liquid redox technology (profiting from subsidized domestic sour natural gas prices in the Middle East). This indicates that using the technical data obtained from lab plant and under assumptions done, electricity production from sour gas is currently more cost-intensive than from sweet gas. Therefore, a sensitivity analysis was conducted and reveals that if the sweet gas prices increase in the future and the domestic prices of the sour natural gas remain subsidized, the new “integrated plant” technology (which enables also the direct electricity production on offshore drilling platforms) can be competitive and even cheaper than the utilization of sweet gas. Even if the sweet gas prices remain stable in the future, in-situ treatment of sour gas to produce electricity is the only option for the regions where no established pipeline infrastructure but only sour gas fields are available – in order not to leave these high potentials lying untapped.

The results of this study supported the expected positive influences of the utilization of the AAS containing chelated iron to achieve the specific targets of the evaluated Siemens liquid redox process. Taking all into account, the “Sol.13” was found to be effective (low capital invest and footprint) and promising (significant reduction potentials in operational expenses – especially by improvement of the solvent losses in the filtration step), and thus, appropriate to be tested and optimized further in a piloting respectively a semi-industrial demonstration phase as next steps to determine absolute rates of performance and costs during long runs. It can be expected that these will be successful, and the economic utilization of sour natural gas reserves for power generation in medium size gas turbines can be accomplished by the liquid redox technique employing AAS.

REFERENCES

AACE. (2003). Conducting Technical and Economic Evaluations as Applied for the Process and Utility Industries TCM Framework: 3.2 – Asset Planning, 3.3 – Investment Decision Making, AACE International Recommended Practice No. 16R-90. Advancement of Cost Engineering International.

Abbott, D. J. et al. (2009). The Impact of Natural Gas Quality on Gas Turbine Performance. European Turbine Network.

Al-Mughiery, S. S. et al. (1992). The SulFerox Process for High Pressure Natural Gas Treating. Paper presented at the 1992 Liquid Redox Sulfur Recovery Conference, Austin, TX/USA, October 4-6, 1992.

Anerousis, J. P. et al. (1984). An Updated Examination of Gas Sweetening by the Iron Sponge Process. SPE 13280, Houston, TX/USA, September 16-19, 1984.

Aronu, E. U. et al. (2013). Understanding Precipitation in Amino Acid Salt systems at Process Conditions. Energy Procedia-GHGT-11, Vol.37, pp.237-240.

Ballaguet, J. P. et al. (2001). Pilot operating experience with a new redox process for the direct high pressure removal of H_2S. in Proceedings 80th GPA Conf., San Antonio, TX/USA, March 12-15, 2001.

Bedell, S. A. (1990). Patent No. U.S.4,891,205. Stabilized chelating agents for removing hydrogen sulfide.

Bedell, S. A. (1992). Patent No. U.S.5,09,691. H_2S abatement with stabilized chelates in geothermal drilling.

Bedell, S. A. (2009). Oxidative degradation mechanisms for amines in flue gas capture. Energy Procedia GHGT-9, Vol.1, pp.771-778.

Bedell, S. A. et al. (1987). Chelation Chemistry in Geothermal H_2S Abatement. Geothermal Resources Council Bulletin, Vol.16, No.3, pp.3-6, August, 1987.

Beenackers, A. A. & Wubs, H. J. (1993). Kinetics of the oxidation of ferrous chelates of EDTA and HEDTA in aqueous Solution. Ind. Eng. Chem. Res., Vol.32, pp.2580-2594.

Behringer, A. (2015). Investigations on the oxidation kinetics of a chelated metal catalyst in amino acid salt solutions for sour gas treatment when applying liquid redox technique. Technische Universität München, Master thesis performed at Siemens AG in Frankfurt am Main, Germany, June 24, 2015.

Bengoa, C. et al. (2007). Phenol oxidation promoted by chelated iron: Degradation pathway. Proceedings of the 10th International Conference on Environmental Science and Technology, Cos Island, Greece, September 5-7, 2007.

Bierdel, T. et al. (2013). Life Cycle Value for Combined Cycle Power Plants - Siemens AG. PowerGen Asia, Bangkok/Thailand, October 2-4, 2013.

Blytas, G. C. (1983). Patent No. U.S.4,421,733. Method of removing hydrogen sulfide from gases utilizing a stabilized metal chelate solution.

Blytas, G. C. & Diaz, Z. (1982). Patent No. U.S.4,356,155. Sulfur process.

Borsboom, H. et al. (2001). New Insights into the Claus Thermal Stage Chemistry and Temperatures. Brimstone 2002 Sulfur Recovery Symposium, Banff, Alberta/Canada, May 2-10, 2002.

Boulegue, J. (1978). Solubility of elemental sulfur in water at 298 K. Phosphorus Sulfur and Silicon and the Related Elements, Vol.5, No.1, pp.127–128.

Boyce, M. P. (2012). Gas Turbine Engineering Handbook (4th ed.). Elsevier Science.

Braatz, R. D. et al. (2003). Measurement of particle size distribution in suspension polymerization using in situ laser backscattering. Sensors and Actuators, Vol.96, pp.451-459.

Brooks Instrument. (2016). Products: GF40 Series Elastomer Sealed Thermal Mass Flow Controllers & Meters. Retrieved from http://www.brooksinstrument.com/products/mass-flow-controllers/thermal-elastomer-sealed/gf40-series, April 14, 2016.

Brown, E. R. et al. (1987). Mechanism of oxidation of ferrous polydentated complexes by dioxygen. Journal of Electroanalytical Chemistry and Interfacial Electrochemistry, Vol.222, pp.173-192, November, 1987.

Bryan Research & Engineering, Inc. (1997). Claus Sulphur Recovery Options. Petroleum Technology Quarterly, Technical papers, pp.57-61, Bryan, TX/USA, 1997.

Buenger, C. W. (1988). The Sulferox Process-Plant Design Considerations. Proceedings of the Gas Processors Association 67th Annual Convention, pp.56-62, 1988.

Butler, J. et al. (1982). Reaction of Iron-EDTA chelates with the superoxide radical. Archives of Biochemistry and Biophysics, Vol.218, No.1, pp.174-178, October 1, 1982.

Canty, D. (2012). The Middle East Sour Oil & Gas Upstream Profile. Retrieved from http://www.arabianoilandgas.com/article-10245-the-middle-east-sour-oil-gas-upstream-profile/1/., February 1, 2016.

Carroll, J. J. et al. (1992). The System Carbon Dioxide-Water and the Krichevsky-Kasarnovsky Equation. Journal of Solution Chemistry, Vol.21, pp.607-621.

CER. (2008). Final Report on the Requirements for a Single Natural Gas Quality Standard for Northern Ireland and the Republic of Ireland. The Commission for Energy Regulation, December 11, 2008.

Chen, D. et al. (1995). Studies on the mechanism of chelate degradation in iron-based, liquid redox H_2S removal processes. Can. J. Chem, Vol. 73, pp.264-274.

Cher, M. et al. (1955). The kinetics of the oxygenation of ferrous iron in phosporic acid solution. Journal of American Chemical Society, Vol.77, No.3, pp.793-798, February 1, 1955.

Clevette, D. J. & Orvig, C. (1990). Comparison of ligands of different denticity and basicity for the in vivo chelation of aluminium and gallium. Polyhedron, Journal for Research in Organic Chemistry, Vol.9, No.2/3, pp.151-161, Pergamon Press, Oxford/UK, 1990.

Connors, K. A. (1990). Chemical Kinetics: The Study of Reaction Rates in Solution. New York; NY/USA: VCH Publishers, Inc.

Creighton, T. H. (1993). Proteins; structures and molecular properties - Chapter 1 (2nd ed.). San Francisco, CA/USA: W. H. Freeman & Co. Ltd., 1993.

CRU Group. (2016). Sulphur Market Outlook. Retrieved from CRU-The Independent Authority: Mining, Metal and Fertilizers: http://www.crugroup.com/market-analysis/products/SulphurMarketOutlook, March 8, 2016

Dalrymple, D. A. et al. (2005). URS Process Technologies, CrystaSulf-One-Step H_2S to Sulfur Conversion. Proceedings of the 84th Annual Convention of Gas Processors Association, San Antonio, TX/USA, March 13-16, 2005.

Danckwerts, P. (1951). Significance of liquid-film coefficients in gas absorption. Ind. & Eng. Chem. Res., Vol.43, pp.1460-1467.

DeBerry, D. (1997). Chemical evolution of liquid redox processes. Environmental Progress, Vol.16, No.3, pp.193–199.

DeCoursey, W. J. (1974). Absorption with chemical reaction: Development of a new relation for the Danckwerts model. Chemical Engineering Science, Vol.29, No.9, pp.1867-1872, September 1974.

Demmink, J. F. et al. (1998). Gas desulfurization with ferric chelates of EDTA and HEDTA: new model for the oxidative absorption of hydrogen sulfide. Ind. and Eng. Chem. Res., Vol.37, No.4, pp.1444 -1453, 1998.

Deshmukh, G. M. et al. (2012). Oxidative Absorption of Hydrogen Sulfide using Iron-chelate Based Process: Chelate Degradation. J. Anal. Bioanal. Techniques 2012, Vol.88, No.3, Special section pp.1.

Devold, H. (2010). Oil and Gas Production Handbook. Oslo/Norway: ABB Oil and Gas.

Diaz, Z. (1983a). Patent No. U.S.4,388,293. H_2S removal.

Diaz, Z. (1983b). Patent No. U.S.4,400,368. H_2S removal process.

Diaz, Z. (1983c). Patent No. U.S.438,291,8. Method of removing hydrogen sulphide from gases utilizing a stabilized iron chelate solution.

Diaz, Z. & Blytas, G. C. (1982). Patent No. U.S.4,3448,368. Method of removing hydrogen sulfide from gases.

DoL. (2015). Economic News Release - Productivity and Costs. Retrieved from U.S. Department of Labor (DoL) - Bureau of Labor Statistics: http://www.bls.gov/bls/newsrels.htm, Februar 2, 2016.

Ebrahimi, S. et al. (2003). Kinetics of the reactive absorption of hydrogen sulfide into aqueous ferric sulfate solutions. Chemical Engineering Science, Vol.58, pp.417-427, 2003.

ECRA. (2006). Updated generation planning for the Saudi electric sector, Prepared for Electricity & Cogeneration Regulatory Authority (ECRA), Document No. PN CER2272. Saudi Arabia: Center for Engineering Research.

EIA. (2014). Electricity market module of the national energy modelling system: Module documentation. Retrieved from EIA: http://www.eia.gov/forecasts/aeo/nems/documentation/electricity/pdf/m068%282014%29.pdf, January 8, 2016.

EIA. (2016a). International Energy Statistics. Retrieved from U.S. Energy Information Administration: http://www.eia.gov/cfapps/ipdbproject/IEDIndex3.cfm?tid=3&pid=3&aid=6, January 15, 2016.

EIA. (2016b). Updated Capital Cost Estimates for Utility Scale Electricity Generating Plants. Retrieved from EIA, U.S. Energy Information Agency: https://www.eia.gov/forecasts/capitalcost/pdf/updated_capcost.pdf, February 12, 2016.

Eliassi, A. et al. (1998). Densities of Poly(ethylene glycol) + Water Mixtures in the 298.15−328.15 K Temperature Range, J. Chem. Eng. Data, Vol.43, No. 5, pp.719-721.

EPRI. (2011). Program on Technology Innovation: Integrated Generation Technology Options, Report No. 1022782. Palo Alto, CA/USA: Electrical Power Research Institute (EPRI).

Fair, J. R. et al. (1997). Gas Absorption and Gas Liquid System Design, Chapter-14. In Perry´s Chemical Engineers´ Handbook (7th ed.). McGraw Hill Companies, Inc.

Fischer, B. (2013). Investigation of the Reactions when applying Amino Acid Salts for Post Combustion Carbon Capture Processes; degradation pathways, environmental and economic impact, Dissertation performed at Siemens AG, Frankfurt am Main. Published by University of Duisburg-Essen, Germany, October 23, 2013.

Foxall, B. (1986). Sulfur Froth Filtration and Washing Prior to Melting. Proceedings of the 1986 Stretford User's Conference, pp. 134, Austin, TX/USA, May 5, 1986.

Gas turbines catalogue. (2016). Siemens gas turbine portfolio - Technical data of industrial gas turbines: SGT-750. Retrieved from http://www.energy.siemens.com/ru/pool/hq/power-generation/gas-turbines/downloads/gas-turbines-siemens.pdf, July 7, 2016.

Goar, B. G. et al. (1986). Sulfur Recovery Technology. Energy Progress, Vol.6, No.2, pp.71-75.

Görner, K. et al. (2013). Optimization of CO_2 capture from flue gas with promoted potassium carbonate solutions. Energy Procedia GHGT-11, Vol.37, pp.1554-1565, 2013.

Grande, M. (1987). Experiences with Rotary-Drum Vacuum Filters. Proceedings of the 1987 Stretford Conference, pp. 185, Austin, TX/USA.

Greaves, D. et al. (2008). Measuring the particle size of a known distribution using the focused beam reflectance measurement technique. Chemical Engineering Science, Vol.63, No.22, pp.5410-5419, November, 2008.

Grozs-Röll, F. B. (1982). Gas-Liquid mass transfer with static mixing units. Paper presented at Fourth Eur. Conf. Mixing, pp.225, 1982.

Hancock, R. D. et al. (1997). Design of ligands for the complexation of Fe(II)/Fe(III) in the catalytic oxidation of H_2S to sulfur. Can. J. of Chem., Vol.75, No.5, pp.591-600, Canada, 1997.

Hardison, L. C. & McManus, D. (1987). Chelated Iron Catalyzed Conversion of Gaseous Sulfur Compounds - What to Expect in the 1990s. Paper No.5a presented at AIChE Summer National Meeting, Minneapolis, MN/USA, August 16-19, 1987.

Hargis, L. G. (1988). Analytical Chemistry: Principals and Technique, Chapter-11: EDTA Titrations (8th ed.). Prentice Hall Inc.

Hauke, S., Joh, R., Sönmez, H. G., Nickelfeld, H. W., & Schüler, M. (2016). Invention disclosure. Verbesserter Prozess zur Abtrennung von H_2S aus Sauergas durch die Verwendung eines Kontaktapparates mit statischen Mischern. Frankfurt am Main: Siemens AG, February 16, 2016.

Heeres, E. J. et al. (2005). Kinetics of the reaction of Fe(II)EDTA with oxygen in aqeuous solutions. Ind. Eng. Chem. Res., Vol.44, pp.8190-8198.

Heguy, D. L. (2003). Consider optimized liquid-redox processes to remove sulfur. Hydrocarbon Processing, Vol.82, No.1, pp.53-57, 2003.

Hessler, R. (2015). Degradation Behaviour of Chelates by Applying Liquid Redox Technique for Sour Gas Treatment. RWTH Aachen, Bachelor thesis performed at Siemens AG in Frankfurt am Main, Germany, November 30, 2015.

Higbie, R. (1935). The rate of absorption of a pure gas into a still liquid during short periods of exposure. Transactions of the American Institute of Chemical Engineers, Vol.35, pp.365-389.

Hoff, K. A. et al. (2012). Solvent development in post combustion CO_2 capture, Proceedings of GHGT-11. Energy Procedia, Vol.37, pp.292-299, Kyoto, Japan, November 18-22, 2012.

Hogendoorn, K. J. A. et al. (2008). Physiochemical Properties of Several Aqueous Potassium Amino Acid Salts. Journal of Chemical & Engineering Data (American Chemical Society Publications), Vol.53, No.6, pp.1286–1291, June, 2008.

Holland, F. A. & Wilkinson, J. K. (1997). Perry´s Chemical Engineers´ Handbook, Chapter 9: Process Economics (7th ed.). McGraw Hill.

Holmes, A. M. (1974). Stretford H_2S Removal Process Proved in Use. Oil and Gas Journal, Vol.72, No.35, pp.56-58, Houston, TX/USA, 1974.

Hook, R. (1997). An Investigation of Some Sterically Hindered Amines as Potential Carbon Dioxide Scrubbing Compounds. Ind. Eng. Chem. Res., Vol.36, No.5, pp.1779-1790.

Hydrocarbon Processing®. (2004). Gas Processes Handbook, TX/USA, Gulf Publishing Company.

IGU. (2015). Wholesale Gas Price Formation - 2015 Edition: A global review of price formation mechanisms 2005-2014. Fornebu: International Gas Union (IGU). Retrieved from http://www.worldenergyoutlook.org/media/weowebsite/2008-1994/weo2004.pdf, March 5, 2016.

IUTA e.V. (2002). PREISATLAS: Ableitung von Kostenfunktionen für Komponenten der rationellen Energienutzung, Teil II: Anlagen zur Kraft-Wärme-Kopplung. Duisburg-Rheinhausen: Stiftung Industrieforschung.

Jain, A. et al. (1978). Design and Testing of a Generalized Reduced Gradient Code for Nonlinear Programming. ACM Transactions on Mathematical Software (TOMS), Vol.4, No.1, pp.34-50, New York, NY/USA, March 1978.

Kohl, A. L. et al. (1997). Gas Purification (5th ed.). Houston, TX/USA: Gulf Publishing Company.

Kumar, A. (1982). Kinetics of complexation and oxidation of ethanolamine and diols by silver(II). The Journal of Physical Chemistry, Vol.86, No.9, pp.1674-1678, April 1982.

Kurimura, Y. et al. (1968). Oxygen oxidation of ferrous ions induced by chelation. Bull. Chem. Soc. Japan, Vol.41, pp.2234-2242.

Lambert, D. G. & Jones, M. M. (1966). Oxidation of Some Chelating Agents and Complexes with Alkaline Ferricyanide. Journal of the American Chemical Society, Vol.88, No.20, pp.4615-4618, 1966.

Lampton, R. D. & Hopkins, T. M. (1986). Patent No. U.S.4,614,644. Process for removal of H_2S from geothermal steam and the conversion to soluble sulfur compounds.

Lockhart, T. et al. (2007). New upstream technologies: Sour oil and gas management. In Encyclopedia of hydrocarbons (Volume III). Roma/Italy: Marchesi Grafiche Editoriali S.p.A.

Ludwig, E. (1997). Applied Process Design for Chemical and Petrochemical Plants (3rd ed.), Vol.2. Houston, TX/USA: Gulf Professional Publishing.

Lundtorp, K. (2001). The Ferrox Process in an Industrial Scale - Developing a Stabilisation Process for Airpollution Control Residues from Municipal Solid Waste Incineration. PhD Thesis, TU Denmark, Copenhagen, Denmark.

Majchrowicz, M. E. (2014). Amino Acid Salt Solutions for Carbon Dioxide Capture, Dissertation published by University of Twente, The Netherlands, Retrieved from http://dx.doi.org/10.3990/1.9789036537803, November 7, 2014.

Martell, A. E. (2009). Catalytic Effects of Metal Chelate Compounds. Pure and Applied Chemistry, Vol.17, No.1, pp.129-178, January, 2009.

Martell, A. E. et al. (1975). Thermal Decomposition of EDTA, NTA, and Nitrilotrimethylenephosphonic Acid in Aqueous Solution. Can. J. of Chem., Vol.53, pp.3471-3476.

Martell, A. E. et al. (1996). Selection of new Fe(lll)/Fe(ll) chelating agents as catalysts for the oxidation of hydrogensulfide to sulfur by air. Can. J. Chem., Vol.74, pp.1872-1879, 1996.

Mathias, P. M. et al. (2012). A Guide to Evaluate Solvents and Processes for Post-Combustion CO_2 paper presented at GHGT-11. Energy Procedia, Vol. 37, pp. 1863-1870, Kyoto, Japan, November 18-22, 2012.

Matsumoto, T. (2013). Abu Dhabi Energy Policy. Tokyo: The Institute of Energy Economics of Japan (IEEJ).

McManus, D. & Kin, F. R. (1988). Patent No. EP0257124, Hydrogen sulfide removal.

Merichem Company. (2012). Comparative H_2S Economics for Shale Gas. Presented at the Gas Processors Association Annual Meeting, February, 2012.

Merichem Company. (2015). Small Capacity Sulfur Recovery Units. Retrieved from http://www.merichem.com/company/overview/technical-lit/tech-papers/small-capacity, December 1, 2015.

Mettler Toledo. (2016). Retrieved from FBRM Method of Measurement: http://www.mt.com/de/en/home/supportive_content/specials/Lasentec-FBRM-Method-of-Measurement.html, July 1, 2016.

Meuly, W. C. (1973). Cataban Process for the Removal of Hydrogen Sulfide from Gaseous and Liquid Streams. Paper presented at the 12th Annual Purdue Air Quality Conference, Purdue Univ., West Lafayette, IN/USA, November 7-8, 1973.

Morsi, B. I. et al. (2015). Mass transfer- Advancement in process modelling-Chapter 9: Mass transfer in multiphase systems. Dr. Marek Solecki, InTech, Retrieved from: http://www.intechopen.com/books/mass-transfer-advancement-in-process-modelling/mass-transfer-in-multiphase-systems, Dezember 4, 2015.

Motekaitis, R. J. et al. (1993). Oxidation of H_2S to S by air with Fe(III)-NTA as a catalyst: catalyst degradation. Can. J. Chem. Vol.71, pp.1524.

Motekaitis, R. J. et al. (1980). The iron(III)-catalyzed oxidation of EDTA in aqueous solution. Canadian Journal of Chemistry, Vol.58, No.19, pp.1999-2005, October 1, 1980.

Myers, J. D. & Bedell, S. A. (1990). Patent No. WO 90/01984.

Nagl, G. (2001). The State of Liquid Redox. The 9th GRI Sulfur Recovery Conference, San Antonia, TX/USA, October 24-27, 1999.

NETL. (2011). Quality Guidelines for Energy System Studies: Cost estimation methodology for NETL assessments of power plant performance, DOE/NETL-2011/1455. National Energy Technology Laboratory, U.S. Department of Energy, April, 2011.

Perry, R. C. et al. (1973). Fundamentals of Gas Treating. The Gas Conditioning Conference, March 15-16, Oklahoma.

Peters, M. S., Timmerhaus, K., & West, R. (2003). Plant Design and Economics for Chemical Engineers, 5th Edition. New York, NY/USA: McGraw-Hill.

Piche, S. et al. (2005). Assessment of a redox alkaline/iron-chelate absorption process for the removal of dilute hydrogen sulfide in air emissions. Chemical Engineering Sciences, Vol.60, No.22, pp.6452-6461.

Purmal´, A. P. et al. (1980). Formation of an intermediate oxygen complex in autooxidation of Fe(II)-ethylenediaminetetraacetate. Bull. Acad. USSR, Div. Chem. Sci., Vol.29, pp.315-320.

Quinlan, M. P. (1991). Characteristics & Handling Options for Sulfur from Liquid Redox. Liquid Redox Sulfur Recovery Conference, pp.317, Austin, TX/USA, Proceedings 1991.

Reicher, M. et al. (1999). The Use of Aqueous Liquid Redox Desulfurization Technology for the Treatment of Sour Associated Gases at Elevated Pressure. Presented at the GPA European Chapter Continental Meeting, Budapest, Hungary, Retrieved from http://www.merichem.com/company/overview/technical-lit/tech-papers/aquaeous-liquid-redox, September 29- October 1, 1999.

Reichl, A. et al. (2014). Process development and scale-up for post combustion carbon capture – validation with pilot plant operation. Energy Proceedings 63, pp.6379-6392.

Rochelle, G. T. et al. (2001). Research needs for CO_2 capture from flue gas by aqueous absorption/stripping, Final report for the U.S. Department of Energy. University of Texas Austin, USA, Department of Chemical Engineering.

Rossati, F. et al. (1982). Sulfint process. Hydrocarbon Processing, pp.169-172, March, 1982.

Rothery, E. (1986). Venturi Absorbers for the Stretford Processes. Proceedings of the 1986 Stretford Users´Conference, pp.40.

Rouleau, W. (2014). LO-CAT®: A Flexible Hydrogen Sulfide Removal Process. Hydrocarbon Engineering, April 2014.

Sada, E. et al. (1987). Oxidation kinetics of Fe(II)EDTA and Fe(II)NTA chelates by dissolved oxygen. Ind. Eng. Chem. Res., Vol.26, pp.1468.

Saelee, R. et al. (2012). Degradation Kincetics of Fe-Edta in Hydrogen Sulfide Removal Process. ISRN Chemical Engineering, Article-ID: 740429.

Satterfield, C. N. (1975). Trickle Bed Reactors. AIChE Journal, Vol.21, pp.209–228.

Schifano, D. (2004). Etude des Mécanismes de base de la dégradation chimique de l'acide nitrilotriacétique, ligand utilisé dans les procédés redox de conversion d'H_2S en soufre élémentaire, PhD thesis. L'Universite des Sciences et Technologies de Lille.

Schumpe, A. (1993). The estimations of gas solubilities in salt solutions. Chemical Engineering Science, Vol.48, No.1, pp.153-158.

Seider, D., Seader, J. D. & Lewin, D. (2010). Product and Process Design Principles (3rd ed.). John Wiley & Sons, Inc.

Siemens AG. (2016). Internal data base.

Smith, R. (2005). Chemical Process Design and Integration (1st ed.). Chichester, England: John Wiley & Sons Ltd.

Smith, R. M. & Martell, A. E. (1987). Critical stability constants, enthalpies and entropies for the formation of metal complexes of aminopolycarboxylic acids and carboxylic acids. The Science of the Total Environment, Vol.64, pp.125-147.

Soares, C. (2015). Gas Turbines Handbook (2nd ed.). The Boulevard, Langford Lane, Kidlington, Oxford, OX5 1AJ/ UK: Elsevier Science.

Sönmez, H. G. (2014). Evaluation of Catalytic Active Washing Processes for Sour Gas Treatment, Master´s thesis, Technische Universität Berlin (work performed at Siemens AG, Frankfurt am Main, Germany), March 31, 2014.

Sönmez, H. G. et al. (2015). Investigations on characterization of catalytically activated liquid systems for sour gas treatment. Paper presented at GPA Europe Technical Conference – Gas Treatment and Liquefaction Processes for Natural Gas, Hamburg, Germany, April 22-24, 2015.

Speight, J. G. (2013). Handbook of Shale Gas Production Processes (1st ed.). Waltham, Mass, USA: Gulf Professional Publishing.

Strigle, R. F. (1994). Packed Tower Design and Applications- Random and Structured Packings (2nd ed.). Houston, TX/USA: Gulf Publishing Company.

Sulfur Information Services. (2016). Sulfur Price. Retrieved from Sulfur Information Services: http://sulfur.nigc.ir/en/sulfurtrade/sulfurmarket/sulfurprice, March 10, 2016.

Tapscott, R. E. et al. (1969). Stereochemistry of Tartrato(4-)-bridged Binuclear Complexes. Coordination Chemistry Reviews, Vol.4, pp.323-359.

The DOW Chemical Company. (2016). Product Safety Assessment-DOW™ Trisodium Nitrilotriacetate-Based Chelants. Retrieved from http://msdssearch.dow.com/PublishedLiteratureDOWCOM/dh_088b/0901b8038088b788.pdf?filepath=productsafety/pdfs/noreg/233-00342.pdf&fromPage=GetDoc, February 17, 2016.

Thompson, R. B. (1980). Patent No. U.S.4,218,342. Composition for Catalytic Removal of Hydrogen Sulfide from Gases.

Travin, S. O. et al. (1981). Kinetics and mechanism of the reaction of iron(II)ethylendiaminotetraacetate (Fe2+EDTA) with molecular oxygen in the presence of ligands. Russian Journal of Physical Chemistry, Vol.55, pp.815.

Tsatsaronis, G. & Morozyuk, T. (2013). Notes for the Class "Entwurf, Analyse und Optimierung von Energieumwandlungsanlagen", WS-2012/2013. Berlin: Technische Universität Berlin, Institute for Energy Engineering.

Tsatsaronis, G. & Yang, Y. (2014). Multi-objective optimization of coal-fired power plants using differential evolution. Applied Energy, Vol.115, pp.254-264, November 28, 2013.

Tsatsaronis, G., Bejan, A., & Moran, M. (1996). Thermal Design and Optimization, Chapter-7: Economic Analysis. New York, NY/USA: John Wiley & Sons, Inc.

Turanyi, T. & Tomlin, A. S. (2014). Analysis of Kinetic Reaction Mechanisms - Chapter 2 "Reaction Kinetics Basics". Springer-Verlag Berlin Heidelberg, Germany.

Turton R. et al. (1984). Analysis, Synthesis and Desing of Chemical Processes. Upper Saddle River, New Jersey/USA: Prentice Hall.

Ulrich, D. G. & Vasudevan, T. P. (2004). Chemical Engineering Process Design and Economics - A practical guide (2nd ed.). Process Publishing.

Vancini, C. A. & R., L. (1985). The Peabody-Stretford Process on Geothermal Incondensable Gas. AIChE Spring National Meeting, No. 82d, Houston, TX/USA, March 27, 1985.

VanKleeck, D. & Morisse-Arnold, D. (1990). Quality of SulFerox Produced Sulfur. Paper presented at the AIChE Summer National Meeting, San Diego, CA/USA, August, 1990.

Wang, H. D. et al. (2008). A Sulfur Removal and Disposal Process through H_2S Adsorption and Regeneration: Ammonia Leaching Regeneration. Process Safety and Environment Protection, Vol.8, pp.296-302, 2008.

Welch, K. et al. (2002). Iron Autoxidation and Free Radical Generation: Effects of Buffers, Ligands, and Chelators. Archives of Biochemistry and Biophysics, Vol.397 No.2, pp.360-369, 2002.

Whitman, W. (1923). The two-film theory of gas absorption. Chemical and Metallurgical Engineering, Vol.29, No.4, pp.146-148.

Winkler, H. J. (1978). Patent No. U.S.4,091,073. Process for the removal of H_2S and CO_2 from gaseous streams.

Wold, S. et al. (2001). PLS-regression: a basic tool of chemometrics. Chemom. Intell. Lab. Syst., Vol. 58, pp.109-130.

Woods, D. R. (1975). Financial Decision-Making in the Process Industry. Englewood Cliffs, N.J.: Prentice Hall.

Wu, Y. et al. (2012). Advances in Natural Gas Engineering-Sour Gas and Related Technologies. Scrivener Publishing LLC.

Wubs, H. J. (1994). Application of Iron Chelates in Hydrodesulphurisation, PhD. Thesis. Rijksuniversiteit Groningen, The Netherlands.

Yan, T. Y. (1980). Removal of Thiosulfate/Sulfate from Spent Stretford Solution. Environ. Science and Technol., Vol.14, No. 6, pp.732-735.

Ying, L. et al. (2014). Selection of Chelated Fe (III)/Fe(II) Catalytic Oxidation. China Petroleum Processing and Petrochemical Technology, Vol.16, No.2, pp.50 -58.

Younger, A. H. (2004). Natural Gas Processing, Principles and Technology Part-I; Further Discussions on Pipeline Specifications. Calgary: Thimm Engineering Inc.

Zang, V. et al. (1990). Kinetics and mechanism of the autoxidation of iron(II) induced through chelation by ethylenediaminetetraacetate and related ligands. Inorganic Chemistry, Vol.29, pp. 1705.

LIST OF PUBLICATIONS

1. Sönmez, H. G. et al. (2014), „Abtrennung von H_2S und CO_2 aus sauren Gasen“, Invention disclosure, Siemens AG, Frankfurt am Main, Germany, April 30, 2014.

2. Sönmez, H. G. et al. (2014). „Festbettreaktor zur Regeneration einer Waschlösung bei der H_2S-Abtrennung“, Invention disclosure, Siemens AG, Frankfurt am Main, Germany, July 14, 2014.

3. Sönmez, H. G. et al. (2014). „H_2S-Abtrennung durch Metalle und deren Regeneration“, Invention disclosure, Siemens AG, Frankfurt am Main, Germany, July 14, 2014.

4. Sönmez, H. G. et al. (2015). Investigations on characterization of catalytically activated liquid systems for sour gas treatment, Paper presented at GPA Europe Technical Conference – Gas Treatment and Liquefaction Processes for Natural Gas, Hamburg, Germany, April 22-24, 2015.

5. Sönmez, H. G. et al. (2016). „Verbesserter Prozess zur Abtrennung von H_2S aus Sauergas durch die Verwendung eines Kontaktapparates mit statischen Mischern“, Invention disclosure, Siemens AG, Frankfurt am Main, Germany, February 16, 2016.

6. Sönmez, H. G. et al. (2016). „Verbesserter Prozess zur Abtrennung von H_2S aus Sauergas durch die Verwendung von Membran-Kontaktoren“, Invention disclosure, Siemens AG, Frankfurt am Main, Germany, June 16, 2016.

NOMENCLATURE

Acronyms

$/a	Dollars per year
$/kWh	Dollars (USD) per kilowatthours
a	Annual (years)
AA	Amino acid
AACE	American Association of Cost Engineering
AAS	Amino acid salt
ADA	Anthraquinone disulfonic acid
AIChE	American Institute of Chemical Engineers
ANEP	Annual net electricity production, (MWhe/a)
APC	Annual power consumption, (MWhe/a)
APC	Polyamino polycarboxylated chelate
APP	Annual power production, (MWhe/a)
Approx.	Approximately
aux.	Auxilaries
Bull. Acad. USSR, Div. Chem. Sci.	Bulletin of the Academy of Sciences of the USSR-Division of Chemical Science
Bull. Chem. Soc. Japan	Bulletin of the Chemical Society of Japan
C	Cost, (M$)
C.I.P.	Chelated Iron Process
Can. J. Chem.	Canadian Journal of Chemistry
CAPEX	Capital expenditures, (M$) or (M$/a)
CC	Carrying charges, (M$)
CDTA	Trans-cyclohexane-1,2-dinitrilo tetra acetic acid
CELF	Constant escalation levelization factor, (-)
CEPCI	Chemical Engineering Plant Cost Index
CER	Commission for Energy Regulation
CF	Capacity factor, (-)
Chemom. Intell. Lab. Syst.	Chemometrics and Intelligent Laboratory Systems
CLD	Chord length distribution
COE	Cost of electricity, (ct(USD)/kWh)
cP	Centipoise, 1 cP = 0.001 Pa.s
CRF	Capital recovery factor, (1/a)
DC	Demand charge of the turbine, ($/kWe)
DCS	Distrubuted control system
DEA	Diethanolamine
DEGEE	Diethylene glycol mono ethyl ether
DGA	Diglycolamine
DIPA	Diisopropanolamine
DMPO	5,5-Dimethyl-1-pyrroline N-oxide
DP	Degradation product
DTPA	Diethylene trinitrilo penta acetic acid
e.g.	Latin: “exempli gratia” (meaning for example)
EASEE	European Association for Streamlining of Energy Exchange
ED3A	Ethylene diamine tri acetic acid
EDTA	Ethylene diamine tetra acetic acid
EIA	U.S. Energy Information Agency
EPRI	Electrical Power Research Institute
ESR	Electro spin resonance

F	Factor
f.o.b	Free on board
FBRM	Focused beam reflectance measurement
FC	Fuel costs, (M$/a)
FCI	Fixed capital investment
GDF	Gaz de France
GHGT	Greenhouse gas technologies
GPA	Gas Processors Association
GRG	Generalized reduced gradients
HEDTA	Hydroxyl ethylethylene diamine tri acetic acid
HHV	Higher heating value, (MJ/Nm^3)
HRSG	Heat recovery steam generation
HSE	Health, safety and environmental issues
Hz	Hertz
i.e.	Latin: “id est” (meaning that is to say)
IC-MS	Ion chromatography with mass spectrometer
ICP-MS	Inductively coupled plasma mass spectrometry
IDA	Imino diacetic acid
IEEJ	The Institute of Energy Economics of Japan
IFP	Institute Francaise du Petrole
Ind. Eng. Chem. Res.	Industrial & Engineering Chemistry Research
IOU	Investor-owned utility
ISO	International Organization for Standardization
ISRN	International Scholary Research Notices
ITX	Income taxes
J. Anal. Bioanal. Ttechniques	Journal of Analytical Bioanalytical Techniques
kWe	Kilowatt electiricity
LC-MS	Liquid chromatography equipped with a mass spectrum
LCoE	Levelized cost of electricity, (ct(USD)/kWh)
LDO	Luminescent dissolved oxygen
LGI	Le Gaz Integral
LHV	Lower heating value, (MJ/Nm^3)
Lig	Ligand (chelating agent)
LNG	Liquefied natural gas
LTPD	Long tons equivalent per day (1 long ton = 1,016.05 kg)
M$	Million dollars (USD)
M$/a	Million dollars (USD) per year
M$/kWh	Million dollars (USD) per kilowatthours
MDEA	Methyldiethanolamine
MEA	Monoethanolamine
MFC	Mass flow controller
MMSCF	Million standard cubic feet (1 MMSCF [at 14.696 psia, 60 °F] = 26,843 Nm^3 [at 1.013 bar, 0 °C])
MMSCFD	Million standard cubic feet per day (1 MMSCFD [at 14.696 psia, 60 °F] = 1,116 Nm^3/h [at 1.013 bar, 0 °C])
MNm^3/d	Million normal cubic meters per day
MW	Molecular weight, (g/mol)
MWhe/a	Megawatthour electricity per year
n.a.	Not applicable
NETL	National Energy Technology Laboratory
Nm^3	Normal cubic meter (at 1.013 bar, 0°C)
NME	Near Middle East
NTA	Nitrilo tri acetic acid

NTU	Number of transfer units, (-)
OMC	Operation and maintenance costs,(M$) or (M$/a)
OPEX	Operational expenditure, (M$/a)
P	Production, (ton/day or ton/a)
PBN	Phenyl-tert-butyl nitrone
PEC	Purchase equipment cost, (M$)
PLSR	Partial least square data regression
PO	Power output, (MWe)
PolyDADMAC	Poly dimethyl diallyl ammonium chloride
PP	Power plant
ppm	Part per million
ppmv	Part per million by volume
ppmvd	Parts per million by volume, dry
ppmwt	Part per million by weight
PSD	Particle size distribution
Q	Capacity
R	Revenue, (M$/a)
Resp.	Respectively
ROI	Return on investment
SCCM	Standard cubic centi meters per minute at 1.013 bar, 0 °C
SCF	Standard cubic feet (1 SCF=0.027 Nm^3)
SCR	Selective catalytic reduction
SGT	Siemens gas turbine
slpmSLPM	Standard liters per minute at 1.013 bar, 0 °C
SRU	Sulfur recovery unit
TCI	Total capital investment, (M$)
TEA	Tri ethanol amine
TGT	Tail gas treatment
TOTEX	Total expenditure, (M$) or (M$/a)
TP	Treatment plant
TRR	Total revenue requirement, (M$/a)
UV-Vis	Ultraviolet-visible spectroscopy
vol	Volume, (L or m^3)
WACC	Weighted averaged cost of capital, (%)
WCI	Working capital investment, (M$)
WI	Wobbe Index, (MJ/Nm^3)
WL	Workload, (h/a)

Subscripts

abs	Absorption
a	Air
ads	Adsorption
aq	Aqueous
BM	Bare module
BM	Bare module
c	Chemical
com	Combustion
DC	Demand charge
del	Delivered
eff	Effective
fuel	Fuel combusted
g or G	Gas
gen	General

i	Inflation and/or interest
i	Specie or ion
in	At inlet
in	Inlet
L	Levelized
l or L	Liquid
M	Material
max	Maximum
n	Nominal
OL	Operating labor
op	Operation
out	At outlet
out	Outlet
P	Equipment
P	Pressure
PP	Power plant
r	Rate
ref	Reference
reg	Regeneration
req	Required
s	Solid
sol	Solution
sour	Sour gas feed
sour	Sour natural gas
sweet	Sweet natural gas
sys	System
t	Time
t=0	Initial
t=∞	End of respective experiment
TP	Treatment plant
u	Utilities
w	Water
x	Number of protons
ε	Extinction coefficient of measured specie, (L/mol.cm)

Superscripts

*	At equilibrium
0, I, II,..	State of oxidation

Chemical Formulas and Substances

Ar	Argon
NH_3	Ammonia
$(NH_4)HSO_4$	Ammonium bisulfate
$(NH_4)_2SO_4$	Ammonium sulfate
As	Arsenic
HCO_3^-	Bicarbonate ion
HS^-	Bisulfide ion
Br	Bromine
C_4H_{10}	Butane
Ca	Calcium
CO_2	Carbon dioxide
CO	Carbon monoxide

CO_3^{2-}	Carbonate ion
CS_2	Carbonyl di sulfide
COS	Carbonyl sulfide
-COOH	Carboxyl group
Cl	Chlorine
Co	Cobalt
C_2H_6	Ethane
$Fe(OH)_3$	Ferric hydroxide
$Fe^{(III)}$	Ferric ion
$Fe^{(II)}$	Ferrous ion
F	Fluorine
CH_2O	Formaldehyde
He	Helium
$Fe(CN)_6^{3-}$	Hexacyanoferrate(III)
H_2O_2	Hydrogen peroxide
H_2S	Hydrogen sulfide
-OH	Hydroxyl group
I	Iodine
Fe	Iron
Fe_2O_3	Iron(III) oxide
Fe_2S_3	Iron(III) sulfide
Pb	Lead
Li	Lithium
Ma	Manganese
RSH	Mercaptane (R = alkane, alkene or other carbon-containing group)
CH_4	Methane
N_2	Nitrogen
NOx	Nitrogen oxides
CX	Organo halides
O_2	Oxygen
P	Phosphor
K	Potassium
$KHCO_3$	Potassium bicarbonate
K_2CO_3	Potassium carbonate
KOH	Potassium hydroxide
K_2SO_4	Potassium sulfate
C_3H_8	Propane
Na	Sodium
$NaHCO_3$	Sodium bicarbonate
Na_2CO_3	Sodium carbonate
NaOH	Sodium hydroxide
Na_2SO_4	Sodium sulfate
$Na_2S_2O_3$	Sodium thiosulfate
SO_4^{2-}	Sulfate ion
-SOOOH	Sulfonic group
S	Sulfur
SOx	Sulfur oxides
$S_2O_3^{2-}$	Thiosulfate ion
V	Vanadium
V_2O_5	Vanadium(V)-oxide
Xe	Xenon

Notations

Ea	Activation energy, (kJ/mol)
f_{air}	Air flow rate per dosed H_2S, (l/min)/(l/min) or m^3/Nm^3
$\Delta H°$	Change in standard enthalpy, (J) (at 1.013 bar, 298 K)
$\Delta S°$	Change in standard entropy, (J/K) (at 1.013 bar, 298 K)
$\Delta G°$	Change in standard Gibbs free energy, (J)
z	Charge number of the ions, (-)
Fe(II).Lig	Chelates of the Fe(II) with various ligands (e.g. EDTA,HEDTA, DTPA etc.)
Fe^{3+}/H_2S	Circulated iron to dosed H_2S, (mol/mol)
wt%	Concentration by weight
$d_{C_{O_2}}/dt$	Concentration gradient of the O_2 within the progress of the time, (mol/L.s)
c[Fe•Lig]	Concentration of iron-ligand complex, (M or mol/L)
c[AAS]	Concentration of respective AAS, (M or mol/L)
$c_{O_{2(l)}}$	Concentration of the O_2 in the liquid phase, (mol/L or mol/m^3)
c_{CO2}	Concentration of the the CO_2 in sour feed gas, (vol%)
c_{H2S}	Concentration of the the H_2S in sour feed gas, (vol%)
α	Degression coefficient, (-)
$\Delta E°$	Difference in standard redox potentials of respective half-cell reactions (Volts or V)
y	Empiric partial order of the reaction with respect to Fe(II)•EDTA
x	Empiric partial order of the reaction with respect to O_2
$c^*_{O_{2(g)}}$	Equilibrium concentration of the O_2 at the gas-liquid-interface, (mol/L or mol/m^3)
Lig/(Fe•Lig)	Excess amount of respective chelator, (mol/mol)
F	Faraday constant (F=96,500 Joule/Volt.mol)
K_{ML}	Formation constant of metal-ligand complex
R	Functional group or side chain of the respective AAS
F-factor	Gas loading factor, ($Pa^{0,5}$)
G	Gas phase
$h_{G,0}$	Gas specific constant at T = 298.15 K, (L/(mol.K))
h_G	Gas specific constant, (L/mol)
v	Gas velocity, (m/s)
He	Henry coefficient (bar.L/mol)
C_0	Initial concentration of sample, (M or mol/L)
W_{int}	Integral corrosion rate, (mm/a)
I_0	Intensity of the incident light, (W/m^2)
I	Intensity of the transmitted light, (W/m^2)
A	Interfacial area, (m^2)
h_i	Ion specific constant, (L/mol)
c[Fe]	Iron concentration, (M or mol/L)
$c[Fe^{3+}]$	Iron(III)-concentrations, (ppmwt or wt%)
c[Lig]	Ligand concentration, (M or mol/L)
L	Liquid phase
L/G	Liquid to gas ratio, (l/min)/(l/min)
L	Liter (l)
k_{l,O_2}	Mass transfer coefficient of the O_2 in the liquid phase, (m/s)
Me•Lig	Metal-ligand complex
MNm^3/d	Million normal cubic meter per day (at 1.013 bar, 0 °C)
MNm^3/h	Million normal cubic meter per hour (at 1.013 bar, 0 °C)
M	Molarity (mol/L)

n	Number of electrons transferred of the half-cell reaction (mol)
d	Optical path through the UV measurement cell, (cm)
Ox	Oxidized form of redox catalyst
A	Pre-exponential factor in Arrhenius law, (L/(mol.s))
P	Pressure, (bar or atm)
r	Reaction rate (mol/(L.s))
k	Reaction rate constant, (unit of this term depends on the order of interacting components in the respective reaction)
k_l	Mass transfer coefficient in liquid phase (m/s)
A	Recorded light absorbance, (-)
E	Redox potential, (Volts (V) or millivolts (mV))
Red^-	Reduced form of redox catalyst
$_{Cr}$	Relative concentrations of sample, (%)
C_t	Remaining concentration at the end of the respective test, (M or mol/L)
$t_{contact}$	Residence time, (s)
f_{sol}	Solvent circulation rate per dosed H_2S, (l/min)/(l/min) or m^3/Nm^3
R^2	Square of the regression coefficient, [-]
$K_{ML}(Ox)$	Stability constant of the oxidized form of chelated metal
$K_{ML}(Red^-)$	Stability constant of the reduced form of chelated metal
v_B	Stoichiometric coefficient of iron, (-)
h_T	Temperature correction parameter for the gas component, (L/mol)
T	Temperature, (°C or K)
N_{O2}	Total number of moles of O_2 absorbed, (mol)
R	Universal gas constant, (R=8.31 $J.mol^{-1}.K^{-1}$)
V	Volume, (m^3)
$\dot{V}_{air}$	Volumetric flow rate of air, (l/min)
$\dot{V}_{sour}$	Volumetric flow rate of sour feed gas, (l/min)
$\dot{V}_{sol}$	Volumetric solution circulation ratio, (l/min)

Greek symbols

α_{ion}	Ionic strength of the respective solution, (M or mol/L)
ε	Phase hold up (G or L), (-)
η	Efficiency
λ	Wavelength, (nm)
μ	Dynamic viscosity, (cP or Pas)
ρ	Density, gas or liquid, (kg/m^3)
τ	Surface tension, (N/m)
υ	Superficial gas velocity, (m/s)
Φ	Reference concentration of O_2 in solution, 25 mol/m^3
Ψ	Reference concentrationof Fe(II) in solution, 100 mol/m^3

APPENDICES

Appendix A-1 gives supplementary informations required for the investigations conducted in the scope of chapter 3.

Appendix A-1.1: In order to understand the economic impacts of the solvent system properties, which are emphasized in section 2.4 and remarked in **Table 3-1**, on the overall process, it is necessary to analyse associated interactions between the addressed characteristics:

- **Stability:** Studying of degradation behavior of the liquid system and identification of its degradation products are crucial, since solvent degradation can pose adverse impacts on performance, economics and environmental character of the process. Decomposition of the constituents may also cause fouling and corrosion, and thus may diminish the operability. Lower degradation tendency reduces the by-product formation, the requirement of reclaiming and/or of chemical make-up and hence leads to less OPEX. High thermal and chemical stability also gives more flexibility to the process design and operation, i.e. it can be run at a wide range of operating conditions. Methods to inhibit degradation can be taken either by adding inhibitors or by adjusting operating parameters.

- **The performance parameters** such as loading capacity, selectivity, regenerability, mass transfer ratio and reaction rates (both for absorption and regeneration) are high of interest, if a solvent system shall be qualified for gas treatment in industrial scale. Solvent systems featuring favorable physical (e.g. viscosity, density and surface tension) and ionic (e.g. ionic strength, α_{ion}) character promote (Wubs, 1994) these parameters, which will increase the loading capacity as well as the regeneration rate of the solvent system and thus lower the energy demand (lower OPEX) which in turn leads to reduced equipment sizes (lower CAPEX, smaller footprint).

- **Viscosity**, (μ), is an important property describing the resistance of a fluid to flow. The power required to move the fluid depends on two intrinsic properties of it: (1) fluid density and (2) viscosity (Ludwig, 1997). Pumps need less energy for circulating low-viscosity-media which results in a lower OPEX. Besides that, low viscosity leads to faster mass transfer: An absorbent solution with low viscosity possesses less interfacial mass-transfer resistance between gas and liquid phases. This means the diffusion coefficient of the components to be transferred into the liquid phase can be increased, thereby increasing overall reaction rates (both absorption and regeneration).

- Components featuring high vapor pressure are characterized as volatile (Kohl, A. L. et al., 1997). High **volatility** causes a higher amount of gaseous solvent losses. This leads to environmental concerns due to emissions, to further investment costs for the implementation of an additional washing section and to an increase in operational expenses caused by replacing the emitted solvent. Therefore, solvent systems which have a negligible vapor pressure are of high interest.

With regard to robust **operability** the following parameters are high of interest:

- **Fouling** is generally defined as the deposition and accumulation of unwanted materials such as suspended solids, decomposition products, non-soluble components but also of crystallized process components on the surfaces of plant equipment (Perry, R. C. et al., 1973). This can have a significant, negative impact on the operational efficiency of the unit, in the worst case blocking and destruction of rotating equipment. Fouling is mainly related to the properties of the solvent systems being handled (e.g. chemical nature, melting point, pH, density, viscosity, diffusivity, etc.) in combination with the equipment design and/or operating conditions such as temperature and velocity. The fouling tendency of a solvent system indicates whether components may precipitate as a solid. For the sake of stable operation, either constituents

featuring lower fouling tendencies or operating conditions hindering the fouling phenomenon are required. As a secondary measure, appropriate mechanical cleaning devices can be installed within the industrial plant.

- **Corrosion** issues can have detrimental impacts on the performance of gas treating and in particular of liquid redox processes since the oxidation and/or reduction rates of the applied catalytic agent may be influenced by the dissolved construction materials in the operating liquid system. Corrosiveness primarily depends on the pH of the operating fluid as well as on its composition, especially on the presence of oxygen and water.

- **Foaming** phenomenon is mostly depending on specific physical properties of the operating liquid (mainly surface tension τ, but also density ρ, viscosity μ, etc.) (Smith R. , 2005). For gas sweetening applications, a significant build-up in the concentration of produced sulfur in the operating liquid system also causes foaming and therefore should be controlled strictly. Excessive foaming of the solvent system can result in high pressure drop, decreased mass transfer efficiency (in turn reduced separation efficiencies) and even failure of the process. Since the foaming tendency of a solvent system cannot or only insufficiently be predicted and prevented prior to operation, elimination/limitation of this operating problem necessitates either through piloting experiments in advance or costly and tricky measurements after start-up: either mechanical adjustments (e.g. installation of a foam breaker) or chemical addition (e.g. injection of antifoaming agents, which however can have other adverse effects on the process).

- **Viscosity** as described above, low viscosity is favorable for good operability of a gas treatment process.

- **HSE issues** influence the handling of the solvent system, the possibility of its re-use and the conditions for disposal of the process waste. Material safety data sheets (MSDS) usually give the required information about the environmental character of the used chemical substances. The hazardousness of the substances themselves, the formation of toxic by-products or environmental impacts of volatile products are of particular concern here. Therefore, only registered chemical substances showing high biodegradability, low volatility and preferably no hazardousness (toxicity) shall be chosen.

- **Cost and availability:** An industrial scale treatment process requires bulk levels of solution inventory. Hence, the use of prohibitively costly and monopoly chemical substances is impractical. Significant cost savings can be realized through the selection of already registered and REACH classified chemicals which are offered by various vendors with high production volume.

Appendix A-1.2 gives an overview and classification of the commercially available liquid absorbents for gas sweetening sweetening **(Younger, 2004)**.

Table A- 1 Commercially utilized gas sweeetening liquid absorbents (Younger, 2004)

1) Chemical Solvent Processes	
1.A) Alkanolamines	
MEA	2.5 N-Monoethanolamine (15% in water)
UCAR	5 N-Monoethanolamine (30%) with inhibitor
DEA	2 N-Diethanolamine (21%)
SNEA-DEA	3 N-Diethanolamine (32%)
DIPA	2 N- Diisopropanolamine (27%)
MDEA	2 N- Methyldiethanolamine (24% or higher)
DGA	6 N- Diglycolamine (63%)
Inhibited Amines	both MEA and DEA (30 – 50%)
1.B) Hot Potassium Carbonate	
Catacarb	Potassium carbonate solution with catalyst
Benfield	Potassium carbonate solution with catalyst
Giammarco - Vetrocoke	Potassium carbonate solution and arsenic trioxide
1.C) Alkaline salts of amino acids	
Alkacid-M	Potassium salt of methyl amino propionic acid
Alkacid-DIK	Potassium salt of dimethyl amino acetic acid
2) Physical Solvent Processes	
Selexol	Dimethyl ether of polyethylene glycol (DMEPG)
Fluor Solvent	Propylene carbonate
Purisol	N- methyl-pyrrolidone (NMP)
Rectisol	Methanol
3) Physical-Chemical (hybrid) Solvent Processes	
Sulfinol	Mixture of sulfolane, DIPA and H_2O
Aminsol	Mixture of MEA, DEA with methanol
4) Direct Conversion Processes	
Feld process, Koppers C.A.S	Polythionate solutions
Fischer, Staatsmijnen-Otto, Autopurification	Iron-cyanide
Manchester, Ferrox, Burkheise, Gluud	Sodium carbonate and ferric oxide solution
GiammarcoVetrocoke-S, Thylox	Alkali thioarsenates and arsenites in solution
Stretford, Hiperion	Quinone + metal salt (sodium carbonate and vanadate)
Takahax, Perox	Sodium carbonate or vanadate with hydroquinone
Sulfolin, Unisulf	Sodium carbonate or vanadate with anthraquinone
LO-CAT®, SulFerox®, Sulfint, Sulfint HP	Chelated iron in solution

Appendix A-1.3 is compiled in the context of quantitative concentration measurements of the metal-ligand solutions (the Fe•Lig) given in **Table 3-6** were carried out with a UV-Visible spectrophotometer according to the procedure described in section 3.5.2.3**.** Three stock solutions with different concentrations of the Fe•Lig were prepared (see **Table 3-8**). In addition, samples only with the free ligand (without Fe) were measured. **Table A- 2** gives an overview of wavelengths of the respective solutions and the obtained square of the regression coefficients (R^2) from the UV-absorbances of the three stock solutions of each respective species.

Table A- 2 Absorbance to wavelength curves of the free ligands and different concentrations of the Fe•Lig at absorption maxima, resulting calibration model (equation and regression)

Sample no. and composition - Wavelength (λ), nm for A=max. - Calibration equation; x=c[Fe•Lig) and y= Amax at λ - R^2	**Absorbance to wavelength curves** -First three curves from top to down represent for three concentrations of Fe:Lig (M:M) 0.15:0.15; 0.10:0.10; 0.06: 0.06, respectively -The last curve at the bottom represents samples containing only free ligand (without Fe)
C1-(Fe•IDA) - λ=285 nm - y= 0.4648x – 0.1673 - R² = 0.9672	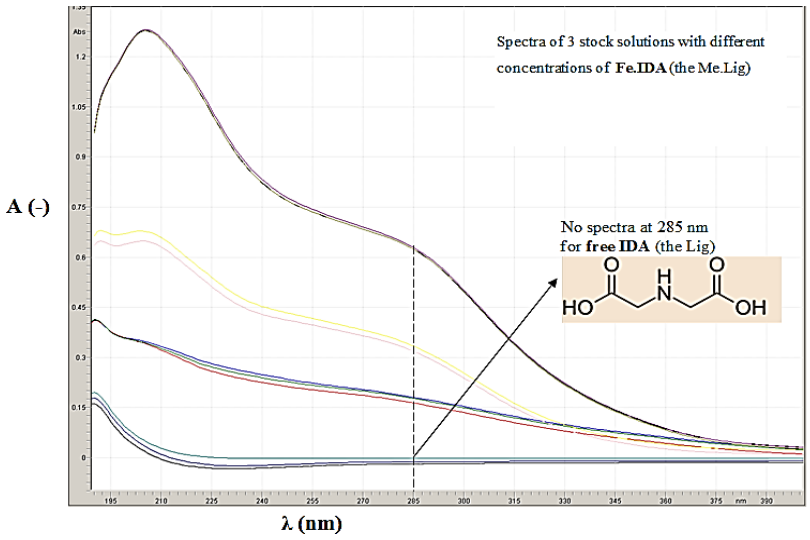
C2-(Fe•NTA) - λ=270 nm - y= 0.4693x + 0.0109 - R² = 0.9881	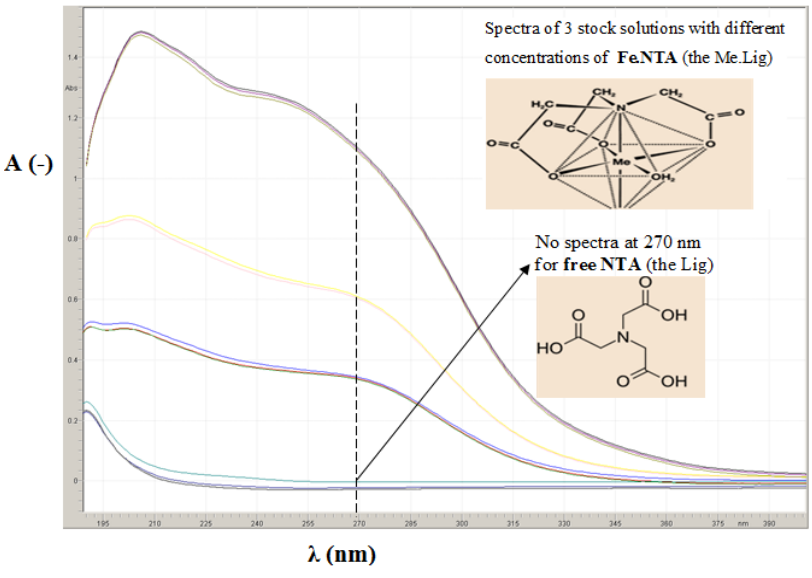

Table A- 2 Absorbance to wavelength curves of the free ligands and different concentrations of the Fe•Lig at absorption maxima, resulting calibration model (equation and regression) **cont´d**

C3-(Fe•HEDTA) - λ=232nm - y = 0.3218x + 0.2866 - R² = 0.99	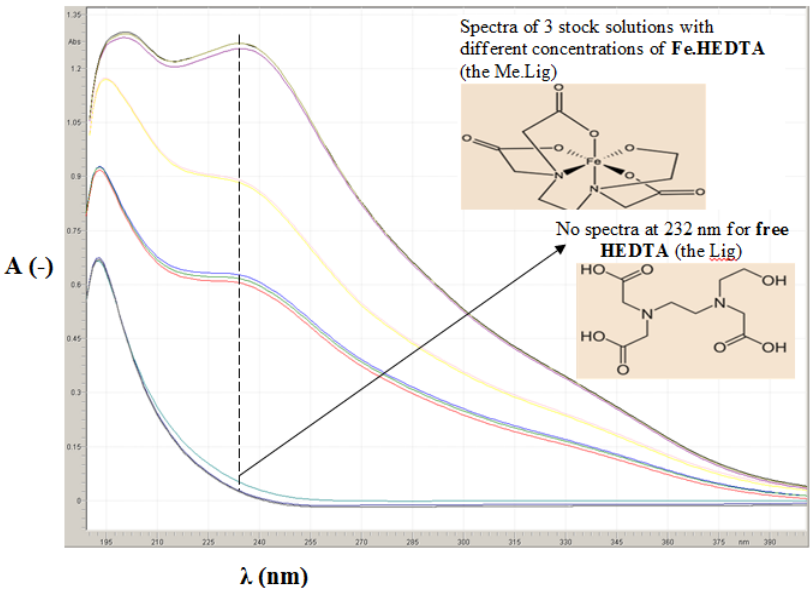
C4-(Fe•EDTA) - λ=243 nm - y = 0.4518x - R² = 0.95	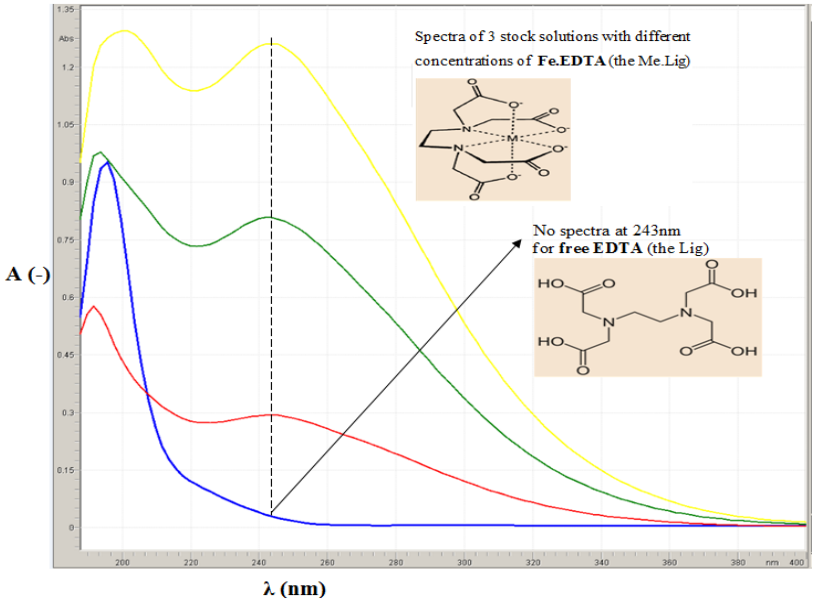

Table A- 2 Absorbance to wavelength curves of the free ligands and different concentrations of the Fe•Lig at absorption maxima, resulting calibration model (equation and regression) **cont´d**

C5-(Fe•CDTA) - λ=255 nm - y = 0.2963x + 0.2934 - R² = 0.95	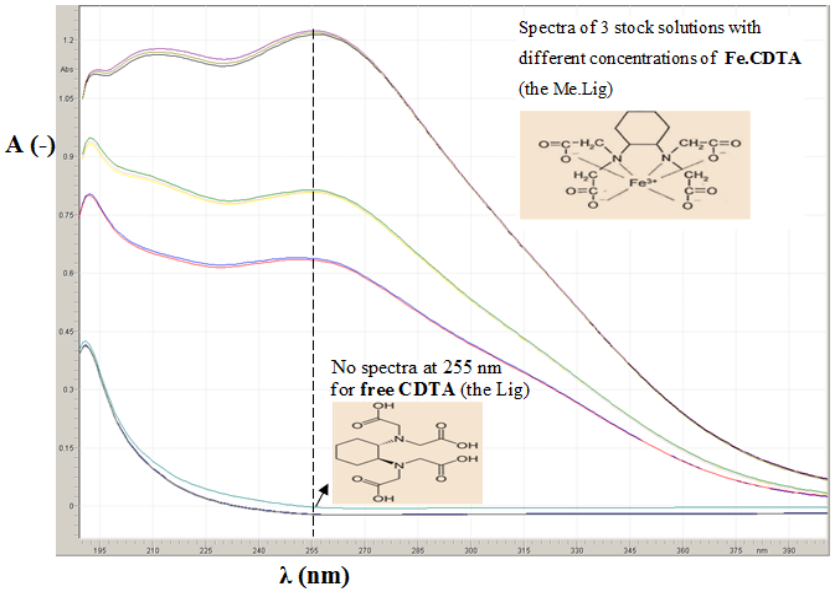
C6-(Fe•DTPA)	see **Figure 3-8** given in section 3.5.1.3
C7-(Fe•Citrate) - λ=245 nm - y = 0.4865x – 0.3608 - R² = 0,95	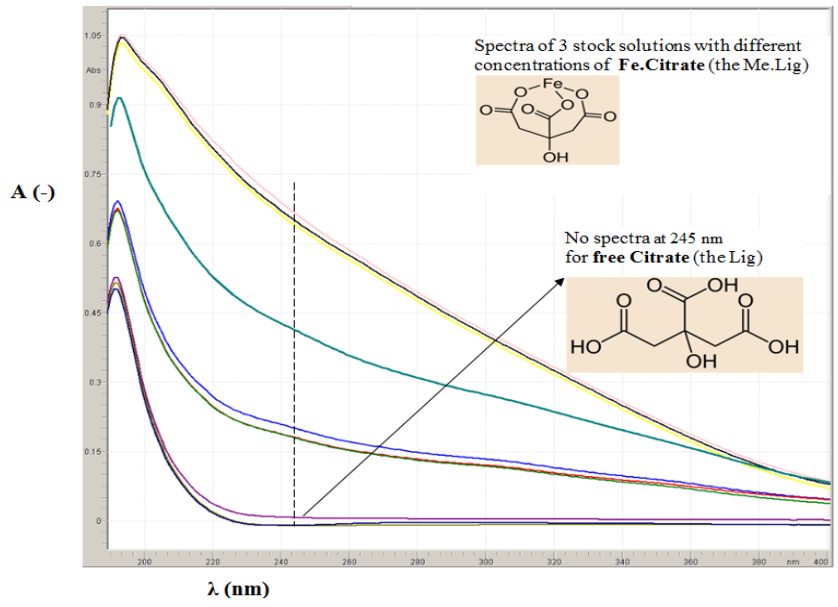

Table A- 2 Absorbance to wavelength curves of the free ligands and different concentrations of the Fe•Lig at absorption maxima, resulting calibration model (equation and regression) **cont´d**

C8-(Fe•Mannitol) - λ=270 nm - y = 0.0768x + 0.195 - R^2 = 0.98	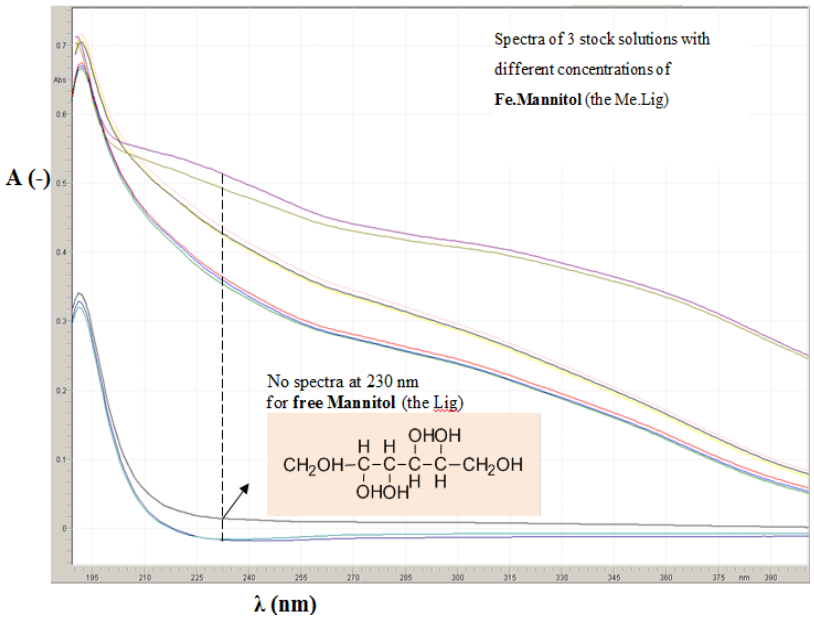

Appendix A-2 involves all appendices regarding chapter 4.

Appendix A-2.1 is related to experimental determination of physical solubility of N_2 and O_2 of the regeneration air in respective solvent system (i.e. Siemens Solvent-1) given in section 4.1.4. The pressure decrease curve of air resulting from the physical absorption of it into Siemens Solvent-1 without chelated catalyst at 30°C is given in **Figure A- 1**.

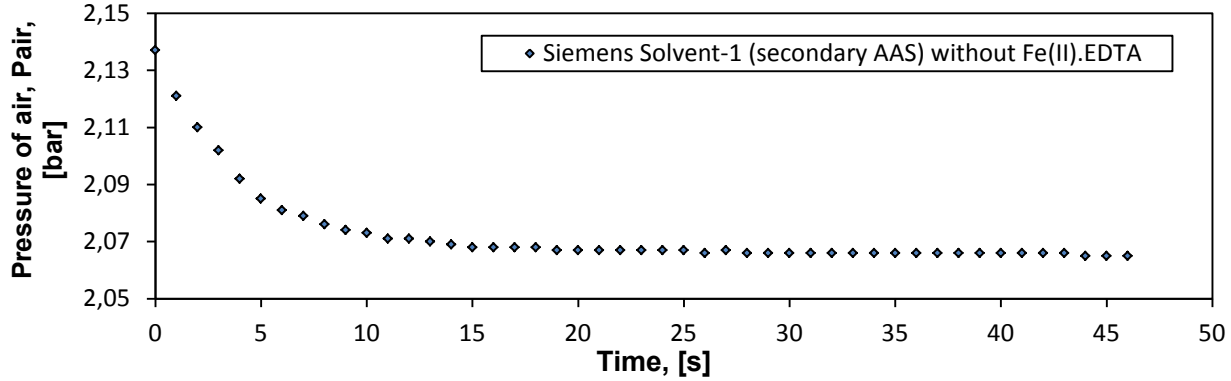

Figure A- 1 Pressure decrease of air resulting from the physical absorption of it into Siemens Solvent-1 without Fe(II)•EDTA at 30°C

For physical absorption of a gas in the solvent in a batch setup, the mass balance gives the following relation for the Henry coefficient (see footnote 15), where the subscripts (t=0), (t=∞) and w stands for initial value at the beginning of the test, final value at the end of the test and for the water, respectively.

$$He,i = \frac{P_{i_{t=\infty}} - P_w}{P_{i_{t=0}} - P_{i_{t=\infty}}} \frac{RTV_L}{V_G} \qquad \text{(Eq.4-9)}$$

The input data for the calculation is given in the table below.

Table A- 3 Data required to calculate the Henry coefficient of O_2 in Siemens Solvent-1 w/o chelated-catalyst at 30 °C by applying Eq.4-9

Required data	Value	Unit
P_w at 30°C	0.042	bar
P_{air}, t=0	2.137	bar
P_{air}, t=∞	2.065	bar
P_{O2}, t=0	0.421	bar
P_{O2}, t=∞	0.406	bar
R	0.08314	L.bar/mol.K
T, t=∞	303.04	K
V_L	0.75	L
V_G	0.773	L
$He_{,O2}$ in Siemens Solvent- 1 w/o Fe(II)•EDTA at 30 °C	592.26	bar L/mol
$He_{,O2}$ in water (Ebrahimi, S. et al., 2003)	781.25	bar L/mol

As it was mentioned in section 4.1.1.1.2.1, the obtained Henry coeffient was corrected by conducting Eq.4-10 where the $h_{G,O2}$ was calculated by inserting the data of h_T, $h_{G,0}$ and h_i taken from (Schumpe, 1993) into Eq.4-11. The values of corrected $He_{,O2}$ (both at 30°C and 60 °C) and the $h_{G,O2}$ calculated for the investigated solutions (i.e. Solution (A) to (C)) and water for the comparison are given in **Table A- 4** in **Appendix A-2.2.**

Appendix A-2.2 is related to methodology for the calculation of solubility of O_2 in regeneration air in respective solutions according to (Schumpe, 1993) given in section 4.1.1.1.2.1 and their results mentioned in 4.1.4.

Table A- 4 Ion specific constants obtained from (Schumpe, 1993) and calculated Henry coefficients of O_2 in the Solutions (A)* to (C)*

Solvent system	hi (m^3/kmol)	$h_{G,O2}$ at 30 °C (m^3/kmol)	h_T (m^3/kmol)	$He_{,O2}$ at 30 °C (bar.L/mol)	$He_{,O2}$ at 60 °C (bar.L/mol)
(A) Fe(II)•EDTA in water	0.0922	-0.00167	-0.1169	2123.14	3144.65
(B) Solvent-1 + Fe(II)•EDTA	0.0680			2976.19	3891.05
(C) Dimethylglycinate + Fe(II)•EDTA	0.0715			2770.08	3937.07
Water (Ebrahimi, S. et al., 2003)	-	-	-	781.25	1290.32

Note: *corrected according to Schumpe and $He_{,O2}$ in water according to (Ebrahimi, S. et al., 2003). The gas specific constant for O_2 is $h_{G,0} = 0$ and the temperature correction constant is h_T =- 0.000334.

Appendix A-2.3: Determination of kinematic viscosities of the solutions given in section 4.1.1 by capillary-tube-type viscometer

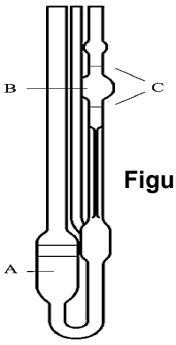

Figure A- 2 Schematic illustration of an Ubbelohde viscometer

Kinematic viscosities (μ/ρ) of the solutions were determined with a capillary viscometer (Ubbelohde viscometer), which is illustrated in **Figure A- 2**. Densities of the samples were measured using a pycnometer as described by (Eliassi, A. et al., 1998). The solutions were fed into the capillary viscometer and heated up to 30 °C for 15 minutes. Subsequently, they were pumped from a lower (A) to a higher (B) reservoir through the capillary. When the solutions passed a photo sensor (C) the pump was turned off and the solutions flowed back to the lower reservoir passing a second photo sensor (C). With the time required for the distance between the two photo

sensors, the viscosities of the different solutions were calculated and are given in the following table.

Table A- 5 Results of kinematic viscosity and density measurements of the investigated solutions at 30 °C given in section 4.1.1

Solution	Density (kg/m^3)	Kinematic viscosity (mm^2/s)
Solution-(A)	1133	1.0715
Solution-(B)	1138	1.9471
Solution-(C)	1141	1.7818

Appendix A-2.4: Determination of the kinetic constant of the oxidation reaction under variation of Fe(II)•EDTA concentration related to section 4.1.4.2: The measured O_2-partial pressure ($P_{O2(t)}$) curve and calculated O_2-pressure gradient (dP_{O2}/dt) of the Solution-(B) half (i.e. 0.5Ψ=50 mol/m^3) and twice (i.e. 2Ψ=200 mol/m^3) of the reference concentration of the Fe(II)•EDTA is illustrated **Figure A- 3** and **Figure A- 4**, respectively.

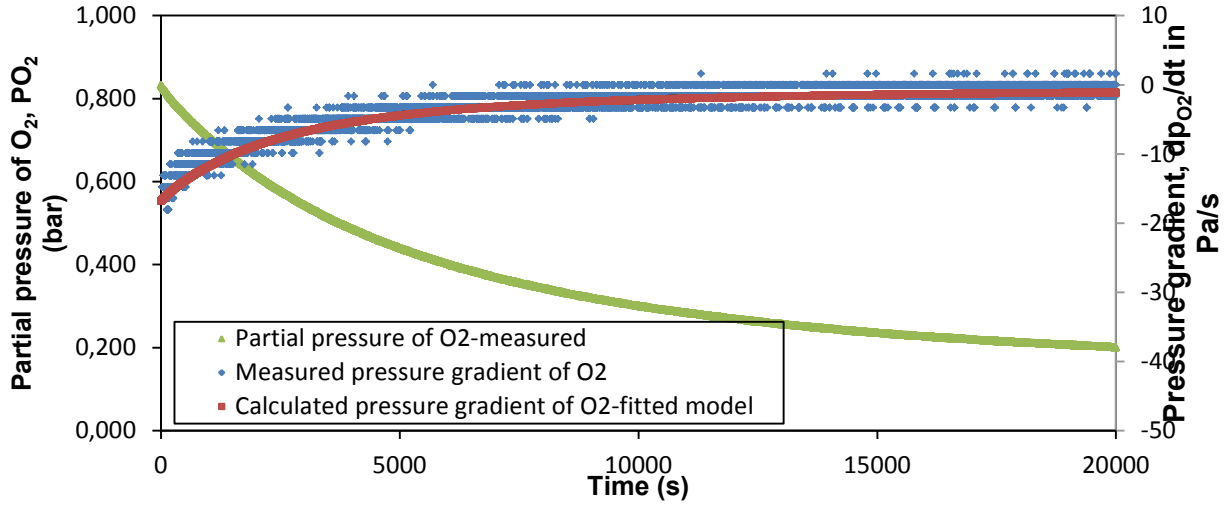

Figure A- 3 Measured partial pressure decrease of O_2 in contact with Solution-(B) under T=30°C, c(Fe(II)•EDTA)=0.5Ψ; cO_2=1.0Φ and other reference conditions as given in **Table 4-4**

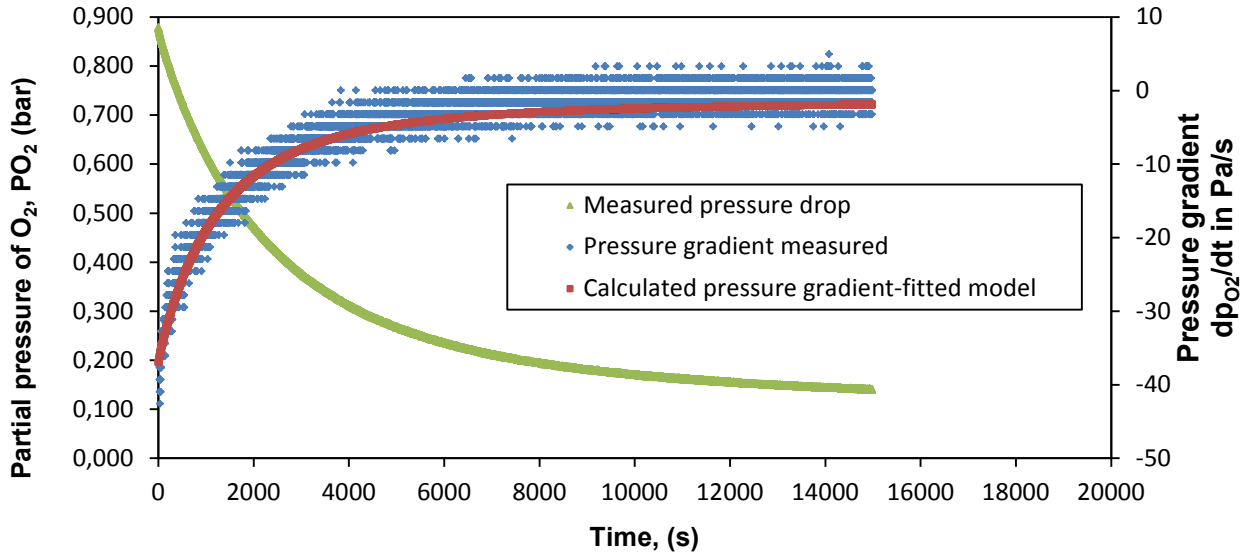

Figure A- 4 Measured partial pressure decrease of O_2 in contact with Solution-(B) under T=30°C, c(Fe(II)•EDTA)=2Ψ; cO_2=1.0Φ and other reference conditions as given in **Table 4-4**

Appendix A-2.5: Mass balance for the formation (as a product of the overall reaction) and the loss of H_2O (caused by destripping by supplied air or inert N_2) during benchmarking tests with lab plant in continuous operation given in section 4.2.3:

In the context of the varied amount of gas feeds and/or concentrations given in **Table 4-11**, the following assumptions were applied for all conducted experiments:

- Air humidity of the off-gas, φ=100%
- Temperatures of the feed and off-gases for both contactors, T= 22 °C; ± 0.3 °C
- Water content of the off-gas, x_{H2O}=29.64 g/m^3
- Molar volume at temperature of the respective feed gas (e.g. at 22°C $V_M air$ = 25.04 l/mol)
- Molecular weight of water, MW_{H2O}= 18 g/mol

$$\Delta m_{H_2O} = 160 * \left[\left(\frac{\dot{V_{H_2S}}}{V_M air} * MW_{H_2O}\right) - \left(\dot{V_{off-gas}} * x_{H_2O}\right)\right] * 0.06 \qquad \text{(Eq. A-4.1)}$$

The term $\dot{V}_{off-gas}$ denotes the volumetric flow rate of the off-gas,($\dot{V}_{off-gas=}\dot{V}_{N_2} + \dot{V}_{Air}$) in l/min. This led to an absolute formation of 0.2 to 2 g H_2O during the 160 hours of operation for each solution. In relation to approximately 6000g of the respective solution in the system and this would therefore be negligible in regard to the accuracy of the conducted analysis.

Appendix A-2.6: Related to measurement of UV-Vis spectra of Fe•EDTA in Sol.1 and Sol.2 during benchmarking tests shown in **Figure 4-12** section 4.2.4.

Since the absorbance at a certain wavelength is directly proportional to the concentration of the measured species, the almost unchanged absorption maxima at 243 nm (shown in **Figure A- 5**) indicate that the Fe•EDTA concentration of the two solutions did not change significantly during the operation under standard conditions and the Case2 given in Table 4-10 and Table 4-11. Thus, the occurrence of chelate degradation can be ruled out.

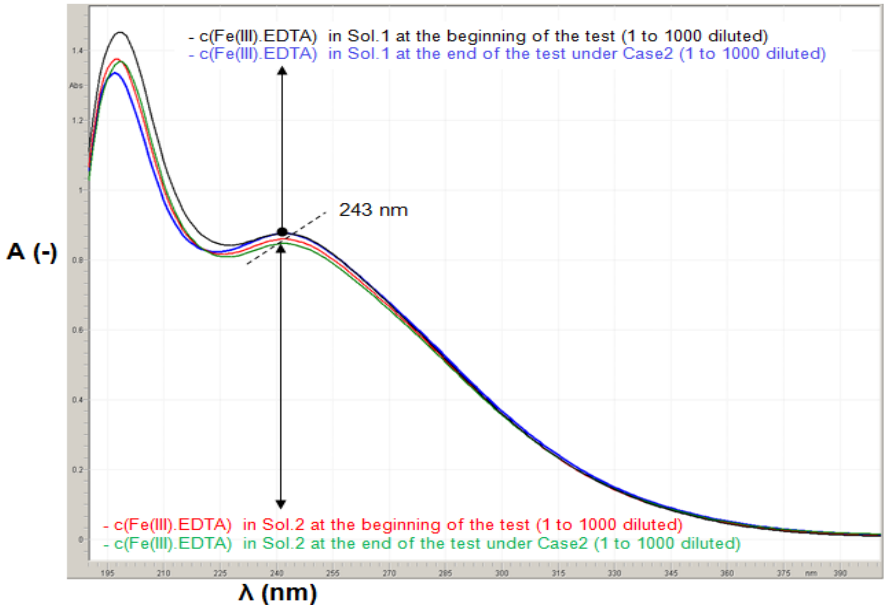

Figure A- 5 Absorbance to wavelength UV-Vis spectra of Fe•EDTA in Sol.1 and Sol.2 at the beginning and the end of the test under Case2 given in Table 4-11

Appendix A-2.7: Comparison of densities and viscosities of the solutions with "low" and "high" chelated catalyst concentrations mentioned in section 4.2.4 measured at 25 °C as described in Appendix A-2.3.

Table A- 6 Densities and kinematic viscosities of the Sol.1 and Sol.3 at 25 °C

Solution	Density (kg/m^3)	Kinematic viscosity (mm^2/s)
Sol.1 (low-cat)	1070	3.05
Sol.2 (high-cat)	1360	14.89

Appendix A-2.8: Related to "Measured of UV-Vis spectra of Fe•EDTA in Sol.1 and Sol.4 tested under standard conditions and Case1 given in Table 4-10 and Table 4-11. Results of the benchmarking tests were shown in **Figure 4-13** given in section **4.2.4**. Absorbance to wavelength spectra of Sol.1 and Sol.4 at the beginning and at the end of the test are given in **Figure A- 6** and **Figure A- 7**, respectively. The absorbance at a certain wavelength is directly proportional to the concentration of the measured species. Since the absorption maximas (243 nm and 250 nm, respectively for the Fe•EDTA and the Fe•Lig2) the occurrence of chelate degradation can be ruled out under testing conditions.

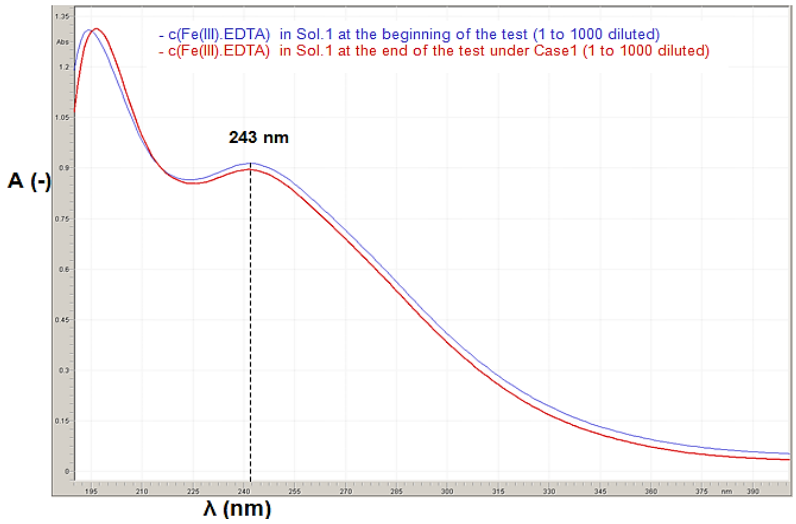

Figure A- 6 Absorbance to wavelength spectra of the Fe•EDTA in Sol.1 at the beginning and end of the test under Case1

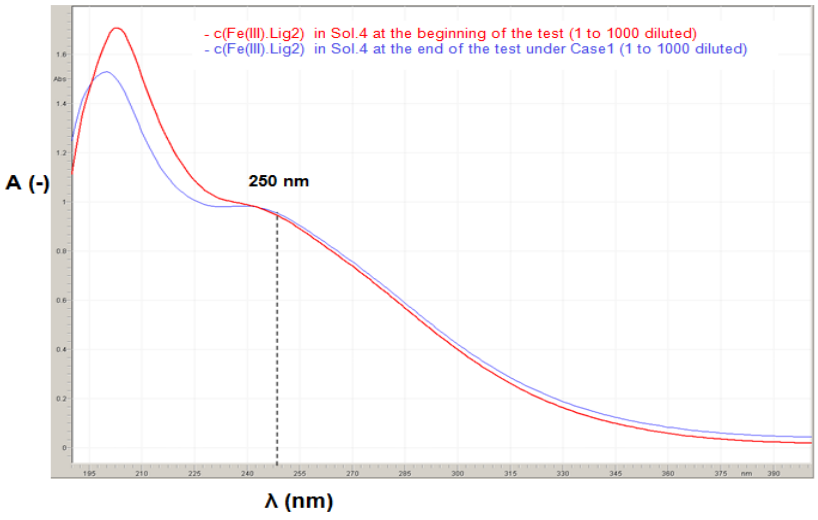

Figure A- 7 Absorbance to wavelength spectra of the Fe•Lig2 in Sol.4 at the beginning and end of the test under Case1

Appendix A-2.9: Related to section 4.2.6.3: The off-line microscopy pictures of all samples (for Sol.1 to Sol.13) are given in **Figure A- 8**.

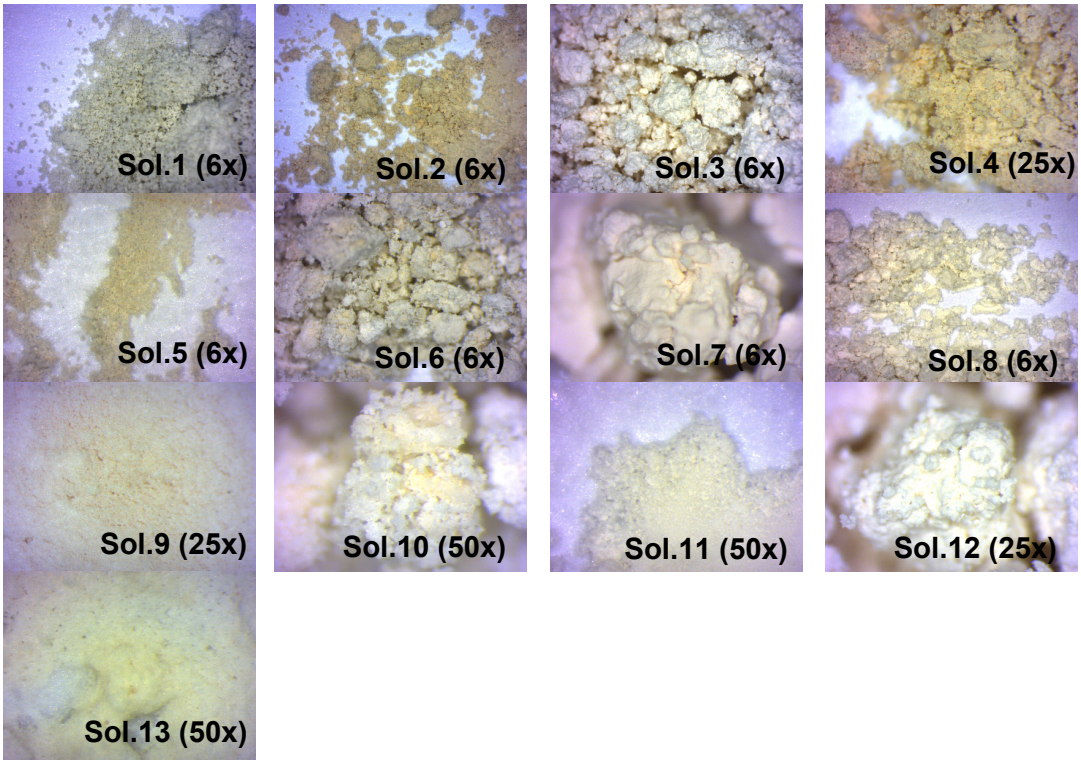

Figure A- 8 Off-line optical microscopy pictures of the sulfur cakes obtained at the end of each test run (160 h) from Sol.1 to Sol.13 with various magnification factors (i.e. 6x, 12x, 25x and 50x)

It shall be noted that their either whitish-appereance or yellowish or brownish appearance depends on the content/type of inorganic or organic compounds in filter cakes.

Appendix A-2.10: shows the official reports of TÜV SÜD related to corrosion tests of the selected materials mentioned in section 4.2.7.

Prüfaufgabe: Durchführung von Korrosionsversuchen

Werkstoffe: 1.0425, Proben normal

Medium: s. u.

Temperatur: 35 °C pH-Wert: Sonstiges:

Versuchsanordnung: Standversuche nach DIN 50 905 Teil 4, Punkte 2.1 und 3
Proben in Glasverspannungen teilweise eingetaucht.

Gasart: Luft ☒ Überlagerung ☐ Einleitung

Belastungsdauer: 15 Tage ☒ Korrosionslabor ☐ Betriebslabor ☐ Betrieb

Ergebnis

Medium 1: [redacted]owcat Absorber + Oxidizer

Werkstoff Probe Nr.	W_{int} [1] mm/a	V [2] $g \cdot m^{-2} \cdot d^{-1}$	Bemerkungen
1.0425 856	<0,01	0,04	Nadelstichartige Lochkorrosion, Spaltkorrosion

Medium 2: [redacted]-Lowcat Absorber + Oxidizer

Werkstoff Probe Nr.	W_{int} [1] mm/a	V [2] $g \cdot m^{-2} \cdot d^{-1}$	Bemerkungen
1.0425 857	0,56	12,04	Mulden- und Lochkorrosion

Medium 3: [redacted]Highcat Versuchsende, fertiges Gemisch aus Absorber + Oxidizer

Werkstoff Probe Nr.	W_{int} [1] mm/a	V [2] $g \cdot m^{-2} \cdot d^{-1}$	Bemerkungen
1.0425 858	1,15	24,50	Mulden- und Lochkorrosion

Medium 4: [redacted] Versuchsende, fertiges Gemisch aus Absorber + Oxidizer

Werkstoff Probe Nr.	W_{int} [1] mm/a	V [2] $g \cdot m^{-2} \cdot d^{-1}$	Bemerkungen
1.0425 859	0,78	16,75	Mulden- und Lochkorrosion

1) W_{int} = Integrale Abtragungsgeschwindigkeit nach DIN 50905, Teil 2, berechnet aus der Massedifferenz der Probe vor und nach dem Korrosionsversuch

2) V = flächenbezogene Massenverlustrate in Gramm pro Quadratmeter und Tag

Appendix A-2.10 cont´d

Prüfaufgabe: Durchführung von Korrosionsversuchen

Werkstoffe: 1.7139 nitriert

Medium: s. u.

Temperatur: 35 °C pH-Wert: Sonstiges:

Versuchsanordnung: Glasverspannung

Gasart: Luft ☒ Überlagerung ☐ Einleitung

Belastungsdauer: 7 Tage ☒ Korrosionslabor ☐ Betriebslabor ☐ Betrieb

Ergebnis

Medium A: [redacted]

Werkstoff Probe Nr.	W_{int} [1] mm/a	V [2] $g \cdot m^{-2} \cdot d^{-1}$	Bemerkungen
1.7139 1	0,19	4,08	Gleichmäßiger Angriff, mattierte Oberfläche

Medium B: [redacted]

Werkstoff Probe Nr.	W_{int} [1] mm/a	V [2] $g \cdot m^{-2} \cdot d^{-1}$	Bemerkungen
1.7139 2	0,01	0,17	Gleichmäßiger Angriff

1) W_{int} = Integrale Abtragungsgeschwindigkeit nach DIN 50905, Teil 2, berechnet aus der Massedifferenz der Probe vor und nach dem Korrosionsversuch

2) V = flächenbezogene Massenverlustrate in Gramm pro Quadratmeter und Tag

Appendix A-3 consists of the results of the measurements done and/or supplementary informations regarding the chapter 5 (degradation studies).

Appendix A-3.1: Figure A- 9 shows the pressure drop curve of air in the Sol. 1 during the first two redox cycles of the Study-1, Test-1 at 30 C° (stirred cell reactor, see section 5.3.3.1).

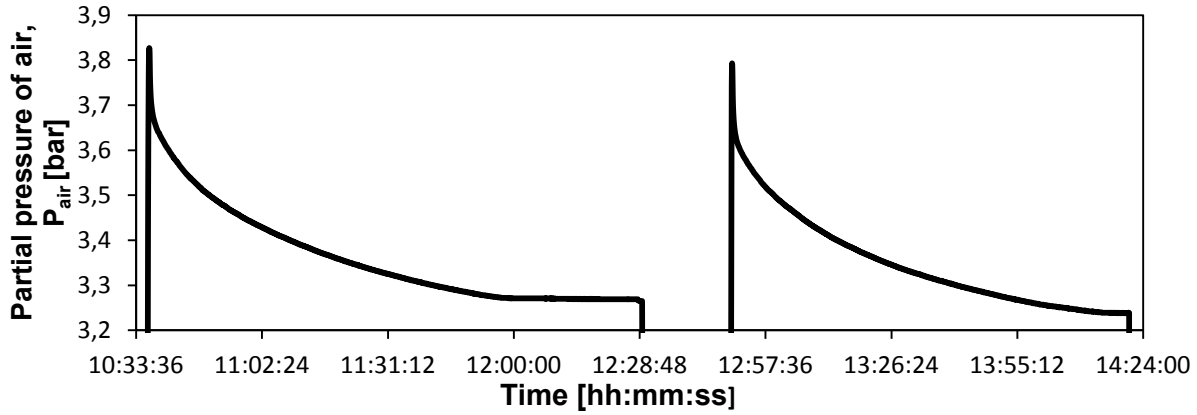

Figure A- 9 Pressure drop of air in the Sol.1 during the first two redox cycles in the run of 20 redox cycles during, Study-1, Test-1, at 30 °C

The experimentally obtained value for the Henry coefficient of N_2 ($He,_{N2}$) in Sol.1 at 30°C is 1284.13 bar.L/mol by applying Eq.4-9 and the experimental data is given in **Table A- 7**.

Table A- 7 Data required to calculate the amount of O_2 supply into system during, Study-1, Test-1 at 30 °C (stirred cell reactor)

Parameter, unit	Value
$V_{reactor}$, L	1.52312
Density of the solution, kg/L	1.09768
Mass of the solution, kg	0.75032
Volume of liquid phase in the reactor, V_L, L	0.68356
Volume of gas phase in the reactor, V_G, L	0.83957
Fe-content in the solution, mol	0.06836
Theoretical stoichiometric coefficient of Fe, $v_{B,theo}$, (-)	4
Stoichiometric O_2 requirement ($(O_2:Fe(II))_{stoichiometric}$=0.25), mol	0.01709
Supplied amount of O_2 (for $f_{O2}=[(O_2:Fe(II))_{supplied}/(O_2:Fe(II))_{stoichometric}]$=1.5), mol	0.0256
Supplied amount of air (20.9 % O_2), mol	0.12817
R, L.bar/mol.K	0.08314
T, t=∞, K	302.45
P_w at 30°C, bar	0.042
Atmospheric pressure measured, bar	0.9985
Pair, t=0, (relative), bar	2.88
Pair, t=0, (absolute), bara	3.8785
Pair, t=∞, (relative), bar	2.292
Δp_N_2 (absolute), bara	0.0289
Absorbed amount of O_2, nO_2, mol	0.01859
Real stoichiometric coefficient of Fe, v_B, (-)	3.677
Absolute amount of excess O_2-consumption, mol	0.001501
Relative amount of excess O_2-consumption, %	8.779
$He,_{N2}$ in Sol.1 at 30 °C, bar.L/mol	1284.13
$He,_{N2}$ in water (Ebrahimi, S. et al., 2003), bar.L/mol	1600

Using the $He_{,N2}$ in Sol.1 at 30°C given in **Table A- 7**, the amount of O_2 consumed from the pressure drop profiles obtained during a redox cycle was calculated by Eq.4-7 and is given **Table A- 8**.

Table A- 8 Calculated excess amount of O_2 in each redox cycle during, Study-1, Test-1, at 30 °C (1 test run =20 redox cycles), stirred cell reactor

ΔpN_2 (bar)	**nO_2 (mol)**	**No. Redox cycle**
rounded up to next whole number		
0.0289	0.0186	1
0.0288	0.0192	2
0.0283	0.0188	3
0.0274	0.0186	4
0.0272	0.0171	5
0.0272	0.0169	6
0.0258	0.0176	7
0.0259	0.0173	8
0.0245	0.0178	9
0.0247	0.0178	10
0.0232	0.0187	11
0.0236	0.0175	12
0.0226	0.0180	13
0.0228	0.0175	14
0.0214	0.0183	15
0.0218	0.0170	16
0.0206	0.0188	17
0.0205	0.0180	18
0.0199	0.0196	19
0.0198	0.0186	20

Appendix A-3.2: As mentioned in section 5.3.5, alternative inhibitors and inhibitor to Fe ratios are given in **Table A- 9**.

Table A- 9 The influences of inhibitors on the degradation of the applied ligand (Wubs, 1994)

References	Inhibitor	Ligand type	c(Fe) (mol/m^3)	Inhibitor/ Fe ratio (mol/mol)	H_2S to Fe ratio (mol/mol)	Degradation rate (b)
(Diaz, 1983c)	-	NTA (a)	270	-	5.3	0.14
	Sodium thiocyanate			0.37		0.06
	Sodium dithionite			0.37		0.06
(Diaz, 1983a)	Thiodiglycolic acid			0.19		0.09
	3,3.thiodipropionic acid			0.19		0.11
(Diaz, 1983b)	N,N-diethylhydroxylamine			0.37		0.09
	Thiourea			0.37		0.07
	Thiosemicarbazide			0.19		0.06
(Blytas, 1983)	Bisulfite			0.37		0.07
(Bedell, 1990) and (Bedell, 1992)	-	HEDTA (c)	100	5.0	2.5	1.83
	Sodium benzoate					0.39
	Paratoluene sulhonic acid					0.33
	Potassium iodide					0.51
	Potassium bromide					0.43
	Potassium chloride					1.72
	2-prapanol					0.74
	1-butanol					0.51
	Ethylene glycol					0.89
	Sodium formate					0.65
	Sucrose			2.5		0.94
(Myers & Bedell, 1990)	-			-		1.83
	Jayfloc™ 803 (d)			0.0058		1.79
				0.0102		1.36
				0.0146		0.98
				0.0292		0.97
				0.0586		0.88
	Jayloc™ 808(d)			0.003		1.08
				0.007		0.70
	Sodium thiosulfate			13.5		0.93

(a) NTA/Fe= 1.4 mol/mol
(b) Degradation rate at pH=7; T= 35°C: Ligand degraded per amount of sulfur produced (g/g).
(c) Degradations rate are recalculated with the data of (Bedell, 1990).
(d)Jayfloc™ 803 and Jayloc™ 808 from Exxon Chemicals are hydrocarbon emulsions containing polyacrylamide-acyrlic acid copolymer with 4.8 mole % and 9.5 mole % of acrylic acid, respectively.

Appendix A-4: Results of the calculations and/or supplementary information regarding chapter 6 (economic analysis of the evaluated technology).

Table A- 10 Treatment plant operation conditions - performance ratios for estimation base (see section 6.2.2)

Parameter	Value	Unit
Volume (capacity) of the sour gas to be treated , V_{sour}	546.28	m^3/h
Concentration of CH_4 in the sour feed gas, c_{CH4}	80	vol%
Concentration of H_2S in the sour feed gas, c_{H2S}	10	vol%
Concentration of CO_2 in the sour feed gas, c_{CO2}	10	vol%
Volumetric flow rate of CH_4 at treatment plant inlet, V_{CH4}	437.03	m^3/h
Volumetric flow rate of H_2S at treatment plant inlet, V_{H2S}	54.63	m^3/h
Volumetric flow rate of CO_2 at treatment plant inlet, V_{CO2}	54.63	m^3/h
Operation temperature in both reactors, T_{op}	35	°C
Operation pressure of absorber, P_{abs}	25	bara
Operation pressure of regenerator, P_{reg}	1.01325	bara
Applied solvent system	Sol.13: Secondary AAS – high cat (0.5 M Fe and 0.75 M EDTA)	
CH_4-slip rate	0.10	vol%
H_2S-separation rate	99.99	vol%
CO_2-desorption rate (see footnote 28)	50	vol%

Table A- 11 Design data of absorber

Parameter	Value	Unit	Notes	
Solution circulation to H_2S ratio, f_{sol}	1.62	m^3/Nm^3	Experimentally found data for Sol.13 for Case4 given in **Table 4-11**	
Density of Sol.13, $\rho_{Sol.13}$ (at 35 °C)	1360	kg/m^3		
Residence time of the solution in absorber, t_{abs}	0.07	h		
Superficial gas velocity in absorber , u_{abs}	5	cm/s		
Volumetric flow rate of required solvent circulation per dosed H_2S, V_{sol}	1930	m^3/h	Eq.4-25	Calculated using the experimentally obtained data given above and equations given in **Table 4-13**.
Volumetric flow rate of the sour gas, V_{sour}	546.28	m^3/h	Base case	
Volumetric flow rate of H_2S in the sour gas , V_{H2S}	54.63	m^3/h	Base case	
Liquid to gas ratio in absorber, L/G_{abs}	3.53	-	Eq.4-27	
Volume of the absorber, V_{abs}	**133.72**	**m^3**	Eq.4-31	
Area of the absorber, A_{abs}	13.76	m^2	Eq.4-29	
Diameter of the absorber, D_{abs}	4.19	m	$=\sqrt{4 * A_{abs}/\pi}$	
Filling height in absorber, h_{abs}	7.78	m		
Solvent hold-up in absorber, HU_{abs}	**107.02**	**m^3**	Eq.4-33	
Material of construction	AISI316Ti=DIN1.4571			
Type of equipment	Bubble column			

Table A- 12 Design data of regenerator

Parameter	Value	Unit	Notes	
Air supply to H_2S ratio, f_{air}	8.0	m^3/Nm^3	Experimentally found data for Sol.13 for Case 4 given in **Table 4-11**	
Density of Sol.13, $\rho_{Sol.13}$ (at 35 °C)	1360	kg/m^3		
Residence time of the solution in regenerator, t_{reg}	0.03	h		
Superficial gas velocity in regenerator, u_{reg}	7.8	cm/s		
Volumetric flow rate of required solvent circulation per dosed H_2S, V_{sol}	1930	m^3/h	Eq.4-25	Calculated using the experimental data given above and the equations given in **Table 4-13**.
Volumetric flow rate of required air per dosed H_2S, V_{air}	9558	m^3/h	Eq.4-26	
Volumetric flow rate of H_2S in the sour gas , V_{H2S}	54.63	m^3/h	Base case	
Liquid to gas ratio in regenerator, L/G_{reg}	0.20	-	Eq.4-28	
Volume of the regenerator, V_{reg}	**55.02**	**m^3**	Eq.4-32	
Area of the regenerator, A_{reg}	40.91	m^2	Eq.4-30	
Diameter of the regenerator, D_{reg}	7.22	m	$=\sqrt{4 * A_{reg}/\pi}$	
Filling height in regenerator, h_{reg}	1.08	m	Eq.4-34	
Solvent hold-up in regenerator, HU_{reg}	**44.03**	**m^3**		
Material of construction	AISI316Ti=DIN1.4571			
Type of equipment	Bubble column			

Table A- 13 Design data of flash vessel

Parameter	Value	Unit	Notes	
Amount of circulated Sol.13 into absorber, m_{sol}	2,625,797	kg/h	Experimentally obtained (Siemens AG, 2016)	
Residence time of solution in flash vessel, t_{flash}	0.019	h		
Molecular weight of CH_4, M_{CH4}	16	kg/kmol		
Henry coefficient of CH_4 in Sol.13 at 35°C, He_{CH4}	0.00018	bar/kmol	Given by (Siemens AG, 2016)	
Volumetric flow rate of required solvent circulation per dosed H_2S, V_{sol}	1930	m^3/h	Eq.4-25	Calculated using the experimentally obtained data given above and equations given in **Table 4-13**.
Averaged molecular weight of the Sol.13, $M_{Sol.13}$	35.01	kg/kmol	calculated	
Amount of circulated Sol.13 into absorber, m_{sol}	74,988.7	kmol/h	$=M_{Sol.13} * V_{sol}$	
Amount of physically dissolved CH_4 in absorber at 25 bar and 35 °C, PD_{CH4}	13.5	kmol/h	$= P_{sys} * He_{CH4} * m_{sol}$	
Amount of physically dissolved CH_4 in absorber at 25 bar and 35 °C, PD_{CH4}	0.84	kg/h	PD_{CH4} (kg/h) = $M_{CH4} * PD_{CH4}$(kmol/h)	
Density of CH_4 at 35 °C 25 bar, ρ_{CH4}	12.915	kg/m^3		
Area of the flash vessel , A_{flash}	7.07	m^2	Eq.4-29	
Diameter of the flash vessel , D_{flash}	3.10	m	$= \sqrt{4 * A_{flash}/\pi}$	
CH_4 amount to be fed into the treated gas at the top of absorber, V_{CH4}	0.065	m^3/h	= PD_{CH4} (kg/h) / ρ_{CH4}	
Volume of the flash vessel , V_{flash}	**36.4**	**m^3**		
Material of construction	AISI316Ti=DIN1.4571			
Type of equipment	Process vessel			

Table A- 14 Design data of sulfur separation unit

Parameter	Value	Unit	Notes
Base case: Sulfur capacity of the sour gas (10 vol % H_2S in the feed compriseses of 11,947 Nm^3/h- sour feed gas)	41.4	LTPD	$LTPD = \dot{V}_{H_2S}\left(\frac{L}{h}\right) * \frac{1\ mol\ H_2S}{22{,}4\ L\ H_2S} * \frac{1\ mol\ S^{2-}}{1\ mol\ H_2S} * \frac{0{,}032\ 1\ kg\ S^{2-}}{1\ mol\ S^{2-}} * \frac{24\ h}{1\ day} * \frac{1\ LTPD}{1016.5\ kg}$
Amount of circulated Sol.13 into absorber	2,625,797	kg/h	Experimentally found
Density of the suspension containing 5 wt% solid sulfur	1768	kg/m^3	Input was given by (Siemens AG, 2016)
Amount of suspension to be separated in proportion to circulated solution	1	wt%	
Volumetric flow rate of the suspension	14.85	m^3/h	
Factor filter area to volumetric flow rate of the suspension	1.6	$m^2/m^3/h$	
Area of the filtration unit	**23.76**	**m^2**	
Material of construction	AISI316Ti=DIN1.4571		
Type of equipment	Pressurized filter		

Table A- 15 Design data of the regenerated solution pump and the air compressor

Parameter	Value	Unit	Notes
Efficiency of the pump, ŋ	0.90	-	$\dot{w}_{s'}[kW] = \frac{\rho * g * h * V_{sol}}{ŋ * 3{,}6 * 10^6}$
Volumetric flow rate of required solvent circulation per sparged H_2S, V_{sol}	1930	m^3/h	
Discharge head, h	25.98	m	
Power requirement of the main circulation pump, $\dot{w}_{s'}$	**247.81**	**kW**	
Air density, ρ	1.15	kg/m^3	$\dot{w}_{f'}[HP] = \frac{0.004363 * \mathrm{V_{Air}} * \left(\frac{\mathrm{K}}{\mathrm{K}-1}\right) * ((\frac{P_2}{P_1})^{\frac{K-1}{K}} - 1)}{ŋ}$
Mass flow rate of air , m_{air}	10948.79	kg/h	
Volumetric flow rate of air , V_{air}	5575.55	ft^3	
Polytropic efficiency of the compressor, ŋ	0.92	-	
Suction pressure (atmospheric), P_1	14.70	psia	
Discharge pressure, P_2	26.11	psia	
Adiabatic expansion coefficient , K	1.41	-	
Theoretical power requirement for the compressor, $\dot{w}_f$	**223.57**	**HP**	
Theoretical power requirement for the compressor	164.44	kW	
Real power requirement for the compressor (incl. friction (+20%))	**197.32**	**kW**	
Material of construction (for pump and compressor, respectively)	AISI316=DIN1.4408 and AISI316Ti=DIN1.4571		
Type of pump	Centrifugal pump		
Type of compressor	Axial, turbo		

Table A- 16 Power generation plant operation conditions - performance parameters

Parameter	Value	Unit
Mass flow rate of fuel at turbine inlet[a]	7997	kg/h
Mass flow rate of CH_4 at turbine inlet[a], m_{CH4}	6824	kg/h
Mass flow rate of CO_2 at turbine inlet[a], m_{CO2}	1172	kg/h
Mass fraction of CH_4 in the treated feed gas at turbine inlet[a], x_{CH4}	85.33	wt%
Mass fraction of CO_2 in the treated feed gas at turbine inlet[a], x_{CO2}	14.17	wt%
Volumetric flow rate of CH_4 at turbine inlet[b], V_{CH4}	9557	Nm^3/h
Volumetric flow rate of CO_2 at turbine inlet[a], V_{CO2}	597	Nm^3/h
Concentration of CH_4 in the treated feed gas at turbine inlet[a], c_{CH4}	94.12	vol%
Concentration of CH_4 in the treated feed gas at turbine inlet[a], c_{CO2}	5.88	vol%
Lower heating value of pure CH_4, LHV_{CH4}	50	MJ/kg
Lower heating value of the fuel gas at turbine inlet for the calculated CH_4 concentration[a], LHV_{fuel}	42.66	MJ/kg
Model of the Siemens gas turbine[c]	SGT-750	60Hz
Power input at turbine inlet[b]	94.77	MJ/s=MW
Operation hours, t	7000	h/a
Gross efficiency, η (for simple cycle)[c]	40.2	%
Power output, PO[c]	38.1	MW (e)
Capacity factor, CF	1.00	-
Pressure ratio[c]	23.8:1	bar:bar
Exhaust mass flow[c]	113.8	kg/s
Exhaust temperature[c]	458	°C
Annual power output	**266700**	**MWhe/a**
a) Calculated as explained in section 6.2.4.4		
b) Calculated as explained in section 6.2.2.1		
c) Retrieved from open literature (Gas turbines catalogue, 2016)		

Table A- 17 Past values and future projections of annual Chemical Enginnering Plant Cost Index (CEPCI) - compiled from (DoL, 2015)

Year	Past values of CEPCI
2000	394.1
2001	394.3
2002	395.6
2003	402
2004	400
2005	468.2
2006	499.6
2007	525.4
2008	575.4
2009	521.9
2010	550.8
2011	585.7
2012	584.6
2013	567.3
2014	576.1
Year	**Future projections of CEPCI** (calculated by the equation given in **Figure A- 10**)
2015	627.9
2016	644.4
2017	660.9
2018	677.5

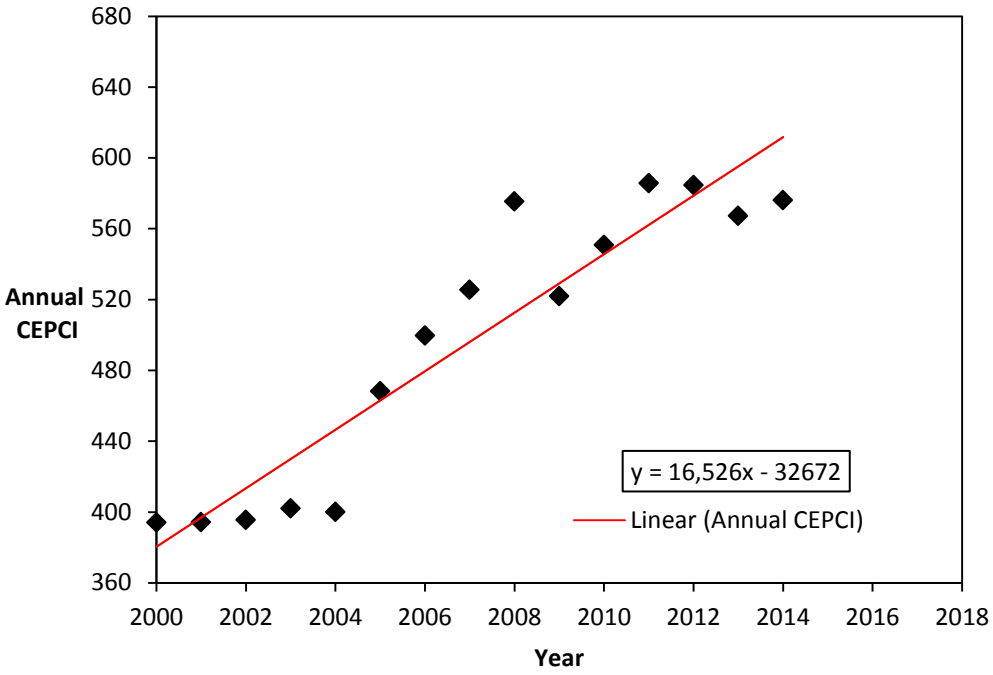

Figure A- 10 Modelling of the historical CEPCI values

Table A- 18 Data (Ulrich & Vasudevan, 2004) and results of bare module cost calculation of the treatment plant equipment applying the Sol.13

Parameter	Unit	Pump	Absorber	Flash vessel	Compressor	Regenerator	Sulfur separation unit
ρ, Density	[kg/m^3]	1360			1.15		1768
Volumetric flow rate of the fluid	[m^3/h]	1930			9558.08		14.85
m, Mass flow rate	[kg/s]				3.04		
g, Gravity	[m^2/s]	9.81					
P_2, Discharge pressure	[bar]	25			1.80		
h, Head	[m]	25.99					
ŋ, Efficiency	[-]	0.90			0.82		
Ps, Power (w/o friction)	[kW]	206.6			164.44		
Ps, Power (with friction + 20%)	[kW]	247.92			197.32		
D, Diameter	[m]		4.19	3.00		7.22	
H, Height	[m]		9.72	5.15		1.35	
V, Volume	[m^3]		133.72	36.39		55.02	
P, Pressure	bar	25	25	2.0	1.8	1.01325	
A, Area of the filtration unit	m^2						23.76
Base area (see Figure 5.57b given in (Ulrich & Vasudevan, 2004)	m^2						8
Base power (see Figure 5.49 for pump and Figure 5.30 for compressor given in (Ulrich & Vasudevan, 2004)	kW	400			200		
Base volume	[m^3]		0.10	1.00		1.00	
Base PEC from the chart at year 2004, C_P	$	70,000.0			109,000.0		60,000.0
Base PEC (f.o.b) from vendor at year 2014, C_P	$		14,560.0	11,500.0		11,500.0	
Cost exponent (degression coefficient,α)	[-]	0.36	0.60	0.60	0.60	0.60	0.12
$F_{p,}$ Correction factor of pressure (refer to Figure 5.50 in (Ulrich & Vasudevan, 2004))	[-]	1.50					
$F_{M,}$ Correction factor of material	[-]	1.90					
$F_{BM,}$ Correction factor of bare module (refer to Figure 5.51 in (Ulrich & Vasudevan, 2004))	[-]	6.00			3.50		2.40
C_{BM}(f.o.b) (year 2004)	$	420,000			381500,00		144,000.0
(CEPCI) on year 2004	-	400			400		400
(CEPCI) on year 2014	-		576.10	576.10		576.10	
(CEPCI) on year 2016	-	644.42	644.42	644.42	644.42	644.42	644.42
C_{BM} (f.o.b)(2016)	$	569,594.1	1,223,354.3	111,168.1	609,664.8	142,450.9	265,231.0
Total $C_{BM\ (f.o.b)}$(2016)	M$	2.92					
Delivery costs	M$	0.29					
Total C_{BM} delivered (2016)	**M$**	**3.21**					

Table A- 19 Individual elements of the fixed capital investment of the treatment plant using Sol.13 as decimal rates of the delivered bare module cost (Seider, Seader, & Lewin, 2010)

Cost elements	Factors for treatment plant (as decimal rates of $C_{BM,del}$)		Calculated cost values, M$
	Direct costs (DC)		
Purchased equipment delivered, $C_{BM,del}$	1.00		3.21
Equipment installation	0.10		0.32
Pipeline (including installation)	0.20		0.64
Electrical systems.instruments and control units	0.30		0.96
Battery limits building and service	0.40		1.28
Auxiliaries (Spares)	0.30		0.96
Site preparation	0.15		0.48
Field expenses	0.10		0.32
Total direct costs, TDC	**2.55**		**8.19**
	Indirect costs as factors of purchased equipment delivered ($C_{BM,del}$)	**Indirect costs as factors of TDC**	
Engineering and construction management	0.77	0.30	2.47
Contractor`s fees, overhead and profit	0.18	0.07	0.58
Contingencies	0.50	0.20	1.61
Total indirect costs, TIC	**1.45**	0.57	**4.65**
Fixed capital investment (FCI_{2016}=TDC+TIC)	**4.00**		**12.84**

Table A- 20 Individual elements of the fixed operational expenses of treatment plant using Sol.13 as percentages of the basis elements

Cost elements	Usual factors of basis elements	Selected factor	Basis elements	Costs, M$/a
Manufacturing costs				
Production costs				
Maintenance (M)	0.01-0.1	0.05	FCI	0.64
Supervision and support (S)	0.2-0.3	0.20	OL	0.38
Operating supplies (S)	0.15	0.15	M	0.10
Laboratory charges (S)	0.1-0.2	0.10	OL	0.19
Fixed Charges				
Local taxes (excluded)	0.01-0.04	0	FCI	0.00
Insurance	0.005-0.01	0.005	FCI	0.06
Plant Overhead Costs				
Plant overhead, general	0.5-0.7	0.50	M+OL+S	1.59
General Expenses				
Distribution and Marketing	0.02-0.20	0.05	OMC	0.07
R&D costs	0.02-0.15	0.05	OMC	0.07
Administration	0.15-0.20	0.15	OL	0.28
Fixed OMC_{2016} (without variable OMC - utilities (C_U), chemical costs (C_C) and operating labor (C_{OL}))				**3.38**

Table A- 21 Individual elements of the fixed operational expenses of power plant as percentages of the basis elements

Cost elements	Usual factors of basis elements	Selected factor	Basis elements	Costs, M$/a
Manufacturing costs				
Production costs				
Maintenance (M)	0.01-0.1	0.04	FCI	1.28
Supervision and support (S)	0.2-0.3	0.20	OL	0.21
Operating supplies (S)	0.15	0.15	M	0.19
Laboratory charges (S)	0.1-0.2	0.10	OL	0.10
Fixed Charges				
Local taxes (excluded)	0.01-0.04	0	FCI	0.00
Insurance	0.005-0.01	0.01	FCI	0.16
Plant Overhead Costs				
Plant overhead, general	0.5-0.7	0.50	M+OL+S	1.41
General Expenses				
Distribution and Marketing	0.02-0.20	0.002	OMC	0.04
R&D costs (excluded)	0.02-0.15	0.00	OMC	0.00
Administration	0.15-0.20	0.15	OL	0.16
Fixed OMC_{2016} (without variable OMC - operating labor (C_{OL}))				**3.55**

Table A- 22 Results of the operating labor costs (C_{OL}) estimations for both power and treatment plant

Contributors of the labor costs	Power plant	Treatment plant
Number of workers per shift	2	4
Shifts per day	3	3
Annual operation time,h/a	7000	
Hourly wages of workers, $/h	20	
Annual wages of workers, M$/a	0.84	1.68
Annual wage of the plant manager, M$/a	0.205	0.205
Operating labor costs (C_{OL}), M$/a	**1.045**	**1.885**

One shift was accounted for eight operation hours whereas three shifts were assumed to be required for daily operation. The labor requirement was considered as four and two workers per shift operation for the power and treatment plants, respectively. Thus, the annual wages of the workers to be employed in the PP and TP were calculated to be 0.84 and 1.68 M$/a, respectively (regarding the total operator requirement, annually operation time of the plant (7000 h/a) and the hourly wages of the workers (20 $/h)). One plant manager, with an annual salary of 0.205 M$/a, was considered for each plant yielding the total C_{OL} of 1.045 and 1.885 M$/a for the PP and TP, respectively.

Table A- 23 Annual utility requirement of the treatment plant (only electricity for pump and compressor, other consumers negligible) (MWhe/a)

Element	Unit	Value
Power requirement of the pump	MWe	0.25
Power requirement of the compressor	MWe	0.20
Total power requirement	MWe	0.45
Annual operation hours	h/a	7000
Annual power consumption, APC	**MWhe/a**	**3117**

Table A- 24 Supplemental data for cost estimation of various applied solvent systems (on the lower part of the table) and the related experimentally found variable data (on the upper part of the table)

Parameter \ Solution	Sol.13	Sol.3	Sol.12	Sol.1
Solution circulation rate, f_{sol}, (-)	1.62	2.46	9.4	10.81
Regeneration air demand, f_{air}, (-)	8.0	6.0	14	17
Density of solution (at 35 °C), kg/m^3	1360	1238	1137	1065
Residual moisture of the filter cake, (wt%)	60	55	55	45
Residence time of solution in regenerator, t_{reg} (h)	0.03	0.04	0.04	0.04
Residence time of solution in absorber, t_{abs} (h)	0.07	0.085	0.03	0.03
Residence time of solution in flash reactor, t_{flash} (h)	0.019 (assumed to be identical for all)			
Methane slip, (vol %)	<0.1 vol% (assumed to be identical for all)			

Equipment	Sizing factor (and desired direction of change)	Function of, (-) Impact on, (➢)	Sol.13	Sol.3	Sol.12	Sol.1
Absorber	Volume (m^3), ↓	- f_{sol} (↓) ➢ Size (↓), TCI (↓) → $CC_{L,TP}$ (↓); LCoE(↓)	133	248	366	390
Regenerator	Volume (m^3) , ↓	- f_{air} (↓) ➢ Size (↓), TCI (↓) → $CC_{L,TP}$ (↓); LCoE(↓)	55	11	462	572
Flash reactor	Volume (m^3) , ↓	- f_{sol} (↓) and methane slip (↓) ➢ Size (↓), TCI (↓); $CC_{L,TP}$ (↓) ➢ Methane slip(↓); $FC_{L,PP}$ (↓) ➢ Thus, LCoE(↓)	36	55	211	243
Circulation pump	Power (kW), ↓	- f_{sol} (↓) ➢ APC(↓),ANEP(↑) → $OMC_{L,TP}$(↓); LCoE(↓)	247	343	1205	1298
Air compressor	Power (kW), ↓	- f_{air} (↓) ➢ APC(↓),ANEP(↑) → $OMC_{L,TP}$(↓); LCoE(↓)	197	148	345	419
Sulfur separation unit	Filter area (m^2) , ↓	- Residual moisture of the filter cake(↓) ➢ Size (↓), TCI (↓); $CC_{L,TP}$ (↓) ➢ Chemical costs (↓),→ $OMC_{L,TP}$ (↓); LCoE(↓)	23	36	138	158
Solvent inventory, HU	Volume (m^3) , ↓	- Loading capacity (↑) and (f_{sol}) (↓) ➢ Size (↓), WCI (↓)→ $CC_{L,TP}$ (↓); LCoE(↓)	116	316	730	848